INL/EXT-19-55888

Light Water Reactor Sustainability Program

Fuel Rod Burst Potential Evaluation under LOCA Conditions for an Existing Plant with Extended Burnup Exceeding the Current Limit by 20%

September 2019

U.S. Department of Energy

Office of Nuclear Energy

INL/EXT-19-55888

Fuel Rod Burst Potential Evaluation under LOCA Conditions for an Existing Plant with Extended Burnup Exceeding the Current Limit by 20%

Hongbin Zhang[1], Cole Blakely[1], Jianguo Yu[1], Ryan Stewart[1], Mehdi Asgari[2]

September 2019

[1]Idaho National Laboratory
Idaho Falls, Idaho 83415

[2]Oak Ridge National Laboratory
Oak Ridge, TN 37830

Prepared for the
U.S. Department of Energy
Office of Nuclear Energy
Under DOE Idaho Operations Office
Contract DE-AC07-05ID14517

SUMMARY

Extending the fuel discharge burnup level from the current limit of rod averaged discharge burnup of 62 gigawatt-days per metric ton of uranium (GWd/MTU) to a proposed new limit of 75 GWd/MTU can provide significant economic benefits to the current fleet of operating nuclear power plants (NPPs). It allows for longer operating cycles and improved fuel utilization. The major economic gain of longer operating cycles is attributable to the increased capacity factor resulting from decreased refueling time as a fraction of total operating time, as well as fewer assemblies to be discharged for a given amount of energy produced. Significant progress has been achieved in the past by the nuclear power industry to increase fuel discharge burnup, which has provided the utilities with considerable reductions in their fuel cycle costs. Further burnup increase would incentivize the utilities to achieve additional fuel cycle cost reduction. Previous studies conducted by the Electric Power Research Institute (EPRI) found that fuel costs decrease with increasing discharge burnups while maintaining the fuel enrichment to less than the current limit of 5 w/o (weight percent). Additional studies by EPRI also showed that enhancements of fuel enrichment greater than 5 w/o (up to 6 w/o) can result in additional decreases in fuel costs and further increases in discharge burnups for both pressurized water reactors (PWRs) and boiling water reactors (BWRs).

There are many technological challenges posed by the increased burnup and warrant more research and development (R&D). These issues include corrosion and hydrogen uptake of the clad, fuel thermal conductivity degradation, dimensional changes of the fuel rod and assembly structure, the rim effect of the pellet, and the potential for the increase of fission gas release. These issues would be exacerbated considering the current industry's trend of adopting flexible operation strategies to maximize the revenue of NPPs. The main licensing challenges for higher burnup fuel are to ensure fuel rod safety under design basis accident (DBA) conditions, especially under large-break loss-of-coolant accidents (LBLOCAs) and reactivity insertion accidents (RIAs). During irradiation, the steep radial thermal gradient results in uranium dioxide (UO_2) pellet cracking and it becomes more prominent as burnup increases. Fuel rod burst, fuel pellet fragmentation, relocation, and dispersal (FFRD) during DBA conditions are the main obstacles for fuel discharge burnup to be extended above the current 62 GWd/MTU limit. Advanced fuel assembly and core designs, as well as advanced safety analysis approaches, are needed to offer sufficient margins to be used with higher enrichments to address these technological and licensing challenges associated with burnup extension.

The Risk-Informed Systems Analysis (RISA) Pathway of the United States (U.S.) Department of Energy (DOE) Light Water Reactor Sustainability (LWRS) Program initiated an Industry Application Pilot Demonstration Project to support the development and deployment of the fuel discharge burnup extension and increased enrichment technologies that are capable of achieving economic improvements, as well as timely widespread adoption by the U.S. nuclear industry. The primary objective of this project is to evaluate the fuel rod burst potential under DBA conditions to assist the nuclear industry to establish the technical basis to achieve burnup extension and provide commensurate fuel cycle cost reductions for the existing NPPs. The focus of the work conducted in fiscal year (FY)-2019 is to further develop the multi-physics best estimate plus uncertainty (MP-BEPU) analysis framework LOTUS by integrating DOE's advanced simulation tools VERA-CS and BISON to perform 24-months equilibrium cycle core designs for a generic PWR with burnup extension and increased enrichment and to carry out integrated evaluation of fuel rod burst potential under LBLOCA conditions.

In this report, five core design evolutions (Core Design Options 1 – 5) are presented for 24-months equilibrium cycles for a generic four-loop PWR with burnup extension up to 75 GWd/MTU and increased enrichment up to 6 w/o. As the core design options progress, the assembly and core designs become more complex and the core power peaking factors would need to be controlled and decreased as needed. Core Design Option 5 has the lowest power peaking factors among all the core design options and it could be a potential candidate for a practical 24-months PWR core design. Due to the high power peaking factors

obtained for Core Design Options 1 and 2, they are unlikely to be adopted in practical core designs and the burst evaluations are not performed for these two core design options. Instead, fuel rod burst potential evaluations are performed under LBLOCA conditions for Core Design Options 3 - 5 using LOTUS. The best estimate calculations using the empirical cladding deformation model in RELAP5-3D are performed for Core Design Options 3 – 5 and found that only the hot rod (i.e., highest power rod in an assembly) in 4 symmetric location once-burned assemblies could experience bursting at the middle of the cycle (MOC) for Core Design Option 3 which has relatively higher power peaking factors. However, more mechanistic evaluations of fuel rod bursting using the advanced fuel performance code BISON indicate that the fuel rod integrity is maintained under LBLOCA conditions. Fuel rods would not experience bursting at other exposure points in the equilibrium cycle for Core Design Options 3 – 5. The MP-BEPU calculations are performed only for Core Design Option 5, it is found that only a small fraction of fuel rods would experience bursting at MOC and EOC (end of the cycle) under LBLOCA conditions. The twice-burned fuel on the periphery would not experience bursting from either the best estimate or MP-BEPU calculations. The results indicate that high burnup does not necessarily contribute to fuel rod bursting. The power history (e.g., high peaking factors) is a more important contributing factor to the fuel rod bursting potential. Advanced fuel and core design techniques are investigated to control the power peaking factors, especially for the once-burned fuel to prevent fuel rods from bursting under LBLOCA conditions. It is noted that the fuel cladding temperature rise from the generic plant model studied in this work exhibits modest rise of cladding temperatures under the LBLOCA conditions. Since the LBLOCA responses are plant specific, plant specific analysis should be performed for those plants with higher temperature rises under LBLOCA conditions to ensure fuel rod integrity.

CONTENTS

FIGURES

TABLES

ACRONYMS

AOO	anticipated operational occurrence
ASTRUM	automated statistical treatment of uncertainty method
ATF	accident-tolerant fuel
ATWS	anticipated transients without scram
BPR	burnable poison rod
BC	boundary condition
BCP	body-centered cubic
BDBA	beyond design basis accident
BE	best estimate
BEPU	best estimate plus uncertainty
BOC	beginning of the cycle
BWR	boiling water reactor
CASL	Consortium for Advanced Simulation of Light Water Reactors
CD	core design
CD-A	core design automation
CD-O	core design optimization
CFR	Code of Federal Regulations
CHF	critical heat flux
CMFD	Coarse Mesh Finite Difference
CSAU	code scaling, applicability, and uncertainty
CTF	COBRA-TF (Coolant Boiling in Rod Arrays – Two Fluid subchannel thermal-hydraulics analysis code)
DBA	design basis accident
DEC	design extension condition
DNB	departure from nucleate boiling
DOE	U.S. Department of Energy
ECCS	emergency core cooling system
ECR	equivalent cladding reacted
EMDAP	evaluation model development and application
EOC	end of the cycle
EPRI	Electric Power Research Institute
F	Fahrenheit
FFRD	fuel fragmentation relocation and dispersal
FOM	figure of merit

FP	fuel performance
FRAPTRAN	Fuel Rod Analysis Program Transient
FSAR	Final Safety Analysis Report
FY	fiscal year
GWd/MTU	gigawatt-days per metric ton of uranium
HCP	hexagonal close packed
IFBA	integrated fuel burnable absorber
INL	Idaho National Laboratory
LBLOCA	large-break loss-of-coolant accident
LHGR	linear heat generation rate
LOCA	loss of coolant accident
LOTUS	LOCA analysis toolkit for the U.S.
LWR	light water reactor
LWRS	Light Water Reactor Sustainability Program
MACCS	MELCOR Accident Consequence Code System
MELCOR	Methods for Estimation of Leakages and Consequences of Releases
MOC	middle of the cycle
MOOSE	Multi-Physics Object-Oriented Simulation Environment
MP-BEPU	multi-physics best estimate plus uncertainty
MTC	moderator temperature coefficient
NPP	nuclear power plant
NRC	U.S. Nuclear Regulatory Commission
NSSS	nuclear steam supply system
OS	overstress
PCT	peak clad temperature
PDF	probability density function
PI	plasticity instability
PIRT	phenomenon identification and ranking table
PNNL	Pacific Northwest National Laboratory
ppm	parts per million
PWR	pressurized water reactor
R&D	research and development
RA	risk assessment
RBR	ratio of bursting rods
RCCA	rod cluster control assembly

RCS	reactor coolant system
RELAP5	Reactor Excursion and Leak Analysis Program 5
RIA	reactivity insertion accident
RIP	rod internal pressure
RISA	Risk-Informed Systems Analysis
RPV	reactor pressure vessel
SA	systems analysis
SAMA	severe accident migration alternative
SRP	Standard Review Plan
SSC	system, structure, and component
STP	South Texas Project
U.S.	United States
UO_2	uranium dioxide
UQ	uncertainty quantification
VERA-CS	Virtual Environment for Reactor – Core Simulator
w/o	weight percent
WABA	wet annular burnable absorber
ZrB2	zirconium diboride

Fuel Rod Burst Potential Evaluation under LOCA Conditions for an Existing Plant with Extended Burnup Exceeding the Current Limit by 20%

1. INTRODUCTION

The nuclear industry in the United States (U.S.) has achieved superb performance in safety and reliability throughout the operating fleet of existing nuclear power plants (NPPs). The nuclear power industry has a long history of working toward achieving improved plant economics through the introduction of many innovative technologies, such as longer operating cycles (i.e., many existing boiling water reactors [BWRs] currently operate on a 24-month cycle, but most existing pressurized water reactors [PWRs] currently operate on a 18-month cycle), higher fuel enrichment (the fuel enrichment is close to the licensing limit of 5%), higher burnup of discharged fuel, and power uprates. Such innovations have led to remarkable improvements in the economic performance of existing NPPs. For instance, the total additional power generated from U.S. NPP uprates is equivalent to the power that would result from building approximately eight new 1,000-MWe NPPs [1].

However, current market conditions associated with the electric power market (i.e., abundant supplies of low-cost natural gas because of hydraulic fracturing extraction techniques, governmental subsidies for wind and solar generation technologies, etc.) have put significant strains on existing NPP economic competitiveness. At the present time, the total generating costs (i.e., fuel, capital, and operating costs) of many NPPs are not able to match the production costs of alternative sources, such as natural gas-fired plants and production tax credits associated with solar and wind power. Therefore, additional innovations will need to be introduced to the existing fleet of NPPs to remedy this situation.

To achieve these objectives, great interest exists for the operating NPP fleet to adopt technologies that can support cost reduction and operational performance enhancements. Significant economic benefits for the current fleet of operating light water reactors (LWRs) are achievable through burnup extension. Increasing the fuel assembly discharge burnup is the most efficient means to achieve fuel cycle cost reduction, which greatly contributes to total generating costs. It allows for longer operating cycles and improved resource utilization. The major economic gain of longer operating cycles is due to the increased capacity factor resulting from decreased refueling times as a fraction of total operating time, as well as a fewer number of assemblies needing to be discharged for a given amount of produced energy. Significant progress has been achieved in the past by the nuclear industry to increase fuel discharge burnup, which has provided these utilities with considerable reductions in their fuel cycle costs. Further burnup increases would incentivize the utilities to achieve additional fuel cycle cost reductions by increasing fuel utilization. Past Electric Power Research Institute (EPRI) studies established economic incentives for burnup extension within the constraints of the 5 w/o enrichment limit [2]. Increased fuel discharge burnup normally requires the use of higher enrichment fuel. Additional studies have also shown that enhancements in fuel enrichment greater than 5 w/o (weight percent) up to 6 w/o can result in additional decreases in fuel costs and further increases in discharge burnups for both PWRs and BWRs [3]. Raising the fuel discharge burnup limit from the current fuel rod averaged value of 62 gigawatt-days per metric ton of uranium (GWd/MTU) to a proposed new limit of 75 GWd/MTU, as well as the enrichment limit from the current value of 5 w/o to a proposed new limit of 6 w/o, would improve fuel cycle economics. For example, increasing fuel enrichment and discharge burnup levels could be used to extend PWR operating cycles from the current 18 months up to 24 months. The main advantages of burnup extension include:

1. Reducing the duration of refueling outage and refueling times as a fraction of total operating time, which directly contributes to a reduction in operating costs.

2. Reducing the number of fresh nuclear fuel assemblies required to be reloaded, and thus reducing the spent nuclear fuel assemblies generated. Both lead to improvements in the economics of fuel cycle.
3. Providing the flexibility to allow advanced fuel designs with additional margins to be installed in a core with higher enrichments in smaller fuel reload batch sizes and with more heterogeneous core loading patterns to flatten out power distributions.
4. Lowering the mass of spent fuel discharged per unit of electricity generated, which can reduce spent fuel handling, storage and transportation costs.
5. Loading of the high burnup assemblies in the periphery reduces the neutron fluence on the pressure vessel.
6. Reducing the potential for the diversion of fissile material from spent fuel for non-peaceful purposes.

However, the impact of longer operating cycles and higher fuel enrichment is that these enhancements will result in larger activity inventory in the core; as such, plant response during operational transient and postulated accident conditions could get closer to prescribed safety limits. There are many technological challenges posed by increased burnup, such as the corrosion and hydrogen pickup of the clad, fuel thermal conductivity degradation, dimensional changes of the fuel rod and fuel assembly structure, the rim effect of the pellet, and the potential for increase of fission gas release. Primary concerns associated with high burnup fuels include:

1. Increased burnup places additional demands on fuel cladding to withstand harsh reactor environments for longer periods of time. The increased loads and more demanding requirements for fuel assemblies could raise the risk of fuel failures and decrease the reliability of the fuel.
2. Longer residence time in the reactor requires a higher corrosion resistance for the cladding materials.
3. Higher accumulation of gaseous fission products inside the fuel rod resulting in a significant increase in rod internal pressure (RIP), which increases the pressure differential between the inside and outside of a fuel rod and poses risks to fuel rod integrity under loss-of-coolant accident (LOCA) conditions.
4. Higher burnup leads to increased radiation-induced growth that can lead to undesirable changes in core geometry (i.e., fuel assembly bow or fuel rod bow). Fuel assembly bow can result in an increased possibility for control rods drop time due to friction between the control rod and bowed guide tubes.
5. Generation of a smaller volume of fuel for reprocessing, but with a higher specific activity.

All of these factors must be considered because they can lead to a decrease in operational reliability and licensing challenges. Additionally, increased discharge burnup necessitates changes in core design such as increased enrichment, core batch fractions, and increases in burnable poisons. Fuel design parameters such as annular, blankets, and gadolinium content are also subject to change. All core design and fuel design changes could raise the risk of fuel failures under both normal operating and abnormal conditions. These issues would be exacerbated considering the current industry's trend of adopting flexible operation strategies to maximize NPP revenue.

The main licensing challenges for higher burnup fuel are design basis accident (DBA) condition analyses, especially for large-break loss-of-coolant accident (LBLOCA) and RIA. The LBLOCA sequence can be divided into three phases: (1) blowdown; (2) refill; and (3) reflood. During the blowdown phase, ballooning and burst of the cladding occur since the RIP becomes much higher than the system pressure of the reactor pressure vessel (RPV) and the strength of the fuel cladding decreases as the temperature increases. During the refill phase, the cladding is severely oxidized by steam and becomes embrittled. During the reflood phase, the embrittled cladding may rupture by thermal shock caused by rapid cooling. Under RIA conditions, the fuel clad local conditions such as oxide layer thickness, oxide spalling, and local hydrides have a strong influence on fuel rod safety; as such, fuel rod local conditions are a strong function of the burnup level. Another obstacle is that there is no internationally accepted RIA

failure limit at high burnup. During irradiation, the uranium dioxide (UO_2) fuel undergoes significant changes in composition and the steep radial thermal gradient results in pellet cracking that allows fission gases migrate to gap and plenum regions in the fuel rod. Fuel rod burst, fuel pellet fragmentation, relocation, and dispersal [4] during these DBA conditions are the main obstacles for fuel discharge burnup to be extended above the current limit of 62 GWd/MTU. Safety analysis should be performed to demonstrate acceptable consequences for these accident conditions. In the safety analyses of NPPs, the consequences of hypothetical accidents such as anticipated operational occurrences (AOOs) and DBAs are analyzed to ensure the suitable safety systems can mitigate them. For DBAs, a fundamental requirement is that there should be no, or very limited radiological consequences released to the public. To fulfill this criterion, derivative acceptance criteria have been formulated for the safety systems of the reactor. For LOCA, the acceptance criteria excerpted from 10 Code of Federal Regulations (CFR) 50.46 [5], are:

1. *Peak cladding temperature*. The calculated maximum fuel element cladding temperature shall not exceed 2200° Fahrenheit (F).
2. *Maximum cladding oxidation*. The calculated total oxidation of the cladding shall nowhere exceed 0.17 times the total cladding thickness before oxidation.
3. *Maximum hydrogen generation*. The calculated total amount of hydrogen generated from the chemical reaction of the cladding with water or steam shall not exceed 0.01 times the hypothetical amount that would be generated if all of the metal in the cladding cylinders surrounding the fuel, excluding the cladding surrounding the plenum volume, were to react.
4. *Coolable geometry*. Calculated changes in core geometry shall be such that the core remains amenable to cooling.
5. *Long-term cooling*. After any calculated successful initial operation of the emergency core cooling system (ECCS), the calculated core temperature shall be maintained at an acceptably low value and decay heat shall be removed for the extended period of time required by the long-lived radioactivity remaining in the core.

Criterion # 4 mandates that the structural integrity of the fuel rods is preserved to maintain their coolable geometries throughout the whole LOCA sequence. When the fuel rods heat up during LOCA and the external high primary system pressure is lost, the RIP is large enough to cause plastic deformation of the cladding, which has the potential to induce cladding ballooning and bursting. The ballooning reduces the coolant flow areas between fuel rods and could potentially be detrimental to cooling the fuel rods. When bursting happens to a fuel rod, cladding oxides from the inside and it picks up a significant amount of hydrogen. Hydrogen pickup embrittles cladding, especially after the quenching phase. Finally, at elevated temperatures, the rate of steam-cladding oxidation may become so high that the heat can no longer be adequately dissipated by cooling, and may eventually lead to autocatalytic or runaway oxidation. If autocatalytic oxidation is not arrested, cladding metal and the reactor core could melt, and causing severe accidents in a reactor. Most countries follow the fuel safety criteria applied by the U.S. Nuclear Regulatory Commission (NRC) under 10 CFR 50.46. Others have more stringent requirements. For example, in Germany, an additional requirement is imposed that the fraction of burst fuel rods shall not exceed 10% of the total rods in the core. The purpose of this requirement is to limit fission products release due to cladding burst.

In the meantime, the NRC is considering a rulemaking change that would revise the requirements in 10 CFR 50.46. In the proposed rulemaking, designated as 10 CFR 50.46c [6], the NRC proposed a fuel performance-based equivalent cladding reacted criterion as a function of cladding hydrogen content before the accident (pre-transient) in order to include the effects of higher burnup on cladding performance, as well as to address other technical issues. The pre-transient cladding hydrogen content,

in turn, is a function of the fuel burnup and cladding materials. The proposed rule would apply to all LWRs and to all zirconium-based cladding types. The key points of the proposed rule are as follows:

- Cladding performance cannot be evaluated in isolation. Cladding performance and ECCS performance need to be considered in a coupled way, which examines the interactions across the disciplines involved.
- Models for cladding performance even within the design basis will need to be updated for regulatory purposes.
- Effort needs to be expended in searching regulatory issue space for the limiting case (i.e., "ECCS performance must be demonstrated for a range of postulated LOCAs of different sizes, locations, and other properties, sufficient to provide assurance that the most severe postulated LOCAs have been identified. ECCS performance must be demonstrated for the accident, and the post-accident recovery and recirculation period.")

The proposed rulemaking imposes more restrictive and fuel rod-dependent cladding embrittlement criteria. If implemented, this proposed new rulemaking presents additional licensing challenges for burnup extension.

It is anticipated that considerable effort would be necessary to obtain regulatory approvals to extend either the current enrichment or burnup limits associated with nuclear fuel, especially the main licensing challenges such as LOCA and RIA for high burnup fuel. It is noted that for international applications, analyses related to beyond design basis accident (BDBA) conditions or design extension conditions (DECs) would provide an additional licensing challenge. It is also noted that the current enrichment limit of 5 w/o U-235 represents a worldwide established limit for fabrication, transport, and storage of nuclear fuel for LWRs.

The Risk-Informed Systems Analysis (RISA) Pathway of the U.S. Department of Energy (DOE) Light Water Reactor Sustainability (LWRS) Program initiated an Industry Application Pilot Project in fiscal year (FY)-2019, called "Modernization of Design Basis Accident Analysis with Application on Burnup Extension," with the main objective to assist the nuclear power industry in establishing the technical basis for fuel rods at burnup extensions beyond 62 GWd/MTU and increased enrichment above 5 w/o. The near-term goal of this activity is to conduct evaluations of fuel rod burst potential under DBA conditions (e.g., LBLOCA and RIA) for increased rod averaged discharge fuel burnup up to 75 GWd/MTU and increased enrichment up to 6 w/o. Since the cost of enrichment is non-linear, at some point the increased enrichment costs may offset the benefits of improved fuel cycle efficiency and the reduced number of fuel assemblies to be discharged. The combination of the optimal level of enrichment, discharge burnup, and fuel cycle length to achieve optimal improvements in fuel cycle economics under a realistic utility environment will be investigated. The long-term goal of this project will be to work with industry partners (including EPRI and industry lead utilities conducting evaluation and testing of fuel burnup extensions and increased enrichment) to address the challenging licensing issues of fuel fragmentation, relocation, and dispersal.

The entire evaluation process involves the review of the licensing limits defined in Section 4.2 of the NRC Standard Review Plan (SRP) (NUREG-0800) [7]. The objective of the evaluation process is to assess the need for modifications or additions to the existing licensing criteria, or to demonstrate the applicability of the present limits to rod averaged burnup levels beyond 62 GWd/MTU.

The licensing requirements of the fuel system specified in Section 4.2 of SRP are:

1. Fuel damage is not expected during Condition I and Condition II events. It is not possible, however, to preclude a very small number of rod failures. These are within the capability of the plant clean-up system and are consistent with plant design basis.

2. The reactor can be brought to a safe state following a Condition III event with only a small fraction of fuel rods becoming damaged, although sufficient fuel damage might occur to preclude the immediate resumption of operation. The fraction of fuel rods damaged must be limited to meet the dose guidelines of 10 CFR 100.
3. The reactor can be brought to a safe state and the core can be kept subcritical with acceptable heat transfer geometry following transients arising from Condition IV events.

For the purpose of completeness, the events under different conditions are briefly described here. Condition I is defined as plant operation within specified operational limits and conditions. Condition I events do not result in any adverse impacts on the plant or the public. The Condition II and Condition III faults are typically referred to as AOOs. An AOO is an operational process that deviates from normal operation and is expected to occur at least once during the operating lifetime of an NPP. In view of appropriate design provisions, AOOs do not cause any significant damage to items that are important to safety and do not lead to accident conditions. Condition IV faults are postulated DBAs that are not expected to occur during the operational lifetime of an NPP. An NPP is designed to withstand DBAs according to established design criteria, and for which the damage to the fuel and the release of radioactive material are kept within acceptable regulatory limits. These postulated DBAs determine the criteria for the design and evaluation of various safety-related systems and equipment. For DBAs, the possibility of limited damage to the fuel is accepted, but offsite consequence release limits should not be exceeded. Figure 1 illustrates the various states or conditions of an operating NPP. In addition to Conditions I through IV described above, an NPP could also undergo an event that is considered to be BDBA conditions. A BDBA or DEC involves accident conditions that are more severe than DBAs and have the potential to result in core degradation.

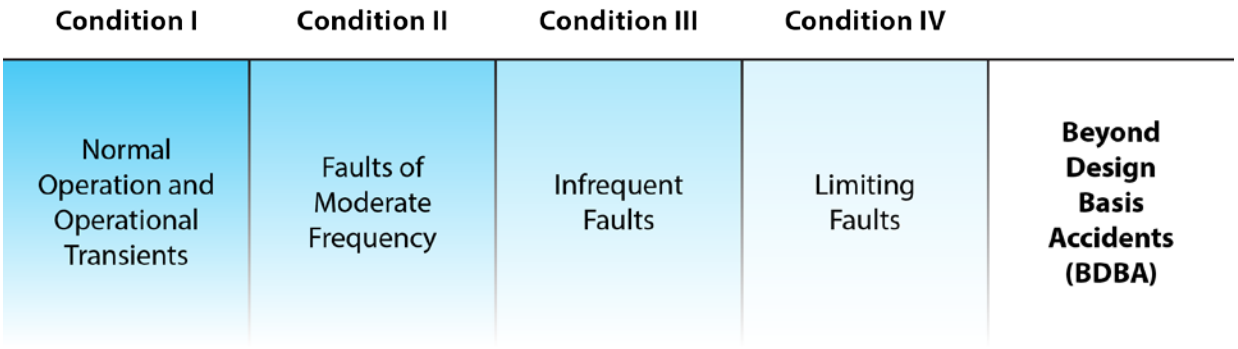

Figure 1. Illustration of NPP states.

In fiscal year (FY)-2019, the primary focus of the research and development (R&D) activities in this project is to perform the evaluation of the fuel rod burst potential under LBLOCA conditions with burnup extension. The evaluation of fuel rod burst potential with burnup extension involves multiple disciplines to address the challenging licensing issues under transient conditions. The disciplines involved in the work conducted in FY-2019 are core design (CD), fuel performance (FP), systems analysis (SA), and uncertainty quantification (UQ)/risk assessment (RA).

Core design work is performed for a four-loop Westinghouse design PWR with increased enrichment up to 6 w/o to achieve a 24-month cycle and around 75 GWD/MTU rod averaged discharge burnup. The Consortium for Advanced Simulation of Light Water Reactors' (CASL's) Virtual Environment for Reactor – Core Simulator (VERA-CS) [8] code is used to perform the equilibrium cycle core design work. The VERA-CS code provides pin-resolved power distributions for the core design followed by detailed fuel performance calculations for individual fuel rods in the core using the FRAPCON fuel performance analysis code [9]. The risk-informed transient safety calculations using the Reactor Excursion and Leak Analysis Program 5 (RELAP5)-3D code [10] is subsequently performed to address

the challenging issues of burst potential evaluation under LBLOCA conditions. The advanced fuel performance BISON code [11] is used to perform more mechanistic evaluation of fuel rod burst potential under LBLOCA conditions. The UQ and RA are performed using the best estimate (BE) and best estimate plus uncertainty (BEPU) methodologies. The evaluation process is performed using the LOCA analysis toolkit for the U.S (LOTUS) controller. A more detailed description on LOTUS can be found in Section 2.

2. FUEL ROD BURST POTENTIAL EVALUATION FRAMEWORK

As pointed in Section 1, evaluating the fuel rod bursting potential under LOCA conditions involves multiple disciplines, such as CD, FP, systems transient analysis, and UQ/RA. The LOTUS framework provides an environment for the integration of multiple codes within the disciplines of core design automation (CD-A), FP, SA, and core design optimization (CD-O). LOTUS also includes UQ, sensitivity analysis, and RA. The LOTUS framework is notionally shown in Figure 2. Both existing and advanced analysis tools are utilized in this work. Due to the high costs associated with the qualification and regulatory acceptance of analytical tools, it is anticipated that the licensing of advanced nuclear technologies will rely predominantly on the current suite of tools used to assess transient events. However, because of the large uncertainties that currently exist with high burnup fuel, the existing tools will need to be informed and enhanced to support the licensing and deployment of the burnup extension technology. The codes that have been identified for use in the execution of burnup extension and increased enrichment analysis. The integration presented in this work demonstrates CD-A using the VERA-CS code, FP using the FRAPCON code for steady-state calculations and Fuel Rod Analysis Program Transient (FRAPTRAN)/BISON for transient calculations, and SA using RELAP5-3D code in conjunction with UQ software. What is presented in this report is only a portion of the eventual capabilities encompassing other disciplines in SAs. As Figure 2 suggests, LOTUS will eventually entail additional codes and stores all data within HDF5 databases [12]. This method of storage allows the results of past cases to be accessed by later works, thereby avoiding redundancies in future code integrations.

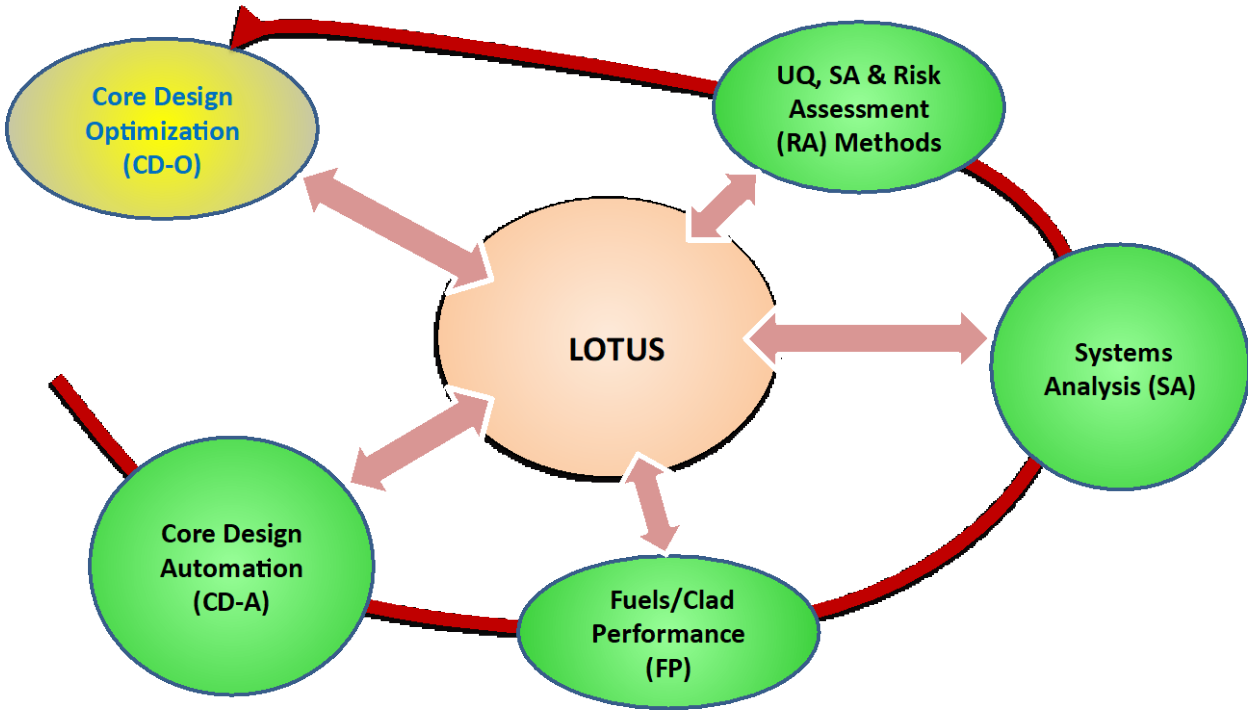

Figure 2. Conceptual schematic of LOTUS capabilities.

Since different models, assumptions and numeric methods are used in different computer codes, inconsistencies exist among them and should be addressed when different computer codes integrated together. Section 2.1 addresses model inconsistencies among different computer codes. Code integration is discussed in Section 2.2 and uncertainty quantification and risk assessment for multi-physics simulations are discussed in Section 2.3.

2.1 Model Inconsistences

Differences between VERA-CS, FRAPCON, BISON, and RELAP5-3D fall into one of three categories: (1) the code domain; (2) the phenomena modeled; and (3) the numerical discretization. These differences are discussed in the sections that follow.

2.1.1 Code Domain

In terms of domain, VERA-CS models a full reactor core, while FRAPCON and BISON model individual fuel rods within an idealized single coolant subchannel. RELAP5-3D models a set of heat structures representing the full core, as well as the entire primary and secondary coolant loops and the ECCS. Essentially, VERA-CS and FRAPCON/BISON model a small subspace of the full RELAP5-3D domain. The largest discrepancies stemming from these domain differences are in the form of boundary conditions.

In order to run FRAPCON and BISON, core inlet temperature, outlet pressure, and mass flow rate or flux are required as boundary conditions. However, they are not boundary conditions within RELAP5-3D as there are no domain boundaries at the core inlet and outlet. In the interests of minimizing the discrepancy to the extent possible, the VERA-CS values and FRAPCON/BISON nominal values of mass flux and outlet pressure were selected based on the results of the nominal case of RELAP5-3D. The inlet nominal temperature for FRAPCON and BISON was selected based on the supplied input to VERA-CS.

2.1.2 Phenomena Modeled

The phenomenological differences between VERA-CS, FRAPCON, BISON, and RELAP5-3D are vast. FRAPCON and RELAP5-3D have evolved separately over forty years to solve very different types of problems, while VERA-CS and BISON are modern computer codes relying on more recently developed methods and an improved understanding of the physics. As a result, there are large variations in the specific phenomena modeled, as well as in the sophistication and numerical accuracy of the individual models involved.

For instance, RELAP5-3D has extensive empirical relations for coolant heat transfer coefficients, while FRAPCON only utilizes two relations (e.g., one for forced film convection and the other for nucleate boiling). Furthermore, dynamic gap conductance models implemented in FRAPCON take into account material deformation, fission gas release, pellet cladding mechanical interaction, and irradiative effects. Conversely, the dynamic gap conductance model of RELAP5-3D uses simplified gap deformation models in conjunction with the ideal gas law (constant gas composition assumed).

The elimination of the majority of these phenomenological discrepancies is neither reasonable nor of little benefit. In most cases, extensive validation has established the simplifications within each code are appropriate for the specific problems they encounter. The primary difference of concern resides in the heat equations of FRAPCON, BISON, and the steady-state simulations of RELAP5-3D. These issues will be resolved in future work centered on calibrating RELAP5-3D to FRAPCON and BISON based on stored internal energy. Within the context of this work, VERA-CS and FRAPCON may be thought of as initialization modules within the RELAP5-3D framework.

VERA-CS provides power histories to FRAPCON and BISON and the core power shapes at the time of LBLOCA to RELAP5-3D. FRAPCON solves a quasi-steady-state depletion problem, which RELAP5-3D is not equipped to model. Fuel performance data from FRAPCON is then supplied to RELAP5-3D as a means to potentially enhance the fidelity of the RELAP5-3D, which then executes a

LBLOCA simulation, which FRAPCON is incapable of performing. The results from RELAP5-3D simulations of LBLOCA are supplied to BISON to perform more mechanistic evaluation of the fuel rod burst potential. The integration of these codes within LOTUS, while not an all-encompassing model of true reactor physics, is an improvement over more compartmentalized approaches.

2.1.3 Discretization

For steady-state simulations of the fuel rods, both the FRAPCON and RELAP5-3D codes use finite difference approximations that solve the heat conduction equation in the radial direction alone, but allow for axial variation in linear heat rates. This is referred to as 1 ½ D in FRAPCON documentation. While there are phenomenological differences in the computation of thermal conductivity, the numerical methods themselves do not contain significant discrepancies.

Within this work, the number of radial and axial nodes differs between code input files. When solving the heat equation, FRAPCON has 17 radial elements in the fuel and 5 in the cladding, while RELAP5-3D has only 5 in the fuel and 2 in the cladding. Note that FRAPCON uses the analytical solution from the thick wall approximation when computing stresses and 45 radial nodes in fission gas release calculations. However, in the interests of comparing similar models, only the discretization used for solving the heat equations in FRAPCON is compared here. The VERA-CS and FRAPCON input files have 15 axial elements within the fuel rod, while RELAP5-3D uses 6 axial elements in the interests of maintaining reasonable run times. Thus within this work, FRAPCON and VERA-CS use greater spatial discretization as compared to the heat structures of RELAP5-3D. Once again, it is stressed that FRAPCON and VERA-CS can be seen as modules used for the initialization of the core within the RELAP5-3D structure. Thus numerical approximations within RELAP5-3D do not affect FRAPCON or VERA-CS. Potential improvements in numerical estimates within VERA-CS and FRAPCON serve only to enhance traditional RELAP5-3D studies.

2.2 Code Integration for Multi-Physics BEPU Simulations

Safety analyses have been traditionally performed sequentially. This means that the analysis performed to address one portion of the physics does not necessarily provide sufficient consideration for the downstream analyses that need to be performed. As a result, the boundary conditions used for one set of analysis frequently assume conservative values from the upstream analyses. As a minimum, this sequential processing of information is inefficient and results in excess expenditures of time and resources. This often is exacerbated by the need to revise previous analyses due to results obtained during later analyses. This need to operate in a cyclic manner can add significantly to the expense and time required to conduct these analyses.

In addition, different models and assumptions went into the computer codes developed for each of the physics being analyzed. As a result, the conventional approach and methods are strongly “code-oriented.” The analyst has to be familiar with the details of the codes utilized, in particular with respect to their input and output structures. This represents a significant barrier for widespread use outside of the small pool of experts that develop and apply the codes. It becomes apparent how difficult it is to make changes and accelerate progress under such a paradigm, especially in a heavily regulated environment where even a single line change in a code can carry a heavy cost of bookkeeping and regulatory review. This “divide-and-conquer” approach currently is adopted in the industry where every physics is resolved independently and coupling is addressed by complex interface procedures. The current process is labor-intensive and inefficient. More importantly, continued use of these current methods has a significant bias to retain excess analytical margins, which cannot be exploited at a later time to enhance operational and economic performance.

Traditionally, the safety margin estimation is mostly based on conservative evaluation model calculations. Thus, the analytical safety margin has a high level of conservatism that can present a skewed understanding of the actual operating situation and limit the potential for enhancement of plant

performance. More realistic analyses should be used to evaluate the evolution and consequences of plant transients and accidents. To remedy the situation, the use of BE analysis together with an evaluation of the uncertainties, or the so-called BEPU approach, is increasing for the following reasons:

1. The use of conservative assumptions may sometimes exclude or mask certain important physical phenomena. Hence, there is a potential to overlook some key sequences of events that are important in assessing the safety of the plant.
2. The use of conservative approaches tends to produce pessimistic results, resulting from the prediction of an incorrect progression or unrealistic timescales of events, and often does not show the true margins to the acceptance criteria that apply in reality. This situation is exacerbated by the fact that the current process for performing safety analysis is sequential in practice with each step providing conservatisms related to its specific physics. This often results in a compounding effect, such that the final analytical results are extremely conservative, leading to the specification of overly conservative operational limitations and requirements. On the surface, this may seem acceptable from a safety perspective; however, since plant resources are finite, overly conservative limits can skew the distribution of resources away from where they could provide more value (in terms of both safety and economic performance).
3. A BEPU approach provides more realistic information about the physical behavior of the plant, assists in identifying the most relevant safety parameters, and allows more realistic comparison with the acceptance criteria. Thus, by providing more realistic outcomes, this approach has the potential to permit reductions in unnecessary operational restrictions and requirements with the ability to enhance operational and economic performance without substantively reducing plant safety.

The BEPU process has become the de-facto standard in the nuclear industry and has been widely used to perform LOCA analyses. Westinghouse developed its realistic LBLOCA evaluation method based on the thermal hydraulic code WCOBRA/TRAC with its biases and uncertainties quantified by the automated statistical treatment of uncertainty method (ASTRUM) [13]. AREVA's realistic LBLOCA analysis is primarily developed based on the S-RELAP5 code, which is a modified version of RELAP5/MOD2 with several updates [14].

The key aspect of the BEPU methodology is to quantify and propagate uncertainties in the calculations across all modeled constituent phenomena (e.g., reactor physics, thermal hydraulics, fuel/clad performance, etc.). However, the computational constraints that arise due to the complex systems and interdependencies of variables historically have prevented the nuclear power industry from executing such multi-physics schemes. Because of these limitations, the existing BEPU methodology primarily focuses on the uncertainties in thermal hydraulics. This methodology is depicted in Figure 3 as an example of a LOCA analysis.

It is noted that the current BEPU methodology still typically contains a high degree of conservatism, primarily as a means to mask knowledge gaps related to certain phenomena, and to simplify licensing and implementation. Further, because the complete propagation of uncertainties across the various disciplines can be prohibitively expensive in terms of computational capability and time, bounding assumptions are often used where multiple phenomena need to be modeled and assessed to address uncertainty considerations. This approach, in turn, limits the ability to consistently propagate uncertainties in multi-physics simulations. Therefore, existing BEPU methods, as currently applied, often provide limited information on the actual margins available in the plants. As a consequence, a portion of the margins that exist in the plants continue to reside in engineering judgment and conservative assumptions, and from which it has proven to be extremely challenging to obtain economic benefits.

There are significant assumptions and engineering judgments used in setting up those procedures that makes the propagation of uncertainties across the disciplines complex and potentially prone to errors. It is noted from the BEPU 2018 conference [15] that the BEPU work was mainly concentrated on uncertainty

evaluation methodologies, rather than on the whole BEPU process. Consistency in all steps of BEPU needs to be ensured; however, a need to reduce the shortcuts in BEPU applications and focus on the exploitation of the full BEPU process has been identified [15].

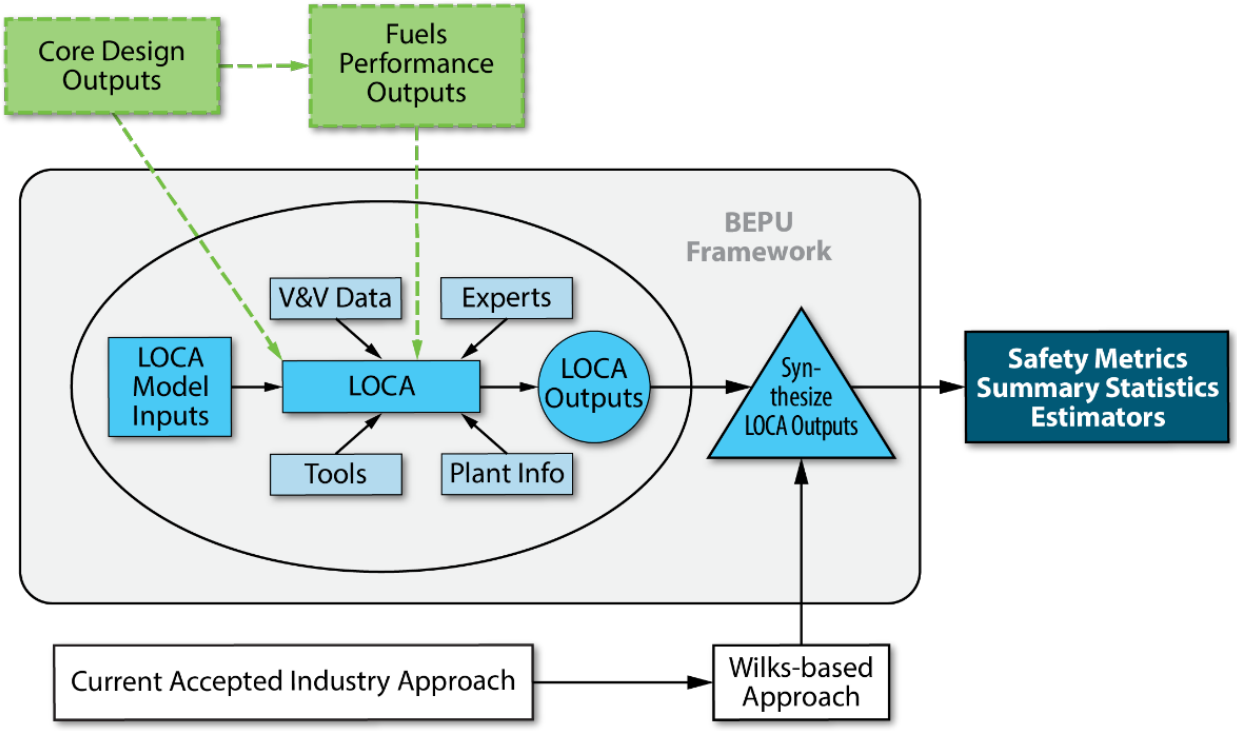

Figure 3. Schematic illustration of the current BEPU process for LOCA analysis.

To address the conservatisms built into the current practice, it is essential to propagate uncertainties across the stream of physical disciplines and manage the data stream. As more automation is adopted into plant processes, it is anticipated that the nuclear industry will develop better standardized databases and improved interfaces that function across the various engineering disciplines. Such standardization and increased automation will be capable of enabling new paradigms to evaluate and manage uncertainties across various disciplines and support a more integrated multi-physics approach that can be applied to the safety analysis problem. This will become more important as the industry adopts new and advanced nuclear technologies, such as further increases in fuel enrichment and discharge burnup to extend operating cycle length and the deployment of accident-tolerant fuel (ATF). The evaluation and adoption of any of these enhancements will require detailed analyses of the fuel and systems, structures, and components (SSCs) behavior within the context of entire plant system dynamics. Fortunately, because of the advancements in computing power over the past several decades, multi-physics simulations are now practical within the context of UQ and sensitivity analysis (i.e., multi-physics best estimate plus uncertainty [MP-BEPU] methodologies [16]). As a result, we are moving toward to a “plug-and-play” or task-oriented approach, as illustrated in Figure 4, for the LOTUS framework, where the codes are integrated together under one roof and each code is simply treated as a module “under the hood” that provides the input-output relationship for a specific analytical discipline. The focus shifts on managing the data stream at a system level, as depicted in Figure 4. The use of an integrated approach in managing the data stream is probably the most important aspect of what is proposed here. The plug-and-play multi-physics environment in LOTUS is essentially a workflow engine with the capability to drive physics simulators, model complex systems, and provide risk assessment capabilities. Such an approach is well-suited with the current trends in industry to enhance automation and develop integrated databases across their organizations.

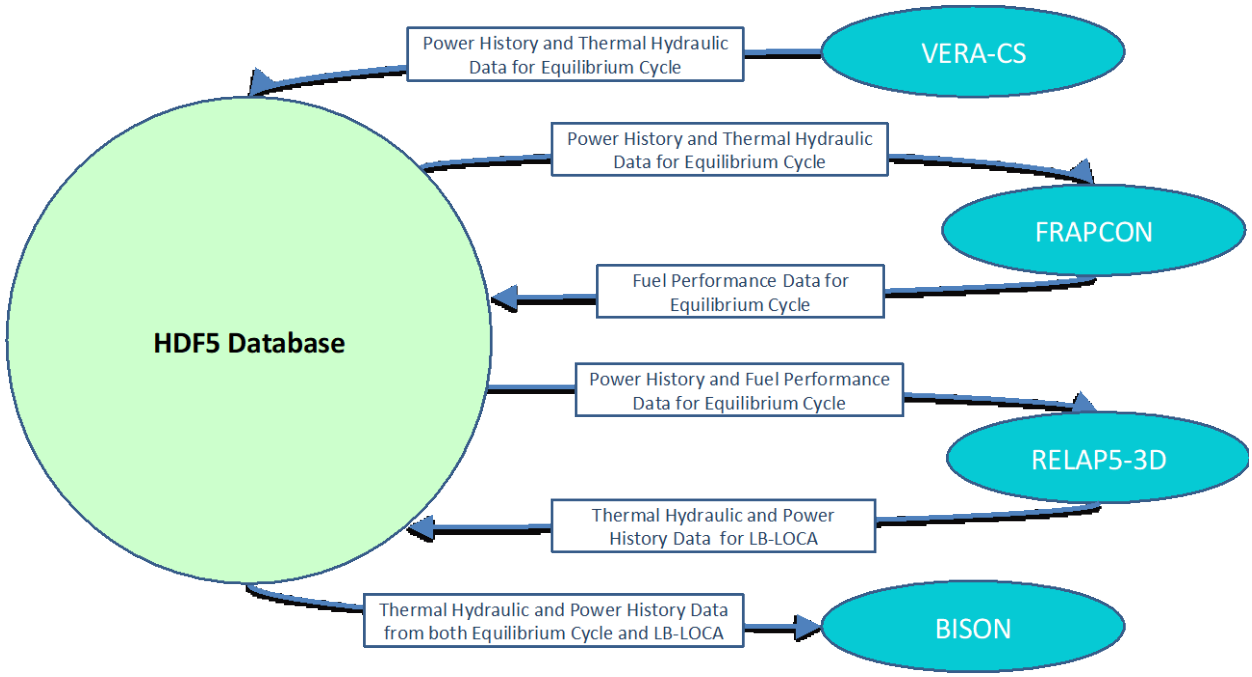

Figure 4. LOTUS data flow structure showing the “Plug-and-Play” concept.

As shown in Figure 4, the plug-and-play multi-physics environment in LOTUS retrieves all values of interest from output files and stores them in a more compact manner in HDF5 format. HDF5 is a data model, library, and file format for storing and managing data. It supports an unlimited variety of data types, and is designed for flexible and efficient input/output, as well as high-volume and complex data. HDF5 is portable and extensible, allowing applications to evolve in their use of HDF5. The HDF5 technology suite includes tools and applications for managing, manipulating, viewing, and analyzing data in the HDF5 format. The data are also easily accessible for use in other codes. Provided that the needed data were calculated and stored, any arbitrary codes can be added into the multi-physics integration environment in an ad-hoc manner and access previously generated data. This flexibility in storage makes the plug-and-play environment in LOTUS more compelling.

The power shapes and power history generated for each fuel rod by VERA-CS are stored within the HDF5 database and later retrieved by FRAPCON, BISON, and RELAP5-3D. The fuel performance data calculated by FRAPCON are also stored in the database, and later used by RELAP5-3D, as well as UQ and SA post processors. Lastly, the safety parameters, such as peak clad temperature (PCT) and equivalent cladding reacted (ECR) data calculated by RELAP5-3D, are stored in the database, and then supplied to the UQ and SA post processors. The RELAP5-3D calculated data are retrieved by BISON to perform more mechanistic fuel performance calculations under LBLOCA conditions. The use of the HDF5 database significantly compresses the amount of data to be stored as opposed to what would occur if all VERA-CS, FRAPCON, RELAP5-3D, and BISON files were to be stored individually. This will be essential in the MP-BEPU analysis using Monte Carlo analysis with sample sizes on the order of thousands.

It is worth noting that the codes within this work are integrated, not coupled. While some sources would consider the data flow shown in Figure 4 to be a one-way or even loose coupling, within this work, the term “coupling” indicates the feedback between the codes. Plans for future work include a tight coupling of transient fuel performance and systems analysis codes for increased fidelity in LOCA simulations.

Managing the data exchange between the different computer codes within the LOTUS framework is essential to ensure the calculations are done automatically, self-consistently, and accurately. The data exchange between different computer codes within the LOTUS framework is discussed in the sections that follow.

2.2.1 VERA-CS Data Exchange

VERA-CS creates an HDF5 database containing a variety of data for each pin and sub channel at 30 states within the depletion. The power histories are stored as a normalized axial linear heat rates for a quarter core symmetry. Note that the power histories are normalized based off the core average linear heat rate. The power histories are reported from VERA-CS as elemental averages. The burnup is reported as elemental averages for all axial elements within each fuel rod. The maximum peak clad surface temperature for each axial element is also reported, and is conservatively treated as the elemental average temperature within the LOTUS framework due to most codes (i.e. FRAPCON, RELAP5-3D) not containing full 3 dimensional fuel modeling capabilities.

The VERA-CS HDF5 database also contains TH data for each subchannel. LOTUS scripts store pin based by TH data by averaging the subchannels each rod comes into contact with. The LOTUS HDF5 database contains coolant mass flux, bulk temperature, and coolant pressure.

LOTUS scripts are designed to restructure the HDF5 file from the VERA-CS format to the LOTUS format. The LOTUS HD5 database has top level groups assigned to each assembly. Within each group are a list of all depletion states. And each state includes the power and thermal hydraulic histories as well as depletions. The pin specific data is stored as three-dimensional data sets, with the first and second indices being used for pin location within assemblies, and the third index denoting axial location.

The LOTUS database also contains core data. These include but are not limited to, the axial mesh, assembly map, average neutron fluxes, inlet temperatures, outlet pressures, critical boron concentrations, and core power. The HDF5 database also includes the geometry and compositions for all assembly types used in the design.

Within this build, no data is passed from LOTUS to VERA-CS. Future work may entail feedback from fuel performance codes such as BISON. Future developments on this integration will be directed based on the evolving needs of VERA-CS as the code continues to progress and evolve.

2.2.2 FRAPCON Data Exchange

LOTUS supplies FRAPCON with power histories extrapolated from the power histories stored from VERA-CS. FRAPCON models the relatively small domain of a single fuel rods as opposed the quarter quarter scale of VERA-CS. As such, the relevant power terms must be converted from core based metrics to rod based metrics. Specifically, FRAPCON requires the average linear rate for the pin of interest, which is obtained via Eq. 1.

$$\overline{q_{Rod}} = \frac{\sum_i^{nElem} q_i^V L_i}{L_{Rod}} \overline{q_{Core}} \tag{1}$$

where $\overline{q_{Rod}}$ is the rod averaged linear heat rate, $nElem$ is the number of elements per rod, subscript i denotes axial position, q_i^V is the element averaged based power shape data from VERA-CS, L_i is the element axial length, L_{Rod} is the rod length, and $\overline{q_{Core}}$ is the core averaged axial linear heat rate.

The power shapes are extrapolated from elemental format with VERA-CS to the nodal format used by FRAPCON input decks. Furthermore, the VERA-CS power shapes which are normalized with respect to core average linear heat rate, are renormalized with respect to rod average linear heat rate. Both of these actions are represented are in Eq. 2.

$$q_i^F = max\left(w_{i-1}q_{i-1}^V + w_i q_i^V, 0\right)\frac{\overline{q_{Core}}}{\overline{q_{Rod}}} \quad (2)$$

where w_i represents the weightings used for extrapolation, q'^N_i Note that the maximum function is put in as a safeguard to avoid nonphysical negative power peaking factors. A similar extrapolation is also performed for the coolant pressure and bulk temperatures, as these two must be supplied as nodal values.

The power and thermal hydraulic histories supplied to FRAPCON also take into account shuffling. Hence the histories of up to three separate assembly locations are inputted into a single FRAPCON case. The LOTUS data stored from are shown in Table 1. The data exchange from FRAPCON output text files to HDF5 databases is automated via LOTUS scripts.

Table 1. Stored data from a single FRAPCON case

Name of Data Stored	**Description of Data**
Average Burnup	Scalar
Average Oxide Layer Thickness	Scalar
Burnup	Dataset (nAxial)
Clad Thickness	Scalar
Fuel Centerline Temperature	Dataset (nAxial)
Gap Conductance	Dataset (nAxial)
Gap Conductance at Peak Power	Scalar
Gap Thickness	Scalar
Gas Compositions	Dataset (nSpecies)
Heat Flux	Dataset (nAxial)
Hydrogen Concentrations	Dataset (nAxial)
Inner Clad Displacement	Dataset (nAxial)
Maximum Centerline Temperature	Scalar
Outer Clad Diameter	Scalar
Outer Clad Displacement	Dataset (nAxial)
Outer Clad Temperature	Dataset (nAxial)
Outer Fuel Displacement	Dataset (nAxial)
Outer Fuel Temperature	Dataset (nAxial)
Oxide Layer Thickness	Dataset (nAxial)
Rod Internal Pressure	Scalar
Stored Rod Internal Energy	Dataset (nAxial)

LOTUS scripts are setup to pull the data from thousands of output files and store them in a single HDF5 database, reducing the necessary storage space by orders of magnitude. The hierarchal structure begins with final state names (i.e. BOC (beginning of the cycle), MOC (middle of the cycle), EOC (end of the cycle)) on top, followed by assembly groups which contain the data of Table 2 for every pin of interest (i.e. Hot, Average).

2.2.3 RELAP-3D Data Exchange

RELAP5-3D is supplied power shapes from VERA-CS and fuel performance data from FRAPCON. The RELAP3-D decks of LOTUS contain two heat structures per assembly, one representing the highest power of the pins, the hot rod, and the other heat structure representing the average of all other rods in the assembly. For each of these heat structures, the data must be mapped the 54 axial element mesh of

VERA-CS to the 6 element axial mesh of RELAP5-3D. Furthermore, RELAP3-D requires the power fraction for each fuel element and the moderation heating associated with it, as compared to the normalized axial linear heat rate of VERA-CS. This conversion for the hot rod heat structure is given in Eq. 3 and Eq. 4.

$$(\Delta Q_i/Q)_{RELAP}^{Hot,Fuel} = \frac{1-F^{DMH}}{L_{Core}}\left(\sum_{j\in i} w_{i,j} q_j^V L_j\right) \tag{3}$$

$$(\Delta Q_i/Q)_{RELAP}^{Hot,DMH} = \frac{F^{DMH}}{L_{Core}}\left(\sum_{j\in i} w_{i,j} q_j^V L_j\right) \tag{4}$$

where $(\Delta Q_i/Q)_{RELAP}^{Hot,Fuel}$ and $(\Delta Q_i/Q)_{RELAP}^{Hot,DMH}$ are the fractions of core power placed in fuel and moderator of the hot pin respectively, F^{DMH} is the fraction of power placed in direct moderator heating, L_{Core} is the cumulative length of all rods in the core ,subscripts i and j represents axial position in RELAP53-D and VERA-CS respectively, q_j^V is normalized axial linear heat rate from VERA-CS, $w_{i,j}$ is a weighting factor, and L_j is the element length.

The summations are performed over every element of VERA-CS power shapes within the much larger elements of RELAP5-3D. For elements VERA-CS elements completely encompassed by the boundaries of an arbitrary RELAP5-3D element, the weighting term ($w_{i,j}$) will be unity. For elements which are stradel elemental boundaries, the weight is assigned according to the fraction of VERA-CS element length within the RELAP3-D element. The relations for calculating the power fractions for the average heat structures are given in Eq. 5 and Eq. 6.

$$(\Delta Q_i/Q)_{RELAP}^{Avg,DMH} = \frac{1-F^{DMH}}{L_{Core}}\left(\sum_{m\neq m_{hot}}\sum_{n\neq n_{hot}}\sum_{j\in i} w_{i,j} q_{m,n,j}^V L_j\right) \tag{5}$$

$$(\Delta Q_i/Q)_{RELAP}^{Avg,DMH} = \frac{F^{DMH}}{L_{Core}}\left(\sum_{m\neq m_{hot}}\sum_{n\neq n_{hot}}\sum_{j\in i} w_{i,j} q_{m,n,j}^V L_j\right) \tag{6}$$

where $(\Delta Q_i/Q)_{RELAP}^{Avg,Fuel}$ and $(\Delta Q_i/Q)_{RELAP}^{Avg,DMH}$ are the fractions of core power placed in fuel and moderator of the average heat structure respectively, and subscripts m and n denotes row and column position within an assembly. The first and second summations in Eqs. 5 and 6 are performed over all pins in an assembly with the exception of the hot pin.

The quarter core format of VERA-CS is expanded to the full core format of RELAP5-3D. The fuel performance data transferred from the LOTUS database to the RELAP5-3D input deck is given in Table 2. The rod internal pressure, rod geometry and displacements, and rod internal pressure are all supplied as modifications to the heat structure inputs. The dependent tables, namely fuel thermal conductivity and volumetric heat capacity, as well as gap gas compositions, are input as new materials, and then referenced by the appropriate heat structure. Essentially, each heat structure has its own custom material which is a function of the average burnup of that heat structure.

Table 2. Fuel performance parameters for each assembly heat structure within RELAP5-3D

Name of Data Stored	Description of Data
Rod Internal Pressure	Scalar
Fuel Displacements	Dataset (nAxial)
Inner Cladding Displacements	Dataset (nAxial)
Initial Fuel Radius	Scalar
Initial Inner Cladding Radius	Scalar
Initial Outer Cladding Radius	Scalar
Fuel Thermal Conductivity	Temperature Dependent Table
Fuel Volumetric Thermal Capacity	Temperature Dependent Table
Gas Composition	Species Dependent Table

The RELAP5-3D output data is stored in the LOTUS HDF5 database in a manner similar to the fuel performance data storage. Each top level group corresponds to the time of LOCA within the depletion (i.e. BOC, MOC, EOC). Within each of these group are all 193 assemblies. Each assembly group contains the data shown in Table 3. The burst Boolean data indicates when a rod has burst at during the course of the LOCA. The burst matrix represents weather an axial section of clad has occurred at a given time step. The remaining terms of table serve as boundary conditions for transient fuel performance codes. The time step size, which effectively sets nTimeStep, is 0.25 seconds, which results in nTimeStep=1201 for the 300 seconds LOCA duration of this work.

Table 3. RELAP5-3D data stored in LOTUS HDF5 database

Name of Data Stored	Description of Data
Burst	Boolean
Burst Matrix	Dataset (nTimeStep,nAxial)
Coolant Pressure	Dataset (nTimeStep,nAxial)
Outer Clad Temperature	Dataset (nTimeStep,nAxial)
Power Shape	Dataset (nTimeStep,nAxial)

2.2.4 BISON Data Exchange

The BISON data exchange entails retrieving both quasi-steady state depletion data from VERA-CS and transient LOCA data from RELAP5-3D. BISON input decks are able to set boundary conditions according to comma separated value (CSV) text files. Thus the integration of BISON is performed by updating five separate CSV files given in Table 4.

The term nAllTimeStep includes of all time steps from the depletion as well as the LOCA transient. The depletion section of average linear heat rate and power peaking CSV files are informed from the VERA-CS power shapes within the LOTUS database, and take into account fuel shuffling. The transient LOCA section of said CSV files is supplied from the RELAP5-3D thermal hydraulic data within the LOTUS database, which is axially coarser, and with the exception of first state, essentially represents decay heat.

The coolant pressure and outer clad temperature are supplied in a manner similar to the power shape data. Thermal data for the quasi-steady state depletion are obtained from VERA-CS date while data from the LOCA transients is supplied from RELAP5-3D data. The neutron fast flux during the depletion is calculated from average flux data in the VERA-CS data. During the comparatively smaller timescales of the LOCA, the effects of neutron fast fluence on cladding are negligible, hence the neutron fast flux is set to zero during the transience.

In the current LOTUS framework, no data is pulled from the BISON output files. Future work will likely entail removing Boolean burst data and other fuel performance parameters such as fission gas release during transience.

Table 4. BISON CSV files updated by LOTUS database.

Name of Data Stored	Data Format
Average Axial Linear Heat Rate	nAllTimeStep
Power Peaking	nAllTimeStep,nAxial
Coolant Pressure	nAllTimeStep,nAxial
Outer Clad Temperature	nAllTimeStep,nAxial
Neutron Fast Flux	nAllTimeStep

2.3 Uncertainty Quantification and Sensitivity Analysis for Multi-Physics Best Estimate Simulations

Since uncertainties exist in the current approach to estimate and manage safety margins, significant research efforts are being made in seeking techniques to obtain more complete characterizations of analytical results. As an outcome of the implementation of updated regulations in 1988 to allow best estimate methods to be used in ECCS/LOCA analysis, the code scaling, applicability, and uncertainty (CSAU) methodology was developed and documented in NUREG-5249 [17]. Accompanying the guidance in NUREG-5249 was NRC Regulatory Guide 1.157 [18] providing best-estimate calculations of ECCS performance, which provides specific details describing acceptable best-estimate LOCA methodologies. The CSAU methodology represents a framework for deriving a quantifiable degree of assurance from a best estimate analysis tool. The CSAU framework outlines a procedure that leads from the identification and characterization of the dominant phenomena influencing the key acceptance parameter, PCT, to quantify a best-estimate of the consequences of an LBLOCA and its associated uncertainty. Additional guidance on the use of an evaluation model development and application (EMDAP) process for the usage of analytical methods and computational codes to support NPP accident and transient analysis is provided in NRC Regulatory Guide 1.203 [19].

In the conduct of this project, the CSAU methodology is extended to support multi-physics simulations to develop the MP-BEPU methodology. This is shown schematically in Figure 5 in which the MP-BEPU approach serves as a wrapper that is applied to each of the constituent single physics-based codes shown schematically in Figure 4. Regardless of the specific codes used to model the physics involved, the methodology discussed here is really a different strategy in managing the uncertainties. Critical to MP-BEPU methodology is consistent uncertainty propagation with which uncertainties are propagated directly from all the uncertain design and model parameters. The interactions between the various model parameters are directly solved within the MP-BEPU framework. This not only facilitates the automation of the process, but it is mathematically more robust as well because the advanced procedures considered to propagate uncertainties and/or perform global sensitivity and risk studies require that the sampled inputs are independent. This requirement is hard to achieve following the traditional “divide-and-conquer” approach. Note that in the current process applied for safety analyses (i.e., the sequential process described previously), the condition of independence is very difficult to achieve (and typically is either just assumed or ignored).

The philosophy used in the LOTUS framework of integrating various computer codes under one roof provides the opportunity to propagate uncertainties consistently in multi-physics simulations. The output of any code has a level of uncertainty. In cases where the frequency of code executions is limited by the hardware constraints, more computationally expensive codes are executed a limited number of times. The resultant sample size is then used to create an estimated probability density function (PDF) for outputs of interest. A large sample size is then generated from these PDFs, which can then be used by less expensive

codes. Fortunately with the large computational resources available at Idaho National Laboratory (INL), a more preferable direct connection method is possible. In this method, the data is passed directly between the codes for each instance of the sample. Essentially, the combination of the codes is treated by the UQ routines as a single code. This direct connection method is preferable as it eliminates the aforementioned multiple samplings and is more numerically accurate as PDF estimation is not required.

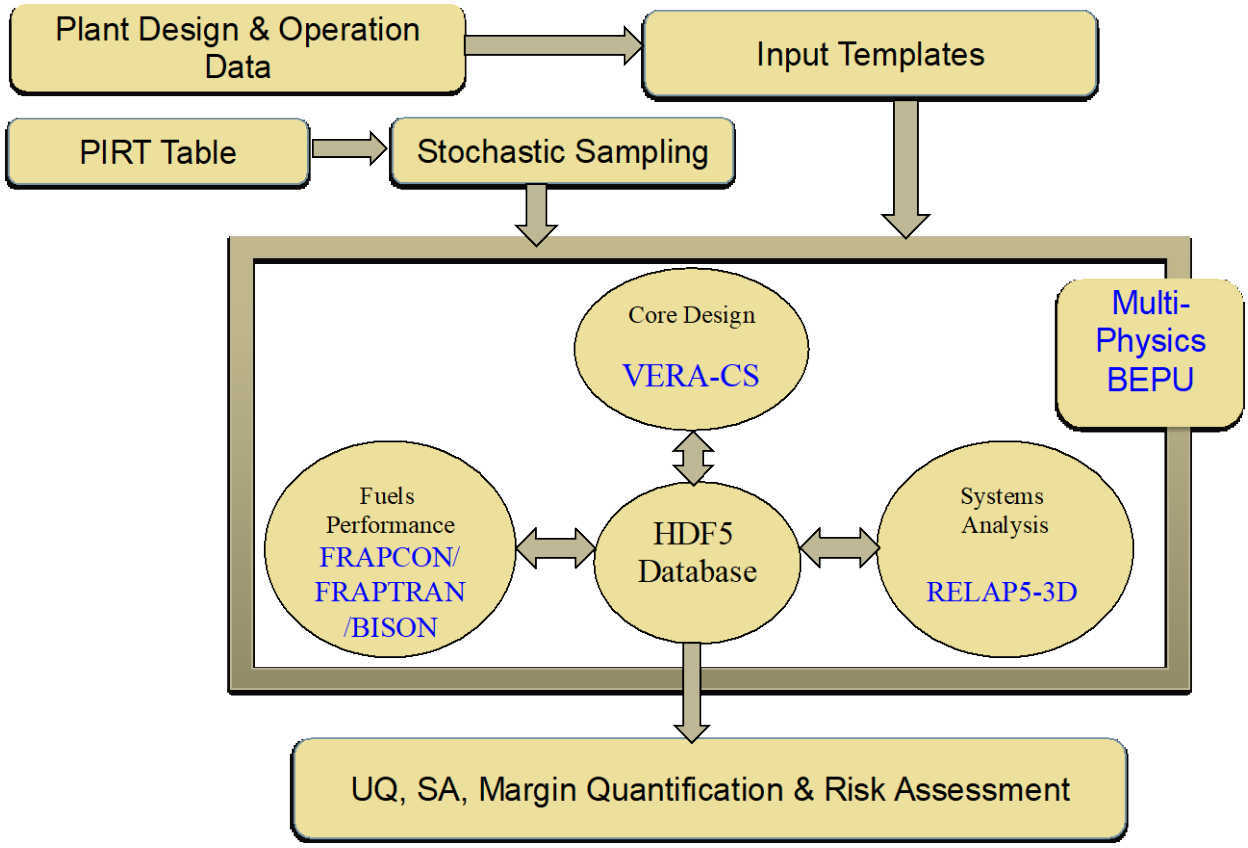

Figure 5. Notational illustration of LOTUS MP-BEPU analysis approach.

3. ANALYSIS OF NEUTRON ABSORBER SELECTION FOR REACTIVITY AND POWER PEAKING CONTROL

To extend the cycle length of current PWRs, an increase in enrichment from 5.0 w/o to 6.0 w/o will be necessary to increase the fissile loading to maintain criticality. Simply increasing the enrichment is not a viable method as the boron concentration at the beginning of life would exceed current allowable limits. To overcome this, additional neutron absorber (poison) methods can be deployed to dampen the effect of the increased enrichment. There are currently two methods used by the nuclear industry for inserting neutron poisons into a fuel assembly—integrated burnable absorbers and burnable poison rods. Typically, integrated burnable absorbers are either mixed in with the fuel or replace a fuel rod in an assembly and are a fixed part of the assembly. Burnable poison rods, on the other hand, can be placed or removed any time the assembly is accessible during the core lifetime (i.e., refueling). These two poison types have their own unique advantages and disadvantages, which will be discussed in the following subsections of this report. Both poison methods have been used extensively by the nuclear industry, which will help reduce the time for implementation and cost of developing a method. Proceeding the discussion on burnable absorbers, a section discussing the effects of each burnable absorber, and combinations of burnable absorbers, for a single assembly calculation will be given.

3.1 Integrated Burnable Absorber

For standard integrated burnable absorbers, there are two methods for adding poison to the fuel—homogenize it into the fuel matrix or coat the outside of the fuel pellets. Homogenizing the poison into the fuel involves creating an oxide out of the poison material (historically gadolinium or erbium) and replacing some w/o of the fuel with the poison. Coating the pellets involves spraying a thin layer of material (historically zirconium boride) over the entirety of the fuel pellet. Both methods add a neutron poison to the fuel to depreciate the reactivity of the pellet. After some time, the poison will be depleted and the fuel pellets will perform similarly to surrounding non-poisoned pins. Three integrated burnable absorbers are discussed in the sections that follow: (1) gadolinia; (2) erbia; and (3) integrated fuel burnable absorbers (IFBAs).

3.1.1 Gadolinia

Gadolinia (Gd_2O_3) is an oxide that can be homogenized into the fuel matrix of a typical UO_2 fuel pellet. The primary poison in the gadolinia is Gd-157 (15.65 wt% Gd), which has a thermal absorption cross-section of ~250,000 barns. Along with this, Gd-155 (14.50 wt% Gd) has an absorption cross-section of ~60,000 barns [20]. Typically, gadolinia is added to the UO_2 during the pellet production process, where it makes up between 4–10 w/o of the fuel. This reduces the mass of uranium present in the gadolinia pellets. Approximately 3–6% of the fuel pins in an assembly are gadolinia-doped pins.

Utilizing gadolinia fuel pins has a few major consequences that must be considered. Increasing the amount of gadolinia increases the complexity of the assembly design in several ways. First, the enrichment of pellets with gadolinia is decreased to reduce the power produced by the fuel pin. Power reduction in gadolinia pins is required due to a decrease in the melting point and thermal conductivity of the fuel due to the presence of gadolinia. The difference in melting points ranges from 2860°C for UO_2 to 2330°C for gadolinia. In addition, the thermal conductivity decreases by 30–60% depending on how the gadolinia is deposited into the fuel matrix [21]. To overcome this, the uranium enrichment in gadolinia pins has typically been reduced by 20–40%, depending on the w/o of gadolinia in the pin. However, if the gadolinia w/o is kept below ~ 3.0 w/o, the melting temperature and thermal conductivity of the fuel is relatively constant [22]. Second, the power shape within an assembly becomes altered due to the initial poison in the fuel matrix and the decreased enrichment. This causes the power shape to be slightly more unpredictable later on when the gadolinia has been mostly depleted. The presence of a strong neutron poison also hardens the neutron spectrum in the assembly due to the preferential absorption of thermal neutrons. In addition, the gadolinia adds a strong self-shielding effect for the fuel pins. This will decrease

the fission rate of uranium-235 and will tend to cause plutonium-239 to build in during the time when the poison is strongest, which causes the reactivity of the assembly to increase over a given time. Finally, the presence of the other gadolinium isotopes leaves a lasting reactivity effect for the life of the assembly due to their absorption's cross-sections of ~ 1-2 barns.

Gadolinia rods have historically been used in assemblies in small quantities to dampen the flux in the section of the core and to act as a poison for the first cycle the assembly is in the core. Compared to other poisons, it has one of the smallest poison rods per fuel assembly. It has been noted that utilizing gadolinia rods in the core provides a quality control for the moderator temperature coefficient during the beginning of core life. Given the small number of gadolinia rods required, the production would only require a small parallel throughput line to create gadolinia-doped fuel pins.

3.1.2 Erbia

Erbia (Er_2O_3) is an oxide, similar to gadolinia, which can be homogenized into the UO_2 fuel matrix. The primary absorber in erbia is Er-167, which has a thermal absorption cross-section of 650 barns with a resonance capture of nearly 3000 barns [20]. This is noticeably smaller than that needed for gadolinia, which can help provide a longer lasting neutron poison. For the fuel pellets, only 1-2 wt% of the fuel is erbia, which prevents the erbia from impacting the thermo-physical properties of the fuel. However, about 20–30% of the fuel pins in a poison assembly are typically erbia pins, which is a drastic increase when compared to gadolinia [23]. This does provide less-pronounced local peaking effects and an increase assembly for power sharing. Finally, erbia tends to harden the neutron spectrum, but in a less pronounced manner in comparison to gadolinia. Erbia fuel pins would require an additional throughput line with a higher throughput than the gadolinia fuel pins, due to the increase in pins required per assembly. Due to the lack of experience with Erbia pins in the U.S., they were not considered a viable option for a neutron poison.

3.1.3 Zirconium Diboride

IFBAs are typically UO_2 pellets coated in thin layers of zirconium diboride. These layers are between 0.01 and 0.02 mm thick, such that the boron-10 concentration is approximately 1.7 mg B-10/cm, where the boron-10 thermal absorption (alpha production) cross-section is around 3500 barns [20]. An IFBA rod can be axially zoned, meaning that not every pellet will receive the zirconium diboride layers, and around 60–70% of the fuel height is covered. On average, between 30–40% of the fuel pins in an assembly are IFBAs. Typically, the concentration of the boron is depleted after the first cycle in the core [23].

Since IFBAs are not homogenized into the fuel, they do not affect the thermophysical properties of the UO_2 fuel pellets. In addition, they only encompass 60–70% of the core, so there is typically a lower axial peaking factor if the zirconium diboride layers are placed on the central fuel region. Natural boron is often used for IFBAs, but enriching the boron-10 content can reduce the number of IFBAs in the assembly, which can in turn reduce the power peaking in the assembly. The major drawback to IFBAs is the high tritium/helium generation. This tends to cause both embrittlement of the cladding and increases the pressure in the plenum. Compared to gadolinia assemblies, IFBAs tend to increase cycle length and reduce power peaking at the cost of increasing the beginning of the cycle boron concentration.

IFBAs require an additional step in the fuel fabrication process; however, this step occurs after the fuel pellet has been produced. This means that a separate facility can process the fuel pellets for IFBA production and be recombined with the original pellets during the fuel loading process. Although an additional facility is required, it does not interfere with the fuel production process and can be handled as a secondary step.

3.2 Burnable Poison Rods

Unlike the integrated burnable absorbers, burnable poison rods (BPRs) are built into the assembly and can be inserted or removed whenever the assembly is accessible. BPRs are inserted into an assembly, which does not contain control rods, and placed into any of the open guide tubes in an assembly. Due to this, BPRs are modular in the sense that they can be added, moved, or removed between any cycle.

3.2.1 Wet Annular Burnable Absorbers

Wet annular burnable absorbers (WABAs) are Al_2O_3-B_4C with 14 w/o boron carbide, with an annular design clad in Zircaloy and a water-filled central region. BPRs in an assembly harden the neutron spectrum by the preferential absorption of thermal neutrons and the displacement of neutron moderators. Due in part to this, there is an increase in the amount of fissions caused by plutonium-239 when compared with assemblies without BPRs. It is also noted that the lower the enrichment, the lower the plutonium. In assemblies with higher enrichments, there is a greater amount of plutonium build up due to the excess of uranium present [24]. When the BPRs are removed, the assembly tends to have a higher worth due to an increase in the fission rate of uranium-235, which was stifled due to the BRPs. For a time after removal, higher enriched fuels (around 5 wt%) will have an increase in reactivity worth for some time before eventually decreasing. The magnitude of the reactivity change is dependent on the number of BPRs in the assembly, where increasing the number of BPRs will increase the reactivity of the assembly after it is removed. In addition, the increase in reactivity effects is linear with respect to the number of BPRs present in the assembly and the w/o of the boron [24]. Overall, the reactivity effect is typically linear with respect to poison loading.

BPRs have been used in various forms throughout the operation of NPPs. Typically, they are inserted during the first cycle to poison the fresh fuel that is being placed into the core. However, some BPRs have been left for two or three cycles depending on the core. In addition, on rare occasions, BPRs have been inserted during the second or third cycle. Since BPRs are not a part of the assembly, their production can occur at a separate facility and shipped directly to a plant. This reduces the number of steps in the fuel production process and provides a simple production path independent of fuel production.

3.3 Single Assembly Analysis

The single assembly calculations were performed with VERA-CS to determine the effect of adding the different poison options to a fuel assembly. A Westinghouse 17x17 assembly was modeled with 24 guide tubes and 1 instrumentation tube. Mirror boundary conditions were used radially, while vacuum boundary conditions were used axially. A multitude of assembly designs were created using the various poisons described in the previous two sections. In addition, two phases of single assembly calculations were performed to determine assembly designs that limited peaking and retained the ability to properly control reactivity. Phase 1 examined a wide variety of assembly designs to get a fundamental understanding of the poison. Phase 2 focused on gadolinia and gadolinia + IFBA assemblies, where the gadolinia + IFBA assemblies attempted to optimize the position of the gadolinia and the IFBAs.

To determine the effect of the poison, a few metrics were examined. The first metric was the effect on k-eff. It is known that adding various poisons can dampen the flux in an assembly and reduce the reactivity of the assembly for a time. However, it will be important to qualitatively and quantitatively understand the reactivity of the assembly as a function of burnup. Specifically, it will be important to see when a particular burnable poison burns out, and if the reactivity will rise after the absorber is gone.

The peaking effects for each assembly will also be measured to investigate how the various poisons impact the spatial neutron flux. The placement of poison pins in the assembly are heterogeneous and may cause a drastic change in local pin peaking. This change can then be accounted for and the designs adjusted as needed to limit axial peaking. These effects will be measured over two cycles (for a total of 4 years) to determine any areas that may require further analysis.

3.3.1 Single Assembly Calculations – Phase 1

For the first phase in single assembly analysis, each burnable poison (except erbia) was examined independently and in combination with each other. The enrichment was also examined at this stage to determine its effect on k-eff and the axial peaking. The results are clustered by assembly type and trends will be commented on and analyzed where appropriate. A few assumptions and design choices should be mentioned before a comparison of the results is discussed:

1. Axial blankets are the same enrichment as the standard rod in the assembly.
2. The last three steps in each burnup cycle correspond to a 'coast down' in power.
3. All neutron absorbers are only placed in the central fuel region and do not extend to the blankets.
4. Uranium enrichment in gadolinia pins was 60% of the standard pin's uranium enrichment.

3.3.1.1 Enrichment

For the enrichment, five enrichment values were examined ranging from 5.0 w/o to 6.0 w/o. The effect on k-eff can be seen in Figure 6. As the enrichment is increased, there is an overall increase in k-eff that lasts for the duration of the two cycles. The axial peaking factor for the different enrichment stays relatively constant, where there is a slight increase due to enrichment, as seen in Figure 7. The peak in the last three steps of each cycle is due to a coast down in power, which decreases the temperature and power of the assembly.

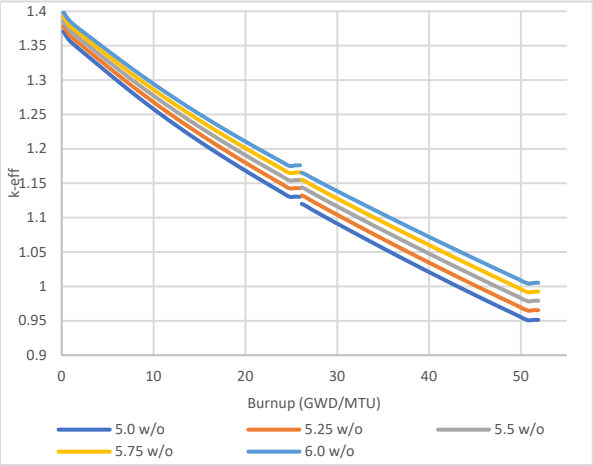

Figure 6. Effect of enrichment on k-eff.

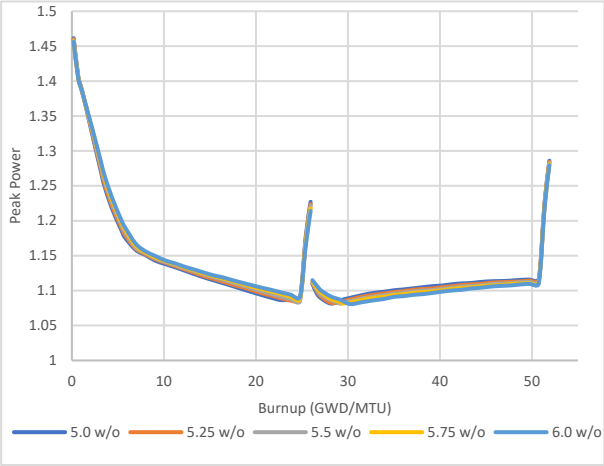

Figure 7. Effect of enrichment on axial peaking.

3.3.1.2 Gadolinia

For gadolinia, the effects of the w/o and the enrichment of the gadolinium was examined. The w/o of gadolinia was examined first, where four different w/o's between 2.5 w/o and 10.0 w/o were selected, with a standard uranium enrichment of 5.0 w/o. Figure 8 shows the effect of adding gadolinia on k-eff, where there is a noticeable decrease in k-eff due to both the addition of a strong poison and the removal of uranium in the gadolinia pins. As the w/o of gadolinia increases, both the potency and duration of the poison increase. For the 2.5 w/o, the poison is effectively gone by around 7–9 GWd/MTU; however, utilizing a 10.0 w/o can prolong the poison effects to nearly 20 GWd/MTU. Along with this, Figure 9 shows a drastic increase in the axial peaking due to the addition of gadolinia pins. This effect is due to the axial enrichment of the gadolinia pins. As noted, the uranium enrichment for all the pins was constant at 5.0 w/o, which causes a large discrepancy between the fission rate in the poison region and the axial

blankets. For the beginning of life, much of the power in the gadolinia pins is due to the blankets, which causes the extreme power peaking effects.

Once the w/o of the gadolinia was examined, the Gd-157 enrichment was examined next with a constant 7.5 w/o of gadolinia. It is noted that examining enriched Gd-157 with 7.5 w/o gadolinia is for exploratory purpose only and would not be used in practical core designs. It is used to demonstrate the potency of enriched Gd and the fact that one would need a very small concentration (<3%) to achieve the intended benefits in actual reload designs. Figure 10 shows the effect on k-eff when the enrichment of Gd-157 is increased from natural to 25 and 75 w/o. Utilizing 7.5 w/o gadolinia with 75 w/o Gd-157 causes a long-term depression of k-eff, well into the second two-year cycle. This is most likely not ideal, but does indicate the w/o of the gadolinia can be decreased to reduce the long-term poisoning of the core. Along with this, Figure 11 shows the axial peaking further increases when enriching the gadolinia due to a further depression of flux in the central region and an increase in flux in the axial blankets.

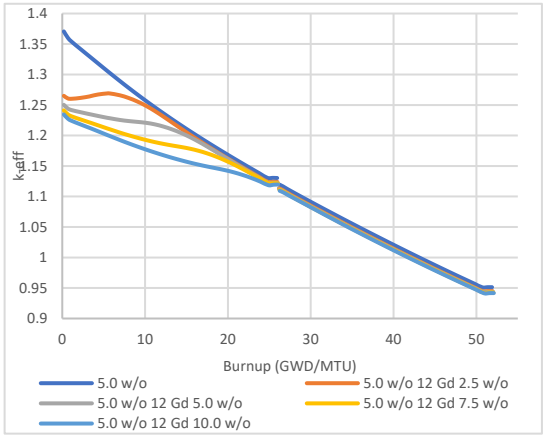

Figure 8. Effect of Gadolinia w/o on k-eff.

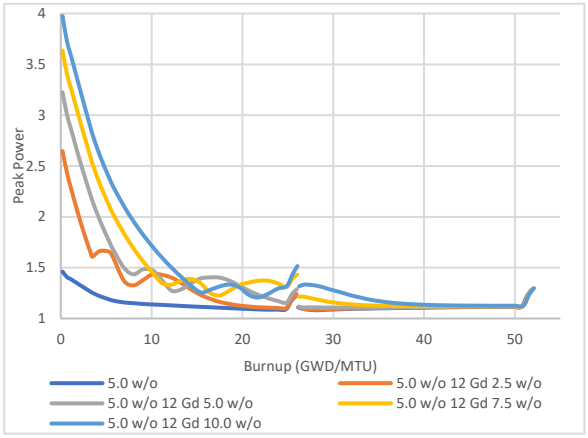

Figure 9. Effect of Gadolinia w/o on axial peaking.

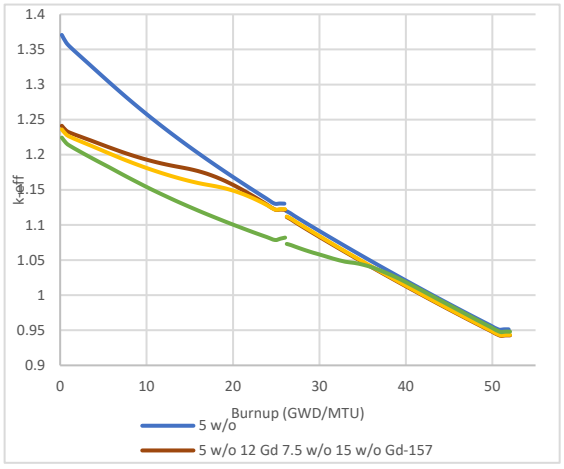

Figure 10. Effect of Gd-157 enrichment on k-eff.

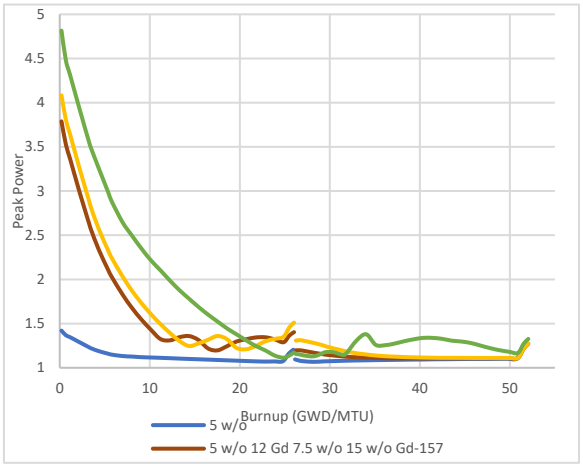

Figure 11. Effect of Gd-157 enrichment on axial peaking.

3.3.1.3 IFBA

The use of IFBAs have been investigated to help dampen the initial reactivity associated with using a higher burnup core [25]. However, to determine integral effects with IFBAs, a set number of IFBA

simulations were created to determine the impact of IFBAs required to hold down the reactivity for the core designs. These patterns would then ideally be used for the inclusion of gadolinia pins as well. For this study, four different patterns were examined to look at assemblies with approximately 50, 100, 150, and 200 IFBA pins. It should be noted that the results for the IFBAs did not utilize the power down scheme seen throughout phase 1. Instead, it maintained a constant power for the last three burnup steps in each cycle due to a slight change in assembly examination that would be carried into phase 3.

Figure 12 shows that as the number of IFBA rods increases, there is a significant decrease in the initial k-eff followed by a sharp increase in reactivity, where the more IFBAs present, the more significant the initial increase becomes. For a large number of IFBA rods, there is a region of flatter reactivity between 5 and 15/20 GWd/MTU. In addition, there is little difference in the reactivity of the assemblies after the first two-year cycle. Figure 13 shows the effect that increasing the number of IFBAs has on the axial peaking factors. As the number of IFBAs is increased, there is a noticeable increase in the initial peaking magnitude, as well as an advent of a secondary peak shortly after cycle 2. It is hypothesized that the 200 IFBA assembly provides the worst peaking due to the plethora of poisoned pins in the assembly, which pushes the power to axial blankets or to nearby non-poisoned pins thereby causing the high peaking effects. However, this assembly type does help provide a strong neutron poison, which is beneficial for the higher enriched core needed for a two-year cycle.

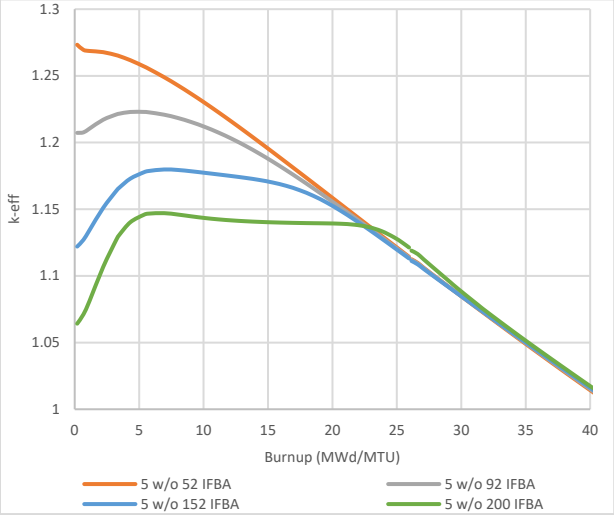

Figure 12. Effect of IFBAs on k-eff.

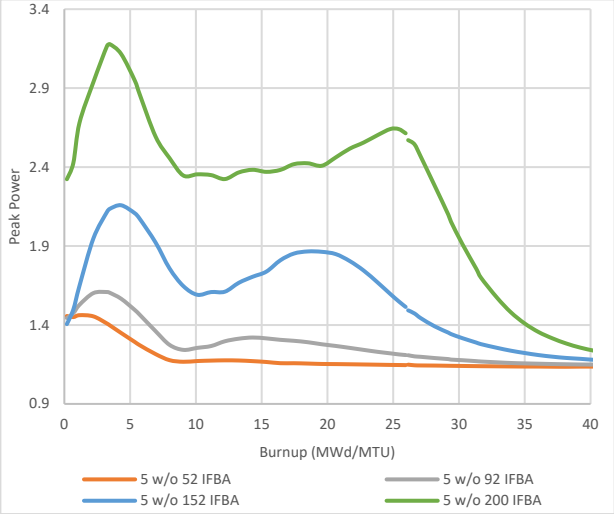

Figure 13. Effect of IFBAs on axial peaking.

3.3.1.4 BPR

The effect of utilizing BPRs was examined by inserting fresh WABAs into the same guide tubes for both cycles. The effects for k-eff can be seen in Figure 14, where about two thirds of the way through the cycle, the BPRs were effectively depleted, and the reactivity is roughly equal to the reference case. However, there is a more pronounced difference in the axial peaking between each configuration, as seen in Figure 15. Including more BPRs tends to increase the axial peaking factor near the end of the first cycle and the beginning of the second cycle. Despite the rather low axial peaking effects the BPRs had, it was determined at this point that BPRs would not be explored for further design analysis. This was because BPRs require additional tools during fuel loading and unloading, which can increase the time, cost, and complexity associated with a fuel outage. In addition, BPRs are inserted into guide tubes, which means they are not able to be placed in assemblies containing control rod drives. This would limit where BPRs can be placed and may prevent their usefulness.

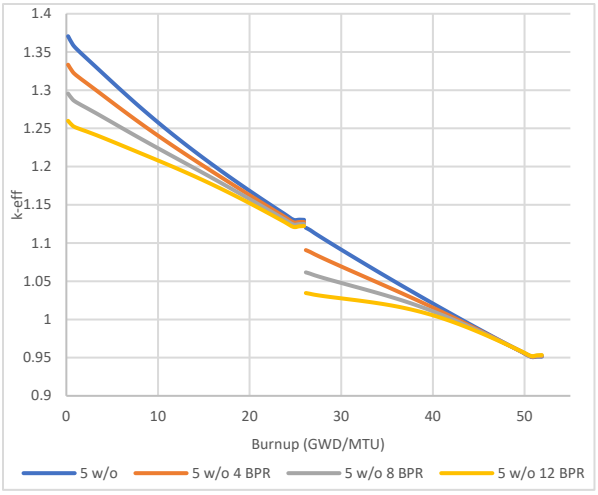

Figure 14. Effect of BRPs on k-eff.

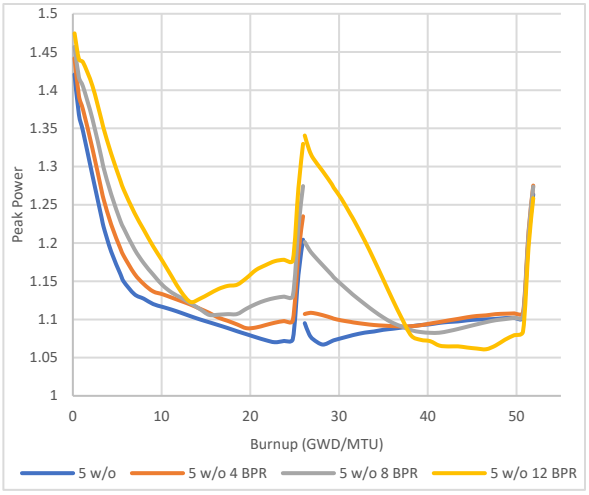

Figure 15. Effect of BPR on axial peaking.

3.3.1.5 Gadolinia + IFBA

To study the effects of using IFBAs and gadolinia in the same assembly, the two were combined with varying numbers of gadolinia and IFBAs present. Figure 16 shows the effect of using both types of poisons on k-eff, where the increase in reactivity typically associated with utilizing IFBAs has been depreciated due to the gadolinia inclusion. In addition, the return to the 5 w/o reactivity value happens closer to 20 GWd/MTU, where the reactivity of the assembly is relatively constant between 5 and 20 GWd/MTU. The IFBAs burn out quickly, around 5 to10 GWd/MTU, and subsequently add reactivity to the assembly. During this time, the gadolinia assemblies are still consuming neutrons, which keeps the reactivity roughly constant. The rate of reactivity insertion is relatively close to the gadolinia depletion, which causes the steady k-eff value. Figure 17 shows a strong degradation in the axial peaking factor from the original gadolinia or IFBA configurations. Again, this is due to the axial blankets producing a large amount of power at the beginning of life due to the gadolinia. Along with this, the addition of IFBAs pushes the flux both axially and radially to non-poisoned fuel pins. It is expected, and later proven, that adjusting the axial blankets reduces this axial peaking to levels that are more appropriate.

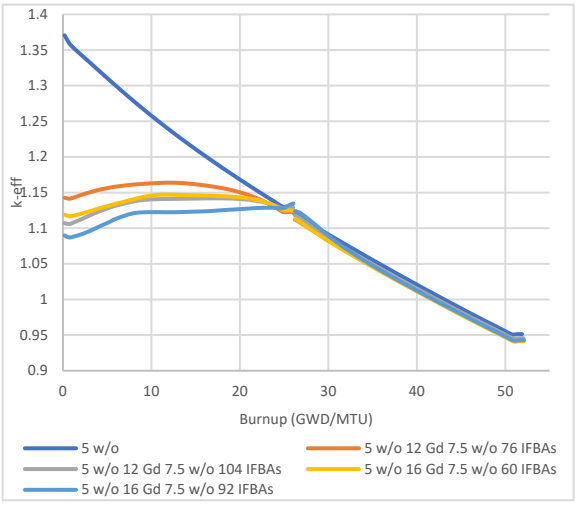

Figure 16. Effect of Gd + IFBAs on k-eff.

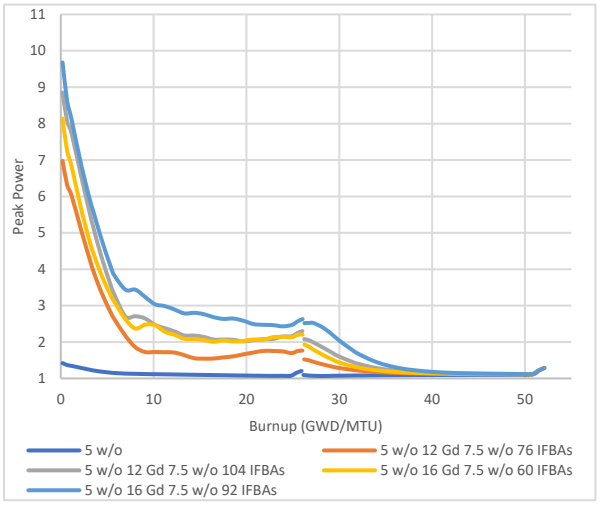

Figure 17. Effect of Gd + IFBAs on axial peaking.

3.3.1.6 Discussion

To wrap up the results from the first phase of the singe assembly study, a brief discussion on the viability of each poison type was given along with the direction for the phase. For the next phase, it was determined that a mixture of gadolinia and IFBAs would be examined. Although the gadolinia/IFBA combinations had the highest axial peaking, the root causes of the axial peaking were determined to be manageable and easily reduced. The next phase maintained the axial blankets for IFBAs and added gadolinia to the blanket for the gadolinia pins. For this combination, gadolinia will be used to reduce the initial reactivity of the assembly, while the IFBAs will be used to reduce peaking. Utilizing Gd + IFBAs is advantageous due to the different consumption rates of the two poisons. IFBAs tend to be consumed within the first 6–12 GWd/MTU, where gadolinia tends to be consumed between 10–15 GWd/MTU, depending on the number and w/o of the gadolinia. As the IFBAs burnout, the reactivity tends to increase; however, due to the inclusion of the gadolinia, this effect is dampened, and the reactivity tends to stay relatively constant during this time. This should help prevent the boron concentration from peaking during the middle of the cycle (MOC). It is the goal of the next iteration to reduce the axial peaking using different approaches and create an assembly that is semi-optimized for gadolinia and IFBA placement.

Gadolinium is meant to depreciate the reactivity of the assembly without causing a large impact on the spatial flux. This was not initially achieved with the first set of assemblies. However, it was found that increasing the Gd-157 enrichment resulted in a much longer poison life when compared to the natural gadolinia assemblies. This allows for the reduction in the w/o of gadolinia in the fuel from 7.5 w/o to 3.0 w/o. This reduction in gadolinia will increase the fuel content in the fuel by replacing the 4.5 w/o gadolinia with fuel. Along with this, by limiting the gadolinia to 3.0 w/o, the uranium enrichment of the fuel is only reduced 15.0%. The adjustment of both axial blankets and gadolinia content will hopefully help address the axial peaking concerns associated with the current design iteration, while maintaining a large poison concentration.

3.3.2 Single Assembly Calculations – Phase 2

A second phase for single assembly calculations was performed to reduce the peaking found in many of the assembly designs. For this section, some of the best assemblies from the previous section were selected and updated. In addition, new assemblies were created to reduce the initial reactivity and retain a k-eff trace similar to the 200 IFBA assembly. Along with this, another set of assumptions is presented:

1. Axial blankets gadolinia pins contain 3.0 w/o gadolinia.
2. Axial blankets for the IFBAs was 5.0 w/o for a 5.0 w/o assembly.
3. Uranium enrichment in gadolinia pins was 4.25 w/o for a standard 5.0 w/o fuel pin.
4. Gadolinia enrichment was 70 w/o Gd-157.

3.3.2.1 Gadolinia

The second phase for gadolinia consisted of examining 24, 28, and 32 gadolinia pin arrangements to find an assembly design that would have the same reactivity control of the 200 IFBA design. The respective designs can be seen in Figure 18, Figure 19, and Figure 20, while Figure 21 shows the k-eff trace for the three separate assembly designs compared to the 200 IFBA case. For k-eff, only the 32 gadolinia pin assembly has enough initial poison to maintain the reactivity; it also has a lower initial peaking factor compared to the 200 IFBA case. This comes at the consequence of a higher peaking factor near the beginning of cycle 2, as seen in Figure 22. As the number of gadolinia rods increases, the magnitude of the axial peaking factors increases, but the overall shape remains relatively constant.

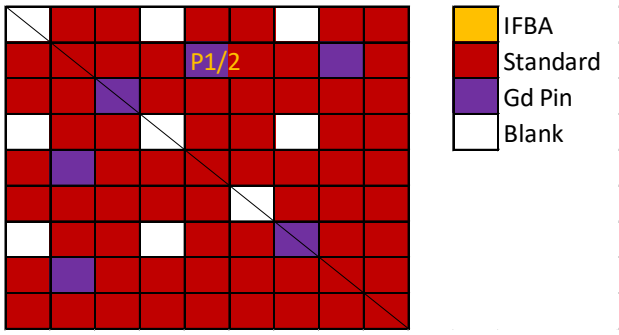

Figure 18. Assembly design for 24 Gd pins.

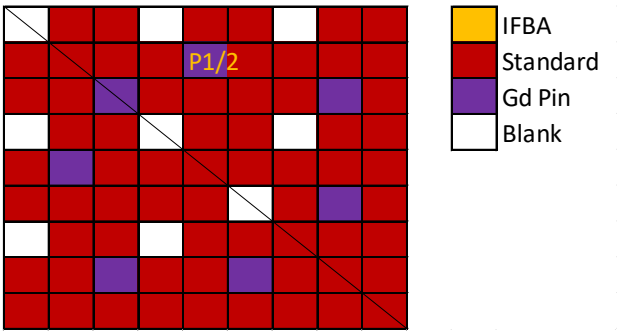

Figure 19. Assembly design for 28 Gd pins.

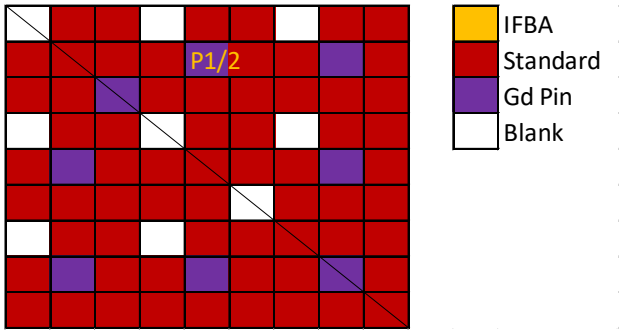

Figure 20. Assembly design for 32 Gd pins.

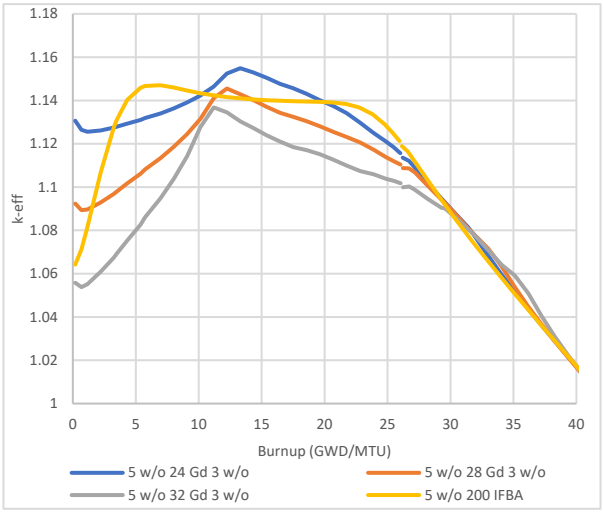

Figure 21. Effect of Gd on k-eff.

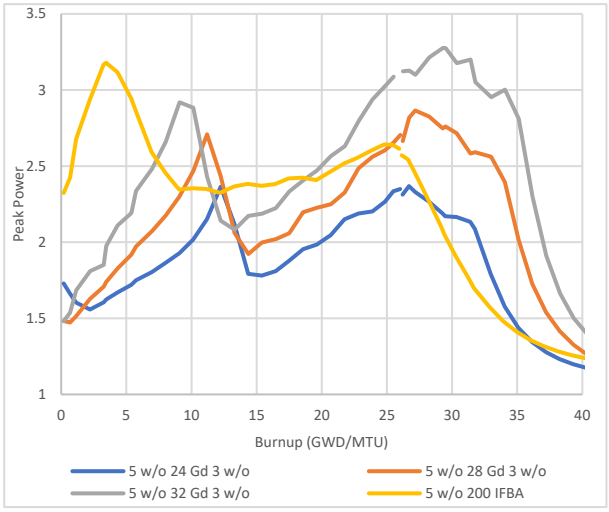

Figure 22. Effect of Gd on axial peaking.

3.3.2.2 Gadolinia + IFBA

The third phase of gadolinia and IFBA designs focused on the change in axial blanket enrichments and examining the effect on both k-eff and axial peaking. Figure 23, Figure 24, and Figure 25 show the assembly designs for the various gadolinia + IFBA assemblies, where each design utilized the 3 w/o and 2 w/o gadolinia pins in two separate cases. For the 3 w/o assemblies, Figure 26 shows the effect on k-eff where nearly all of the designs maintain reactivity below the 200 IFBA design. Only the 20 Gd + 64 IFBA design has an initial k-eff above the 200 IFBA design; however, it is still within reason. For the

axial peaking, shown in Figure 27, all of the designs have axial peaking that are either equal to or less than the 200 IFBA case, while the 20 Gd + 64 IFBA case has lower peaking for almost the entirety of the two cycles as compared to the 200 IFBA case.

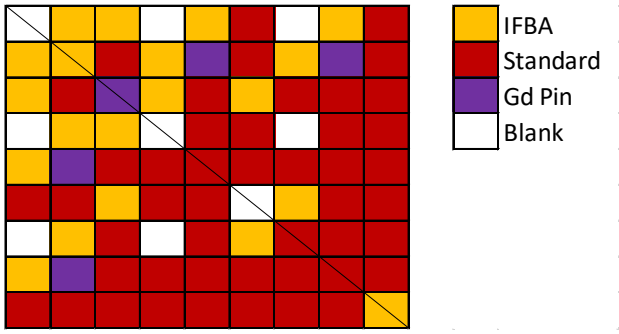

Figure 23. Assembly design for 20 Gd + 64 IFBAs.

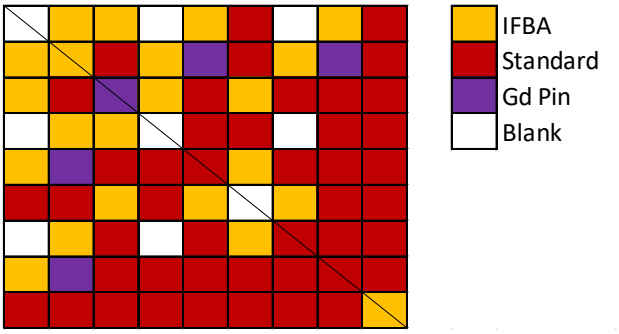

Figure 24. Assembly design for 20 Gd + 72 IFBAs.

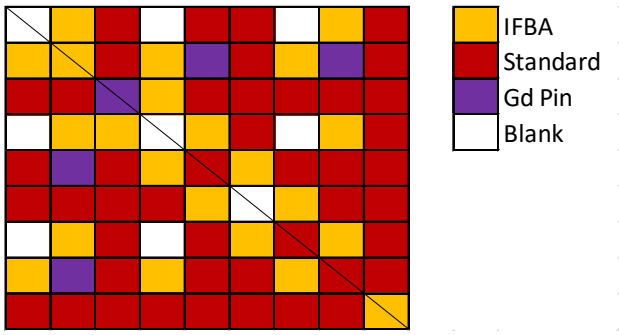

Figure 25. Assembly design for 20 Gd + 80 IFBAs.

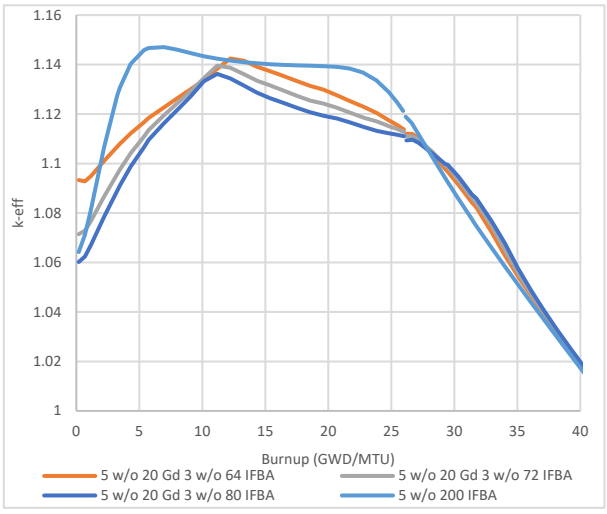

Figure 26. Effect of 3 w/o Gd + IFBA on k-eff.

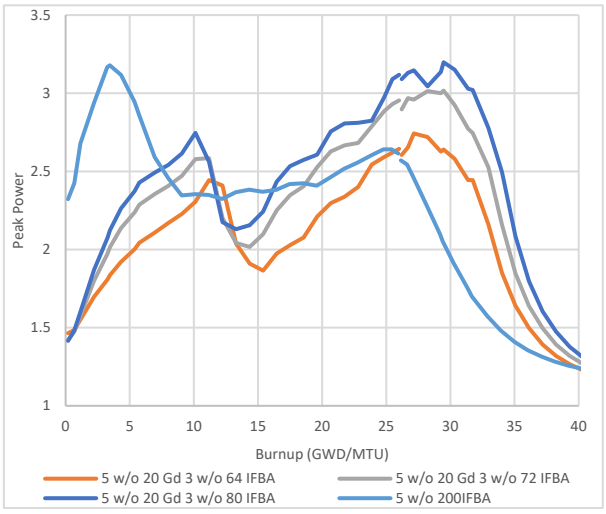

Figure 27. Effect of 3 w/o Gd + IFBA on axial peaking.

3.3.2.3 Enrichment

The last thing that was examined in phase 2 was the effect of enrichment on the axial peaking factors for the IFBA and gadolinia + IFBA assemblies. This was done by examining the IFBA and gadolinia + IFBA assemblies that would ideally dampen the initial reactivity for a full core. Figure 28 produced an unexpected result showing that the higher the enrichment of the fuel with 200 IFBAs, the lower the axial peaking factors. As the enrichment increases from 5.0 w/o to 6.0 w/o, the axial peaking goes from highly peaked at the BOL to nearly uniform throughout the cycle lengths. This trend was also examined by adding 8 gadolinia pins to the 200 IFBA assembly. These additional gadolinia pins further poisoning the initial reactivity would be used to dampen the assemblies that may peak in the core. It was found that increasing the enrichment provides a similar effect on the axial peaking, as seen in Figure 29. For the 6 w/o case, the peaking stays below 2.0, but increases up to nearly 2.5 for the 5.0 w/o case.

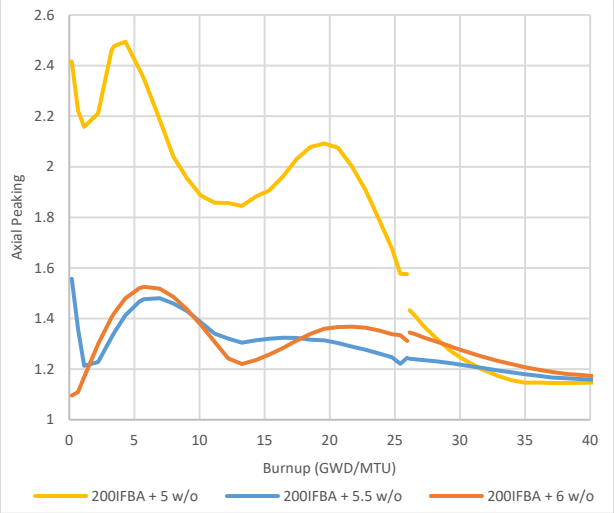

Figure 28. Effect of enrichment on 200 IFBA assembly's axial peaking.

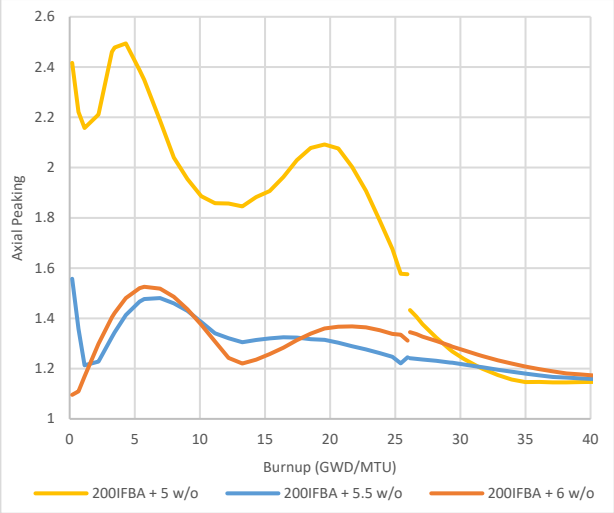

Figure 29. Effect of enrichment on 8 Gadolinia + 200 IFBA assembly's axial peaking.

3.3.2.4 Discussion

Phase 2 analysis sought to reduce the axial peaking by matching the axial blankets with their corresponding materials. This greatly reduced the BOL peaking seen throughout phase 1. In addition, an increase in the number of gadolinia rods and IFBAs could be achieved with reasonable axial peaking factors. In addition, it was found that both the gadolinia and gadolinia + IFBAs can be utilized to create a k-eff trace, which nearly mirrors the 200 IFBA case.

Another important factor that was examined was the effect of enrichment on axial peaking. The enrichment has a large effect on the peaking factors for assemblies with both IFBAs and gadolinia + IFBAs. This was quantified by examining the axial peaking shape for the six different assemblies throughout the first cycle and can be seen in Figure 30, Figure 31, Figure 32, Figure 33, Figure 34, and Figure 35, respectively, where the 6 w/o pin has a relatively stable axial profile throughout the entirety of the cycle, as it transitions from a flat profile to a central peak, and finally an axial peaked pin. Throughout the cycle, the entire axial length of the pin contributes to the overall power. This trend starts to decay with the 5.5 w/o assembly, and the 5 w/o pin has a completely different axial power profile throughout the cycle length. For the 5 w/o assembly, the power peaking is severe and starts off peaked near the bottom and transitions to the top of the pin throughout the cycle, where the non-power producing portion of the pin is consistently lower. These axial trends help quantify the results from Figure 28 and Figure 29, as to why the axial peaking was so much stronger for the 5 w/o fuel than the 6 w/o fuel. The current hypothesis

is that the 6 w/o fuel has enough excess fissile material that the central region can continue to produce power, even in the presence of a poison. This implies that the 5 w/o fuel pushes the power to specific region of the assembly where the poison is not present and to continually burn though the IFBA. As this happens, it tends to severely deplete each region that causes the power profile to act as a wave towards the top of the assembly.

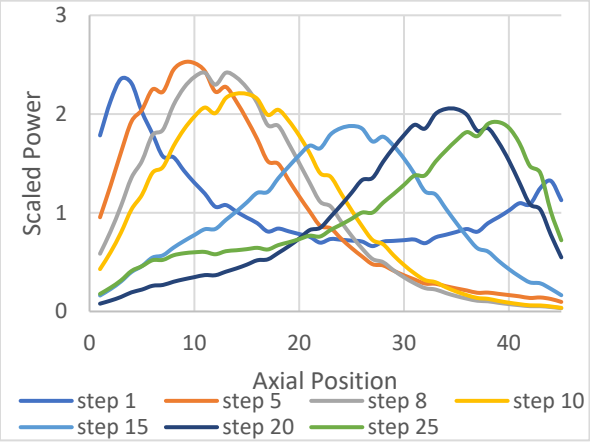

Figure 30. Axial profile for 5 w/o 200 IFBA.

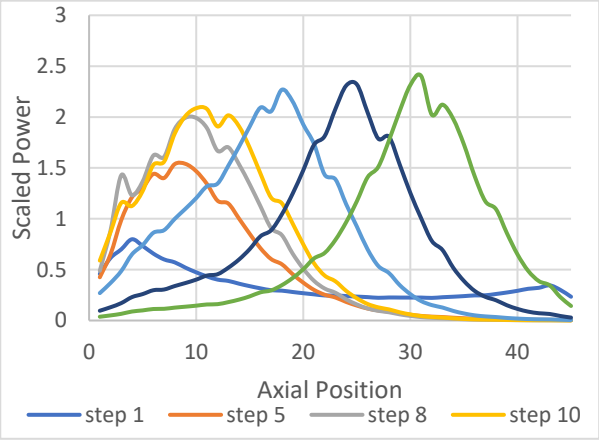

Figure 31. Axial profile for 5 w/o 200 IFBA + 8 Gd.

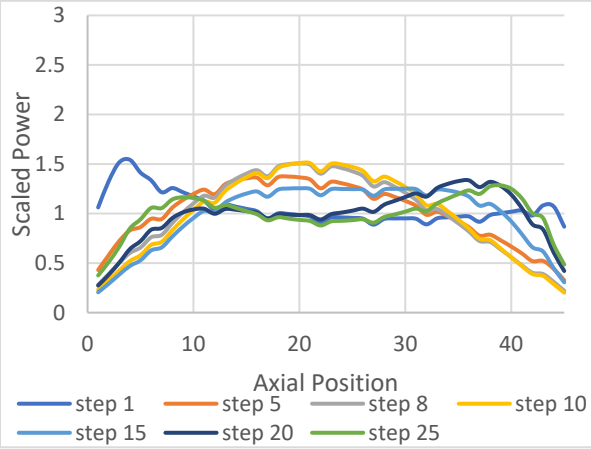

Figure 32. Axial profile for 5.5 w/o 200 IFBA.

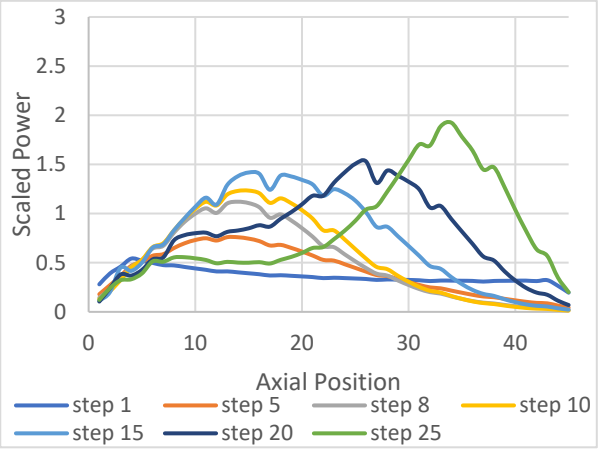

Figure 33. Axial profile for 5.5 w/o 200 IFBA + 8 Gd.

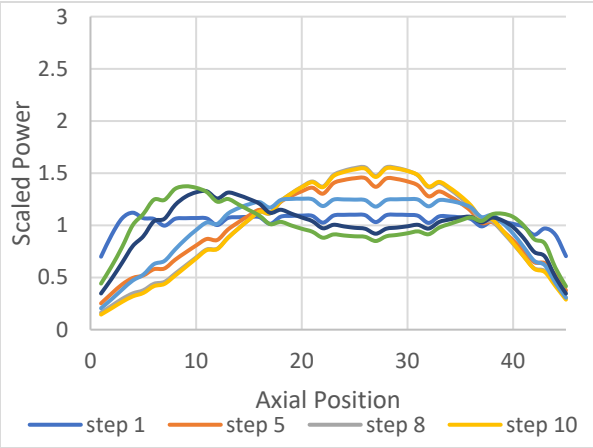

Figure 34. Axial profile for 6 w/o 200 IFBA.

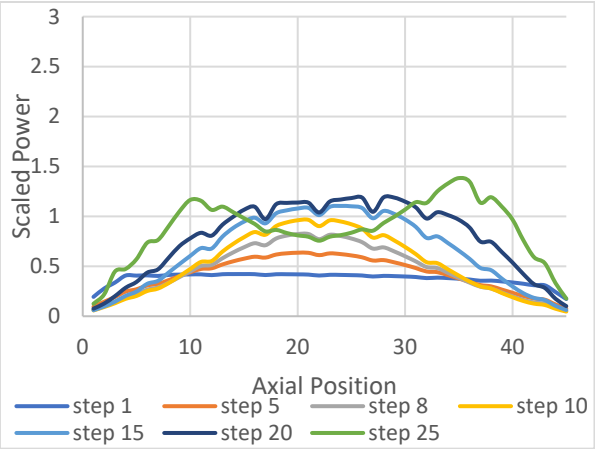

Figure 35. Axial profile for 6 w/o 200 IFBA + 8 Gd.

3.3.3 Recommendations for Assembly Designs

The purpose of this section is to provide a tool to select an assembly design that could then be placed into a full reactor model and limit axial peaking, while simultaneously providing enough reactivity dampening to maintain appropriate boron concentrations. Full core calculation results are not expected to provide a one-to-one comparison for axial peaking. Despite this, the single assembly analysis provides a useful insight into how the neutron poisons behave during a two-year cycle length. It was found that peaking factors are highly dependent on the surrounding assemblies, which indicate that the single assembly estimates of axial peaking are unrealistic. Due to this, it is recommended to examine single assembly designs for their poison loading and attempt to match the k-eff profile with a known assembly that provides adequate reactivity dampening for a full core. This process can help core designers examine various gadolinia/IFBA configurations to find optimal amounts of each. Utilizing the single assembly process, the number of full core models that need to be created and run can be reduced by examining the k-eff trace for a variety of single assemblies to find an assembly that provides adequate poisoning. This assembly can then be placed into the full core model to determine its peaking factors without needing to concentrate on the core reactivity.

This process has also produced a few viable assembly designs that are useful for full core analysis and will be combined in later sections to generate full core designs. The first is utilizing the 200 IFBA assemblies with 5.0 w/o and 6.0 w/o fuel. This provides nearly enough poison to maintain the two-year cycle length and the boron concentration limits. Along with this, it was found that adding 8 gadolinia pins to a 200 IFBA assembly provides enough reactivity suppression at the beginning of life required to maintain a boron concentration below 1700 pcm at hot zero power. It was determined that these two assembly types would be used for the core design options described in Section 4. These assemblies were also found to have the best axial peaking results when the axial blanket fuel for gadolinia pins matched the fuel for the gadolinia pins. This led to all the axial blankets maintaining a fuel composition that was identical to the fuel pin it was surrounding.

Other designs that could be promising include utilizing 20 gadolinia pins and 80 IFBAs; however, they were not explored in this work and may be examined later as an appropriate alternative to reduce the number of IFBAs present. In addition, it appears that utilizing 32 gadolinia pins without any IFBAs would provide the needed reactivity dampening, but may cause extreme peaking when applied to full core design due to the vast difference in power generation between the gadolinia pins and the standard pins.

4. 24-MONTHS CYCLE PWR CORE DESIGN WITH INCREASED ENRICHMENT AND BURNUP EXTENSION

PWRs are the most common type of nuclear reactors and account for two-thirds of the currently installed nuclear generating capacity in the U.S. and worldwide. A PWR core uses normal water as both a moderator and primary coolant, which is kept under considerable pressure (about 15 MPa) by the pressurizer in order to obtain a relatively high boiling point, and its temperature rises about 30°C after its upward passage past the fuel. The fuel used in U.S. PWRs are built with open cage square lattice arrangement assemblies, which are mechanically identical to each other. The fuel assemblies are normally characterized by the number of rods they contain, typically 15x15, 16x16, and 17x17 in current designs. A PWR fuel assembly stands between four and five meters high and is about 20 cm across and weighs about half a ton [26]. Each assembly has vacant rod positions or guide thimbles that are spaced to the left for the vertical insertion of control rods with a space designated as an instrumentation guide thimble into which a neutron source rod, specific instrumentation, or a test fuel segment can be placed. For example, for an assembly with a 17x17 fuel rod array, it typically consists of 264 fuel rods, 24 guide thimble tubes for control rods, and 1 instrumentation guide thimble. The instrumentation guide thimble is located in the center position. The absorber rod guide thimbles provide channels for the insertion of a rod control cluster assembly (RCCA). The RCCAs or control rods, as shown in Figure 36 [27], provide a rapid means for reactivity control during both normal operating and accident conditions. The absorber material used in the control rods is a silver-indium-cadmium (AgIn-Cd) alloy. The AgIn-Cd alloy is in the form of extruded rods, which are sealed in stainless steel tubes to prevent the poisoning material from coming in direct contact with the coolant.

Figure 36. PWR rod control cluster assembly (RCCA).

Fuel rods provide no structural function for the fuel assembly, which are supported by the top and bottom nozzles, the dimples on the grid spacers, and the control rod guide thimbles. The bottom and top nozzles are heavily constructed as they provide much of the mechanical support for the fuel assembly structure. A typical large PWR core may contain 193 fuel assemblies composed of over 50,000 fuel rods. A nuclear fuel assembly stays in the core for several years depending on the design of the operating cycle. Most PWRs in the U.S. are still operating on 18-month cycles, while the fuel discharge burnup is constrained by the current licensing limit of 62 GWd/MTU. During refueling, usually one third of the fuel

in the core is removed to the spent fuel storage pool, while the remainder is shuffled to a location in the core better suited to its remaining level of enrichment. The objective of our core design activities is to extend the cycle length from the current 18 months to 24 months. In our design, the discharge burnup is extended to the proposed new limit of 75 GWd/MTU, while the enrichment is increased to the proposed new limit of 6 w/o. It is noted that most BWRs in the U.S. are already operating on the cycle length of 24 months.

This section presents the simulation results performed by using CASL's VERA-CS for the generic PWR model based on the South Texas Project (STP). The STP is a Westinghouse design PWR with a 4-loop nuclear steam supply system (NSSS), which has a rated thermal power of 3853 MWth and 193 assemblies in the core with a 17x17 design. Among all the core design and analysis tools available, the VERA-CS tool has the highest fidelity and is the choice of the code in this work.

4.1 VERA-CS

VERA-CS stands for Virtual Environment for Reactor Applications – Core Simulator, which couples MPACT for neutron transport, COBRA-TF for subchannel thermal hydraulics, and ORIGEN for isotropic depletions. VERA-CS was developed by the Consortium for Advanced Simulation of Light Water Reactors (CASL), which is a DOE energy innovation hub. VERA-CS includes coupled neutronics, thermal-hydraulics, and fuel temperature components with an isotopic depletion capability. The neutronics capability is based on MPACT [28], a three-dimensional (3-D) whole core transport code. The thermal-hydraulics and fuel temperature models are provided by the COBRA-TF (CTF) subchannel code [29]. The isotopic depletion is performed using the ORIGEN [30] code system.

4.1.1 MPACT

As stated in the MPACT Theory Manual [28], MPACT is a 3-D whole core transport code that is capable of generating subpin-level power distributions. This is accomplished by solving an integral form of the Boltzmann transport equation for the heterogeneous reactor problem in which the detailed geometrical configuration of fuel components, such as the pellet and cladding, is explicitly retained. The cross-section data needed for the neutron transport calculation are obtained directly from a multi-group cross-section library, which has traditionally been used by lattice physics codes to generate few-group homogenized cross-sections for nodal core simulators. Hence, MPACT involves neither *a priori* homogenization nor group condensation to achieve the full core spatial solution.

The integral transport solution is obtained using the method of characteristics, and employs discrete ray tracing within each fuel pin. MPACT provides a 3-D method of characteristics solution; however, for practical reactor applications, the direct application of method of characteristics to 3-D core configuration requires considerable amounts of memory and computing time associated with the large number of rays. Therefore, an alternative approximate 3-D solution method is implemented in MPACT for practical full core calculations, based on a "2-D/1-D" method in which MOC solutions are performed for each radial plane and the axial solution is performed using a lower-order 1-D diffusion or SP3 approximation. The core is divided into several planes, each on the order of 5 to 10 cm thick, and the planar solution is obtained for each plane using 2-D method of characteristics. The axial solution is obtained for each pin, while the planar and axial problems are coupled through transverse leakage. The use of a lower order 1-D solution, which is most often the nodal expansion method with the diffusion or P3 approximation, is justified by the fact that most heterogeneity in the core occurs in the radial direction rather than the axial direction. Alternatively, a full 3-D method of characteristics solution can be performed, if necessary, should the computational resources be available.

The Coarse Mesh Finite Difference (CMFD) acceleration method, which was originally introduced to improve the efficiency of the nodal diffusion method, is used in MPACT for the acceleration of the whole core transport calculation. The basic mesh in the CMFD formulation is a pin cell, which is much coarser than the flat source regions defined for the method of characteristics calculations. (Typically, there are

approximately 50 flat source regions in each fuel pin.) The concept of dynamic homogenization of group constants for the pin cell is the basis for the effectiveness of the CMFD formulation to accelerate whole core transport calculations. The intra-cell flux distribution determined from the method of characteristics calculation is used to generate the homogenized cell constants, while the method of characteristics cell surface-averaged currents are used to determine the radial nodal coupling coefficients. The equivalence formalism makes it possible to generate the same transport solution with CMFD as the one obtained with the method of characteristics calculation. In addition to the acceleration aspect of the CMFD formulation, it provides the framework for the 3-D calculation in which the global 3-D neutron balance is performed through the use of the method of characteristics generated cell constants, radial coupling coefficients, and the nodal expansion method-generated axial coupling coefficients.

In the simulation of depletion, MPACT can utilize the ORIGEN code, which is included in the SCALE [31] package. However, MPACT has its own internal depletion model, which is based closely on ORIGEN, with a reduced isotope library and number of isotopes. The internal depletion model will be used in the Use Case applications where MPACT is applied.

4.1.2 COBRA-TF

Coolant Boiling in Rod Arrays – Two Fluid (COBRA-TF or CTF) [29] is a transient subchannel code based on the two-fluid formulation, in which the conservation equations of mass, energy, and momentum are solved for three fields, namely the vapor phase, continuous liquid, and entrained liquid droplets. The conservation equations for the three fields and for heat transfer from and within the fuel rods are solved using a semi-implicit finite-difference numerical scheme, with closure equations and physical models to account for interfacial mass transfer, interfacial drag forces, interfacial and wall heat transfer, inter-channel mixing, entrainment, and thermodynamic properties. The code is applicable to calculate various flow and heat transfer regimes beyond critical heat flux (CHF), and is capable of calculating reverse flow, counter flow, and crossflow with either 3-D Cartesian or subchannel coordinates for thermal-hydraulic or heat transfer solutions. It allows for full 3-D LWR core modeling and has been used extensively for LWR LOCA and non-LOCA analyses, including the departure from nucleate boiling (DNB) analysis.

The CTF code was originally developed by the Pacific Northwest National Laboratory (PNNL) and has been updated over the last few decades by several organizations. CTF is being further improved as part of the VERA multi-physics software package as part of the CASL DOE Modeling and Simulation Hub. These enhancements include:

- Improvements to user-friendliness of the code through the creation of a preprocessor utility
- Code maintenance, including source version tracking, bug fixes, and transition to modern Fortran
- Incorporation of an automated build and testing system using CMake/CTest/Tribits [32]
- Addition of new code outputs for better data accessibility and simulation visualization
- Extensive source code optimizations and full parallelization of the code, enabling fast simulation of full core subchannel models
- Improvements to closure models, including the Thom boiling heat transfer model, the Yao-Hochreiter-Leech grid-heat-transfer enhancement model, and the Tong factor for the W-3 CHF correlation
- Addition of a consistent set of steam tables from the IAPWS-97 standard [33]
- Application of an extensive automated code regression test suite to prevent code regression during development activities
- Code validation study with experimental data.

In a steady-state or transient CTF simulation subchannel data, such as flow rate, temperature, enthalpy, pressure, and fuel rod temperatures are projected onto a user-specified or pre-processor generated mesh and written to files in a format suitable for visualization. The freely available Paraview [34] software is used for visualizing the 3-D data resulting from large, full core models and calculations.

4.2 Input Data for Core Design Calculations

To develop the VERA-CS input models based on the STP core design, publicly available data from the STP Final Safety Analysis Report (FSAR), Rev. 18 [35], has been used. Data that is not publicly available in the FSAR has either been taken from another public source [36] or assumed according to best engineering judgment. The main parameters used in the core design are shown in Table 5. The reactor core has 193 fuel assemblies with a 17x17 fuel rod design using UO_2 fuel and ZIRLO cladding material in each assembly. Table 5 shows the core characteristics assembled from the STP FSAR with the exception of the batch sizes and cycle length. Currently, the STP units are operating at 18-month cycles. In this work, the cycle length is extended to 24-months. Table 6 shows the assembly parameters. A cross-sectional view of the assembly design is shown in Figure 37. It's a 17x17 assembly with 264 fuel rods and 25 non-fuel locations. All non-fuel locations are guide or instrument tubes. The number of IFBA rods, as shown in Figure 37, used in this work is 200. IFBA fuel pellets refer to the UO_2 fuel pellets coated with thin layers of zirconium diboride (ZrB2). ZrB2's daughter products—helium and lithium—are essentially transparent to neutrons. The absorption rate of ZrB2 is closely matched to the fuel's reactivity depletion, so no residual penalties result. To prolong the cycle length of a reactor core, it is desirable to initially load an excess of reactivity into the reactor core and, at the same time, use IFBAs for the reactivity to be maintained relatively constant throughout core life. IFBA material has high neutron absorption during the initial period of operation and then its neutron absorption ability is reduced through transformation during the later period of operation.

Table 5. Core characteristics for the generic PWR based on STP.

Core Parameter Name	Core Perimeter Values
Rated Power (MW)	3853
Heat Deposited in Fuel	97.4%
Number of Assemblies	193
Active Core Height	168 in (426.72 cm)
Effective Rated Flow (kg/s)	16745
Cycle Length (EFPD)	690
Inlet Temperature (°C)	291.667
Outlet Pressure (MPa)	15.513
Number of Fresh Assemblies	80
Number of Once-Burned Assemblies	81
Number of Twice-Burned Assemblies	32

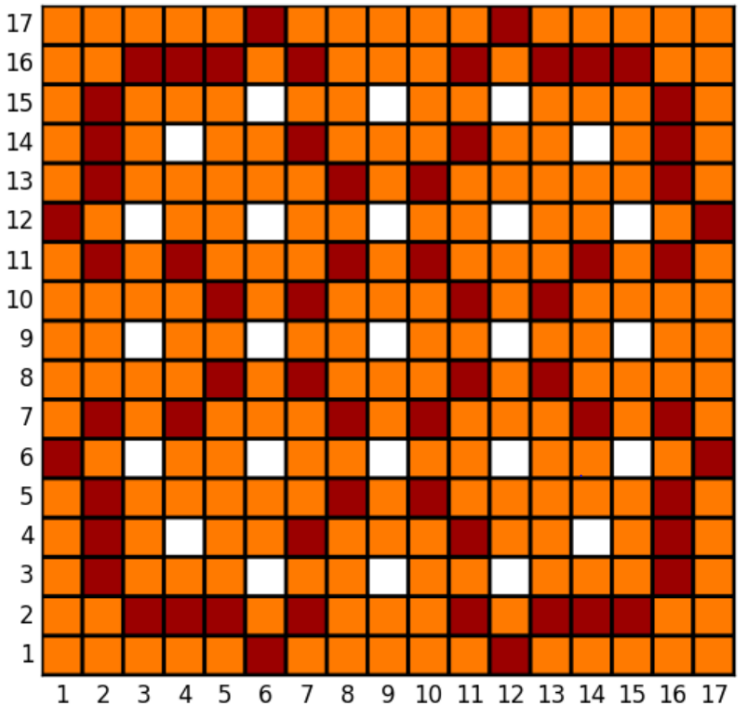

Figure 37. Assembly design; the orange color indicates IFBA rods, while the burgundy color indicates standard fuel rods.

Table 6. Assembly parameters.

Fuel Assembly Characteristics	Fuel Assembly Parameter Values
Active Fuel Length (m/ft)	4.267/14
Number of Fuel Rods per Assembly	264
Rod Array	17 x 17
Rod Pitch	0.496in (1.25984 cm)
Grids per assembly	11
Axial Blankets	Top/bottom using annular pellets
Annular Pellet Length in Assembly	8 in (20.32 cm) top/bottom
Assembly Pitch	8.466 in (21.50364 cm)
Lattice Cell Pitch	8.426 in (21.40204 cm)
Assembly Water Gap	0.04 in (0.1016 cm)
Number of IFBA rods	200

The fuel rod parameters are shown in Table 7 and Figure 38 illustrates the fuel rod design. The cross-sectional view and axial schematic of a fuel rod are shown in Figure 38. The fuel rods contain a low enriched zone at the top and bottom. Neither the geometrical data nor the enrichment is available for the low enriched annular pins forming the blanket at the top and bottom of the fuel pin. It has been assumed that the annular pellets are solid. The enrichment has been adjusted to 3.2% according to the original enrichment value indicated in [35]. The IFBA coating does not extend to the blanket regions (i.e., the burnable absorber is only sprayed on the high-enriched part of the fuel rods).

Table 7. Fuel rod parameters.

Number of IFBA Rods	200
Fuel Pellet Radius (cm)	0.4096
Cladding Thickness (cm)	0.05715
Cladding Outer Radius (cm)	0.475
Gap Thickness (cm)	0.008255
IFBA Loading	1.57 mg/inch B-10
Cladding Material	ZIRLO™
Fuel Material	Uranium Dioxide
Fuel Density (g/cm^3)	10.3828
Instrument Tube Wall Thickness (mm)	0.508
Inner Annulus Radius (cm)	0.1948
Guide Tube Inner Radius (cm)	0.572
Guide Tube Outer Radius (cm)	0.612
Number of Guide Tubes per Assembly	25
Grid Spacer Material	ZIRLO™ (mid)/74.44% Inconel and 24.56% ZIRLO™ (end)
Number of Grid Spacers	8 (mid)/2(end)
Grid Spacer Heights	3.81 cm (mid)/3.866 cm (end)
Middle Spacer Grid Loss Coefficient	0.97 (mid)/0.75 (end)
Initial Enrichment (w/o)	5.0 (5.4) and 6.0
Initial Blanket Enrichment (w/o)	3.2
IFBA B-10 Linear Concentration (mg/cm)	0.618
Number of IFBA Rods	200

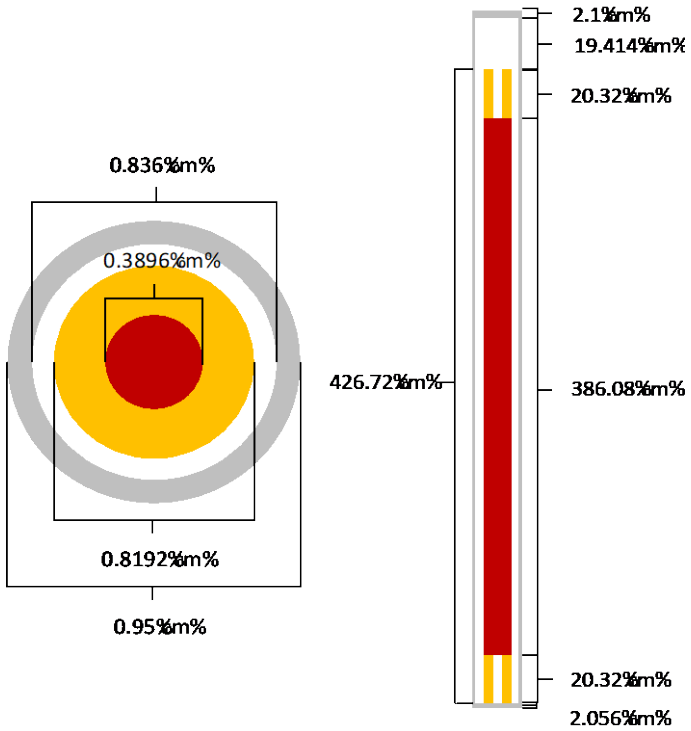

Figure 38. Illustration of fuel rod design, the left figure shows a cross-sectional view of the fuel rod design and the right figure shows the vertical view of the fuel rod design.

Core design is performed for this generic 4-loop Westinghouse PWR design based on STP with increased enrichment limit up to 6 w/o to achieve a 24-months cycle and a maximum rod average discharge burnup of approximately 75 GWd/MTU. The rated thermal power and mass flow for the core are 3853 WMth and 16745 kg/s, respectively. The core inlet temperature is 291.667°C and the core outlet pressure is 15.513 MPa. The VERA-CS code is used to provide pin-resolved power distributions for the core design.

The following sections summarize the 24-month core design evolutions done in FY-2019. There are five variants of core design options presented. These core design options are documented here to help future core designers on lessons learned and to avoid pitfalls on their practical core design activities with burnup extension.

4.3 Core Design Option 1 – Loading with 5.4% and 6% Enrichment Fuel

In this design option, a batch size of 80 fresh assemblies is considered with 40 assemblies loaded with 5.4% enrichment and 40 assemblies with 6% enrichment. The 5.4% assemblies are loaded in the interior region of the core and along the one row in from the periphery. The 6% assemblies are loaded in the outer region of the core. All of the fuel rods have the blanket regions with 3.2% enrichment at the top and bottom with 20.32 cm length respectively. The core loading pattern is shown in Figure 39.

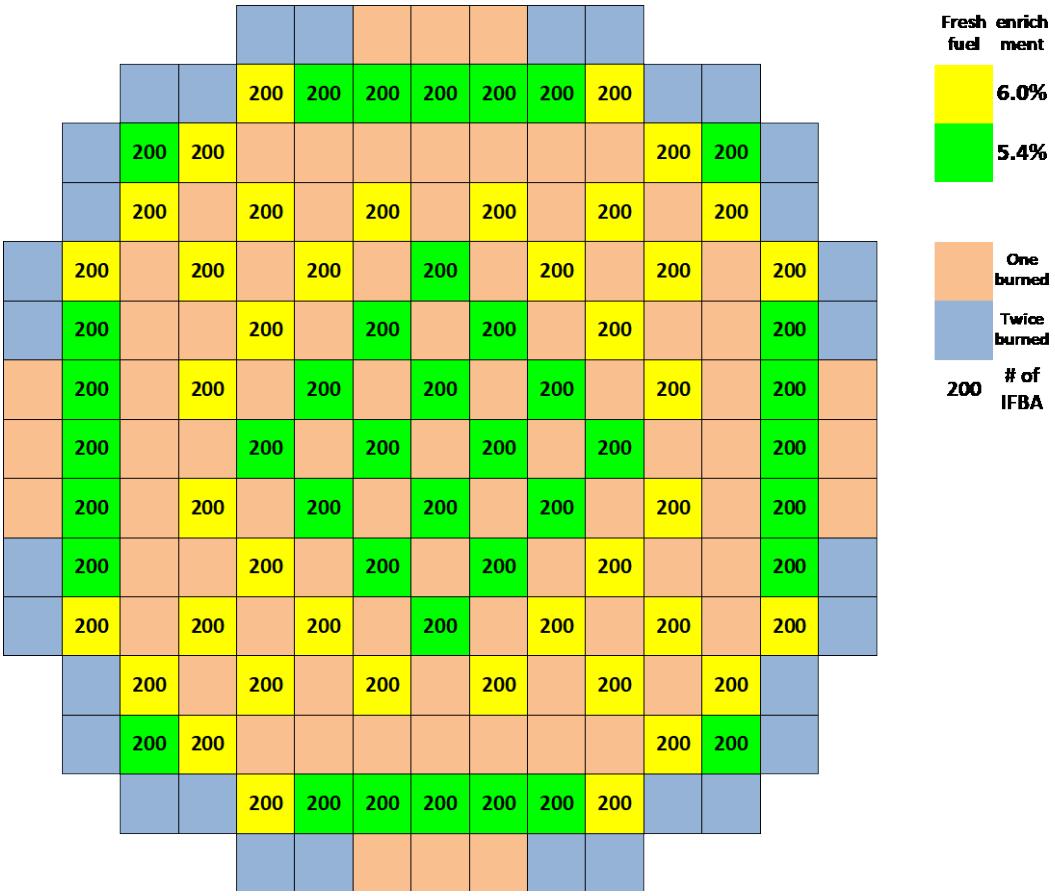

Figure 39. Core loading pattern for Core Design Option 1.

In order to speed up the calculation time, VERA-CS calculations for the cycle depletion were performed with quarter core symmetry. The calculations were carried out on INL's high performance computing cluster, FALCON, with 975 processors. In order to decrease the length of transience to the

equilibrium cycle, the so-called “jump-in” scheme is used with which the depletion calculations were first done for single fuel assemblies and the calculated results were put into the calculations as the initial conditions for the once-burned and twice-burned fuel in the quarter core cycle depletion calculations. The “jump-in” allows for quasi-equilibrium to be reached in a fewer number of cycles. The quasi-equilibrium cycle is normally achieved with five to seven cycles of depletion calculations with the same shuffling scheme and loading pattern. It normally takes about 24 hours for one cycle to complete and about one week to complete the entire equilibrium cycle calculations. An equilibrium cycle is defined as a steady-state loading pattern with a fixed number of fresh fuel, feed enrichment, inventory of the burnable poison, and fuel reloading between two consecutive cycles. So the core characteristics such as discharge burnup and cycle length do not change cycle by cycle (i.e., these characteristics are identical in every cycle). The equilibrium cycle can be attained through the repetition of cycle burnup calculations assuming identical fuel reloading throughout consecutive cycles. In practical NPP operations, fuel assemblies are loaded in-core during several cycles and the fuel loading pattern in each cycle depends on that of the previous cycle; furthermore, the reactor operating period is not the same in each cycle, therefore the loading pattern is different in every cycle. However, with the absence of plant specific and cycle specific analyses, an equilibrium cycle can be considered as a typical core. Analyses of the equilibrium cycle are useful for evaluating economics and/or safety of the newly designed fuel assemblies, such as those used here.

In order to keep the reactor critical during the cycle, the critical boron search option was used in the VERA-CS calculations to find the proper boron concentration in the moderator. Figure 40 shows the critical boron concentration letdown curve found for the equilibrium cycle. It can be seen that in the BOC, the critical boron concentration is slightly above 1500 parts per million (ppm). The boron concentration goes up to close to 1800 ppm, due to the plutonium build-up in the core, before it decreases until the end of the cycle (EOC) at about 690 days. Figure 41 shows the thermal-hydraulic quantities F_q (1st row), F_Δh (2nd row) and the radial assembly power peaking factors (P_bar) (3rd row) at Peak (burnup state with the maximum F_q value in the cycle). Peak normally happens when the IFBAs are burnt out.

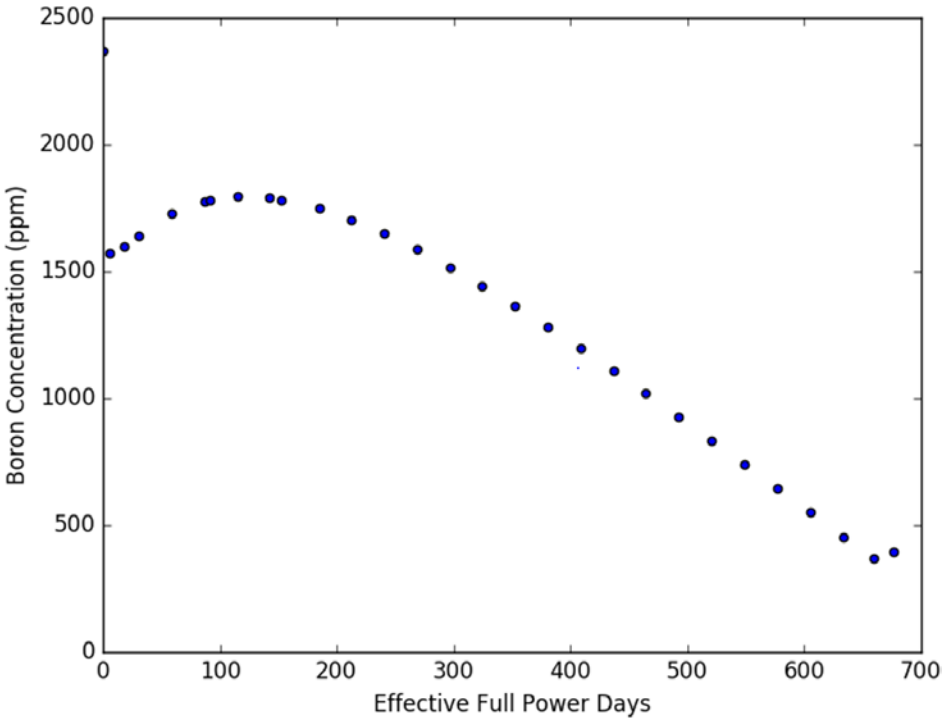

Figure 40. Critical boron concentration in ppm during the equilibrium cycle for Core Design Option 1.

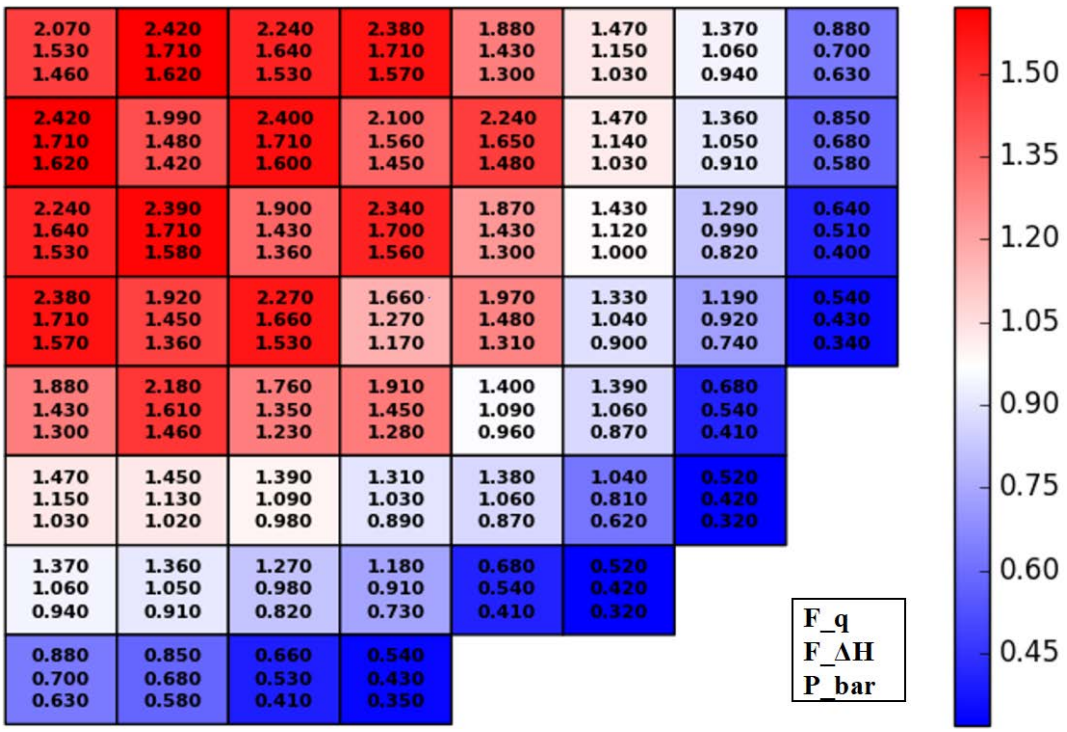

Figure 41. Peaking factors for the equilibrium cycle at Peak for Core Design Option 1.

F_q, the heat flux hot channel factor, is defined as the ratio of the linear heat generation rate at an elevation over the average linear heat generation in the core [37]. Limiting F_q would ensure that the peak power density does not exceed its limit and that the peak cladding temperature after a LOCA will not exceed 2200°F. F_Δh, the enthalpy rise hot channel factor, is defined as the ratio of maximum integrated rod power over the average integrated rod power [37]. F_Δh is used to ensure that DNB will not occur. Since the highest peaking factors happen near BOC, only the peaking factors at BOC are shown. Figure 41 shows that the high peaking region happens in the interior region of the core. Future improvements will investigate ways to reduce the peaking in the interior region to flatten out the power distribution in the core.

The burnup distributions at the EOC are shown in Figure 42. The first row shows the maximum local burnup value in an assembly. The second row shows the maximum rod averaged burnup value in an assembly. The third row shows the assembly averaged burnup value. It can be seen from Figure 42 that the maximum rod averaged burnup achieved for this equilibrium core design is 74.18 GWd/MTU and is close to the target discharge burnup of 75 GWd/MTU. The maximum rod averaged burnup happened in a twice-burned assembly loaded on the periphery. Table 8 provides a summary of the peaking factors and burnup values at the BOC, MOC, and EOC of the equilibrium cycle. The maximum F_q value is 2.424 at the BOC and is much higher than the normal values used in a practical core design. Table 9 provides a summary of the critical boron concentration, maximum offset, and moderator temperature coefficient (MTC) values.

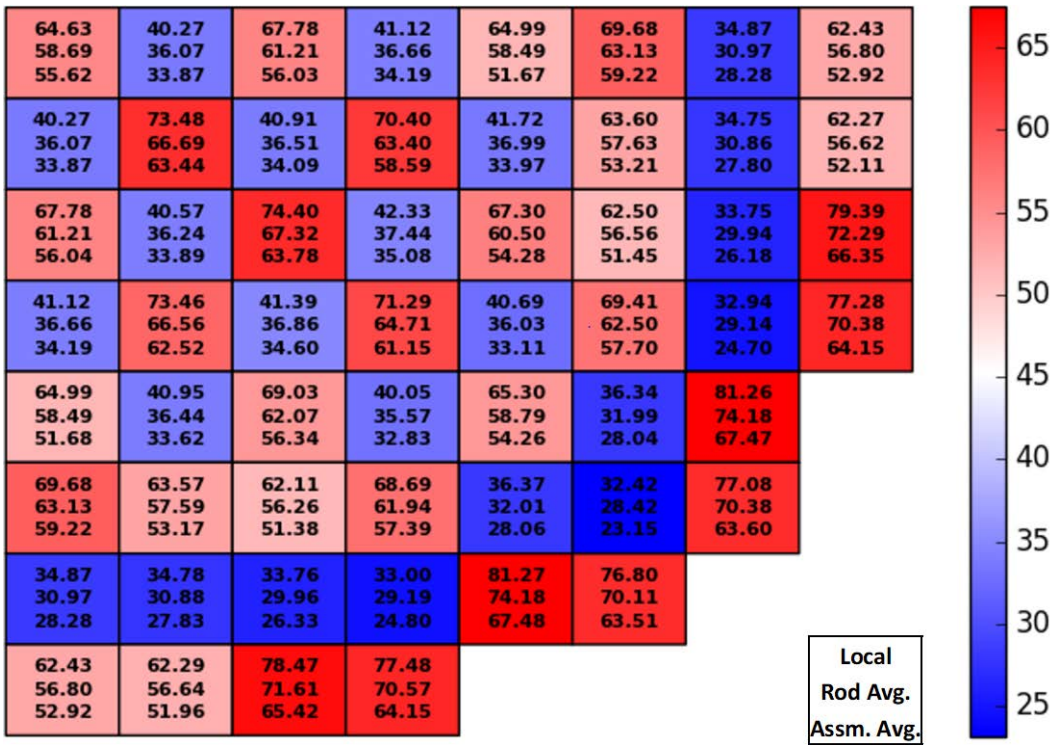

Figure 42. Burnup distribution for the equilibrium cycle at the EOC for Core Design Option 1 (first row local, second row rod averaged, and third row assembly averaged).

Table 8. Summary of peaking factors and burnup values for Core Design Option 1.

	PEAK	MOC	EOC
P_bar	1.618	1.360	1.286
F_ΔH	1.714	1.452	1.413
F_q	2.420	1.765	1.715
Radial assembly burnup (GWd/MTU)	53.21	59.26	67.48
Radial pin burnup (GWd/MTU)	58.49	64.83	74.18
Peak burnup (GWd/MTU)	64.98	71.65	81.27

Table 9. The critical boron concentration, axial offset, and MTC values for Core Design Option 1.

Critical boron concentration at hot zero power	2371.15 ppm
Peak critical boron concentration at full power	1794.77 ppm
Maximum axial offset	15.52%
Moderator temperature coefficient	-2.499 pcm

4.4 Core Design Option 2 – Loading with 5% and 6% Enrichment Fuel

Recognizing the high peaking factors calculated from Option 1 and the high critical boron concentrations required to suppress the excess reactivity, the core design in Option 1 needs some de-toning to lead to less excess reactivity. In this design variation, Core Design Option 2, all of the assemblies with 5.4% enrichment, as shown in Figure 39, are replaced with 5.0% assemblies. All of the other parameters stay the same as those in Core Design Option 1. The same ‘jump-in’ scheme was used in

the VERA-CS calculations to speed-up the attainment of the equilibrium cycle, which is achieved after five cycles of repetitive loading and shuffling schemes. The fuel assembly loading pattern for Core Design Option 2 is shown in Figure 43. As what has been observed from Core Design Option 1, the highest peaking factors occurred at BOC for this core design option. The peaking factor distributions for BOC of the equilibrium cycle are shown in Figure 44. The burnup distribution at the EOC of the equilibrium cycle are shown in Figure 45. Table 10 provides a summary of the peaking factors and burnup values at BOC, MOC, and EOC of the equilibrium cycle. Table 11 provides a summary of the critical boron concentration and axial offset values. The maximum rod averaged burnup value calculated for the equilibrium cycle is 72.99 GWD/MTU, which is less than the target value of 75 GWD/MTU. The critical boron concentration letdown curve is shown in Figure 46. Compared to Core Design Option 1, the peaking factors in this core design option stayed about the same, while the critical boron concentration reduced slightly. These results indicate that more improvements are needed to reduce the power peaking in the reactor core.

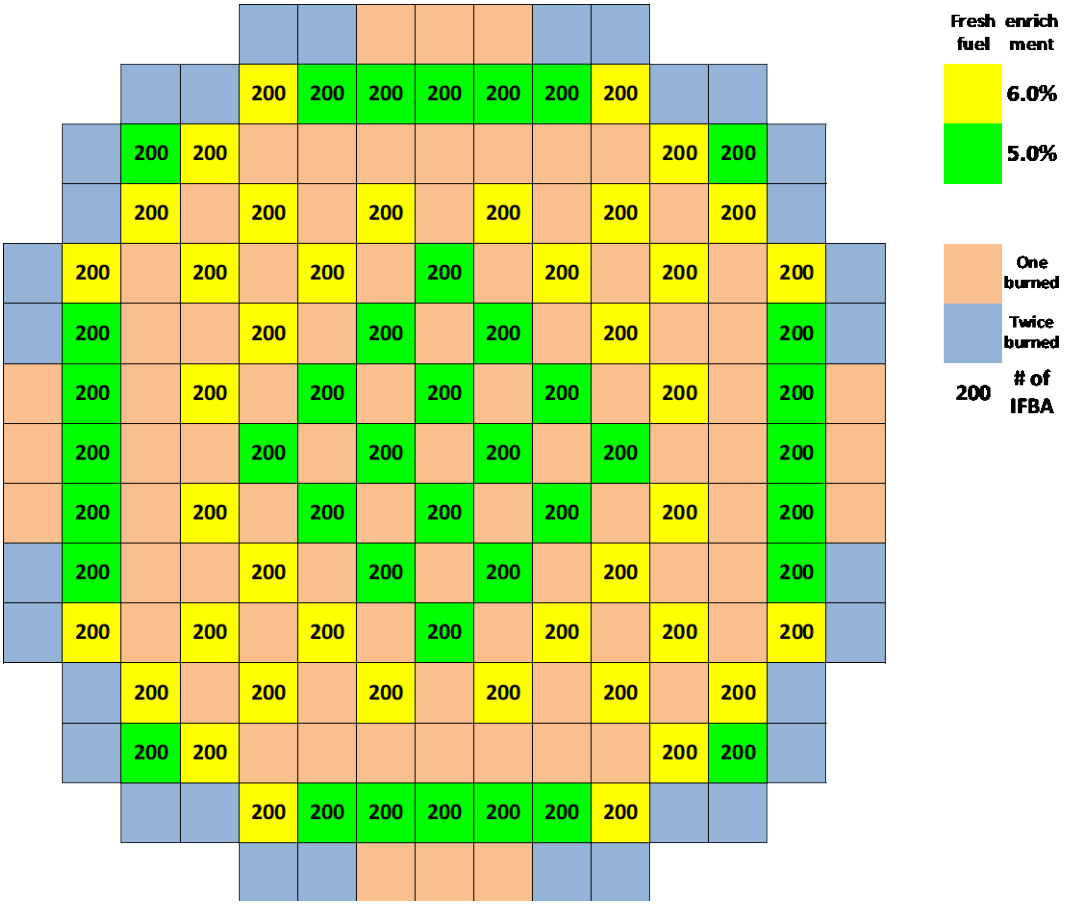

Figure 43. Core loading pattern for Core Design Option 2.

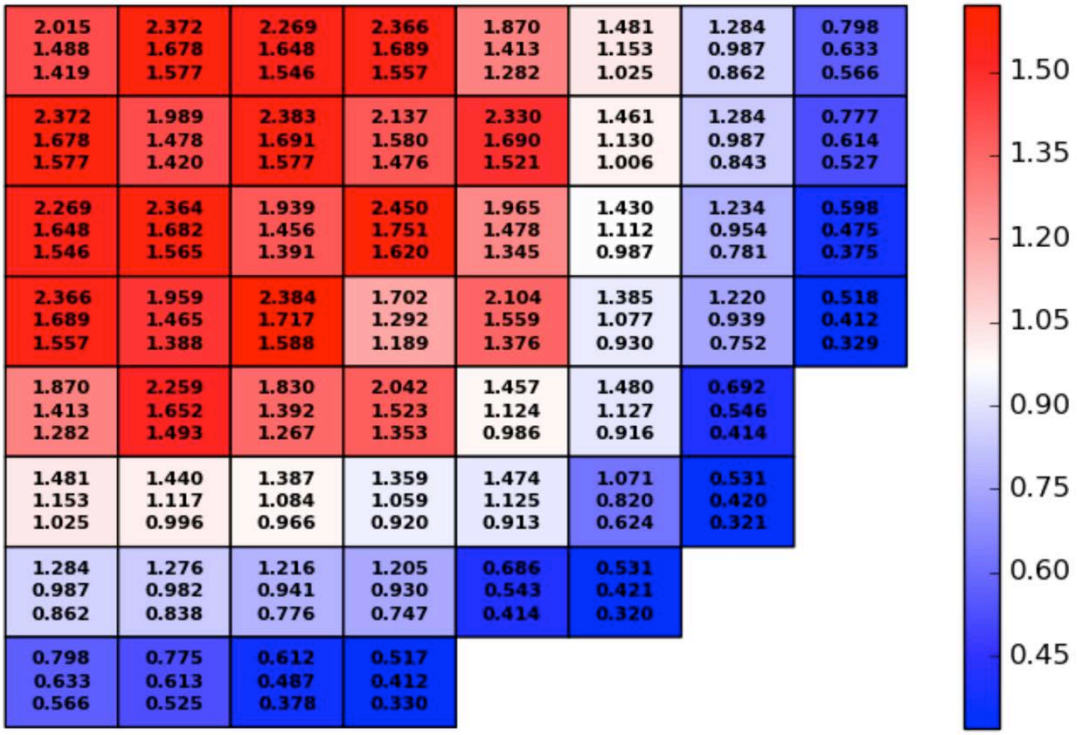

Figure 44. Peaking factors for the equilibrium cycle at Peak for Core Design Option 2 (first row F_q, second row F_ΔH and third row P_bar).

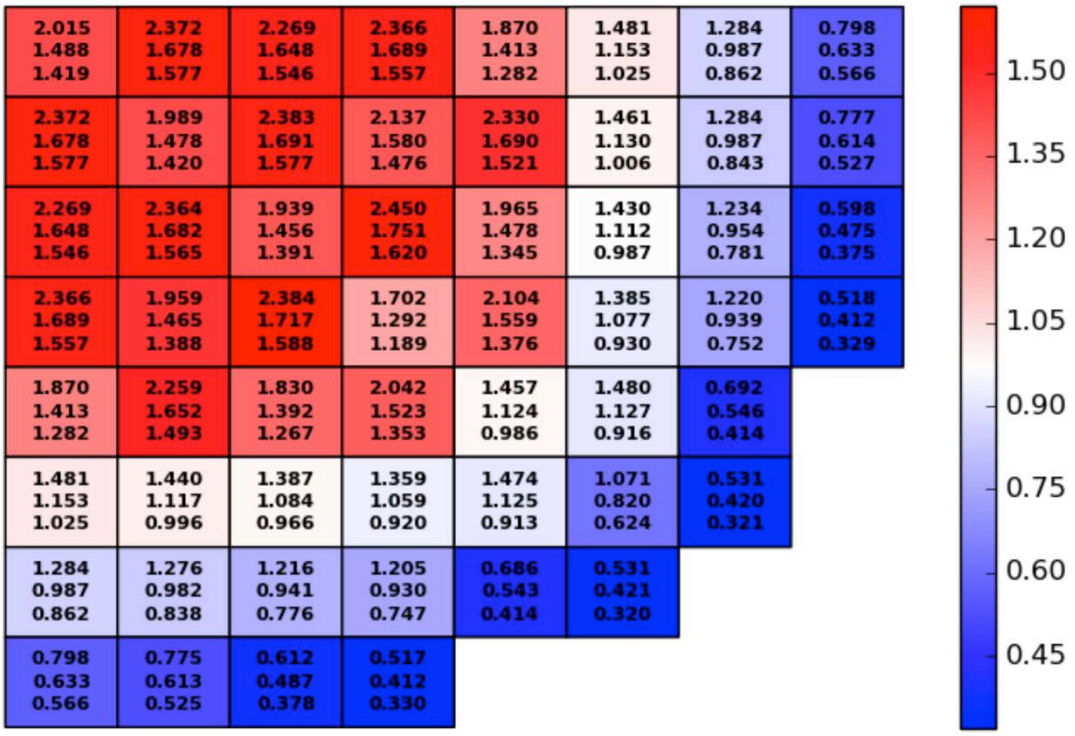

Figure 45. Burnup distribution for the equilibrium cycle at EOC for Core Design Option 2(first row local, second row rod averaged and third row assembly averaged).

Table 10. Summary of peaking factors and burnup values for Core Design Option 2.

	PEAK	MOC	EOC
P_bar	1.620	1.396	1.289
F_ΔH	1.751	1.488	1.405
F_q	2.450	1.840	1.724
Radial assembly burnup (GWd/MTU)	53.33	57.96	66.16
Radial pin burnup (GWd/MTU)	59.40	63.62	72.99
Peak burnup (GWd/MTU)	65.68	70.02	79.69

Table 11. The critical boron concentration and axial offset values for Core Design Option 2.

Critical boron concentration at hot zero power	2160.41 ppm
Peak critical boron concentration at full power	1605.32 ppm
Maximum axial offset	18.20%

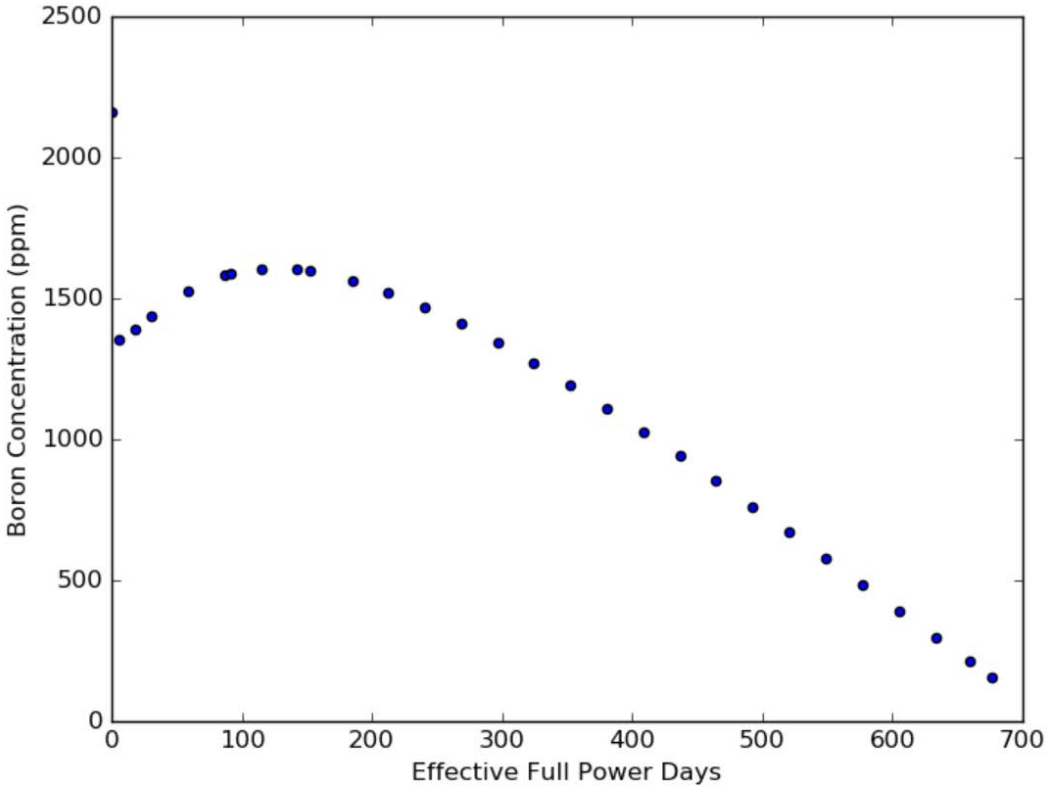

Figure 46. Critical boron concentration in ppm for the equilibrium cycle for Core Design Option 2.

4.5 Core Design Option 3 – Loading with 5% and 6% Enrichment Assemblies and no Reduction of Enrichment in the Blanket Regions

As stated in prior subsections, compared to the results obtained from Core Design Option 2 to those from Core Design Option 1, the peaking factors did not change very much. This indicates there is a higher probability of fuel failure for the high power fuel rods during LBLOCA conditions for those two core design options. Consequently, other innovative design features and concepts should be considered in order to lower the core peaking factors. In both of the Option 1 and Option 2 designs, the upper and lower annular blanket regions of the fuel rods have reduced enrichment compared to that of the solid middle

region. This type of design increases axial peaking factors. After discussions with the core design group at Xcel Energy Electric Services Company, it was suggested to use the same enrichment for the blanket regions as that of the solid region of the fuel rods. In this design variation, Core Design Option 3, the enrichment for the blanket regions is increased to be the same as that in the solid region of a fuel rod. With the higher enrichment in the blanket regions of the fuel rods, more fuel is loaded into the reactor core as compared to that in Core Design Option 2. In this core design option, a fewer number of assemblies with 6% enrichment is loaded in the core. The total number of fresh assemblies is still 80, the same as in Options 1 and 2. However, the number of fresh assemblies with 6% enrichment is reduced to 24, while the number of fresh assemblies with 5% enrichment is increased to 56. The assembly loading pattern in the core for this design option is shown in Figure 47.

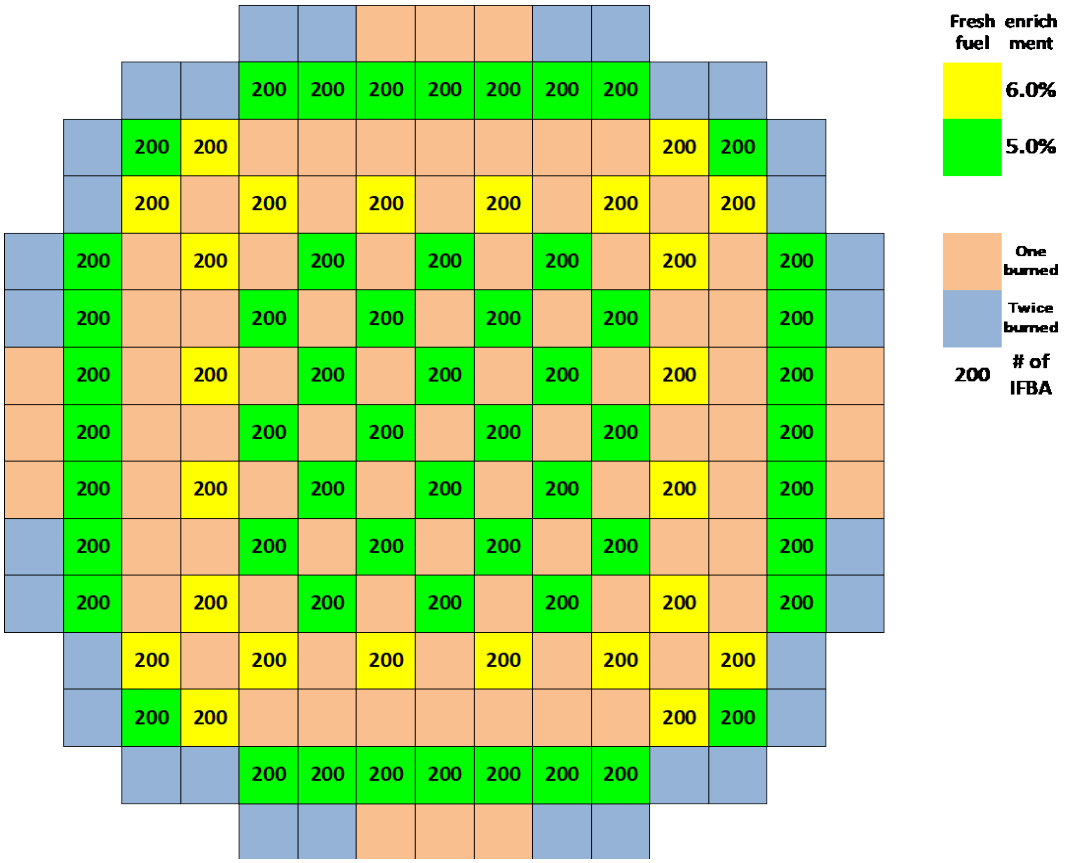

Figure 47. Core loading pattern for Core Design Option 3.

Figure 48 shows the peaking factors at Peak (burnup state with the maximum F_q value in the cycle) for Core Design Option 3. The maximum F_q calculated is 2.086, which is over 10% lower than that calculated from Core Design Option 2. Figure 49 shows the burnup distributions at the EOC of this core design option. The maximum rod averaged burnup achieved is 74.93 GWD/MTU.

Table 12 provides a summary of the peaking factors and burnup values at BOC, Peak, MOC, and EOC of the equilibrium cycle. Table 13 provides a summary of the critical boron concentration and axial offset values for Core Design Option 3. The critical boron concentration letdown curve is shown in Figure 50.

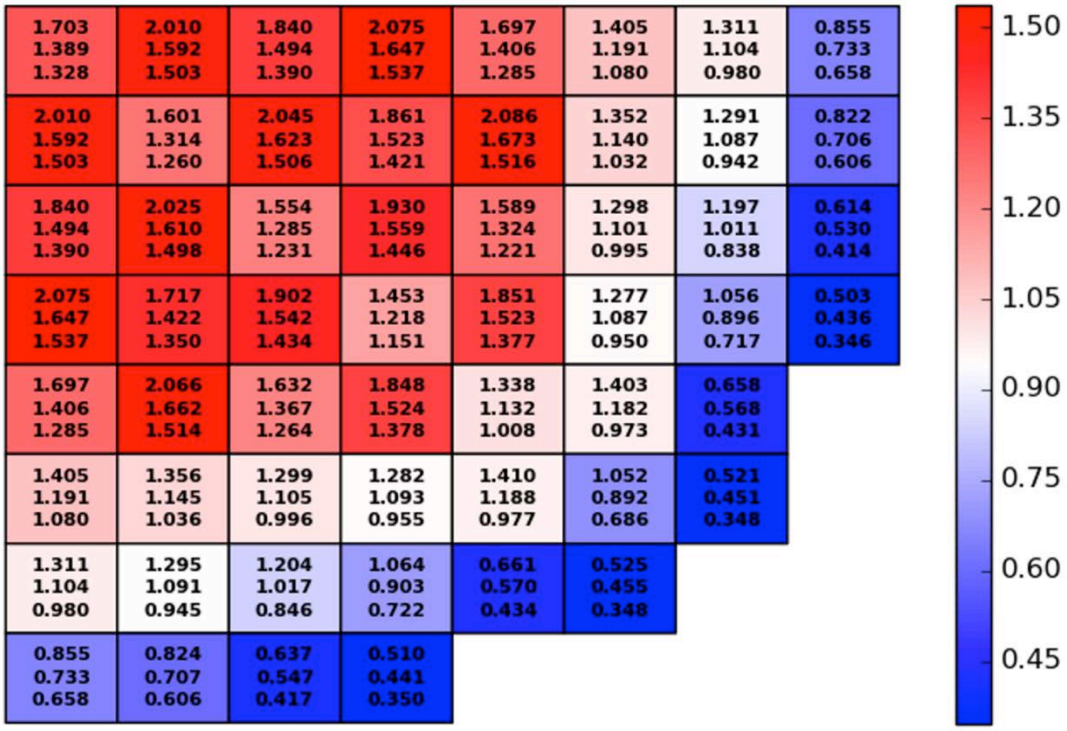

Figure 48. Peaking factors at Peak (burnup state with the maximum F_q in the cycle) for Core Design Option 3 (first row F_q, second row F_ΔH and third row P_bar).

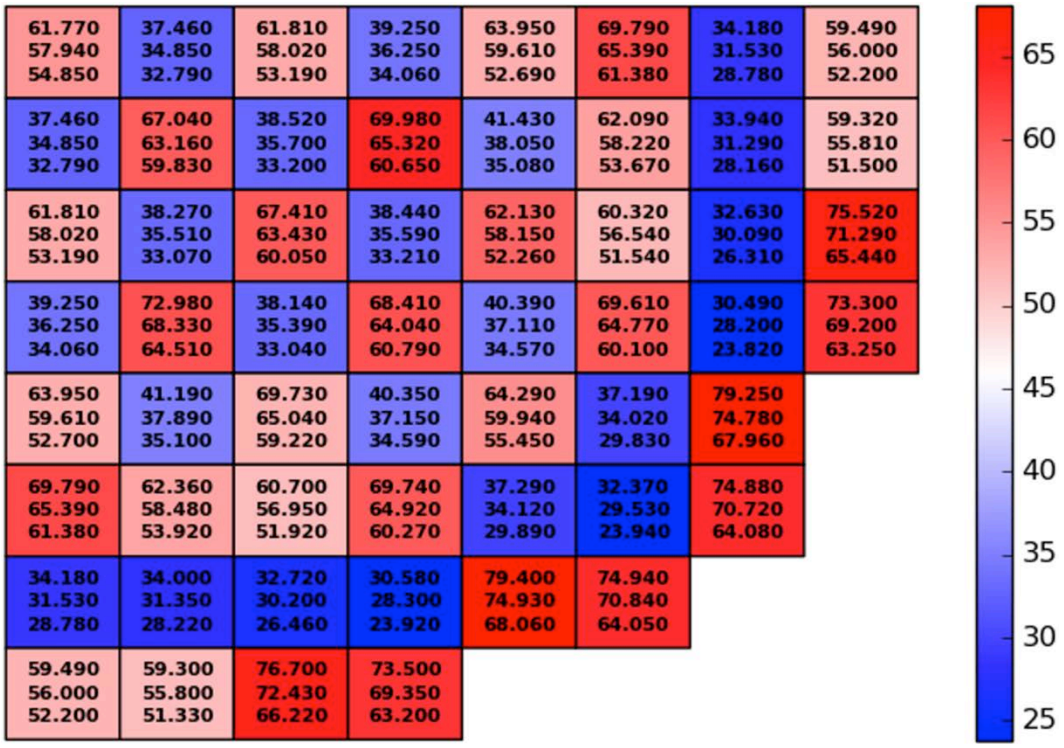

Figure 49. Burnup distribution at EOC for Core Design Option 3 (first row local, second row rod averaged and third row assembly averaged).

Table 12. Summary of peaking factors and burnup values for Core Design Option 3.

	BOC	Peak	MOC	EOC
P_bar	1.498	1.537	1.364	1.303
F_ΔH	1.611	1.673	1.465	1.423
F_q	1.842	2.086	1.663	1.660
Radial Assembly Burnup (GWd/MTU)	53.91	55.48	59.85	68.06
Radial Pin Burnup (GWd/MTU)	59.69	61.20	65.58	74.93
Peak Burnup (GWd/MTU)	63.93	65.42	69.84	79.40

Table 13. The critical boron concentration and axial offset values for Core Design Option 3.

Critical boron concentration at hot zero power	2030.14 ppm
Peak critical boron concentration at full power	1527.50 ppm
Maximum axial offset	28.48%

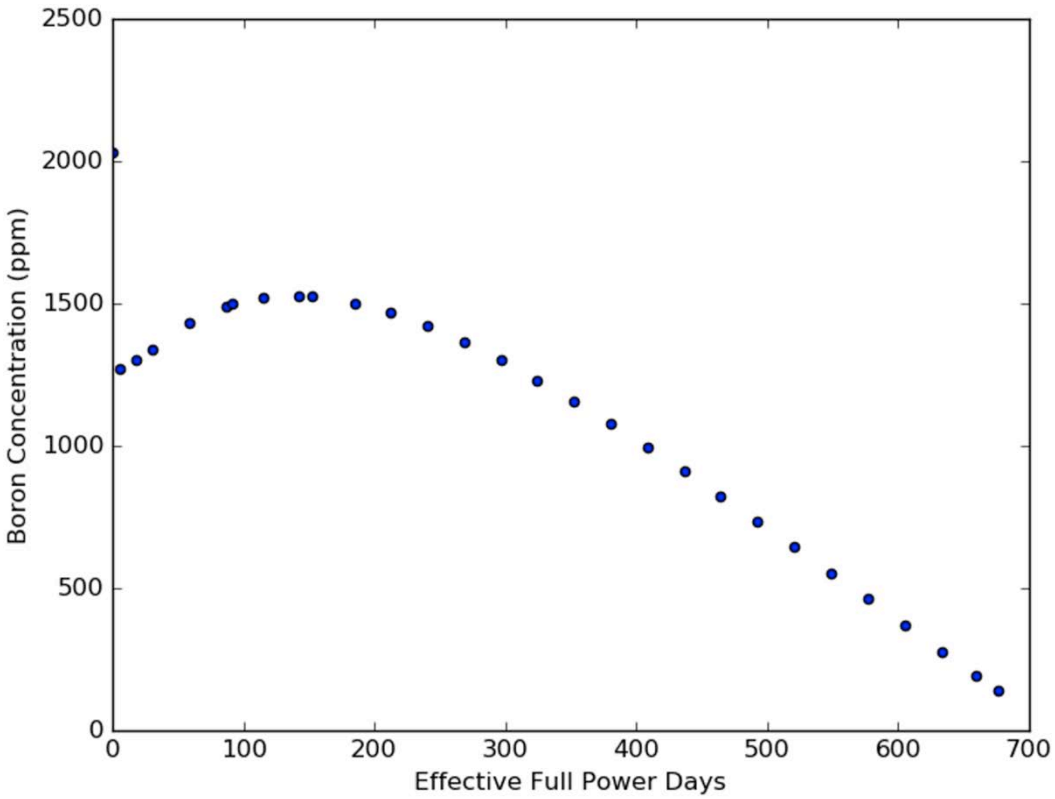

Figure 50. Critical boron concentration in ppm for the equilibrium cycle for Core Design Option 3.

Comparing the results obtained from Core Design Option 3 with those from Options 1 and 2, the peaking factors and critical boron concentrations are much reduced.

4.6 Core Design Option 4 – Loading with 5% and 6% Enrichment Assemblies and 8 Assemblies with Gadolinia Rods

Core Design Option 4 is essentially the same as Core Design Option 3, with the addition of 8 assemblies containing gadolinia rods. The gadolinia assemblies are located so as to lessen the burnup and power peaking of the once burned assemblies with excessive fission gas release. For this option, only assemblies with an initial enrichment of 6% contain gadolinium rods. The core locations of these assemblies are shown in Figure 51. The loading map of the gadolinium assembly configuration is shown in Figure 52. The gadolinium rods contain 8% gadolinia and 3.6 w/o U-235.

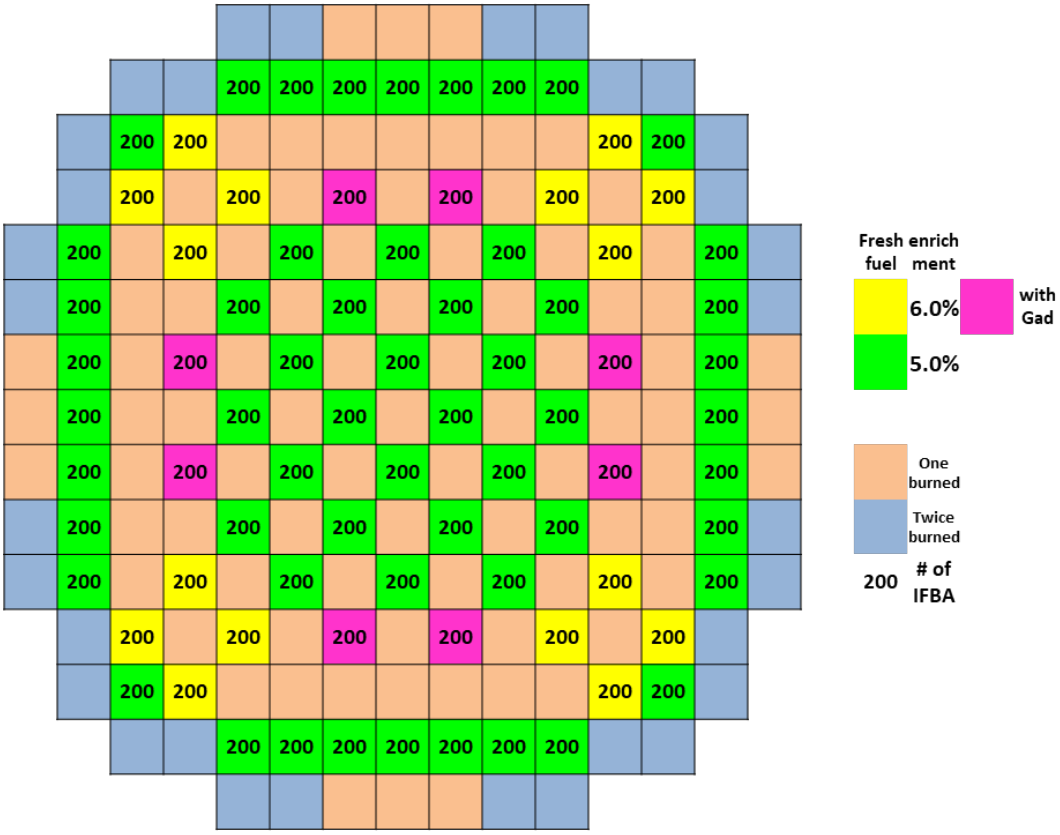

Figure 51. Core loading pattern for Core Design Option 4.

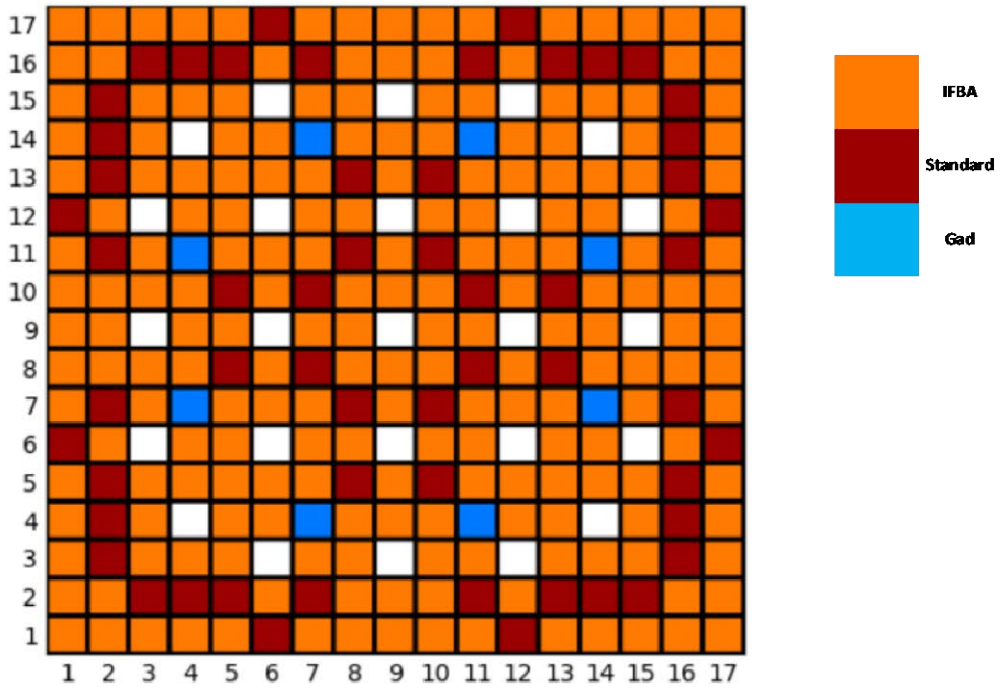

Figure 52. Illustration of an assembly with gadolinia rods.

The inclusion of the gadolinium assemblies resulted in peaking being lowered considerably. This is especially true at the BOC, and in the gadolinium assemblies. At BOC, theses assemblies coincide with the location of F_q, both in Core Design Option 3 and Core Design Option 4.

A comparison of F_q values between Core Design Option 3 and Core Design Option 4 is more complex at the peak, where the effects of IFBA have largely waned. The effects of gadolinium are still present at the peak, resulting in a local peaking factor decrease from 2.086 to 1.934. However, with the absence of IFBA, all of the interior fresh assemblies with 5% enrichment have a relatively large reactivity resulting in high cross-sections. The presence of gadolinium shifts the core peak from the gadolinium assemblies to the most interior fresh assemblies, which increases the local peaking from 2.010 to 2.080. This results in a similar maximum F_q of 2.086 to 2.080, between Core Design Option 3 and Core Design Option 4, respectively.

One of the primary objectives in introducing the gadolinium assemblies was to lower the peaking of the once-burned assemblies with excessive fission gas release. The peaking from these assemblies lowered from 1.606 to 1.562 between Core Design Option 3 and Core Design Option 4. Despite this decrease being relatively small, Core Design Option 4 serves to partially quantify lowering the once-burned assembly peaking by adding gadolinium to a neighboring fresh assembly.

Figure 53 shows the peaking factors at Peak for Core Design Option 4. Figure 54 shows the burnup distribution at EOC for Core Design Option 4. The maximum rod averaged burnup achieved is 74.97 GWd/MTU. Table 14 shows the summary of the peaking factors and burnup values for Core Design Option 4. Table 15 shows a summary of the critical boron concentrations. Figure 55 shows the critical boron concentration letdown curve for Core Design Option 4.

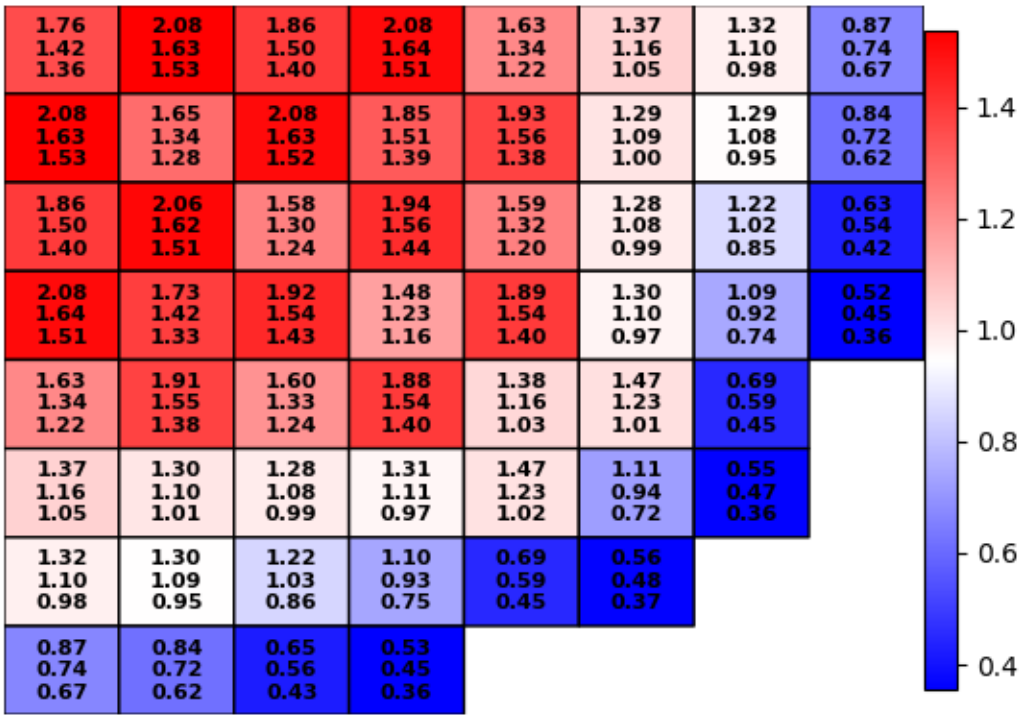

Figure 53. Peaking factors at Peak for Core Design Option 4 (first row F_q, second row F_ΔH and third row P_bar).

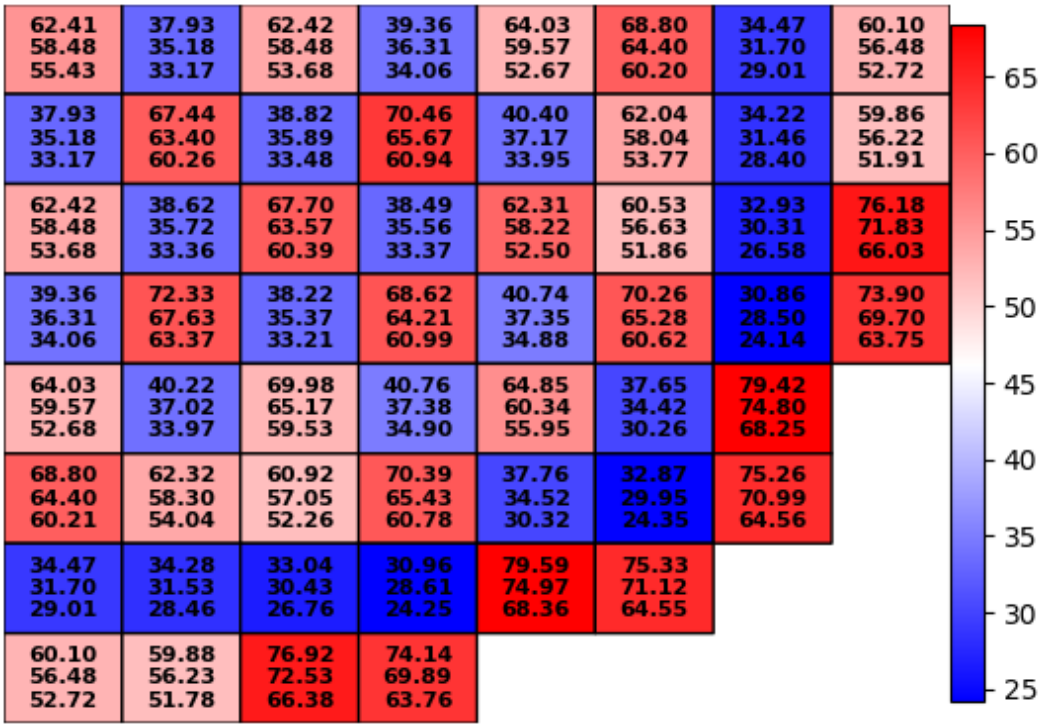

Figure 54. Burnup distribution at EOC for Core Design Option 4 (first row local, second row rod averaged and third row assembly averaged).

Table 14. Summary of peaking factors and burnup values for Core Design Option 4.

	BOC	Peak	MOC	EOC
P_bar	1.382	1.535	1.366	1.296
F_ΔH	1.487	1.638	1.468	1.417
F_q	1.687	2.080	1.631	1.651
Radial Assembly Burnup (GWd/MTU)	54.02	55.68	60.17	68.36
Radial Pin Burnup (GWd/MTU)	59.65	61.22	65.62	74.97
Peak Burnup (GWd/MTU)	64.01	65.55	70.06	68.36

Table 15. The critical boron concentration and axial offset values for Core Design Option 4.

Critical boron concentration at hot zero power	1936.00 ppm
Peak critical boron concentration at full power	1463.73 ppm
Maximum axial offset	27.56%

The addition of gadolinium assemblies lowered critical boron concentrations. In comparing Core Design Option 3 and Core Design Option 4, the hot zero power boron concentrations lowered from 2030.14 ppm to 1936 ppm. Peak critical boron concentration at full power decreased from 1527.50 ppm to 1463.73 ppm. The axial offset also decreases from 28.48% to 27.56%. These trends clearly demonstrate the benefits of gadolinium assemblies.

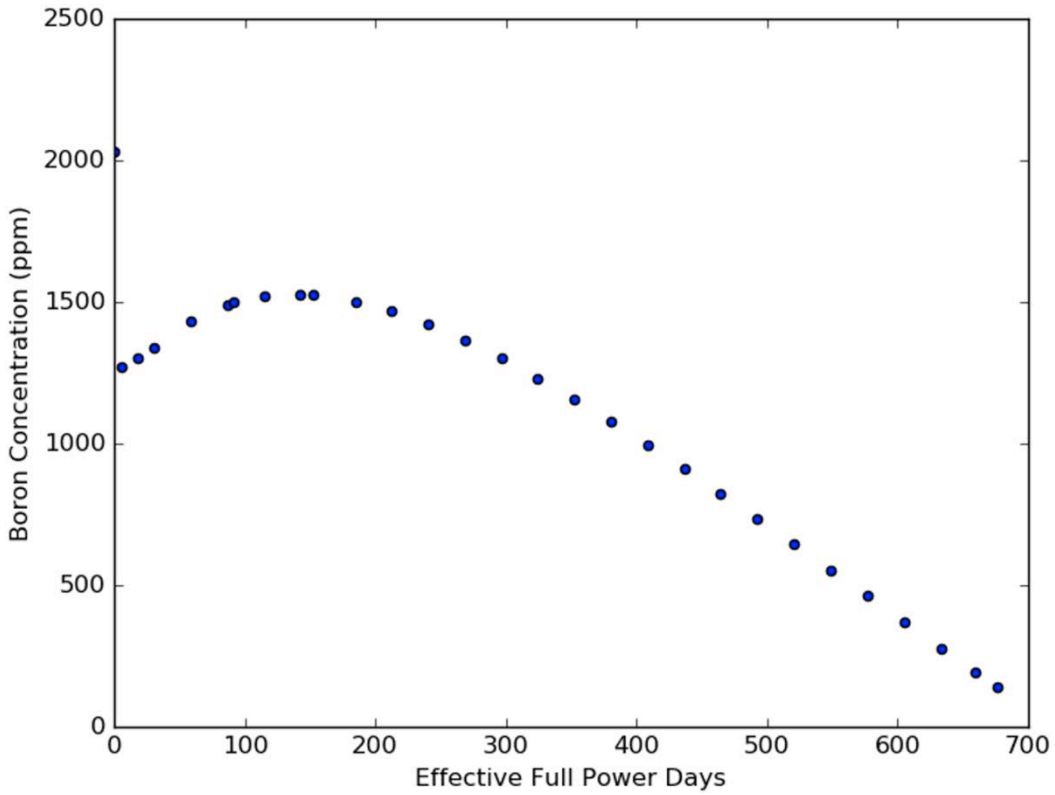

Figure 55. Critical boron concentration in ppm for the equilibrium cycle for Core Design Option 4.

4.7 Core Design Option 5 – Loading with 5% and 6% Enrichment Assemblies and 28 Assemblies with Gadolinia Rods

In this core design variation, Core Design Option 5, the number of fresh assemblies is still 80, the same as the one used in Core Design Options 1–4. There are 24 assemblies with 6% enrichment fuel rods and 56 assemblies with 5% enrichment fuel rods. To flatten out the power distributions in this design option, more assemblies with gadolinia rods are loaded into the fuel rods loaded in the interior region of the reactor core. Eight gadolinium rods are loaded in each assembly, and there are 28 fresh assemblies with gadolinium rods. Among the 28 assemblies with gadolinium rods, 8 assemblies have fuel rods with 6% enrichment, while 20 assemblies have fuel rods with 5% enrichment. The loading pattern is shown in Figure 56. The gadolinium rods loading in an assembly is the same as that shown in Figure 52. There are 8 fuel rods containing 8% mass fraction of Gd_2O_3. The enrichment of U-235 in the gadolinium rods has to be reduced to avoid the spiking of power peaking when the gadolinium is depleted. The enrichment for the 5% fuel without gadolinium is reduced to 3% with gadolinium and for the 6% fuel without gadolinium is reduced to 3.6% with gadolinium. Figure 57 shows the distributions for the power peaking factors at Peak for this core design option. Figure 58 shows the distributions for the burnup distributions at EOC. The maximum rod averaged burnup achieved is 76.17 GWD/MT which is slightly above the design target of 75 GWD/MT. Figure 59 shows the critical boron concentration and Figure 60 shows the axial offset for this core design option.

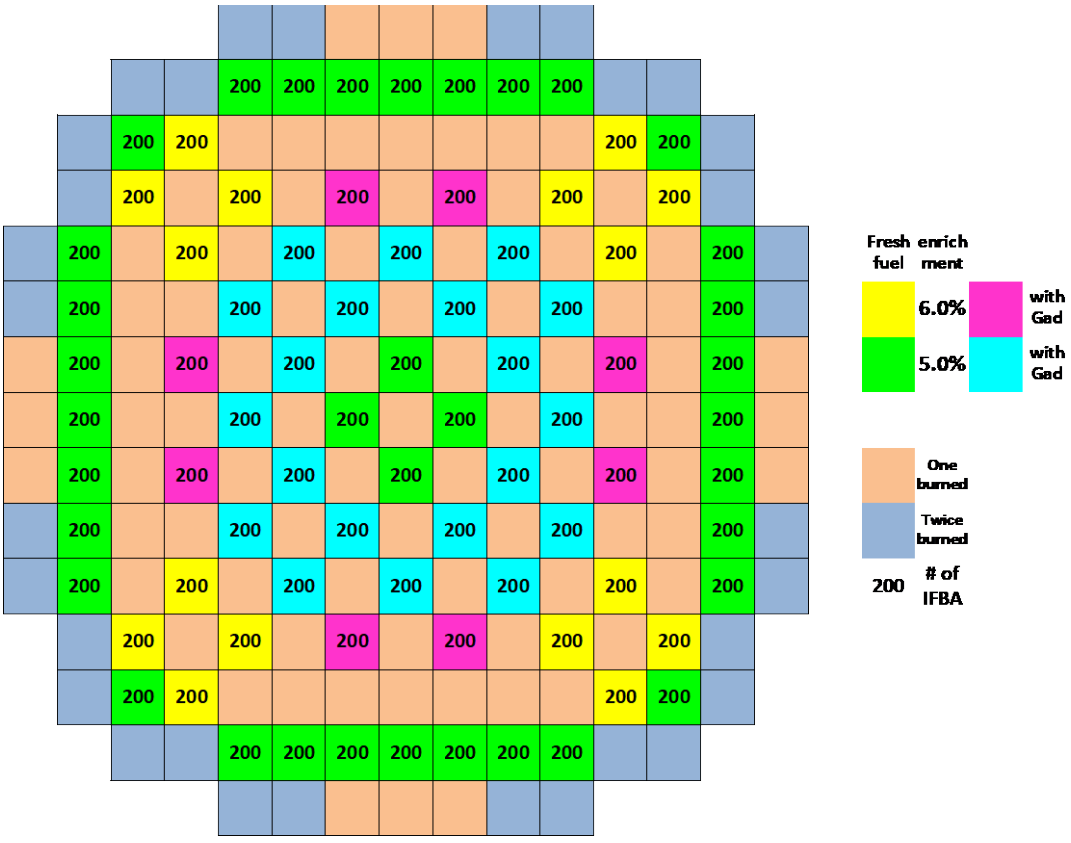

Figure 56. Loading pattern for Core Design Option 5.

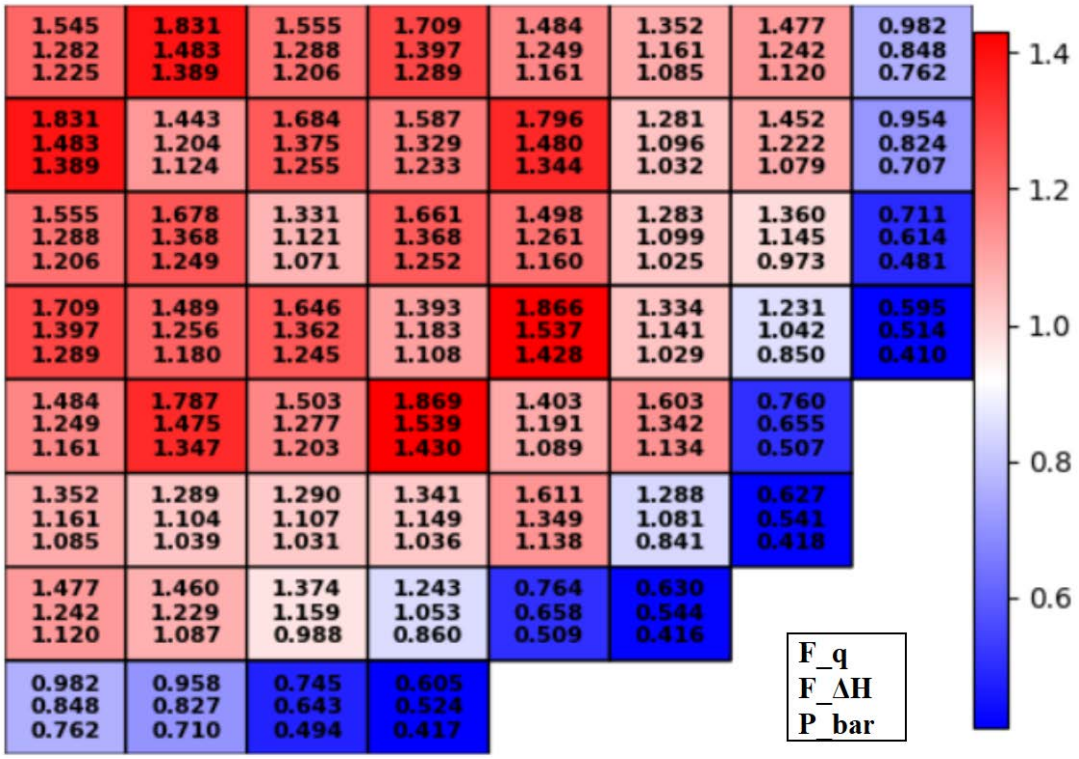

Figure 57. Peaking factors at Peak for Core Design Option 5.

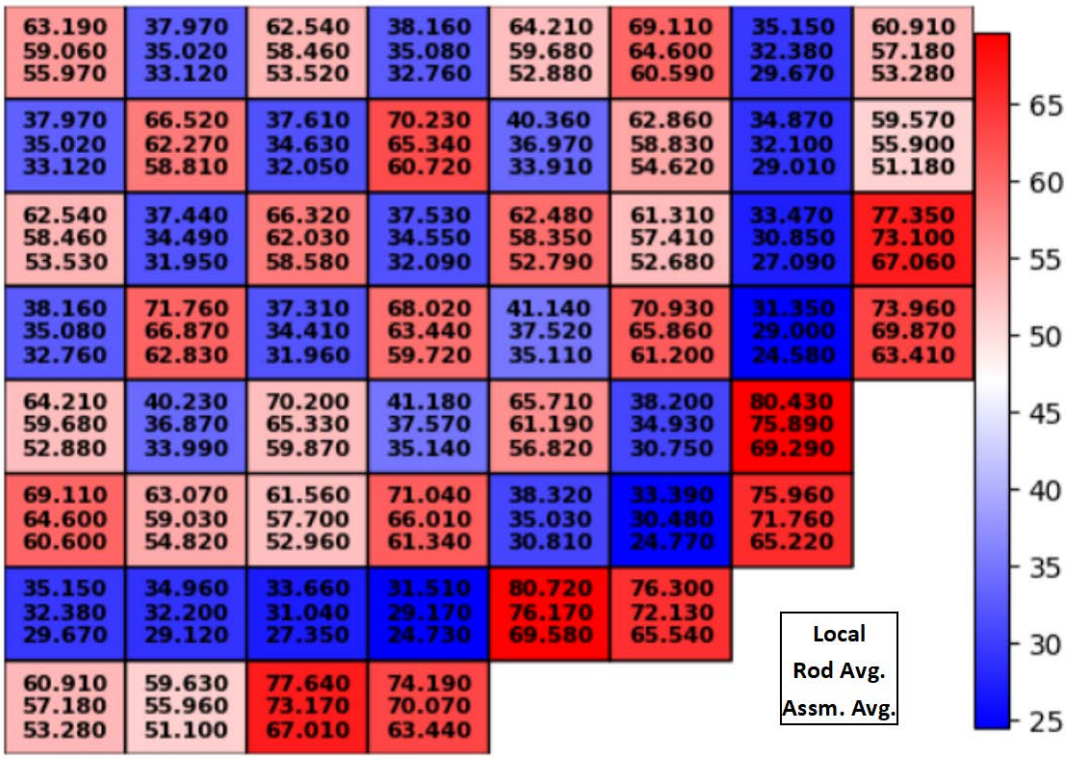

Figure 58. Burnup distribution at EOC for Core Design Option 5.

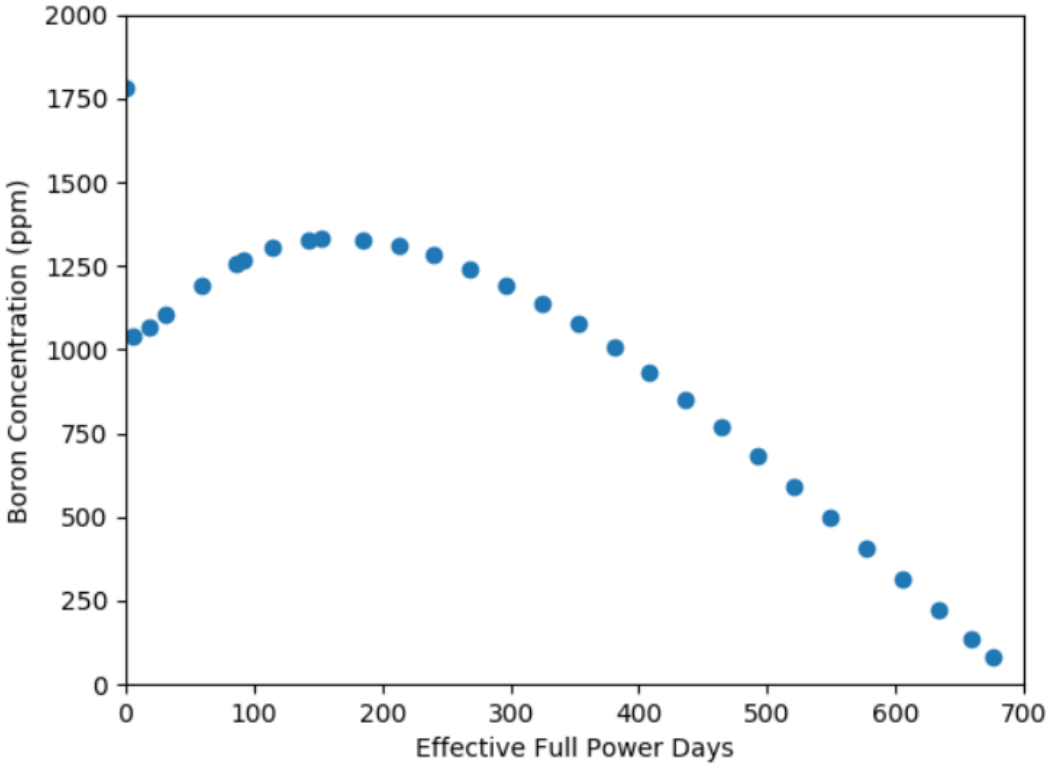

Figure 59. Critical boron concentration in PPM for the equilibrium cycle for Core Design Option 5.

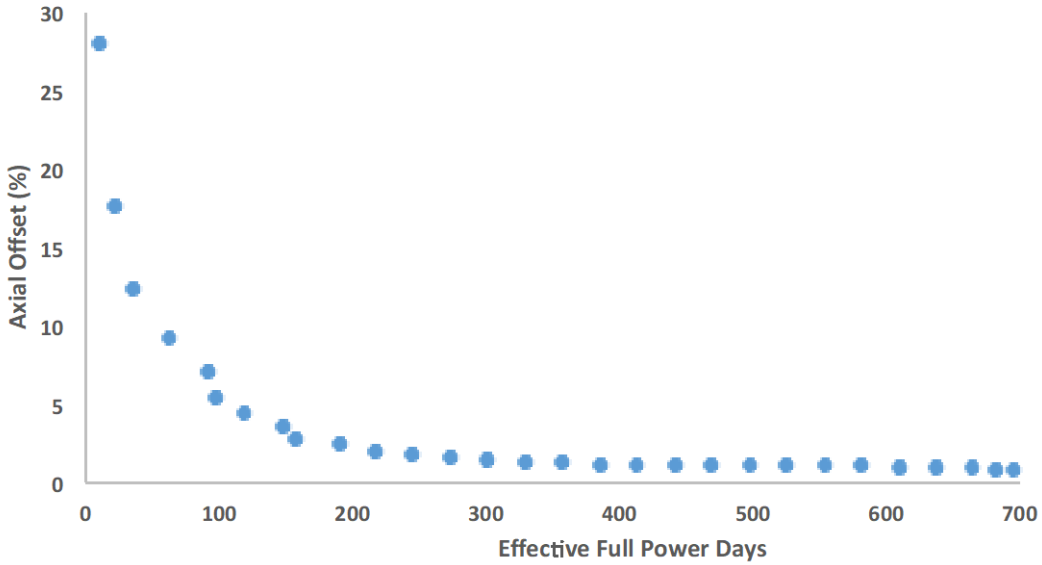

Figure 60. Axial offset for Core Design Option 5.

Table 16 provides a summary of peaking factors and burnup values at BOC, MOC, and EOC at the equilibrium cycle for this design option. The highest F_q value is 1.869, which is much lower than that from the previous four options. Table 17 shows the critical boron concentration and axial offset values. The critical boron concentration is now within the range of normal operating conditions, but the axial offset values are outside the design target range in the initial few states. This situation can be remedied by

the insertion of control rods into the operations. To summarize, this design option represents the best core design we have achieved thus far.

Table 16. Summary of peaking factors and burnup values for Core Design Option 5.

	BOC	**Peak**	**MOC**	**EOC**
P_bar	1.417	1.430	1.659	1.270
F_ΔH	1.493	1.539	1.476	1.388
F_q	1.700	1.869	1.361	1.605
Radial assembly burnup (GWd/MTU)	55.20	57.62	61.75	69.58
Radial pin burnup (GWd/MTU)	60.05	62.41	67.21	76.17
Peak burnup (GWd/MTU)	64.57	66.91	71.62	80.72

Table 17. The critical boron concentration and axial offset values for Core Design Option 5.

Critical boron concentration at hot zero power	1782.86 ppm
Peak critical boron concentration at full power	1331.57 ppm
Maximum axial offset	28.10%

5. FUEL PERFORMANCE

Nuclear fuel operates in a harsh environment in which high temperature, chemical reactions, radiation damage, and mechanical stresses may challenge the ability of a fuel rod to withstand a transient without losing its integrity and cause a fuel failure. Fuel failure refers to a situation when the cladding is breached (e.g., fuel rod ballooning and rupture during a LBLOCA) and radioactive material leaks from the fuel pellet into the reactor coolant water. The radioactive materials with most tendency to leak through a cladding breach into the reactor coolant are fission-product gases and volatile elements, such as krypton, xenon, iodine, and cesium. To protect the integrity of the fuel rods and minimize the probability of fuel failures, the NRC imposes a fuel burnup limit (i.e., the current limit rod averaged burnup of 62 GWd/MTU) to regulate how long a fuel assembly can stay in a reactor core.

With fuel burnup extension (e.g., to the proposed new burnup limit of 75 GWd/MTU), the extended operational exposure that accompanies high burnup causes changes to the fuel and cladding that may affect its integrity. These changes occur gradually over the life of the fuel rod and can be considered as initial conditions for an accident. There are many changes that occur to the fuel and cladding as a result of prolonged exposure to the irradiation field present in a reactor core. The combination of high temperatures, radiation damage, transmutations, mechanical stresses, and chemical corrosion causes the microstructure of cladding and fuel to evolve considerably during reactor exposure and is responsible for the changes in material behavior at high burn-up. Therefore, it is essential to understand the fuel behaviors (or performance) under both steady-state and transient conditions to evaluate the fuel rod bursting potential under LBLOCA conditions.

LWR fuel rods consist of UO_2 ceramic pellets, which are placed inside a slightly cold worked Zircaloy (e.g., Zircaloy-4 or other high performance fuel cladding material such as ZIRLO) tube due to low absorption of thermal neutrons and corrosion resistance. The fuel pellets are right circular cylinders consisting of slightly enriched UO_2 powder compacted by cold pressing and sintering (e.g., high-temperature fusing of metal particles) to the required density. The ends of each pellet are dished slightly to allow greater axial expansion at the center of the pellets due to higher temperatures there. Void volumes, such as the plenum region above the fuel pellets within a fuel rod, and clearances, such as clad and pellet gaps, are provided within the rods to accommodate fission gases released from the fuel and differential thermal expansion between the cladding and the fuel. The tube is plugged and seal-welded at both ends to encapsulate the fuel. A nuclear fuel rod plenum spring assembly is used to hold fuel pellets in their positions. The spring has a substantially flat surface on its underside that presses against the upper surface of the upper fuel pellets to spread the load of the spring over the top surface of the upper-most fuel pellet. All fuel rods are internally pressurized with helium during the welding process in order to minimize compressive clad stresses and to prevent cladding flattening due to coolant operating pressures. Fuel rod pressurization is dependent on the planned fuel burn-up, as well as other fuel design parameters and fuel characteristics, particularly densification potential. The fuel rods are designed such that the internal gas pressure will not exceed the nominal system coolant pressure even during anticipated transients, and clad flattening will not occur during the core life. With enrichment and burnup extension, the fuel resides in the core for a much longer period of time and has the potential to have greater fission gas release, and thus increased fuel rod internal pressure. As such, sophisticated fuel rod designs should be investigated to reduce the fuel rod internal pressure.

Fuel behaviors in a reactor core involve complicated multiphysics phenomena with multiple spatial and time scales. The multiphysics include neutronics, fully-coupled nonlinear thermomechanics, multiple species diffusion, thermalhydraulics, and chemical reactions. These complex and interacting physics must be adequately modeled mathematically with a self-consistent approach to simulate the dynamic situation in a fuel rod. The effects of changes in any one of these physical phenomena on all of the others have to be considered. Figure 61, reproduced from [38] by INL's BISON team, illustrates the complex interacting multiphysics phenomena to be considered to simulate fuel behaviors. These multiphysics phenomena have important physics at multiple spatial scales ranging from the atomistic, microstructural, and

engineering levels. Multiple time scales are also involved for the multiphysics phenomena for the time step size ranging from milliseconds for power ramps and accidents to months for steady-state operations. There has been a long history to develop computer codes to simulate the fuel performance for LWR fuel. These notable codes include the NRC's legacy codes FRAPCON/FRAPTRAN, and the advanced fuel performance code, BISON, still being developed at INL. These fuel performance computer codes are developed only for single fuel rod calculations. The calculated parameters include gap conductance, temperatures, pressures, fission gas release, stored energy, cladding stress and strain, cladding oxidation, and cladding hydrogen uptake, etc.

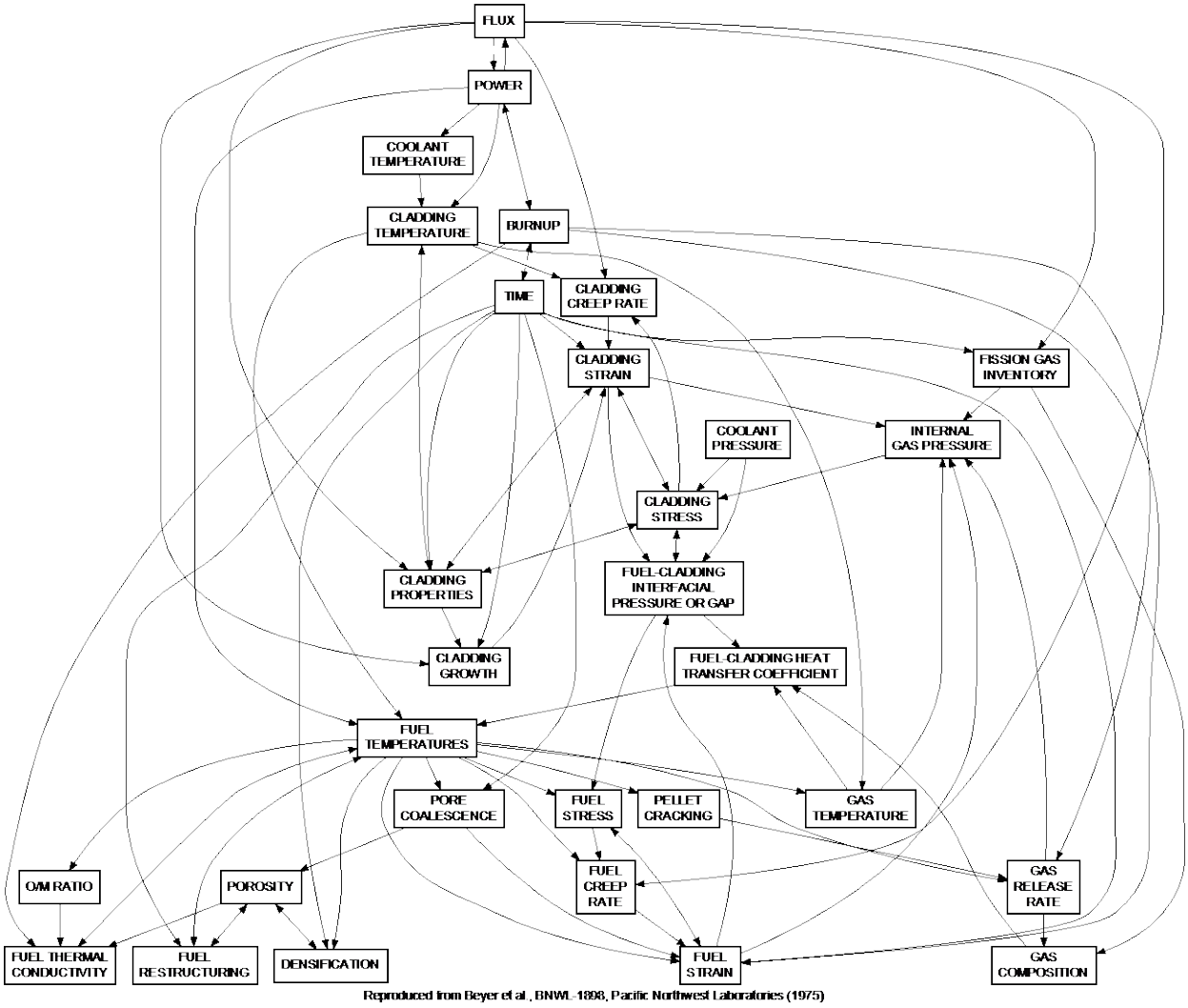

Figure 61. Illustration of the complicated multiphysics phenomena considered in fuel performance simulations (reproduced by the BISON developers at INL from [38]).

The fuel performance codes were developed only for single fuel rod calculations so they are not capable of capturing the detailed thermal hydraulic conditions, due to the impact from neighboring fuel rods and assemblies. For the steady-state fuel performance calculations, the FRAPCON code is chosen. Power history and axial power profile from the output of core design analysis using VERA-CS are required as inputs to FRAPCON. The linear heat generation rate (kW/m) at each time step of FRAPCON simulation is also provided. The VERA-CS code incorporates the subchannel code, CTF, to provide the thermal hydraulic feedback to the neutronics code, MPACT. CTF has fluid dynamics and heat transfer

models that provide local steady-state thermal hydraulic data at different depletion cycle points as an input for FRAPCON simulations. By using axial dependent cladding surface temperature and coolant pressure for each fuel rod of interest, more accurate results can be obtained from fuel performance codes. In the meantime, part of the outputs from the FRAPCON simulations are used to prepare for the steady-state run of a system LBLOCA model, ensuring correct stored energy and initial conditions for the transient fuel performance models.

Under LBLOCA conditions, the high-pressure differentials across the cladding and high temperatures make the cladding highly vulnerable to swelling and rupture (bursting) behavior. LOCA testing on high burnup fuels has revealed that fuel in the ballooned region of a fuel rod has the tendency to fragment into very fine powders, which can be expelled out through the burst opening. While a fuel rod swelling and rupture does not necessarily challenge the core geometry criteria, the dispersal of large volumes of fuel through the cladding burst opening can lead to valid concerns as to whether the core geometry is maintained. Additionally, the release of large volumes of fragmented fuel can significantly alter the results of the dose consequence analysis performed as part of the LOCA safety analysis. Strong evidence exists that the swelling and rupture behavior of the cladding and the fuel fragmentation relocation and dispersal (FFRD) behaviors are connected. Cladding rupture is required for the dispersal of any fuel fragments. It is also required to relieve the hydrostatic pressure that has built up in the fuel rod that is the result of pellet, cladding contact, and the buildup of fission gas in the fuel rod plenum. Zircaloy fuel cladding is both cold work and partially annealed, resulting in anisotropic behavior, especially in its unirradiated state. The crystal structure is hexagonal close packed (HCP), which is referred to as the alpha phase [39]. Zircaloy begins to undergo a phase change at ~800°C from the HCP alpha structure to a body-centered cubic (BCP) beta phase structure. Between ~800°C and ~980°C, a two-phase region exists, and above ~980°C, a pure beta phase exists. The mixed phase region and beta phase region have significantly lower creep strength than the alpha phase, and, unlike the alpha phase, the beta phase behaves isotopically. As such, strain rates in parts of the cladding exhibiting higher concentrations of beta phase grains are likely to be much higher. Zircaloy used as nuclear fuel cladding is an alloy of zirconium with minor alloying additions of tin, niobium, iron, chrome, nickel, and oxygen. The extent of the alloying mixture will affect the alpha/beta transition, which will in turn affect the deformation behavior. Some elements like niobium, chrome, and iron are beta stabilizers, so they will have the effect of lowering transition temperatures. Other elements like tin and oxygen are alpha stabilizers, so their effect will be the reverse. Early rupture at low overall strain will occur in cases where local ductility is exhausted by non-uniform straining. This occurs when axial or azimuthal temperature variations lead to non-uniform straining. Azimuthal temperature variations can occur in the nuclear fuel due to varying temperatures of neighboring rods, the pellet stack not remaining co-axial during the ballooning, axial fuel fragment relocation into the ballooned region, or due to the cladding's anisotropic behavior. Additionally, fast temperature ramps can result in cladding rupture before large deformations due rapidly decreasing cladding strength in the beta phase prior to appreciable cladding deformation.

For the transient fuel performance calculations, the advanced fuel performance code, BISON, is chosen to perform more detailed mechanistic modeling of the fuel behaviors. System analysis codes, such as RELAP5-3D, have best-estimate two-phase flow and heat transfer models, which can provide local transient thermal hydraulic data at a different time in the transients as an input for BISON simulations.

Fuel rod design information is necessary for reactor core design, fuel performance, and reactor system analysis codes as input parameters. To ensure data consistency, a common set of fuel rod design input data should be shared among all the codes. Table 18 shows the input data from several common fuel rod designs needed for different codes. Note that these fuel rod data may vary with time and have to be updated under different conditions.

Table 18. Common data from fuel rod design for different physics in LOCA analysis.

Fuel Rod Data	Fuel Performance	Core Design	System Code
Rod geometry information, such as cladding outer diameter, cladding thickness, fabricated gap, active fuel length, and plenum length.	☑	☑	☑
Spring dimensions, such as the outer diameter of the plenum spring, the diameter of the plenum spring wire, and the number of turns in the plenum spring.	☑	☑	☐
Pellet shape, such as height (length) of each pellet, height (depth) of pellet dish, pellet end-dish shoulder width, and Chamfer height and width.	☑	☐	☐
Pellet isotopics, such as fuel pellet U-235 enrichment, oxygen-to-metal atomic ratio, weight fraction of gadolinia in urania-gadolinia fuel pellets, Boron-10 enrichment in ZrB2, ppm by weight of moisture in the as-fabricated pellets, and ppm by weight of nitrogen in the as-fabricated pellets.	☑	☑	☐
Pellet fabrication, such as as-fabricated apparent fuel density, open porosity fraction for pellets, the fuel pellet surface arithmetic mean roughness, etc.	☑	☑	☑
Cladding fabrication, such as cladding type, the cladding surface arithmetic mean roughness, as-fabricated hydrogen in cladding, etc.	☑	☑	☑
Rod fill conditions, such as initial fill gas pressure, initial fill gas type, and their mole fractions.	☑	☑	☑
Fuel assembly geometry, such as pitch.	☑	☑	☑

Fuel performance calculations, under both the steady-state and transient conditions, are required in this work to demonstrate the integrity of fuel rods with burnup extension under large-break LOCA conditions. Steady-state fuel performance calculations are required to ensure that the initial conditions prior to fuel rods going into transients are set correctly. Transient fuel performance calculations provide more mechanistic simulations of the fuel rod bursting potential under LBLOCA conditions. The following section describes the FRAPCON code used to perform fuel performance analysis under both steady-state fuel depletion, as well as the FRAPTRAN code used for transient conditions.

5.1 FRAPCON/FRAPTRAN

FRAPCON/FRATRAN is a suite of codes developed by PNNL for the NRC for the purposes of performing fuel performance analyses under steady-state (FRAPCON) and transient (FRAPTRAN) conditions. FRAPCON is used to analyze the steady-state response of LWR fuel rods. The code calculates the temperature, pressure, and deformation of a fuel rod as functions of time-dependent fuel rod power and coolant boundary conditions. The phenomena modeled by FRAPCON include: (1) heat conduction through the fuel and cladding to the coolant; (2) cladding elastic and plastic deformation; (3) fuel-cladding mechanical interaction; (4) fission gas release from the fuel and rod internal pressure; and (5) cladding oxidation. The code contains the necessary material properties, water properties, and heat-transfer correlations.

The Fuel Rod Analysis Program Transient (FRAPTRAN) is a Fortran computer code that calculates the transient performance of light-water reactor fuel rods during reactor transients and hypothetical accidents such as LOCAs, anticipated transients without scram (AWTS), and reactivity-initiated accidents. FRAPTRAN calculates the temperature and deformation history of a fuel rod as a function of time-dependent fuel rod power and coolant boundary conditions. Although FRAPTRAN can be used in

"standalone" mode, it is often used in conjunction with, or with input from, other codes. The phenomena modeled by FRAPTRAN include: (1) heat conduction; (2) heat transfer from cladding to coolant; (3) elastic-plastic fuel and cladding deformation; (4) cladding oxidation; (5) fission gas release; and (6) fuel rod gas pressure.

5.2 Steady-State Fuel Performance Data for Core Design Option 3

Since Core Design Option 1 and Core Design Option 2 show very high power peaking factors and are way above the normal practical core designs allowed, fuel performance and fuel rod bursting evaluations were not performed. In this subsection, fuel performance data under steady-state conditions are presented for Core Design Option 3. This core design option loads 24 fresh assemblies with 6 w/o enrichment and 56 fresh assemblies with 5% enrichment. The fuel rods have no enrichment reduction in the blanket regions. For this core design option, the FRAPCON input files for all the fuel rods in the quarter core geometry have been automatically prepared and executed by the LOTUS scripts. The FRAPCON calculated fuel rod internal pressures at MOC are shown in Figure 62. It shows the fuel rod internal pressures versus rod averaged burnup and rod average linear heat generation rate. It can been seen from Figure 62 that rod internal pressures for the fresh fuel rods and the twice-burned fuel rods remain relatively low; however, for the once-burned fuel rods, the rod internal pressures are high for certain rods. Figure 63 shows the rod internal pressures for the once-burned fuel with 6 w/o enrichment. These high rod internal pressure rods also correspond to high average linear heat generation rate (LHGR), which indicates high power peaking for those rods. These high rod internal pressure rods are most susceptible to bursting under LBLOCA conditions.

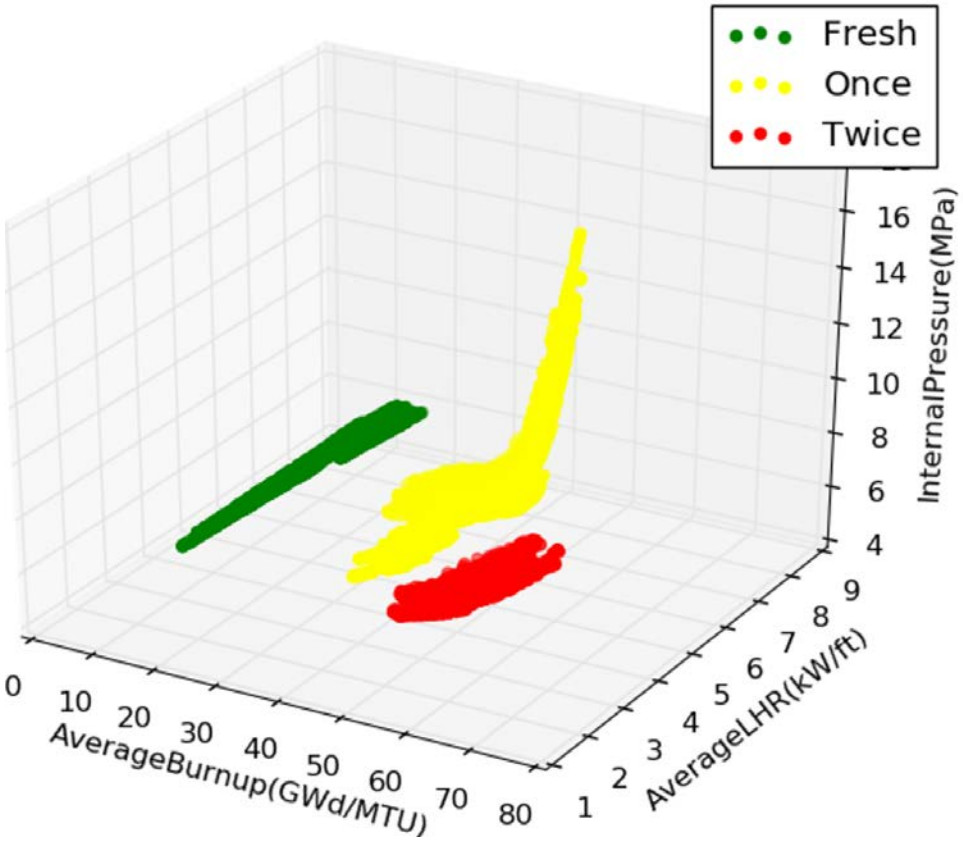

Figure 62. Fuel rod internal pressures at MOC for all of the fuel rods in Core Design Option 3.

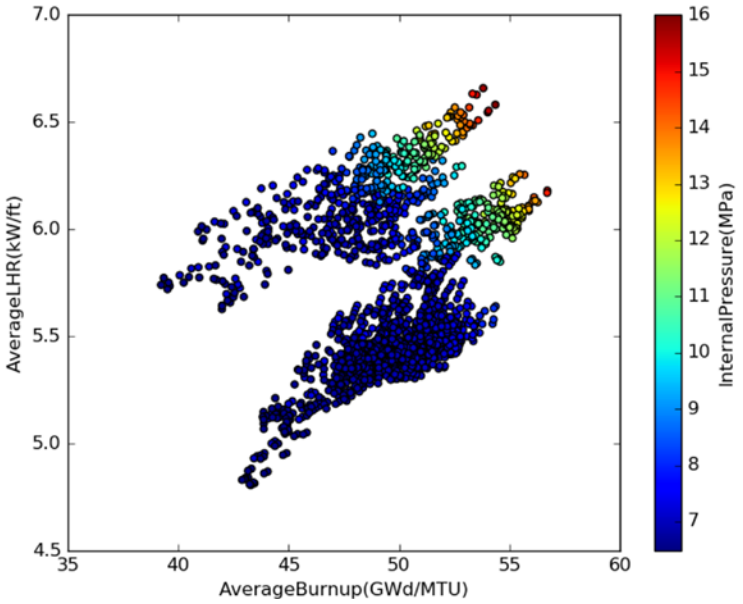

Figure 63. Fuel rod internal pressure at MOC for the once-burned fuel with 6 w/o enrichment.

5.3 Steady-State Fuel Performance Data for Core Design Option 4

In this core design option, there are 24 fresh assemblies with 6 w/o enrichment and 56 assemblies with 5 w/o enrichment. Among the 6 w/o enrichment assemblies, 8 of them are loaded with gadolinium rods. For this design option, only two FRAPCON calculations were done for each assembly—one for the hot rod and the other for the average rod. The hot rod is defined as the hot power rod in the assembly at the various burnup states. The average rod represents the lumping of the remaining 263 fuel rods in an assembly. Figures 64 – 67 show the fuel rod internal pressures for all of the hot rods at BOC, Peak, MOC, and EOC, respectively. It can be seen that the rod internal pressure increases as the burnup increases. The rods with highest rod internal pressure are once-burned fuel rods.

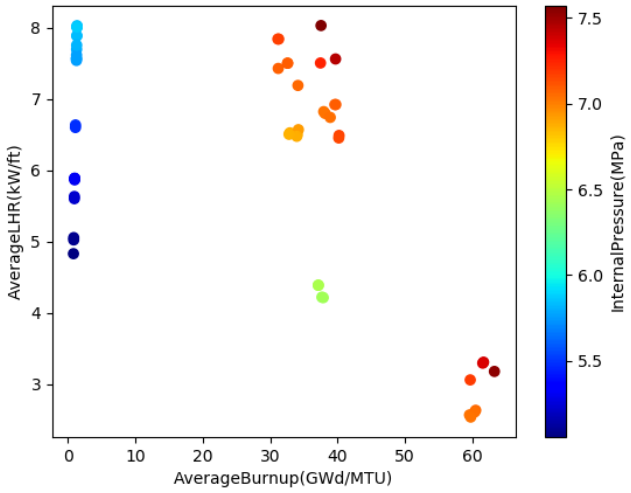

Figure 64. Fuel rod internal pressures for the hot rods at BOC for Core Design Option 4.

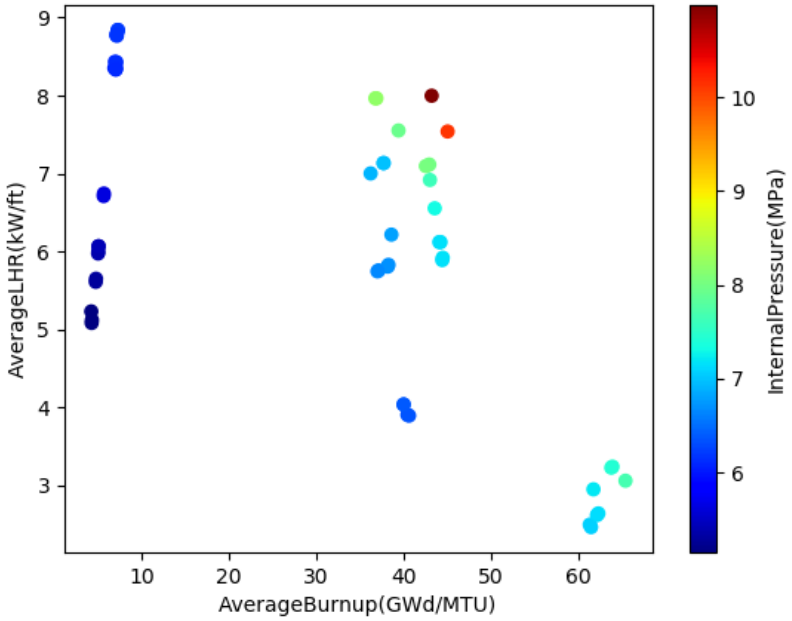

Figure 65. Fuel rod internal pressures for the hot rods at Peak for Core Design Option 4.

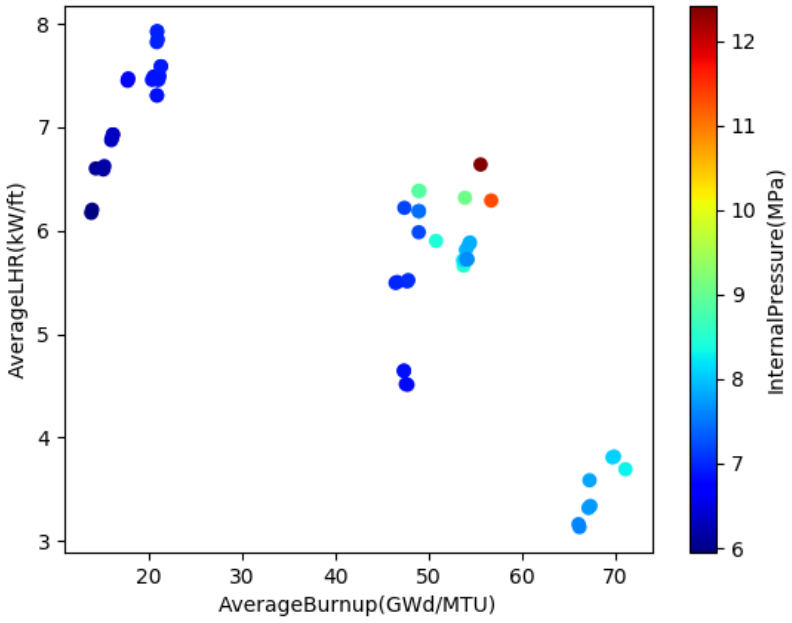

Figure 66. Fuel rod internal pressures for the hot rods at MOC for Core Design Option 4.

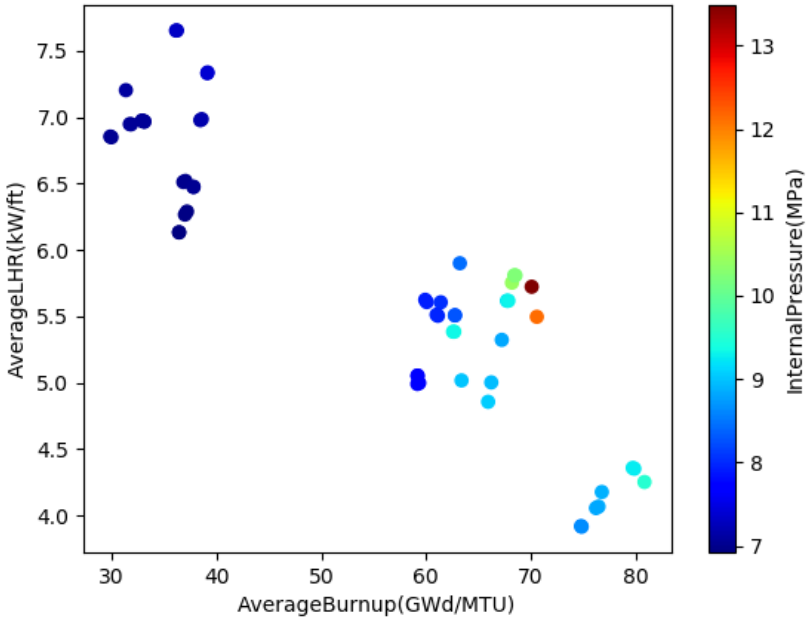

Figure 67. Fuel rod internal pressures for the hot rods at EOC for Core Design Option 4.

5.4 Steady-State Fuel Performance Data for Core Design Option 5

In this core design option, there are 24 fresh assemblies with 6% enrichment and 56 assemblies with 5% enrichment. Among these 80 fresh assemblies, 28 of them have gadolinium rods. For this design option, only two FRAPCON calculations were done for each assembly—one for the hot rod and the other for the average rod. The rods with highest rod internal pressure are once-burned fuel rods.

Figure 68, Figure 69, Figure 70, and Figure 71 show the fuel rod internal pressures for all of the hot rods at BOC, Peak, MOC, and EOC, respectively. It can be seen that the rod internal pressure increases as the burnup increases.

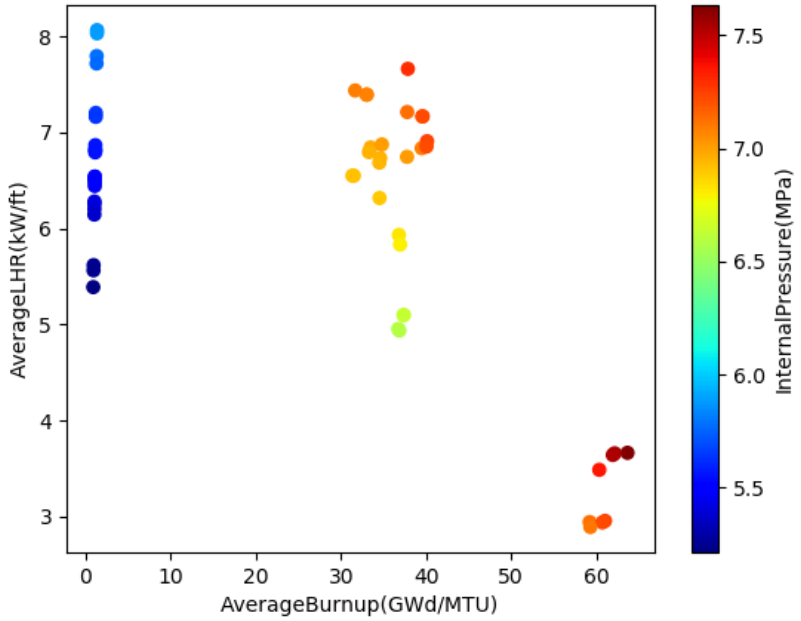

Figure 68. Fuel rod internal pressures for the hot rods at BOC for Core Design Option 5.

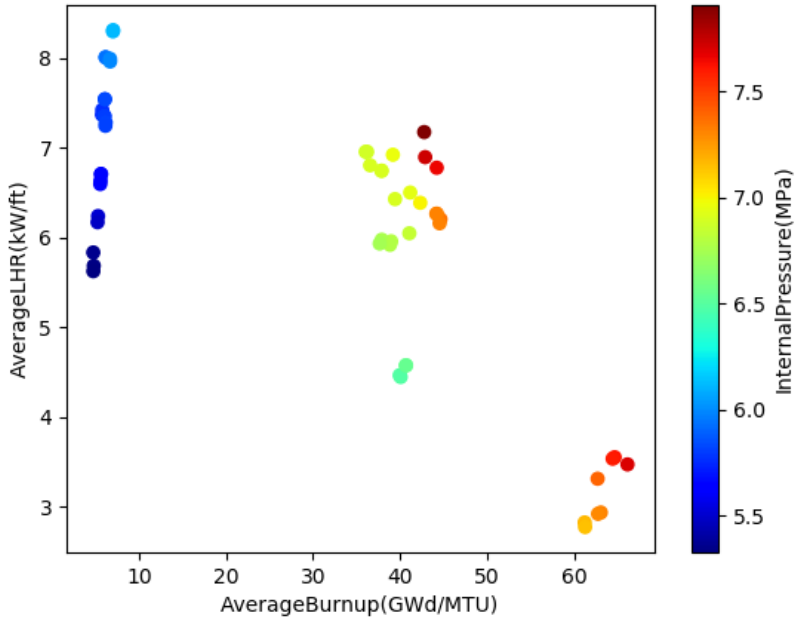

Figure 69. Fuel rod internal pressures for the hot rods at Peak for Core Design Option 5.

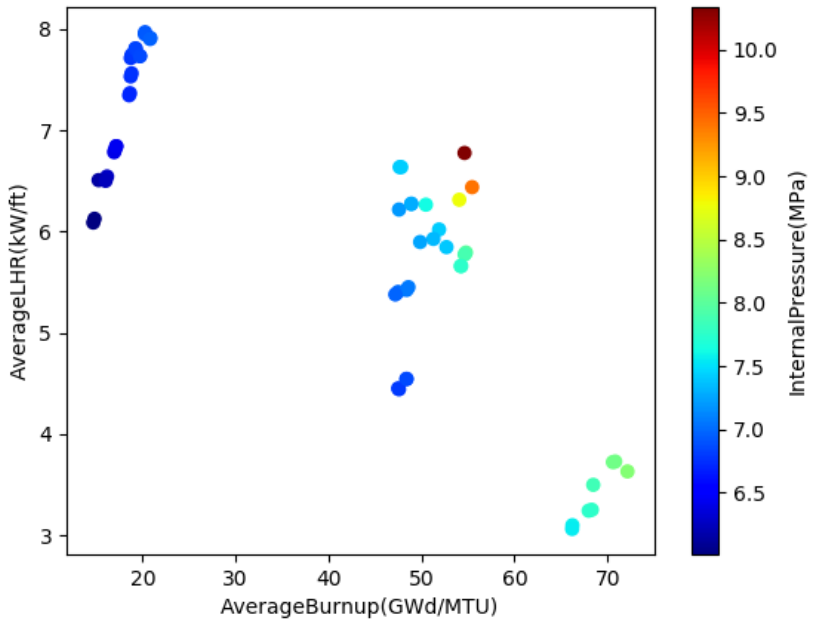

Figure 70. Fuel rod internal pressures for the hot rods at MOC for Core Design Option 5.

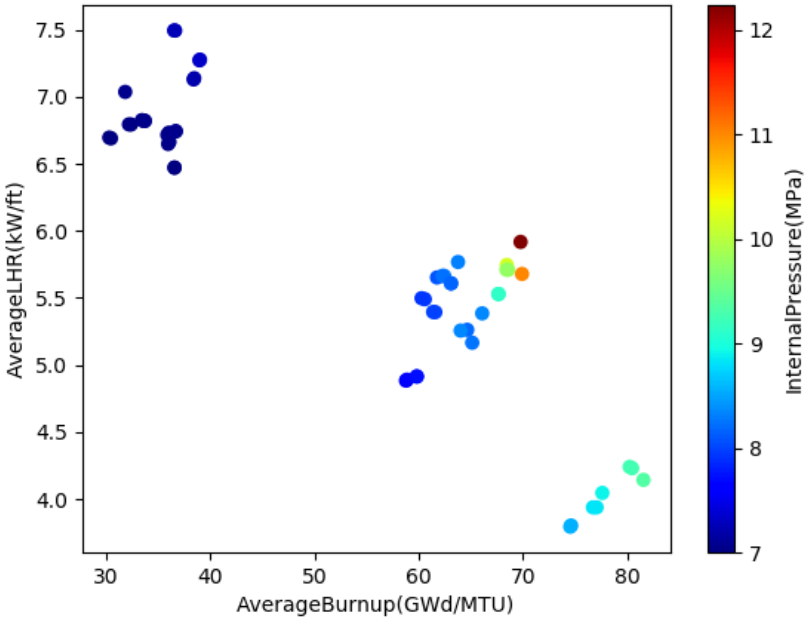

Figure 71. Fuel rod internal pressures for the hot rods at EOC for Core Design Option 5.

6. SYSTEMS ANALYSIS

The NPP systems analysis codes are required to perform the system response under abnormal conditions, such as AOO, DBA, and BDBA events at commercial NPPs operating in the U.S., to demonstrate the NPPs remain safe under various abnormal conditions. INL has a long history of developing NPP systems analysis codes with RELAP5-3D as its flagship product. RELAP5-3D is the code of choice to perform systems analysis.

6.1 RELAP5-3D

The RELAP5-3D code has been developed for BE transient simulation of LWR coolant systems during postulated accidents. Specific applications of the code have included simulations of transients in LWR systems, such as LOCAs and ATWS, and operational transients, such as loss of feedwater flow, loss of offsite power, station blackout, and turbine trip. RELAP5-3D, the latest in the series of RELAP5 codes, is a highly generic systems code that, in addition to calculating the behavior of the reactor coolant system (RCS) during a transient, can be used to simulate a wide variety of hydraulic and thermal transients in both nuclear and nonnuclear systems involving mixtures of vapor, liquid, noncondensable gases, and nonvolatile solutes.

RELAP5-3D is suitable for the analysis of all transients and postulated accidents in LWR systems, including both large- and small-break LOCAs, as well as the full range of operational and postulated transient applications. Additional capabilities include space reactor simulations, gas-cooled reactor applications, fast breeder reactor modeling, and cardiovascular blood flow simulations.

The RELAP5-3D code is based on a nonhomogeneous and nonequilibrium model for the two-phase system that is solved by a fast, partially implicit numerical scheme to permit economical calculation of system transients. The objective of the RELAP5-3D development effort from the outset was to produce a code that included important first-order effects necessary for accurate prediction of system transients, but that was sufficiently simple and cost-effective so that the conduct of parametric or sensitivity studies would be possible.

The code includes many generic component models from which general systems models can be developed and the progress of various postulated events can be simulated. The component models include pumps, valves, pipes, heat releasing or absorbing structures, reactor kinetics, electric heaters, jet pumps, turbines, compressors, separators, annuli, pressurizers, feedwater heaters, emergency core cooling (ECC) mixers, accumulators, and control system components. In addition, special process models are included for effects such as form loss, flow at an abrupt area change, branching, choked flow, boron tracking, and noncondensable gas transport.

The system mathematical models are coupled into an efficient code structure. The code includes extensive input-checking capability to help the user discover input errors and modeling and input inconsistencies. Also included are free-format input, restart, renodalization, and variable output edit features. These user conveniences were developed in recognition that the major cost associated with the use of a system transient code generally is in the engineering labor and time involved in accumulating system data and developing system models, while the computational cost associated with the generation of the final result is usually small.

6.2 Description of RELAP5-3D Plant Model

Plant system level calculations are required to evaluate the fuel rod burst potential for burnup extension under LOCA and other accident conditions. The reference system to be simulated in this work is a generic 4-loop PWR power plant based on STP with a rated thermal power of 3853 MW. The reactor system is simulated using RELAP5-3D with 1-D components and includes all of the main reactor features of importance when simulating LOCA scenarios. This includes a detailed representation of the primary

system (e.g., reactor vessel and internals, four independent loops with cold and hot legs, primary coolant pumps, and steam generators), pressurizer, and ECCS.

The secondary loop includes the secondary side of the four steam generators up to the main steam isolation valves. The auxiliary feedwater system was included in the secondary side modeling. The model is equipped with control logic to simulated automatic signals, and procedures adopted during LOCA.

The reactor core is simulated with six vertical pipe components (e.g., radially connected through cross-junctions) and six axial nodes. Each assembly is represented as two heat structures (one for the hot rod and one for the average rod). The hot rod is defined as the highest power rod in an assembly and the average rod represents the lumping of the remaining 263 rods in the assembly.

It is not practical to simulate every single fuel rod and all of the subchannels in a reactor core in plant level simulations using RELAP5-3D. Homogenization techniques are used in the reactor core simulations to reduce the number of fuel rods and flow channels to be simulated. The reactor core modeling in RELAP5-3D used different homogenization approaches for thermal fluid dynamics calculations than for the heat conduction and clad oxidation calculations in the fuel rods. A multiple channel approach was used for the thermal fluid dynamics calculation. Specifically, the assemblies in the core were grouped into various regions based on their burnup history. The assemblies with fresh fuel, once-burned fuel, and twice-burned fuel were grouped together, respectively. Two flow channels were built to represent each group of assemblies. Hence, there are a total of six flow channels in this study. The flow channels are connected in the lateral direction to allow crossflow to be calculated. Crossflow is modeled at each axial elevation in the core between the core channels. This allows the flow to be redistributed around a blockage caused by cladding ballooning or rupture. The crossflow area is based on the minimum gap between the fuel rods along one side of a fuel assembly and the number of fuel assembly sides at the interface between the core channels.

Two sets of heat structures were used for each assembly—one set represents the highest power rod or the hot rod in the assembly and the other set represents the average of the remaining fuel rods in the assembly. This is a reasonable approximation given that the fuel rod burnup normally does not vary too much within a PWR assembly and the hot rod in an assembly would be the limiting rod for that assembly. Each heat structure is comprised of six axial elements in order to partially capture the variations within axial power regions for each assembly. Each of these heat structures is connected to the appropriate hydrodynamic pipe component.

A simplified representation of the RELAP5-3D model of the reactor system is shown in Figure 72. The parameters within the RELAP5-3D input deck are vast and are not included here for the sake of brevity.

The LBLOCA scenario [39] considered is initiated by a double-ended guillotine break, as illustrated in Figure 73, in a cold leg between the reactor coolant pump and the reactor vessel. The cold leg is typically considered as the most limiting location as it limits the ECCS injection in the cold leg, it promotes flow stagnation in the core, and it causes ECCS injection bypass. Due to the pressure decrease, reactor and turbine trips follow. Simultaneously with the turbine trip, the offsite power is lost and the main recirculating coolant pumps start to coast down. Due to the loss of coolant, the core is uncovered. The water in the accumulators is injected to the primary loop when the accumulator pressure set point is reached. After a delay, the emergency diesel generators are started and the high-pressure injection systems, and later on low-pressure injection systems, start to inject water into the reactor core to quench the core. The entire accident consists of blowdown, refill, reflood, and long-term cooling phases.

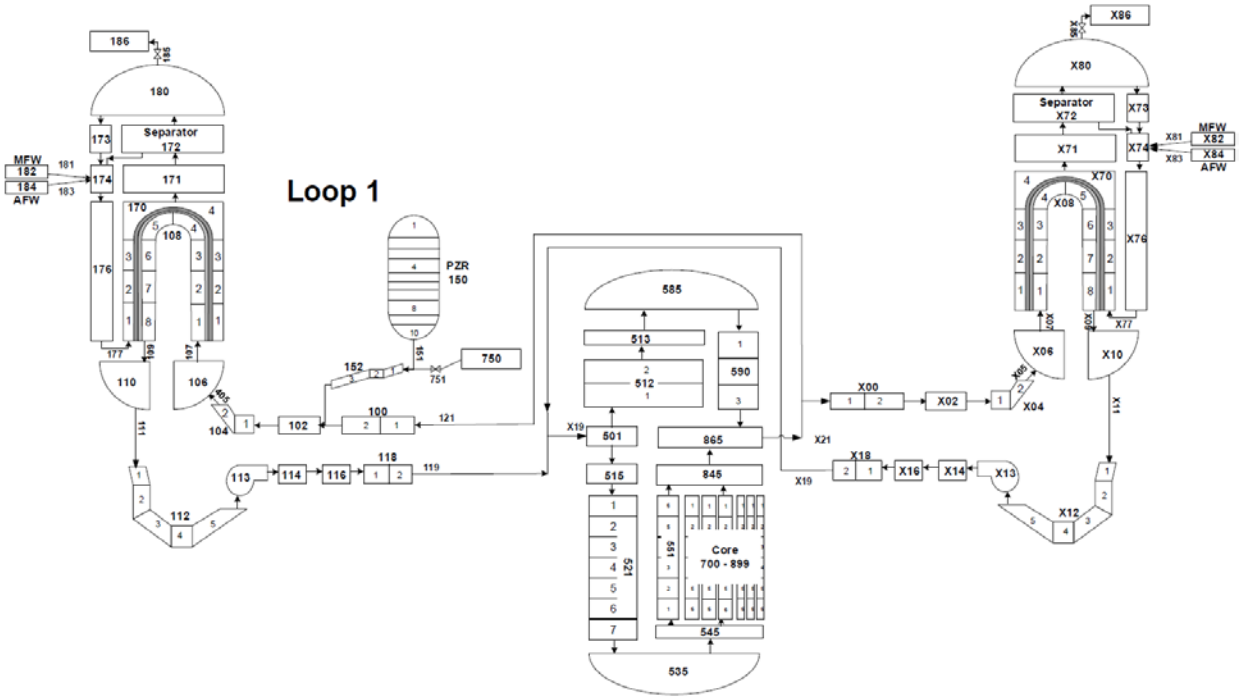

Figure 72. RELAP5-3D nodalization diagram of the generic 4-Loop PWR based on STP.

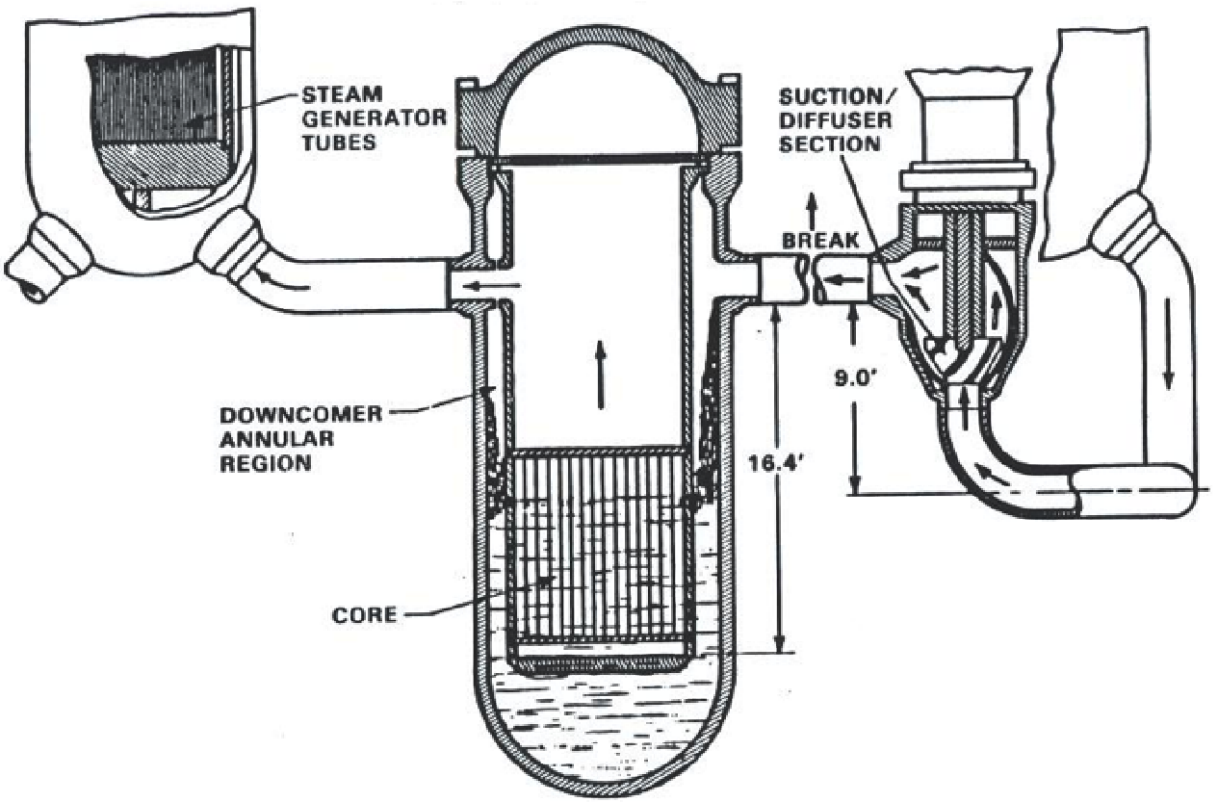

Figure 73. Schematic of double-ended guillotine break.

The blowdown phase occurs, between 0 and 30 seconds, as a result of a break in the coolant system through which the primary coolant is rapidly expelled. Within a fraction of a second after the break, the coolant in the core voids and goes through DNB, resulting in a sharp reduction in heat transfer to the coolant. The boiling and flashing, which occurs in the core as a result of the rapid depressurization, is sufficient to shut down the fission process due to negative reactivity feedbacks. No control rod insertion is credited in the event. Interactions between the primary pump and the break dynamics cause intermittent flow reversals. With the diminished cooling and the redistribution of stored energy in the fuel, the cladding heats up due to decay heat. The primary system pressure rapidly decreases and the high-pressure safety injection begins, but most of this flow is lost out of the break. The flow out of the break is large, but limited by critical flow phenomena. Injection from the cold-leg accumulators begins, but much of the injected flow is swept around the downcomer into the broken-loop cold leg and out the break. As the blowdown progresses, the RCS pressure decreases below the accumulator pressure. The accumulators begin injecting cold water into the cold legs, but the initial injection is swept out of the vessel and into the broken cold leg by the continuing high flow of steam from the core. This is called ECCS bypass. As the pressure decreases, the reversed flow induced by the break diminishes and positive core flow can be reestablished, while an increasing amount of the accumulator-injected coolant stays in the downcomer and some water begins to enter the lower plenum.

During the blow-down phase, the cladding temperature first rises rapidly as the initial stored energy in the fuel pellets is transferred to the cladding. After the initial heat-up, the cladding temperature will decrease due to the down flow of high velocity steam through the core. The lower power regions in the core may even quench during this blow-down cooling phase.

The refill period normally occurs between 30 and 40 seconds following the start of LBLOCA. The primary pressure has decreased to a level at which the low-pressure injection system activates and begins to inject water into the system. The lower plenum of the RPV begins to fill with accumulator water as coolant bypass diminishes. While refilling of the lower plenum is underway, however, the core heats up in a near adiabatic mode due to decay heat. Some fuel rods may balloon and burst, causing blockage of some of the flow channels during the refill of coolant.

The reflood phase occurs between 40 and 300 seconds. It begins when the lower plenum of the RPV has filled and the core begins to refill. Water injected by the accumulators fills the downcomer and creates the driving head for refilling the core. The lower elevations of the core quench, generating a two-phase mixture that provides some cooling to the upper elevations of the core. However, the fuel rods continue to heat up until the quench front begins to move upward through the core. Some additional number of fuel rods may balloon and burst during the reflood period. Zirconium-water reactions can occur for high temperature regions of the core. As the quench front continues to advance, the fuel rod upper elevations are cooled by a dispersed non-equilibrium two-phase mixture of superheated steam and entrained droplets. Eventually, there is sufficient cooling in advance of the quench front to terminate the increase in the cladding temperature. The cladding temperature starts to decease after the PCT is reached.

The fuel rod burst potential evaluations under LBLOCA conditions are done using BE and BEPU approaches. Section 6.3 presents the fuel rod burst criteria used in RELAP5-3D. Sections 6.4 and 6.5 present the details and results of these two approaches, respectively.

6.3 RELAP5-3D Fuel Rod Burst Criteria

The cladding deformation model in RELAP5-3D was used to evaluate the fuel rod burst potential. This model is an empirical model that accounts for the plastic deformation of the cladding in the calculation of the cladding of the fuel rod during LOCA simulations. This empirical model can be used to inform users of the possible occurrence of rod bursting and flow blockage. It is invoked in conjunction with the dynamic gap conductance model. More detailed simulations of the behavior of the fuel rods should be conducted once the possible occurrence of rod bursting is indicated. In the RELAP5-3D

cladding deformation model, the total cladding strain is the sum of the thermal strain, the creepdown strain, the elastic strain, and plastic strain.

The plastic strain is given by Eq. 7:

$$\varepsilon_p = 0.25\varepsilon_{rup}\exp\left[-0.0153(T_r - T_c)\right] \tag{7}$$

where ε_p is the plastic hoop strain before bursting (rupture), ε_{rup} is the cladding strain at bursting, T_r is the bursting temperature, and T_c is the average cladding temperature. The rupture temperature is given by Eq. 8:

$$T_r = 3960 - \frac{20.4S}{1+H} - \frac{8.51\times 10^6 S}{100(1+H)+2790S} \tag{8}$$

where S is the cladding hoop stress and $H = \frac{\min[heating\ rate)}{28\frac{C}{s}}, 1.0$.

The burst strain versus rupture temperature is shown in Figure 74.

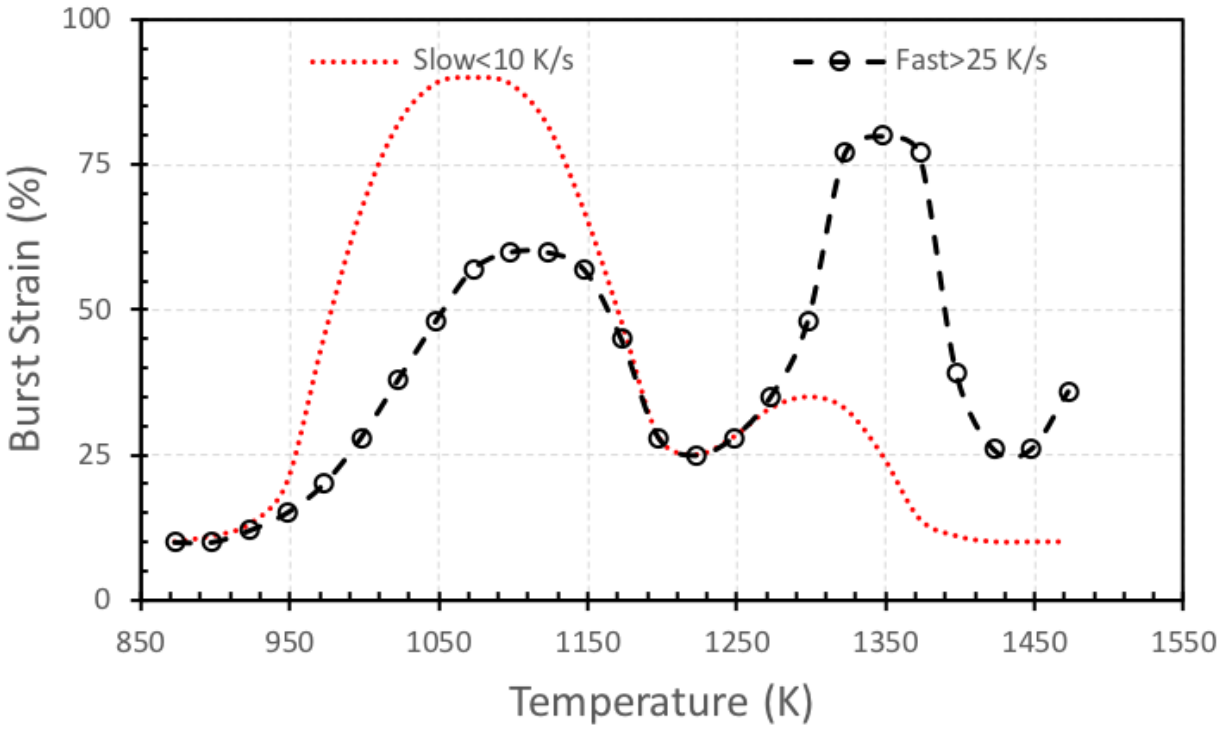

Figure 74. Burst strain criteria used in RELAP5-3D.

6.4 BE Calculations for Fuel Rod Burst Potential Evaluation

In the BE calculations, uncertainties on the input parameters and models are not considered; instead, all of the input parameters represent the true design parameters and operating conditions as close as possible. All of the calculation models and parameters in the core design, fuel performance, and systems analysis are BE ones.

The LBLOCA BE simulations using the RELAP5-3D code were driven by the LOTUS framework. The cladding deformation model in RELAP5-3D was used to evaluate the fuel rod burst potential. This model is an empirical model that accounts for the plastic deformation of the cladding in the calculation of the cladding of the fuel rod during LBLOCA simulations. It is invoked in conjunction with the dynamic gap conductance model. In the RELAP5-3D cladding deformation model, the total cladding strain is the sum of the thermal strain, the creepdown strain, the elastic strain, and the plastic strain. The burst strain versus rupture temperature is shown in Figure 74. The LBLOCA simulations were carried out at the BOC, Peak, MOC, and the EOC of the equilibrium cycle of core design.

Since the power peaking factors for Core Design Option 1 and Core Design Option 2 are high and they are unlikely to be adopted in the practical core designs, the fuel rod burst potential evaluations are not performed for these two core design options. Instead, the fuel rod burst potential evaluations using BE calculations are done only for Core Design Option 3, Core Design Option 4, and Core Design Option 5.

6.4.1 BE Rod Burst Evaluation for Core Design Option 3

In Core Design Option 3, there are 24 assemblies with 6% enrichment and 56 assemblies with 5% enrichment. The fuel rods have annular blanket regions on the top and the bottom, but with no reduction on fuel enrichment. The LOTUS-driven BE simulations of fuel rod bursting during LBLOCA using the RELAP5-3D are performed for Core Design Option 3. The PCTs calculated by RELAP5-3D for each assembly in the core at BOC, Peak, MOC, and EOC are shown in Figure 75, Figure 76, Figure 77, and Figure 78, respectively. The RELAP5-3D simulation results indicate that fuel rods would not experience any bursting at the BOC, Peak, and EOC. The highest burnup happens at EOC and none of the rods, including the twice-burned fuel on the periphery with burnup up to 75 GWd/MTU, would experience bursting under LBLOCA conditions, which indicates that fuel rod integrity is maintained with burnup extension. However, at MOC, the hot rod in four symmetric location assemblies experiences bursting, as indicated by the “yellow” color in Figure 77. The assemblies with hot rod bursting at MOC are the once-burned fuel assemblies with high power peaking factors and fuel rod internal pressure as shown in Figure 62. This indicates that the core design needs to be improved to reduce the peaking for the once-burned fuel to prevent clad bursting from happening.

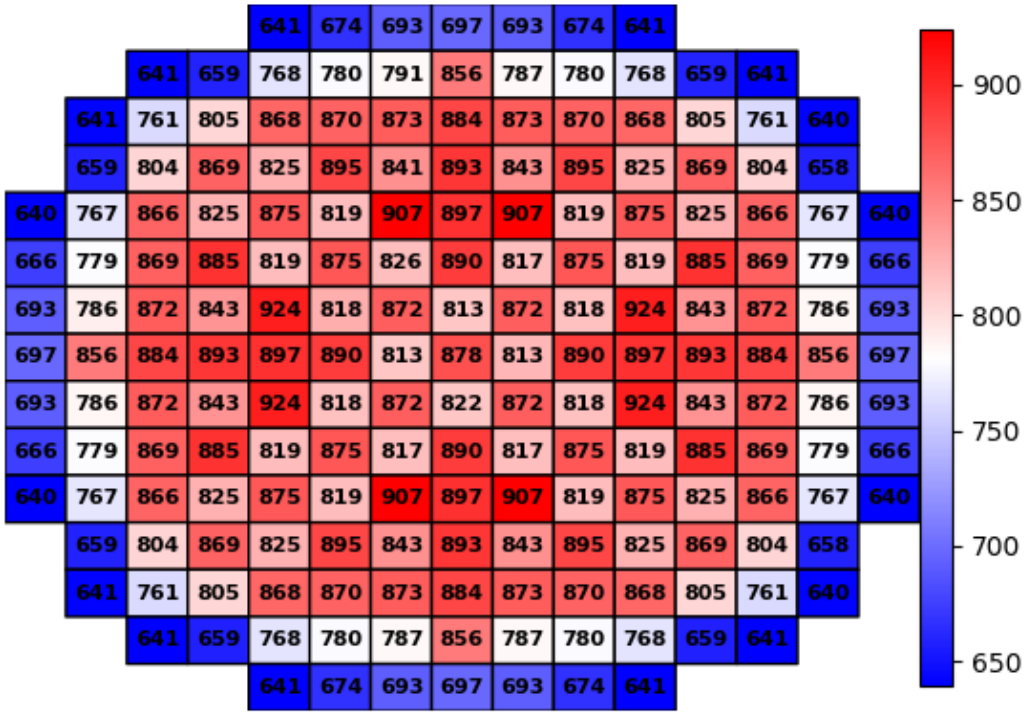

Figure 75. PCT in K for the hot rod in each assembly at BOC for Core Design Option 3. No rods experience bursting.

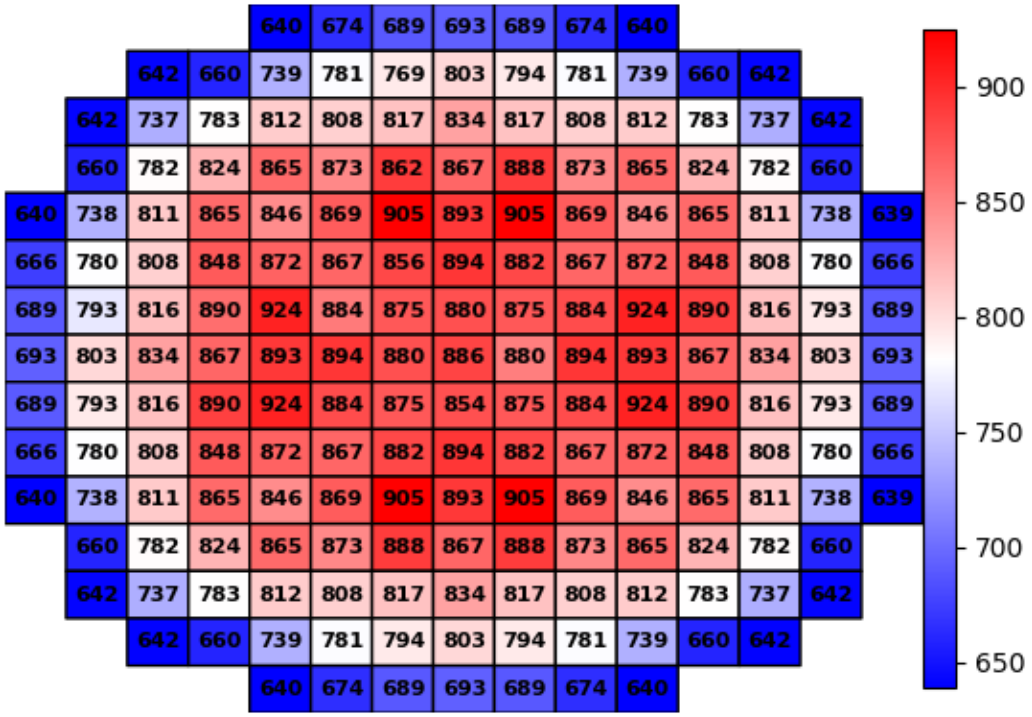

Figure 76. PCT in K for the hot rod in each assembly at Peak for Core Design Option 3. No rods experiencing bursting.

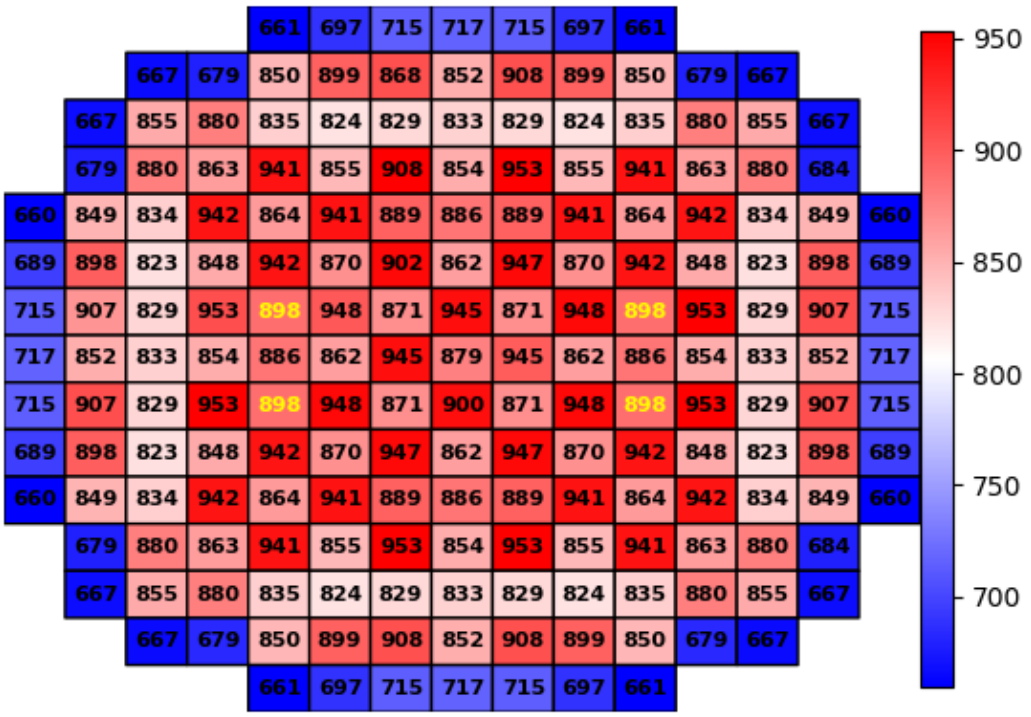

Figure 77. PCT in K for the hot rod in each assembly at MOC for Core Design Option 3. The hot rod in four symmetric assemblies experience bursting, as indicated by the “yellow” color.

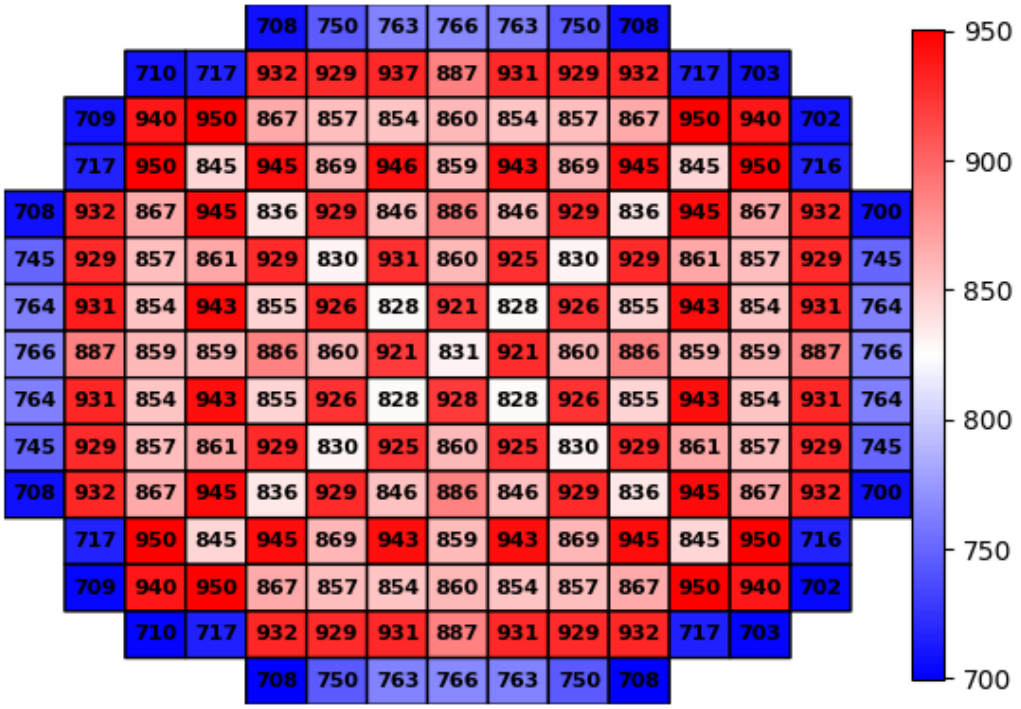

Figure 78. PCT in K for the hot rod in each assembly at MOC for Core Design Option 3. No rods experiencing bursting.

6.4.2 BE Rod Burst Evaluation for Core Design Option 4

In Core Design Option 4, the loading pattern is the same as that in Core Design Option 3. There are 8 fresh assemblies with 6 w/o enrichment loaded with gadolinia rods in Core Design Option 4. These 8 assemblies are placed adjacent to the once-burned assemblies (i.e., experience hot rod bursting at MOC in Core Design Option 3) to control the power peaking for those once-burned assemblies. The LOTUS driven BE simulations of fuel rod bursting during LBLOCA using the RELAP5-3D are performed for Core Design Option 4. Figure 79, Figure 80, Figure 81, and Figure 82 show the PCTs calculated under LBLOCA conditions by RELAP5-3D for each assembly in the core at BOC, Peak, MOC, and EOC, respectively, which were shown in Figure 75, Figure 76, Figure 77, and Figure 78 previously. The RELAP5-3D calculations indicate that no fuel rods experience bursting under LBLOCA conditions at BOC, the burnup state with the peak F_q value, MOC, and EOC. Adding gadolinia rods in the fuel assemblies is an effective means to control power peaking and remedy the potential for fuel rod bursting.

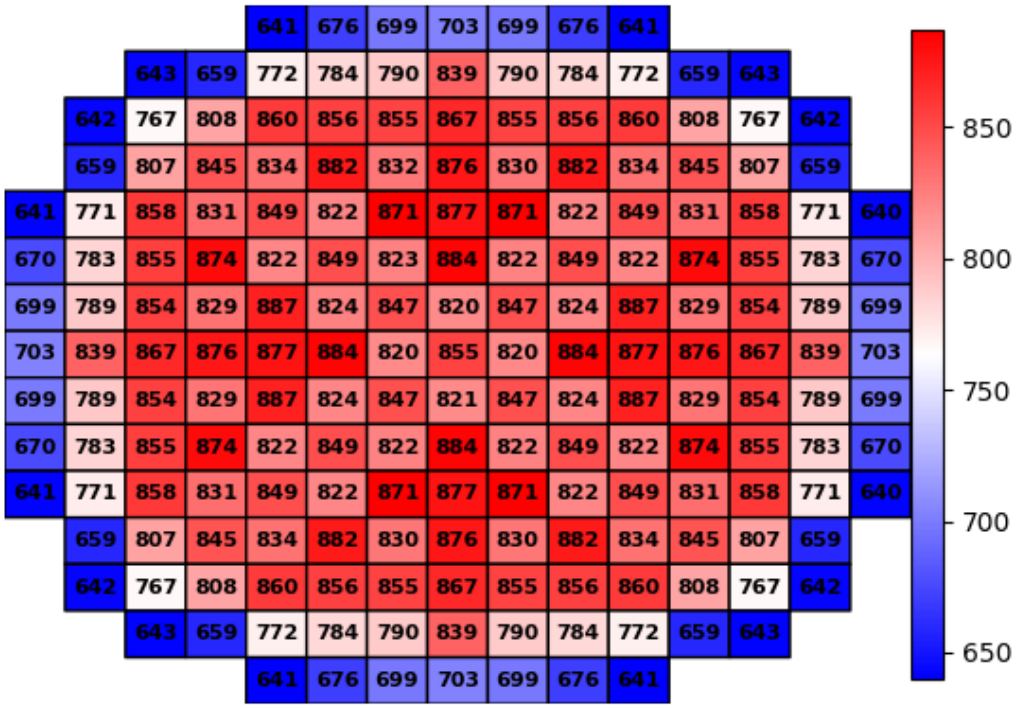

Figure 79. PCT in K for the hot rod in each assembly at BOC for Core Design Option 4. No rods experience bursting.

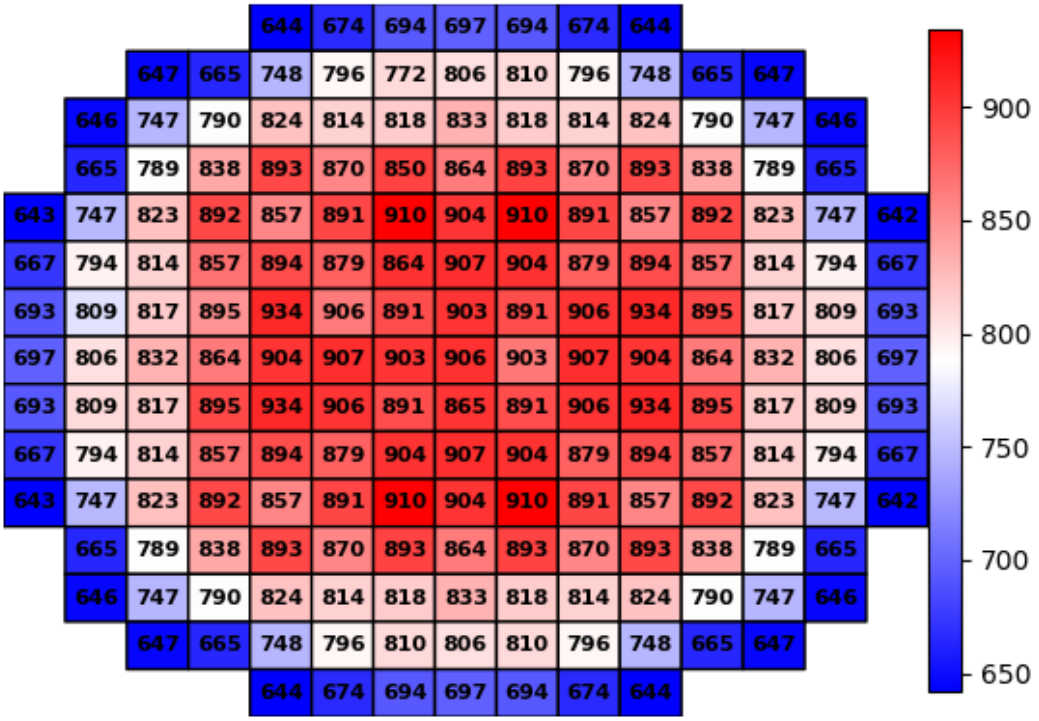

Figure 80. PCT in K for the hot rod in each assembly at the burnup state with maximum F_q for Core Design Option 4. No rods experience bursting.

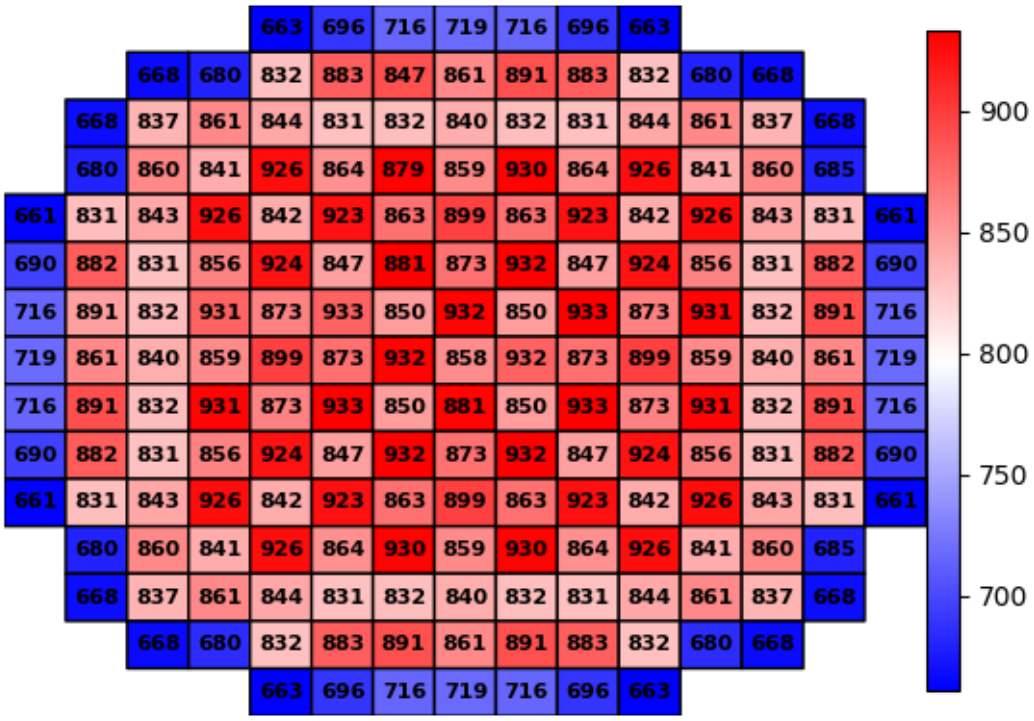

Figure 81. PCT in K for the hot rod in each assembly at MOC for Core Design Option 4. No rods experience bursting.

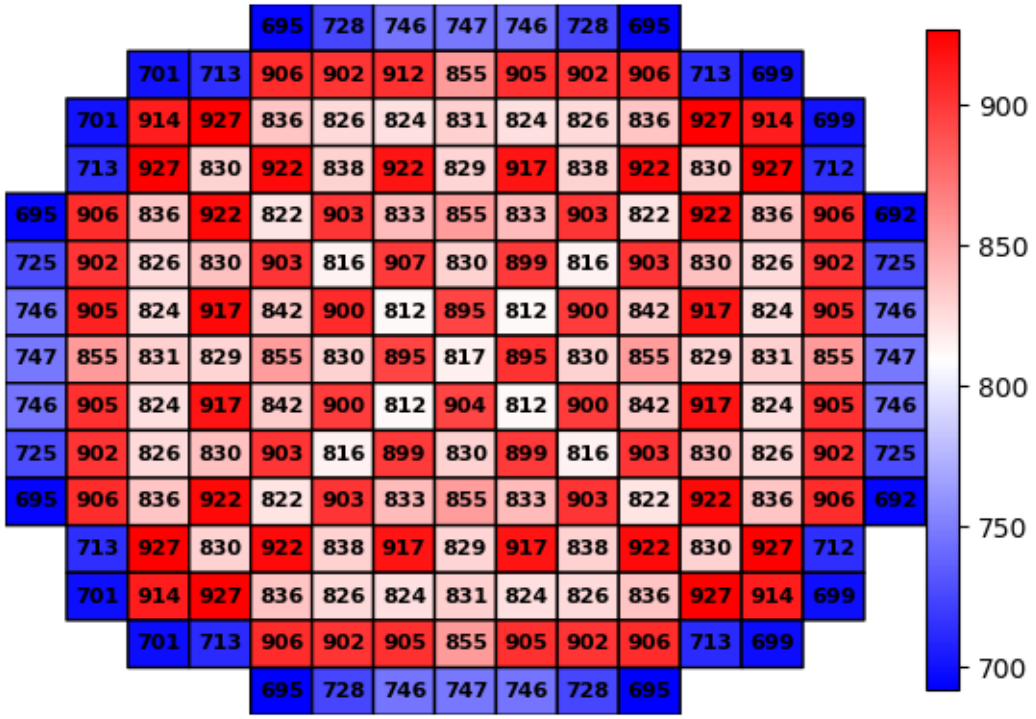

Figure 82. PCT in K for the hot rod in each assembly at EOC for Core Design Option 4. No rods experience bursting.

6.4.3 BE Rod Burst Evaluation for Core Design Option 5

In order to further flatten out the power distribution in the core to reduce the probability of fuel rod bursting, more assemblies with gadolinia rods are loaded in Core Design Option 5. In this core design option, 28 assemblies are loaded with gadolinia rods as compared to 8 assemblies with gadolinia rods loaded in Core Design Option 4. The LOTUS-driven BE simulations of fuel rod bursting during LBLOCA using the RELAP5-3D were performed for Core Design Option 5. The RELAP5-3D calculations were performed at the burnup state at the BOC, the peak F_q value, the MOC, and the EOC. The maximum PCTs calculated during LBLOCA for each assembly are shown in Figure 83, Figure 84, Figure 85, and Figure 86 for the burnup state at the BOC, the peak F_q value, the MOC, and the EOC, respectively. It is noted that the simulation results showed that no fuel rods experience bursting during LBLOCA in the equilibrium cycle of Core Design Option 5, with the fuel rod bursting criteria used in RELAP5-3D.

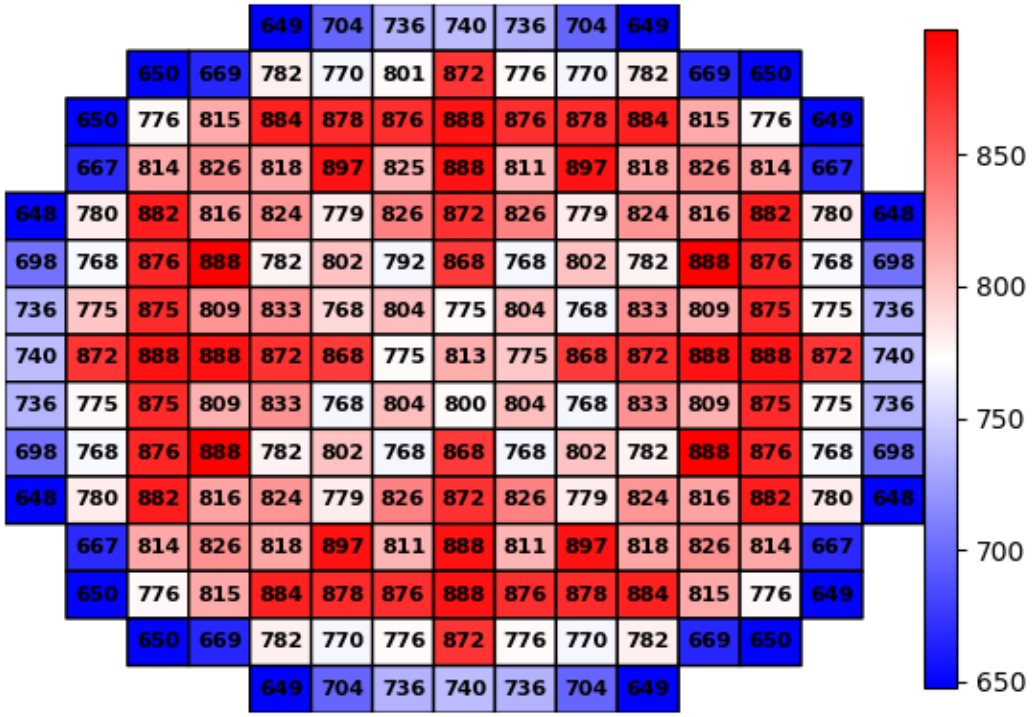

Figure 83. PCT in K for the hot rod in each assembly at BOC. No rods experience bursting.

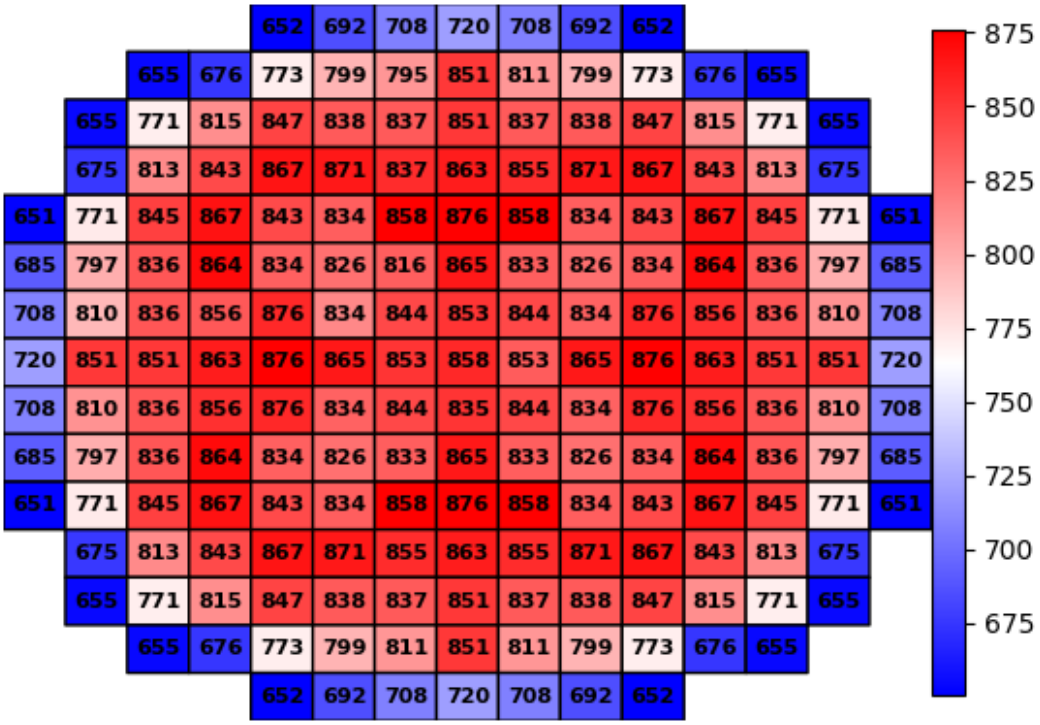

Figure 84. PCT in K for the hot rod in each assembly at Peak F_q. No rods experience bursting.

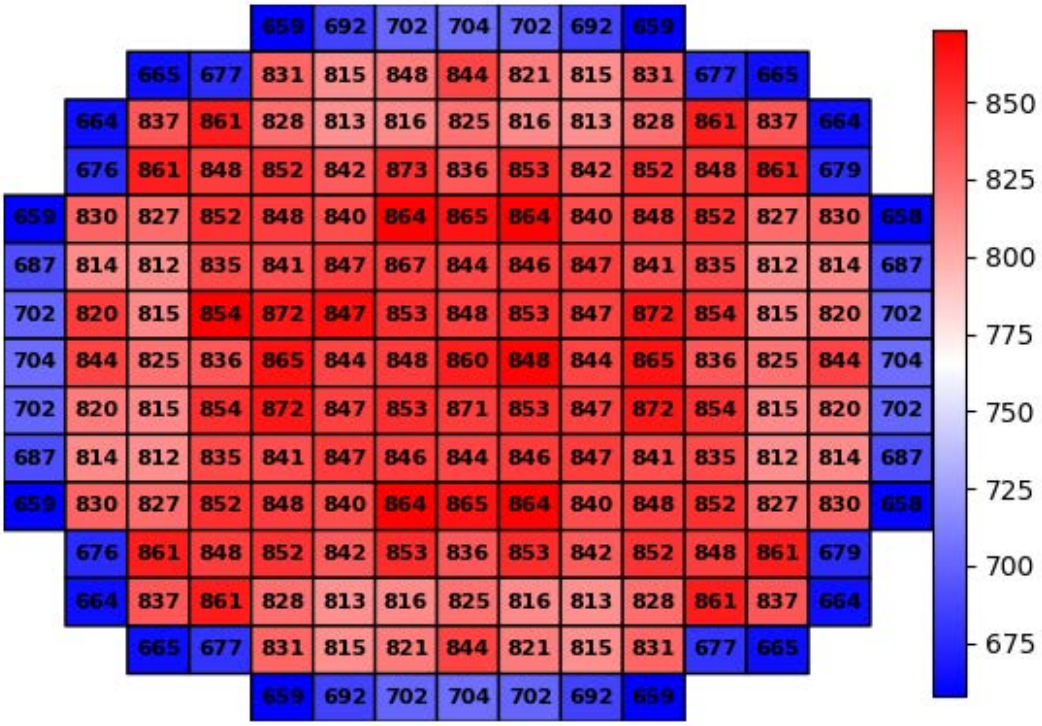

Figure 85. PCT in K for the hot rod in each assembly at MOC. No rods experience bursting.

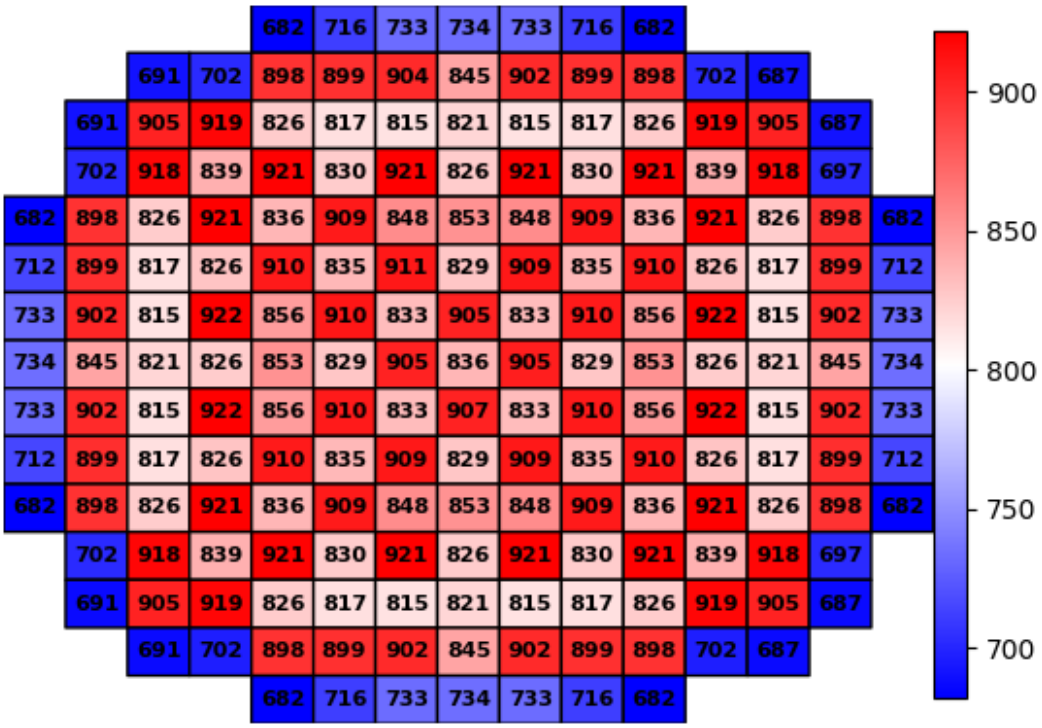

Figure 86. PCT in K for the hot rod in each assembly at EOC. No rods experience bursting.

The LOTUS-driven BE simulations of fuel rod bursting under LBLOCA conditions for Core Design Option 3, Core Design Option 4, and Core Design Option 5 indicate that by gradually improving the core design to lower the power peaking factors, the fuel integrity is better ensured by preventing fuel rods from bursting.

6.5 MP-BEPU Calculations for the Fuel Rod Burst Potential Evaluation for Core Design Option 5

Uncertainties exist in the models and parameters of computational codes; however, they are not considered in BE calculations. MP-BEPU analysis seeks to refine the analysis to return the margin to the operator and better characterize plant operation. It is noted that the BEPU methodology has become the de-facto industry standard to demonstrate compliance under the existing rule specified in 10 CFR 50.46. Key to the BEPU approach in margin characterization is the propagation of input uncertainties to statistics of the figures of merit (FOMs). Traditional approaches to quantifying uncertainty for NPP include the Wilks' method [40] and the more costly, but arguably more reliable, Monte Carlo method. Studies have suggested that while Wilks' method requires relatively few samples to produce statistics, the fluctuation of those statistics is significant; the Monte Carlo method, on the other hand, requires many samples to produce reliable statistics, but does so in a consistent and reliable manner. The MP-BEPU approach we developed in the LOTUS framework emphasizes on computer codes integration and on consistent uncertainty propagation in multi-physics simulations.

The MP-BEPU methodology consists of several sequential and logical steps in the evaluation process. The following provides a brief description of the major steps used in this work. It is noted that the MP-BEPU calculations are performed for Core Design Option 5 only.

6.5.1 Selection of a Plant Model, Accident Scenario and Figure of Merit

The plant selected for analysis in this work is the generic 4-loop PWR design based on STP with a rated thermal power of 3853 MW (see aforementioned discussions in this section). The accident scenario selected is a LBLOCA with a double-ended guillotine break in a cold leg. The thermal hydraulic system analysis code used is RELAP5-3D with its latest version of release. The FOMs are the generic acceptance criteria specified in 10 CFR 40.46 for the PCT. Another FOM is the ratio of bursting rods (RBR) in LBLOCA.

6.5.2 Identifying Relevant Physical Phenomena and Uncertain Parameters with Their Probability Distribution Functions

The important phenomena affecting the progression of the LBLOCA accident are normally determined by the phenomena identification and ranking table (PIRT) process. A large number of studies have been done previously that identified the important phenomena relevant to LBLOCA. The uncertainty ranges and distributions of relevant parameters were generated from past UQ/SA work on fuel performance [41], coupled thermal hydraulics and neutronics [42], and systems analysis [43]. It should be noted that many of the ranges of the perturbed inputs exclusive to RELAP5-3D were selected based off of common practices for expected uncertainties within thermal hydraulics (i.e., 30% uncertainty in heat transfer coefficients).

Table 19 provides a list of the common uncertain parameters with corresponding uncertainty ranges. The * in Table 19 indicates that the perturbed input of that row strongly influences the program of the corresponding column, despite it not being a direct input. For instance, the initial plenum fill gas pressure of FRAPCON is not inputted to RELAP5-3D; however, the plenum gas pressure at various states, which are highly dependent on the initial pressure, are included in RELAP5-3D input decks. The direct moderator heating fraction is also not directly supplied; however, the LOTUS scripts use the fraction in determining the portion of the core power to be placed in direct moderator heating within RELAP5-3D.

Lastly in the nominal value column, a '-' entry indicates that a continually varying value within the code is biased by a specified amount; thus, a nominal value does not exist.

Table 19. List of common uncertain parameters with corresponding uncertainty ranges.

Parameter	Nominal	Range (+/-)	Distribution	FRAPCON	RELAP5-3D
Fuel Radius	0.40956 cm	0.001 cm	Normal	X	X
Clad Outer Radius	0.47498 cm	0.002 cm	Normal	X	X
Clad Thickness	0.05715 cm	0.002 cm	Normal	X	X
Plenum Fill Gas Pressure	2.0 MPa	0.08 MPa	Normal	X	*
Percent Theoretical Density	94.5%	1.6%	Normal	X	X
Fuel Thermal Conductivity	-	10%	Normal	X	X
Core Power	3.85 GW	2%	Normal	X	X
Direct Moderator Heating	0.02	10%	Normal	X	*
Decay Heat Multiplier	1	0.06	Uniform		X
Accumulator Pressure	606 psi	10%	Normal		X
Accumulator Liquid Temperature	52.222°C (126°F)	13.889°C (25°F)	Uniform		X
Accumulator Liquid Volume	35.397 m^3 (1250 ft^3)	0.227 m^3 (8 ft^3)	Uniform		X
Sub-Cooled Counter Flow Multiplier (Pump Side)	1	0.2	Uniform		X
Two-Phase Counter Flow Multiplier (Pump Side)	1	0.2	Uniform		X
Super-Heated Counter Flow Multiplier (Pump Side)	1	0.2	Uniform		X
Sub-Cooled Counter Flow Multiplier (Vessel Side)	1	0.2	Uniform		X
Two-Phase Counter Flow Multiplier (Vessel Side)	1	0.2	Uniform		X
Two-Phase Counter Flow Multiplier (Vessel Side)	1	0.2	Uniform		X
Turbulence Heat Transfer Multiplier	1	0.3	Uniform		X
Nucleate Boiling Heat Transfer Multiplier	1	0.3	Uniform		X
Critical Heat Flux Multiplier	1	0.3	Uniform		X
Transition Boiling Heat Transfer Multiplier	1	0.3	Uniform		X
Film Boiling Heat Transfer Multiplier	1	0.3	Uniform		X

Parameter	Nominal	Range (+/-)	Distribution	FRAPCON	RELAP5-3D
Condensation Heat Transfer Multiplier	1	0.3	Uniform		X
Natural Convection Heat Transfer Multiplier	1	0.3	Uniform		X
Laminar Heat Transfer Multiplier	1	0.3	Uniform		X
Fuel Enrichment	2.6/4.2/4.6	0.003%	Normal	X	
Fuel Roughness	2.0 μm	0.33333 μm	Normal	X	
Clad Roughness	1.0 μm	0.2 μm	Normal	X	
Fuel Thermal Expansion	-	15%	Normal	X	
Fission Gas Release Biasing	-	+200%/-67%	Normal	X	
Fuel Swelling	-	20%	Normal	X	
Clad Creep	-	30%	Normal	X	
Clad Axial Growth	-	50%	Normal	X	
Clad Oxidation	-	40%	Normal	X	
Clad H2 Pickup	-	80 ppm	Normal	X	
Outlet Pressure	15.686 MPa (2275 psi)	2%	Normal	X	
Inlet Mass Flux	3533.596 kg/s-m^2 (2605453 lbm/hr-ft^2)	2%	Normal	X	

* Indicates inputs supplied to code are directly affected by perturbed value of row. Normal indicates truncated normal distribution of two standard deviations.

6.5.3 Developing Simulation Models for LBLOCA Analysis

The previous sections and this section have detailed descriptions of the simulation models. The simulation models for core design are presented in Section 6.5.4. The simulation models for fuel performance are presented in Section 5. The plant level simulation models are described in this section.

6.5.4 Random Sampling of Uncertain Parameters and Uncertainty Quantification

Generally, there are two types of methods that can be used to perform UQ within the context of BEPU, Wilks' method, and the direct Monte Carlo method. The Wilks' method is widely used with current industry practice to perform UQ. Wilks' method, originally proposed by S.S. Wilks in 1941 for use in manufacturing processes, is a nonparametric statistical analysis method that provides a bounding value of the samples with a given confidence level. This method can be referred to as the "distribution-free" method as well. Wilks' method entails finding tolerance limits for a population based off of a limited sample size. The method may be used for any output probability distribution function so long as it is continuous. While this is not technically true of floating point numbers, it is nevertheless a very fair assumption to treat code outputs as continuous variables. The Wilks' method randomly samples all of the uncertainty parameters in the space defined by the uncertainty ranges and all of the uncertainties are combined. However, it only uses a small number of samples to aggregate the effect of the uncertainty parameters to quantify the total uncertainty in the LOCA analysis. This method decouples the number of uncertain parameters from the number of required calculations in order to perform UQ analysis. It has the advantage of using a relatively small number of samples of LOCA transient calculations to obtain the limiting transient case, as well as the 95/95 (i.e., 95% probability with 95% confidence level) upper

tolerance limits of the FOM. A set of equations was derived through the number of required data samples that can be solved for a desired tolerance limit and confidence level. The equation for a one-sided tolerance limits is given as (Eq. 9):

$$1 - \beta^N > \gamma \tag{9}$$

where β is the desired probability of coverage, γ is the confidence level, and N is the minimum number of required data samples. If we are interested in finding out the minimum number of data samples for 95/95 upper tolerance limits, substituting β=0.95 and γ=0.95 in Eq. 9, and N is found to be 59. Eq. 9 is applicable to situations where only one outcome (e.g., PCT), is measured from the sample.

However, if more than one outcome is measured from the sample, then multidimensional bounds (i.e., rectangular bounds for two outputs, or cube bounds for three outputs such as the PCT, the ECR, and RBR) will be constructed. The required sample sizes and ranks must be modified. The number of runs can be found by solving the following equation for N [44] (Eq. 10):

$$\beta = \sum_{j=0}^{N-p} \frac{N!}{(N-j)!\,j!} \gamma^j (1-\gamma)^{N-j} \tag{10}$$

where p is the number of outcomes considered and N is number of required sample size. For evaluation of PCT and RBR ($p = 2$), Eq. 10 indicates that if a β of at least 0.95 is desired with no lower bounds and the highest, and the second highest values have been set as upper bounds for the first and second outputs, respectively, then a sample size of at least 93 is required. In order to ensure outputs are treated equally, it has become a common practice in the nuclear safety community to take the highest rank of all outputs as bounds [13]. While this is more conservative, it still qualifies as bounding 95% or more of the population with *at least* 95% confidence.

In the previous practice of LOCA analysis, the limiting fuel rod in the limiting transient case can be easily identified with the safety metric being defined as the PCT and the limiting rod as the fuel rod with the highest PCT, which is normally the highest power rod (hot rod) in the core. The reactor core modeling in a LBLOCA analysis normally uses a simplified approach with the core flow represented by a hot channel and an average channel. The hot channel represents the flow channel adjacent to the highest power rod and the average flow channel represents the remaining flow in the core. The fuel and clad temperature distributions and clad oxidation rates within the hot rod are calculated by building a heat structure for the rod and attaching it to the hot channel. Average heat structures are built for the remaining fuel rods in the core and attached to the average flow channel, such that the fuel and clad temperature distributions and clad oxidation rates can be calculated for the average rods.

In the present work of evaluating fuel rod bursting potential, PCT and RBR are the FOMs. Since fuel rod bursting involves complex mechanisms and is dependent on local power peaking and fission gas release, the limiting rods may not be the hot rods and could even move from certain fuel rod locations to others depending on fuel burnup and other conditions in an operating cycle. Therefore, all of the fuel rods have to be considered in LOCA analyses in order to identify the limiting cases.

The acceptance criteria for the safety metrics are the following:

1) PCT_{max} < 2200 F
or
2) RBR < Criterion TBD

It is noted that the ratio (or percent) of bursting rods is not in the NRC's acceptance criteria. It is used only as a FOM to demonstrate the percentage of the potentially failed rods in LBLOCA.

Using the above criteria, the limiting fuel rods can be identified as the fuel rods with the maximum PCT value (PCT_{max}) or the maximum RBR value (RBR_{max}) during LOCA transients. Using Wilks' theorem, compliance can be demonstrated by ranking the PCT and the RBR obtained from the simulations in the 93 samples. The highest ranked set of PCT and RBR from the 93 samples can be chosen as the limiting cases to represent the 95/95 estimates of the upper tolerance of the chosen FOMs from a small sample.

Despite the widespread adoption of the Wilks' method by the industry, the use of small sample sizes to infer statement of compliance to the 10 CFR 50.46 rule has been a major cause of unrealized operational margin in today's BEPU methodology. With a small sample size, the Wilks' method has the risk of under-prediction or over-prediction of FOMs. Additionally, reliable sensitivity analysis results are not attainable with a small sample size to gain the insights in what is truly limiting in the design in order to assess the impact of design changes. Moreover, the debate on the proper interpretation of Wilks' theorem in the context of safety analyses is not fully resolved yet, more than two decades after its introduction in the nuclear industry. This represents both a regulatory and operational risk in rolling out new methods.

The direct Monte Carlo approach offers a robust alternative to perform UQ within the context of BEPU analyses. The direct Monte Carlo method simply samples the input distributions a large number of times (*N*) and then uses computer codes to generate *N* output files, which are then used to generate the distribution of safety metrics or FOMs. The direct Monte Carlo method requires formidable computing resources if directly using system analysis codes and is considered to be impractical for industrial applications in the past. Lately, with the ever-increasing computing power, this approach has the potential to be widely adopted by the industry. It should be pointed out that using the direct Monte Carlo method, very large sample sizes may be needed to reduce the confidence interval on the estimate of FOMs to the desired magnitude. However with the direct Monte Carlo simulations, SAs can be performed such that the impact and significance of input parameter changes can be assessed with high confidence. With the Monte Carlo method, the common "95/95" estimators of the upper tolerance limits for FOM (e.g., PCT, RBR) can be constructed. The 95/95 estimators are compared to the 10 CFR 50.46 or the proposed 10 CFR 50.46(c) rules to demonstrate compliance. According to Ref. [45], the 95% values with 95% confidence interval can be expressed as Eq. 11:

$$Y_{95/95} = \mu_{95\%} \pm 1.96 * SE_{Q95\%} \tag{11}$$

$$SE_{Q95\%} = 2.11 * SE_M \tag{12}$$

where $\mu_{95\%}$ is the 95th percentile values of PCT and RBR, and SE_M is the standard error of the sample mean value.

6.5.5 Determining the Limiting Values of the FOM

The Monte Carlo based uncertainty quantification was performed with 300 perturbed cases for 4 states: BOC, Peak (state corresponding to maximum core peaking), BOC, and MOC. The results of these cases were then ranked with respect to peak clad temperature (PCT). The 95/95 values were then taken as the 95th percentile case, or the 285th highest case. The results for this UQ are summarized in Table 20.

The core temperature map of the 95/95 case for each state are shown in Figures 87 through 90. Note that the PCT with respect to state does not follow a clear trend. This is likely due to the serendipitous nature of the 95/95 value for a sample size of 300. This stochastic behavior eclipses the smaller trend attributable to changes in core peaking. The trend is also further obscured by the somewhat arbitrary partitioning of heat structures with respect to core coolant channel within RELAP5-3D.

It is worth noting that no bursting occurs at the 95/95 PCT case at EOC. This is due to bursting being heavily dependent on both systems level thermal hydraulics and fission gas release biasing. While the 95/95 PCT case at EOC results in relatively high temperature boundary conditions for the cladding, this particular case was supplied low fission gas release biasing from the global Monte Carlo sampling, resulting in a significantly lower plenum pressure.

Table 20. 95/95 PCT values for each state.

State	PCT 95th Percentile	+/- 95% Confidence Interval
BOC	935.336 K (1223.935 °F)	7.447 K (13.405 °F)
Peak	932.485 K (1218.803 °F)	6.753 K (12.155 °F)
MOC	952.222 K (1254.329 °F)	7.149 K (12.868 °F)
EOC	967.925 K (1282.595 °F)	7.548 K (13.586 °F)

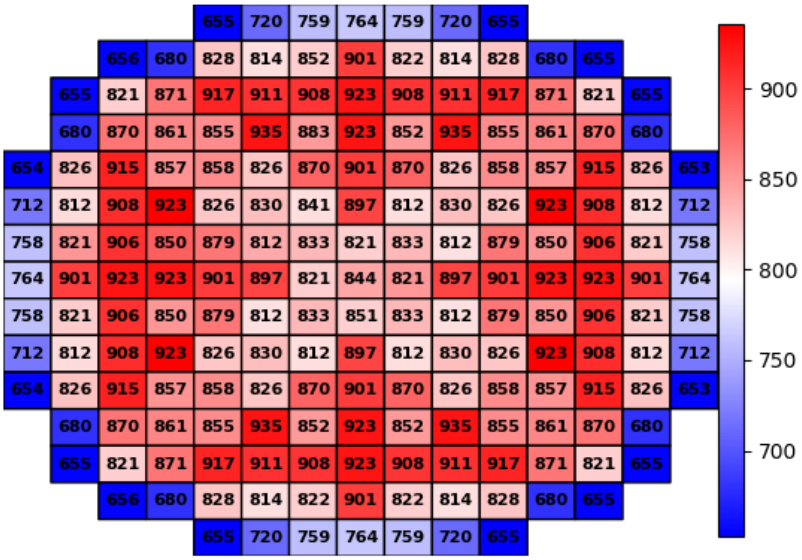

Figure 87. PCT in K for the hot rod in each assembly at BOC for PCT 95/95 Case. No rods experience bursting.

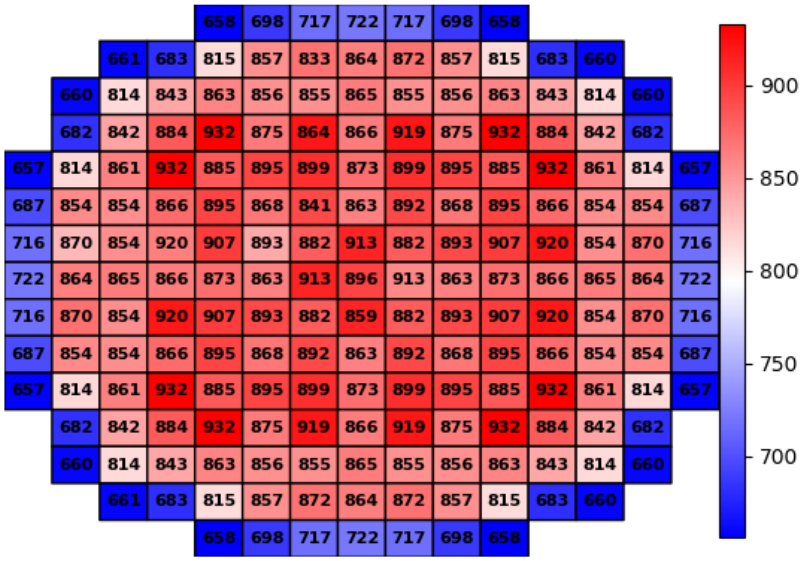

Figure 88. PCT in K for the hot rod in each assembly at Peak for PCT 95/95 Case. No rods experience bursting.

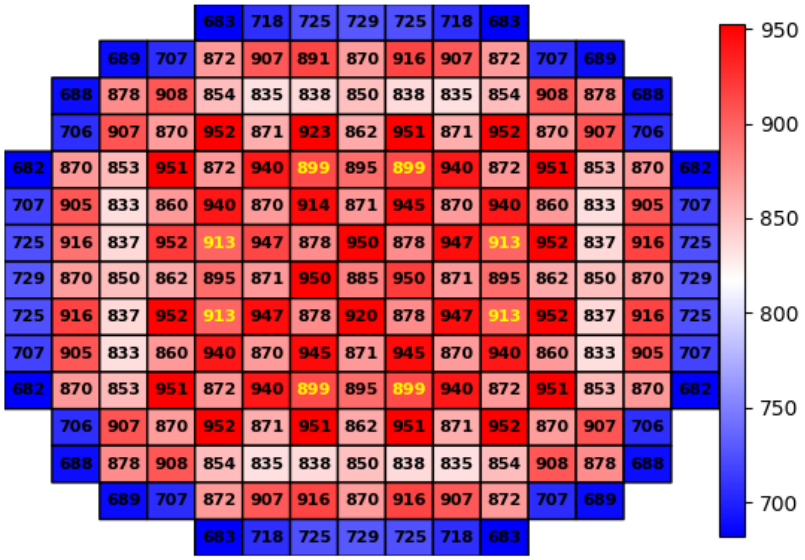

Figure 89. PCT in K for the hot rod in each assembly at MOC for PCT 95/95 Case. Rods with bursting indicated in yellow.

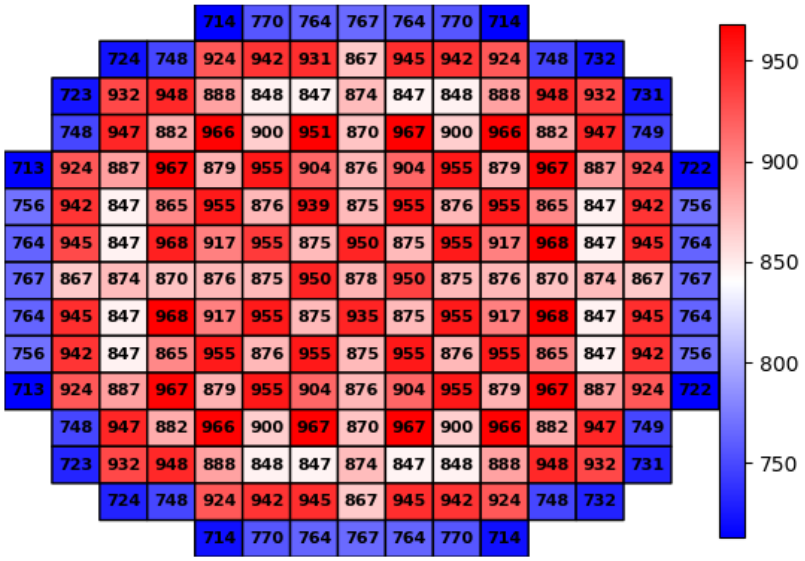

Figure 90. PCT in K for the hot rod in each assembly at EOC for PCT 95/95 Case. No rods experience bursting.

The Monte Carlo based UQ was also applied to the ratio of bursting rods (RBR). In this work, three different methods are used for estimating this value based off the available RELAP5-3D data. The input decks used by this work assign two heat structures to each assembly, one representing the hot rod, the other representing the average rod. The RELAP5-3D output files indicate if these heat structures had any bursting. From these 2x193 heat structures, one can provide reasonable estimates for what ratio of the 264x193 rods experienced bursting.

The first estimate (RBR I) serves as a lower bound. Since the assemblies are 1/8 symmetry, it is assumed that if the hot rod bursts, at least 8 rods in the assembly burst. If both the hot and the average rod burst, it is assumed that the 8 average rods, plus all other rods with greater power, also burst (136/264).

The second estimate (RBR II) is the most reasonable given the amount of data. RBR II assumes that if the hot rod bursts and the average rod does not, then half of the rods burst. This is safe to assume due to the fact that if the mean rod doesn't burst, any rod from the lower half of the pin power rankings is not likely to burst either. If both hot and average burst, then all rods are assumed to have burst. In reality, the true RBR is between RBR I and RBR II.

RBR III serves as an upper bound. If the hot rod bursts, then all rods in the assembly are assumed to have burst. The average assembly burst data is not used in this estimation. This assumption yields the most conservative estimate possible for the available data.

The 95/95 RBR values are summarized in Table 21. Note that Eq. 5 and 6 are assume a Gaussian distribution, which is obviously not the distribution for any of the RBR metrics. Incorporating a more universal Monte Carlo based UQ will be a focus of future research. The 95/95 cases at both BOC and Peak contain no rods with bursting. MOC and EOC both show rods with bursting for their 95/95 cases. The ranking of these cases has a small amount of subjectivity, due to the fact that many cases have an identical amount of rods with bursting. For this work, cases with an identical amount of bursted rods

were ranked on a secondary criterion of PCT. Note that this secondary criterion has no effect on the RBR 95/95 values, only on the selection of the limiting cases for core visualization. Due to BOC and Peak not experiencing bursting, no graphical representation is necessary. The RBR 95/95 cases for MOC and EOC are shown in Figures 91 and 92. Since the real RBR is between RBR I and RBR II, it can be deduced from Table 21 that the probability (with 95% confidence) of fuel rod bursting is less than 2.22% at MOC and less than 3.49% at EOC.

Table 21. 95/95 RBR values for each state

State	RBR I 95th Percentile (If hot rod bursts, 8 symmetric rods in an assembly would burst)	RBR I +/- 95% Confidence Interval	RBR II 95th Percentile (If hot rod bursts, half of the rods in an assembly would burst)	RBR II +/- 95% Confidence Interval	RBR IIII 95th Percentile (If hot rod bursts, all rods in an assembly would burst)	RBR III +/- 95% Confidence Interval
BOC	0.0 %	0.0017 %	0.0 %	0.0286 %	0.0 %	0.0571 %
Peak	0.0 %	0.0047 %	0.0 %	0.0775 %	0.0 %	0.155 %
MOC	0.126 %	0.00907 %	2.07 %	0.149 %	4.15 %	0.297 %
EOC	0.188 %	0.0229 %	3.11 %	0.378 %	6.22 %	0.756 %

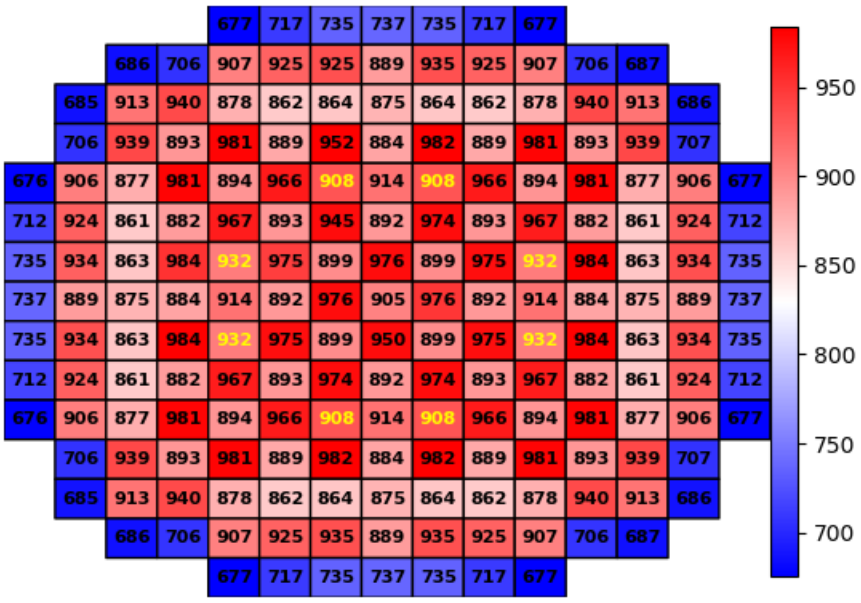

Figure 91. PCT in K for the hot rod in each assembly at MOC for RBR 95/95 Case. Rods with bursting indicated in yellow.

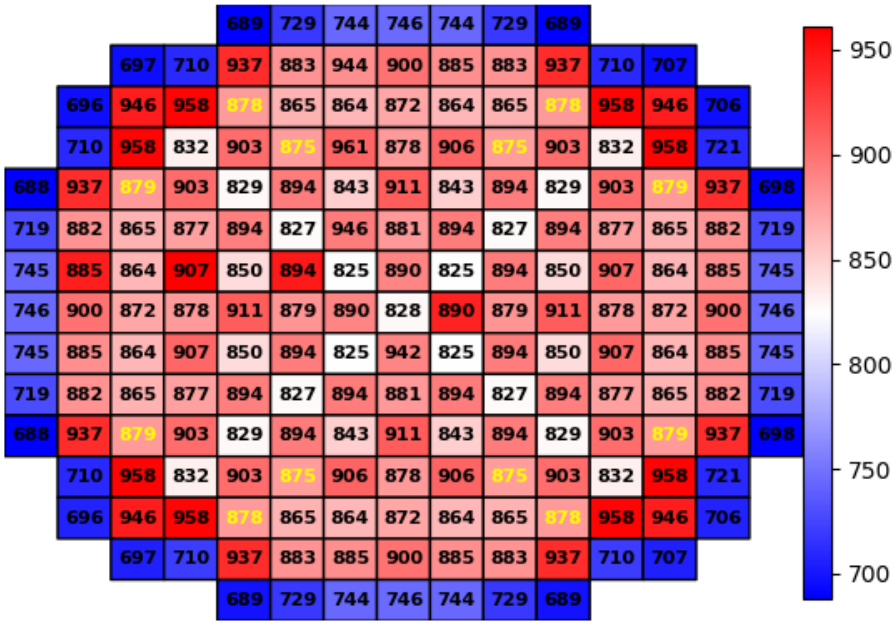

Figure 92. PCT in K for the hot rod in each assembly at EOC for RBR 95/95 Case. Rods with bursting in yellow.

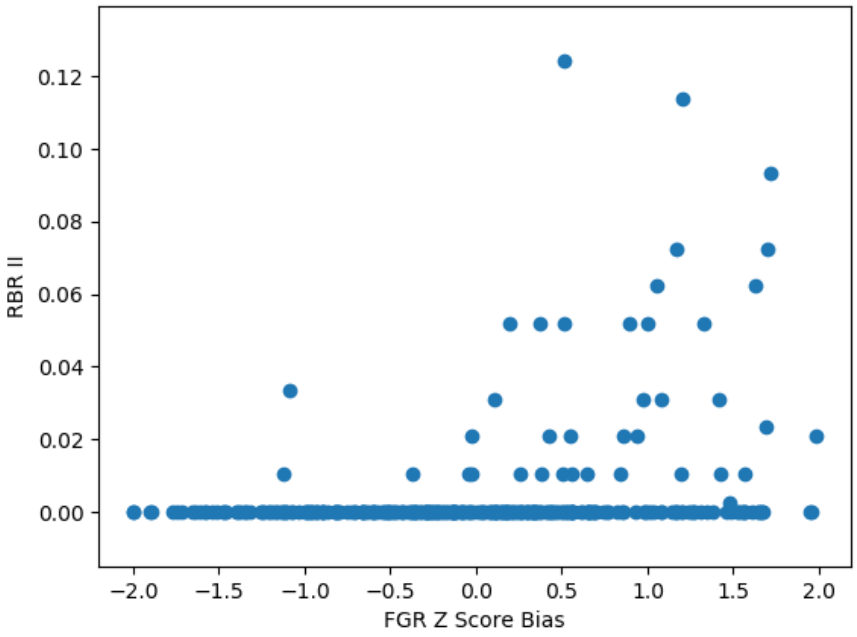

Figure 93. of Bursted rods versus fission gas release Z score bias at EOC.

A plot of the RBR II criteria versus the Z score for fission gas release biasing at EOC is given in Figure 93. The Z score of a given instance of a random variable is the difference between said instantiation and the statistical mean, all over the standard deviation of the random variable. For the fission gas release model of FRAPCON, a Z score range of -2 to 2 corresponds to the fission gas diffusion coefficient being biased between 33% and 300% of the nominal value. Note that nearly all cases with negative fission gas release biasing do not contain bursting. Furthermore as the biasing increases the bursting becomes more common. Thus the bursting behavior of rods with higher burnup design is heavily influenced by fission gas release biasing.

There are three primary methods of alleviating the fission gas release problem for future designs. The first is to reduce fission gas diffusion by modifying the power history to avoid high linear heat rates at high burnup. The second is to increase the available gas volume within the clad. This may be accomplished by increased plenum length, gap sizes, fuel annulus dimensions, and pellet chamfers and shoulders. Lastly, the incorporation of new fuel materials outside of traditional ceramic fuel may reduce the production and release of fission gas products.

7. FUEL ROD BURSTING POTENTIAL EVALUATION USING BISON

BISON [11] is a finite element-based nuclear fuel performance code applicable to a variety of fuel forms, including LWR fuel rods, tristructural isotopic (TRISO) particle fuel, and metallic rod and plate fuel. This advanced fuel performance code is being developed at INL and offers distinctive advantages over FRAPCON/FRAPTRAN, such as 3-D simulation capability, etc. BISON solves the fully coupled equations of thermomechanics and species diffusion for either 1-D spherical, 2-D axisymmetric, or 3-D geometries. Fuel models are included to describe temperature and burnup dependent thermal properties, fission product swelling, densification, thermal and irradiation creep, fracture, and fission gas production and release. Plasticity, irradiation growth, and thermal and irradiation creep models are implemented for clad materials. Models also are available to simulate gap heat transfer, mechanical contact, and the evolution of the gap/plenum pressure with plenum volume, gas temperature, and fission gas addition. BISON has been coupled to the mesoscale fuel performance code, MARMOT [46], demonstrating its fully coupled multiscale fuel performance capability. BISON is based on the Multi-Physics Object-Oriented Simulation Environment (MOOSE) framework [47]; therefore, BISON can efficiently solve problems using standard workstations or very large high-performance computers. BISON is currently being validated against a wide variety of integral LWR fuel rod experiments.

7.1 Cladding Burst Failure Models in BISON

Criteria to determine the occurrence of cladding burst (rupture) are available in BISON [48]. More precisely, the cladding burst of Zircaloy-4 claddings during LOCA can be predicted by the use of four different burst criteria: (1) overstrain; (2) overstress (OS); (3) plasticity instability (PI); and the combination of OS/PI. These four correlations are described in the following sections.

7.1.1 OS Criterion

When the OS burst criterion is used, it is assumed that failure will occur when the local hoop stress σ_θ exceeds a limiting burst stress σ_b [49] (Eq. 13):

$$\sigma_\theta \geq \sigma_b \tag{13}$$

The burst stress σ_b depends on the temperature and oxygen concentration in the cladding, which is defined as (Eq. 14):

$$\sigma_b = a * e^{(-bT)} * e^{[-(\frac{\eta-\eta_0}{9.5*10^{-4}})^2]} \tag{14}$$

where T (K) is temperature, η is the current weight fraction of oxygen picked up in the cladding, and a and b are material dependent constants. A set of constants based on an evaluation of Zircaloy-4 high-temperature burst data by Erbacher and co-workers [49] is listed in Table 20. The values for the a and b parameters are given in Table 20 for material parameters depending on the phase. In the mixed phase (α+β) region, linear interpolations of ln(a) and b are made between the values for pure α and middle of α+β (50%α 50%β) phase, and between 50%α 50%β and pure β phase.

Table 22. Material parameters used to calculate the burst stress of Zircaloy-4.

Zr Phase	Temperature region (K)	a (MPa)	b (K^{-1})
α	$< T_\alpha = 1085$	830	$1 \cdot 10^{-3}$
50%α–50%β	$T_{\alpha\beta} = 1166$	3000	$3 \cdot 10^{-3}$
β	$> T_\beta = 1248$	2300	$3 \cdot 10^{-3}$

The current oxygen weight fraction η may be determined through (Eq. 15):

$$\eta = \frac{2r_{clad,\,outer}}{\rho_{Z_{y*}(r^2{}_{metal,\,outer} - r^2{}_{clad,\,inner})}} \times g + \eta_0 \tag{15}$$

in which η_0=1.2·10^{-3} is the oxygen weight fraction at fabrication.

Under low-stress situations, OS criterion may lead to non-conservative predictions [50]. To overcome this drawback with the OS failure criterion, a PI criterion was developed.

7.1.2 PI Criterion

PI is another burst mechanism, which can be triggered upon attaining a limiting value for the effective plastic (including creep and plasticity) strain rate (Eq. 16):

$$\dot{\varepsilon}_{pl,eff} \geq \dot{\varepsilon}_b \tag{16}$$

in which $\dot{\varepsilon}_{pl,eff}$ is the effective plastic strain rate, and $\dot{\varepsilon}_b$is the limiting strain rate. In BISON, the limiting value $\dot{\varepsilon}_b = 100\ h^{-1} \cong 2.78 * 10^{-2} s^{-1}$ is adopted from data by Marcello et al. [50].

7.1.3 Combination Failure Criterion

A combination of OS and PI criterion establishes that cladding burst occurs when either condition of OS or PI is fulfilled. The combined failure criterion is recommended, especially in low-stress situations when the load on the cladding changes relatively suddenly, such as during a power ramp or scram. Thus, the prediction of failure occurrence avoids unsafe predictions in low-stress situations as a consequence of non-negligible strain rate. These three ballooning/burst models implemented in BISON have been validated to several separate-effects of ballooning/burst tests [51, 52]. In general, the combination of OS/PI is recommended as the failure criterion for clad during transient conditions.

7.1.4 Overstrain Criterion

Cladding burst can also be studied through an overstrain criterion, in which cladding burst occurs once the permanent engineering total hoop strain (i.e., creep) exceeds 40%. In BISON, the true strain is used, and therefore, the permanent engineering hoop strain limit is converted through Eq. 17:

$$\varepsilon_{hoop,limit} = ln(1.0 + 0.4) = 33.6\% \tag{17}$$

where burst occurs if $\varepsilon_{hoop} \geq \varepsilon_{hoop,limit}$. Note that this overstrain burst criterion is overly too simplified and the effect of temperature is not considered. For more realistic studies of the burst mechanism, the overstrain model is not recommended.

Note that these burst criteria implemented in BISON are purely empirical, which means they are either too simplified as with the overstrain failure criterion or derived by fitting correlations to different sets of experientially measured data on cladding burst as with other three criteria.

7.2 Fuel Rod Bursting Evaluation using BISON for Core Design Option 3

The fuel rod burst mechanisms under LBLOCA conditions were evaluated through the BISON simulations for Core Design Option 3. Unlike the simplified fuel rod deformation model used in RELAP5-3D, BISON provides more mechanistic modeling of the fuel rod bursting.

7.2.1 Methods and Boundary Conditions

The main parameters to simulate a full-length fuel rod with burnup extension are listed in Table 23. Specifically, the cladding is ZIRLO with UO_2 fuel in a 17x17 fuel assembly design based on the STP NPP. For this special STP NPP, the total active fuel column length is 4.267 m, which is distinguished from the commonly used value of 3.658 m. As listed in Table 23, the cold plenum length is 323.2 mm, which includes the original cold plenum length in the core design of 203.2 mm and the correction of 120 mm by taking into account the contribution from by the top annular pellets as blankets, dish of pellets, and wire spring. Two types of enrichment used in the STP NPP are 6.0% for fresh and once-burned fuel and 5.0% for twice-burned fuel. In Table 23, 6.0% enrichment is used to simulate once-burned fuel.

Table 23. Fuel rod parameters used in BISON.

Parameter	Value
Pellet outer radius (mm)	4.096
Pellet quantity	434
Pellet height (mm)	9.832
Cladding thickness (mm)	0.57
Top/bottom cladding thickness (mm)	2.24
Gap thickness (side) (mm)	0.084
Gap thickness (bottom) (mm)	1
Total (active) fuel column length (m)	4.267
Cold plenum length (mm)	323.2
Enrichment (%)	6.0/5.0
Pellet density (%TD)	94.5
Cladding type	Zirlo

During a LBLOCA scenario, it is anticipated that internal pressurization and high temperature may eventually induce cladding OS. The combined effect of the outward creep deformation of the cladding tube and OS may lead to cladding ballooning and burst. Thus, a failure criterion for clad during transient conditions is required to analyze the fuel rod behavior under accident conditions. Four fuel rod burst criteria are used in this comparative study: (1) overstrain; (2) OS; (3) PI; and (4) the OS/PI combination.

In order to reliably predict the thermo-mechanical behavior and integrity (deformation and burst) of the full-length nuclear fuel rods during accidents, it is a pre-requirement to complete BISON simulation during normal reactor operation. The final outputs from these BISON simulations will serve as the initial inputs for the followed LBLOCA simulations. In addition, in order to perform a realistic fuel rod analysis under LBLOCA, specific user inputs to control the BISON simulations are also required. In particular, five boundary conditions (BCs) are generated by VERA-CS for steady-state and RELAP5-3D for LBLOCA as user inputs. The first BC is the power, which is associated with an LWR fuel rod and is typically given as rod averaged linear power (or linear heat rate) in units of kW/m or W/m and a function of time. During the LBLOCA, the power is switched into the decay heat. The power should vary in time

and space, which leads to the second BC, the axial variation in power. It is given as a scaling factor as a function of distance from the bottom of the rod and time, and it is fixed in the BISON simulations during both normal reactor operation and LBLOCA. Fast neutron flux is the third BC, which is supplied by VERA-CS for steady-state and set to zero during LBLOCA condition. The last two BCs are coolant temperature and pressure, which are as a function of distance from the bottom of the rod and time.

For the steady-state BISON simulations, all five BCs are the outputs from the simulations of CASL's VERA-CS code. Under the LBLOCA scenario, four BCs are the outputs from RELAP5-3D simulations, except the BC of neutron flux, which is zero. For the MOC case, among three types of fuel (e.g., fresh, once-burned, twice-burned), according to RELAP5-3D failure criteria, only once-burned fuel was predicted to burst during LBLOCA. The corresponding BCs are shown in Figure 94 and Figure 95 for steady-state and LBLOCA, respectively.

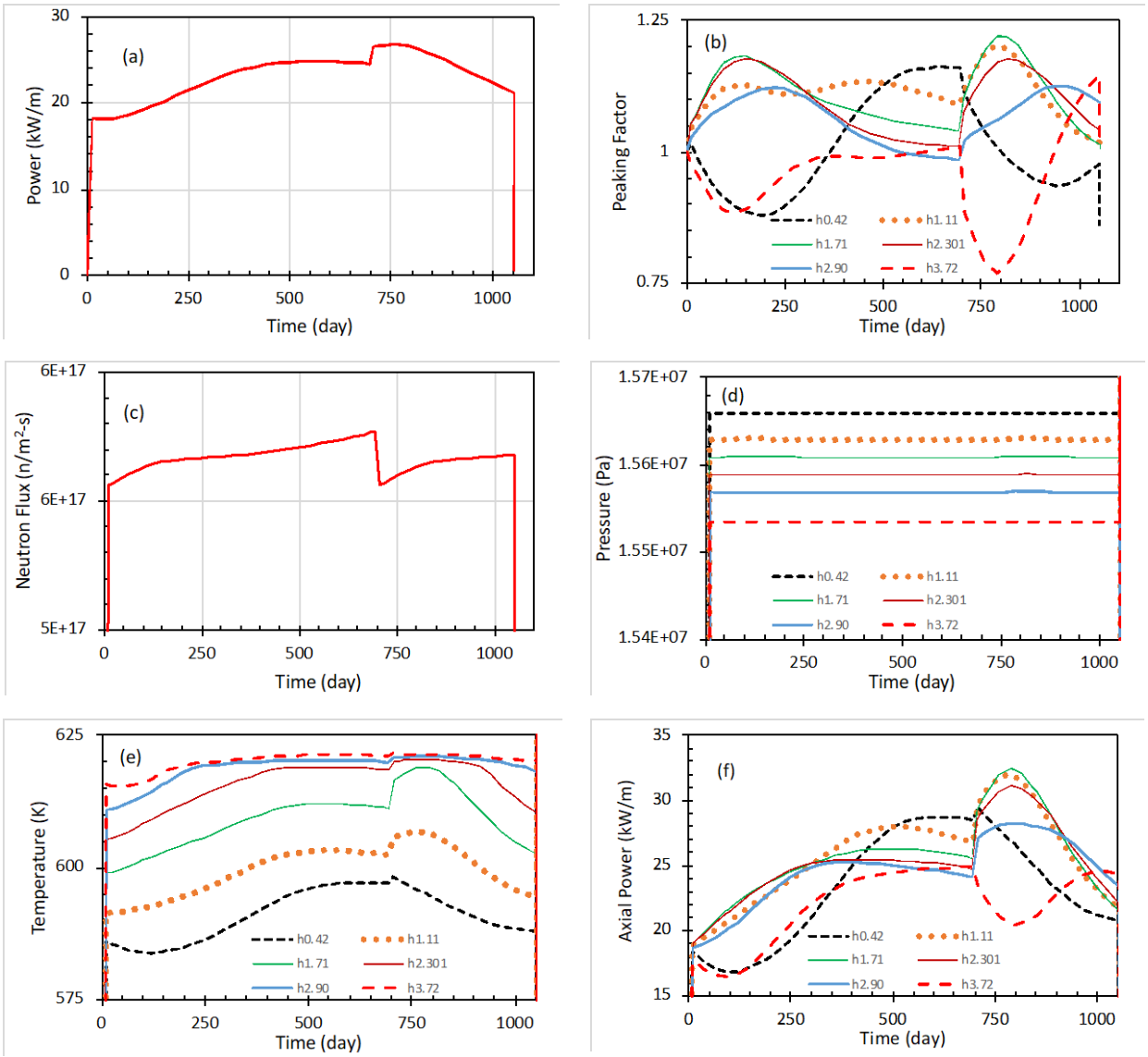

Figure 94. Five BCs are generated by VERA-CS for steady-state for the full-length fuel rod after one cycle of normal operation with burnup extension (~2 years) until MOC for (a) average linear power (heat rate); (b) axial peaking factor; (c) fast neutron flux; (d) coolant pressure; (e) coolant temperature; and (f) axial average power.

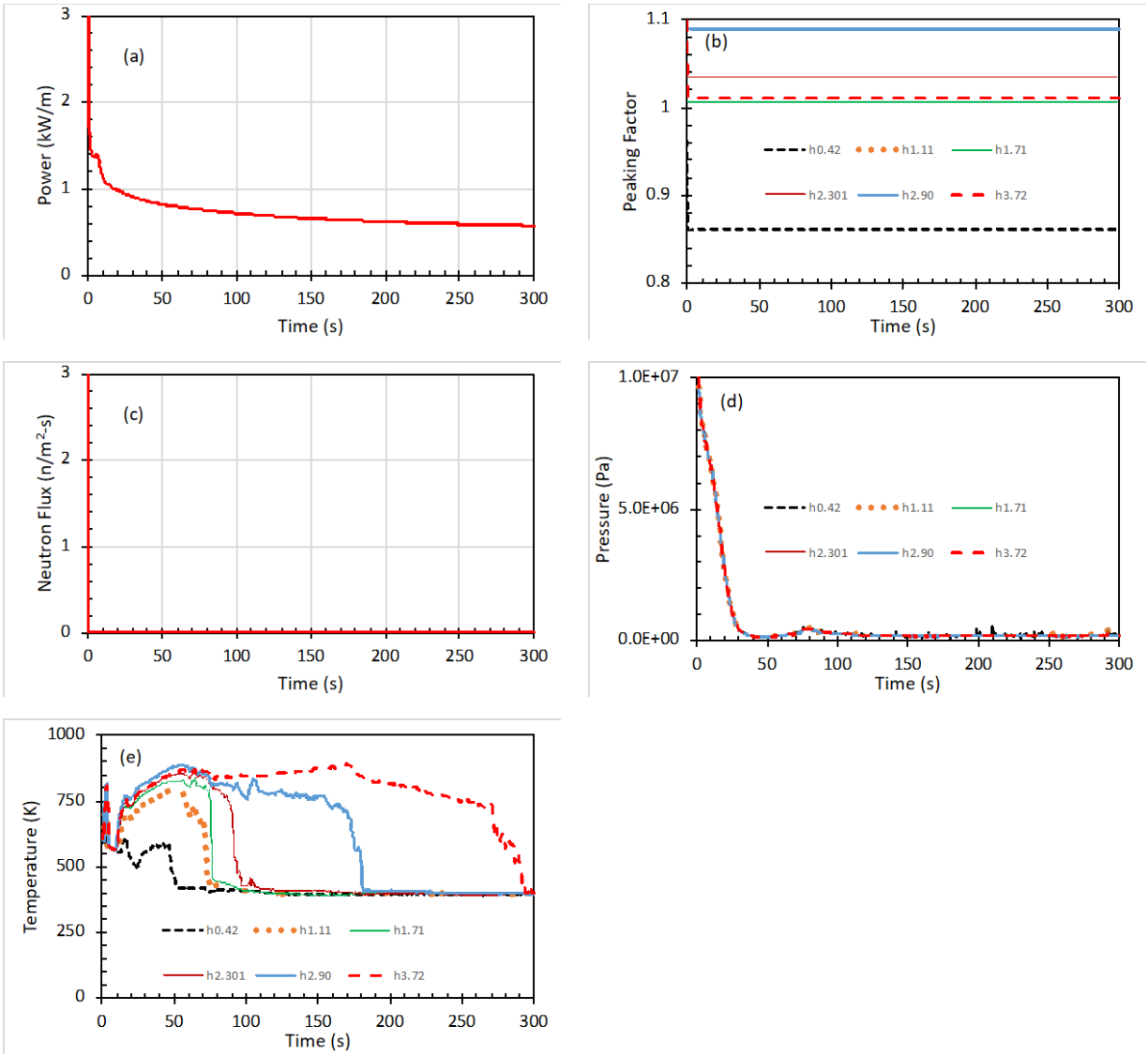

Figure 95. Five BCs for LOCA for (a) the power; (b) peaking factor; (c) fast neutron flux; (d) coolant pressure; and (e) coolant temperature. Zero in the LOCA time is the beginning of LOCA and the end of the steady-state. Four BCs are generated by RELAP5-3D, except for the BC of neutron flux.

7.2.2 Fuel Rod Burst Evaluation Results and Discussion

Fuel temperature is a primary factor determining the thermal and mechanical performance of a fuel rod. Figure 96 shows the maximum temperature evolution of fuel and cladding in the steady-state (left) and LOCA (right). It can be seen that, in the steady-state, the maximum cladding temperature around 650 K is quite stabilized in the whole steady-state operation. This indicates the BC of coolant (or outer cladding surface) temperature as shown in Figure94(e) carries away the heat generated by the fuel well. Meanwhile, the maximum fuel temperature increases from ~1150 K to ~1572 K on the 695th day near the end of the first cycle. However, there is a significant fuel temperature increase around 700 days and reaches the peak value of ~1868K on the 810 day. At the end of MOC in the steady-state operation, the maximum fuel temperature decreases to ~1650 K, which may be higher than the expected fuel temperature (~1350 K). It is interesting to note that the maximum fuel temperature profile is very similar

with the axial average power profile as shown in Figure94(f). Thus, it suggests that the fuel temperature is determined by the power distribution strongly.

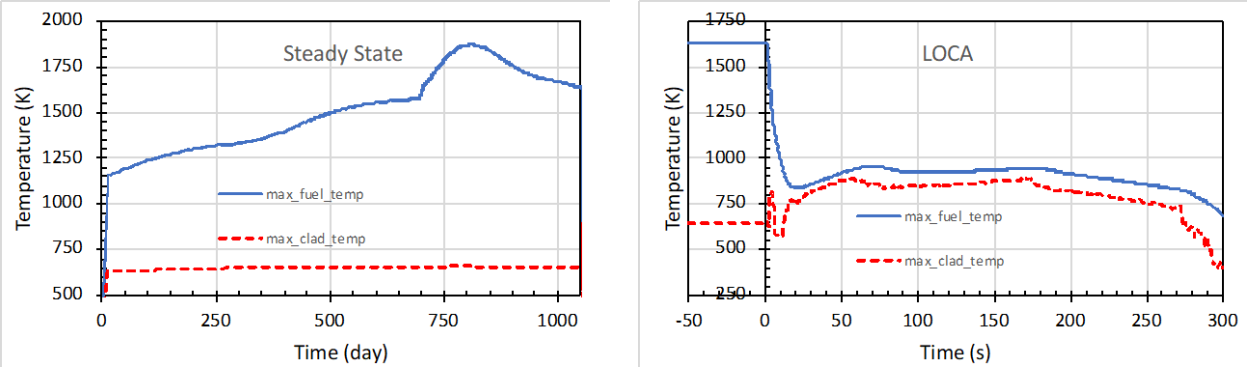

Figure 96. Maximum temperature evolution of fuel and cladding in the steady-state (left) and LOCA (right) with the Core Design Option 3. Zero in the LOCA time is the beginning of LOCA and the end of the steady-state operation.

As LBLOCA starts after the reactor scram, the maximum fuel temperature drops rapidly from ~1650 K at the steady-state to below 1000 K in a few seconds, then stays below 1000 K until the end of LBLOCA. Meanwhile, the maximum cladding temperature initially increases from about 650 K to ~790 K in five seconds, then drops to below 575 K at 11 seconds. This corresponds to the blow-down phase, the cladding temperature first rises rapidly as the initial stored energy in the fuel pellets is transferred to the cladding. After the initial heat-up, the cladding temperature will decrease due to the down flow of high-velocity steam through the core. The lower power regions in the core may even quench during this blow-down cooling phase, the maximum cladding temperature located in the upper region will increase after 11 seconds, as shown in Figure 96. The maximum fuel temperature is at least 50 K than the maximum cladding temperature during LBLOCA, no matter which phase it has reached (i.e., blow-down, refill, and reflood).

Cladding hoop stress and plenum pressure are another two critical factors determining the thermal and mechanical performance of a fuel rod. Figure 97 shows the evolution of the maximum cladding hoop stress and plenum pressure evolution in the steady-state (left) and LBLOCA (right). In the steady-state, the maximum cladding hoop stress is near zero (below 16 MPa) for ~435 days, increases to the peak value of ~203 MPa on the Day 810, then decreases to ~114 MPa at the end of MOC. Meanwhile, the plenum pressure increases slowly from ~6 MPa in the beginning of steady-state to ~22 MPa at the end of MOC. As shown in the left side of Figure 97, the evolution of the maximum cladding hoop stress is very similar with the axial average power profile, as shown in Figure 94(f). Thus, it is expected that the cladding hoop stress is determined by the power distribution strongly.

As LOCA starts after the reactor scram, the plenum pressure drops from ~22 MPa at the steady-state to below 6 MPa in end of LOCA. Meanwhile, the maximum cladding hoop stress initially decreases from about 114 MPa to ~62 MPa at 11 seconds, then increases to ~92 MPa at 30 seconds. This indicates that in LBLOCA, the maximum cladding hoop stress is determined by the coolant temperature, as shown in Figure 95(e), significantly. Meanwhile, corresponding to the blow-down phase, the initial stored energy distribution may not play significant role on cladding hoop stress in LBLOCA.

Under LBLOCA, it is expected to observe significantly higher RIP (i.e., plenum pressure) and cladding temperature. However, with the current Core Design Option 3, we didn't observe such behavior under LBLOCA. In contrast, significantly higher hoop stress and fuel temperature were observed in the steady-state, induced by the axial average power. Thus, it is crucial to optimize power distribution in order to keep the maximum RIP and temperature below a limit value for the operational safety.

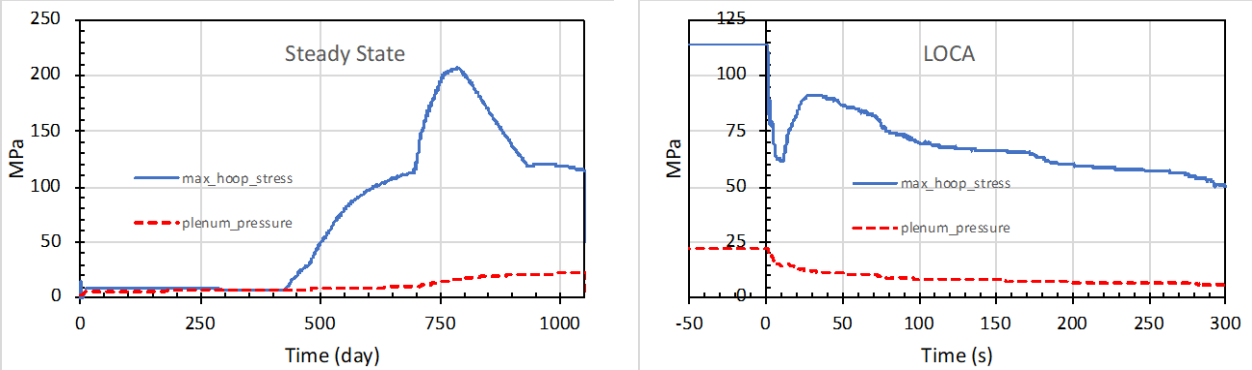

Figure 97. Evolution of max hoop stress and plenum pressure in the steady-state (left) and LOCA (right) with the Core Design Option 3. Zero in the LOCA time is the beginning of LOCA and the end of steady-state operation.

The hoop stress depends on the temperature and oxygen concentration in the cladding. Under LBLOCA, it may reach extremely high value at some locations, leading to rod burst as local hoop stress exceeds a limiting burst stress. Although cladding burst was predicted by RELAP5-3D with this core design for the burnup extension, bursting was not observed using BISON with BCs provided through RELAP5-3D and VERA-CS.

7.2.3 Fuel Rod Burst Evaluation Results and Discussion

As found in the previous section, the BC of coolant temperature in LBLOCA is paramount since it determines the cladding hoop stress and whether or not the fuel rod will burst. With the current Core Design Option 3, no rod burst is observed as local hoop stress never exceeds the limiting burst stress in LBLOCA. Thus, it is important to evaluate sensitivity measures of the importance of parameter uncertainties for the uncertainties of the results; in this case, the coolant temperature in LOCA. Here the margin to acceptance criterion on coolant temperature is performed.

Figure 98 shows the profile of shifted coolant temperature in LBLOCA at the pellet height of 3.73 m. Zero in the LOCA time is the beginning of LBLOCA and the end of the steady-state operation. The unshifted coolant temperature generated by RELAP5-3D is marked as 0 K.

Figure 99 shows the results of failure time based on the cladding burst under LOCA predicted by BISON for different burst mechanisms driven by the shifted coolant temperature, as shown in Figure 46. The shifted temperatures are 50, 100, 150, 200, and 250 K, respectively. Four different burst criteria: (1) overstrain; (2) OS; (3) PI; and (4) the combination of OS/PI were utilized. Furthermore, these four burst models also take into account the contributions of the β-phase and/or high-temperature oxidation, which form four combinations. These four combinations are applied to the PI and overstrain criteria. For the OS and OS/PI models, the only result is presented with the β-phase. Since the β-phase must be considered in the OS and OS/PI models implemented in the BISON code, no data is available for the cases of either high-temperature oxidation only, or no choice of high-temperature oxidation and the β-phase. As both oxidation and the β-phase are taken into account in the OS and OS/PI models, the rod is predicted to burst even in the steady-state, which suggests that the oxidation in the OS and OS/PI models is not suitable to study LBLOCA, even in the steady-state. Thus, there are a total of ten cases.

As one can see, when coolant temperature is only shifted by 50 K, no burst is observed by BISON among ten cases of four failure criteria. When coolant temperature is shifted by 150 K or more, burst is observed by BISON among ten cases of four failure criteria, and the burst time is less than 50 seconds. When the coolant temperature is shifted by 100 K or more, both burst (~ 50 seconds) and no burst are observed. Thus, it seems that the margin for coolant temperature is between 50 K and 150 K.

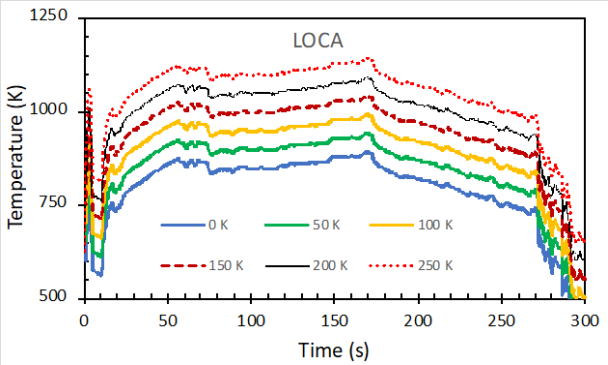

Figure 98. The profile of shifted coolant temperature in LOCA at the pellet height of 3.73 m. Zero in the LOCA time is the beginning of LOCA and the end of the steady-state operation. The unshifted coolant temperature generated by generated by RELAP5-3D is marked as 0 K.

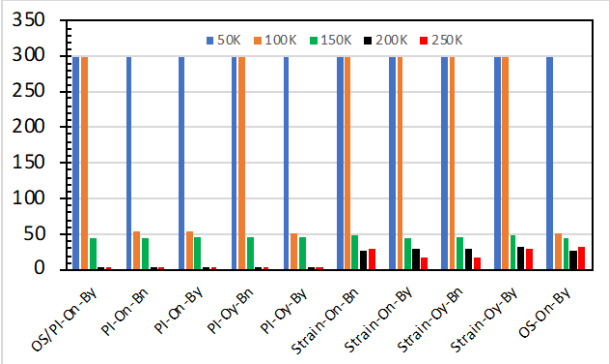

Figure 99. Evaluation of the temperature margin as acceptance criterion for fuel rod burst under LBLOCA with different burst mechanisms. On: no high temperature oxidation; Oy: high-temperature oxidation; Bn: no β-phase; By: β-phase.

7.3 Fuel Rod Bursting Evaluation using BISON for Core Design Option 4

For Core Design Option 4, the fuel rod burst mechanisms under LOCA were evaluated through the BISON simulations. The main parameters to simulate a full-length fuel rod with burnup extension are the same with Core Design Option 3, which is listed in Table 23. Here, the combination of OS/PI is selected as the failure criterion for clad during transient conditions. BISON simulations were carried out for 300 ECO cases based on random sampling of uncertain parameters and uncertainty. No burst is found among these 300 EOC cases.

With Core Design Option 4, the rods with the highest RIP are once-burned fuel rods. Figure 100 shows the maximum temperature evolution of fuel and cladding in the steady-state (left) and LBLOCA (right) for the same once-burned fuel rod in the same assembly presented for Core Design Option 3. It can be seen that in the steady-state, the maximum cladding temperature around 650 K is quite stabilized in the whole steady-state operation, which is similar with the result for Core Design Option 3. Meanwhile, the maximum fuel temperature increases from ~1100 K to ~1500 K on Day 695, near the end of the first cycle. Still, there is a significant fuel temperature increase around 700 days and reaches the peak value of ~1680 K on Day 810. At the end of EOC in the steady-state operation, the maximum fuel temperature decreases to ~1430 K. For Core Design Option 4, the maximum fuel temperature is relatively lower than that for Core Design Option 3. This is due to a flat power distribution.

As LBLOCA starts after the reactor scram, the maximum fuel temperature drops rapidly from ~1430 K at the steady-state to below 704 K in a few seconds, then increase slightly and stays below 900 K until the end of LBLOCA. Meanwhile, the maximum cladding temperature initially increases from about 650 K to ~780 K in five seconds, then drops to below 569 K at 11 seconds. With a relatively lower magnitude of cladding temperature, the evolution of the maximum cladding temperature is very similar with that for Core Design Option 3.

Figure 101 shows the evolution of the maximum cladding hoop stress and plenum pressure evolution in the steady-state (left) and LBLOCA (right). In the steady-state, the maximum cladding hoop stress is near zero (below 8 MPa) for ~435 days, increases to the peak value of ~163 MPa on Day 810, then decreases to ~90 MPa at the end of the EOC. Meanwhile, the plenum pressure increases slowly from

~6 MPa in the beginning of steady-state to 18 MPa at the end of EOC. Again, with Core Design Option 4, both cladding hoop stress and plenum pressure are relatively lower than that for Core Design Option 3.

As LBLOCA starts after the reactor scram, the plenum pressure drops from ~18 MPa at the steady-state to below 6 MPa at the end of LBLOCA. Meanwhile, the maximum cladding hoop stress initially decreases from about 86 MPa to ~46 MPa at 11 seconds, and then increases to ~99 MPa at 30 seconds. This probably indicates that in LBLOCA, the maximum cladding hoop stress is determined by the coolant temperature. With current Core Design Option 4, we did not observe such behavior under LBLOCA among 300 EOC cases.

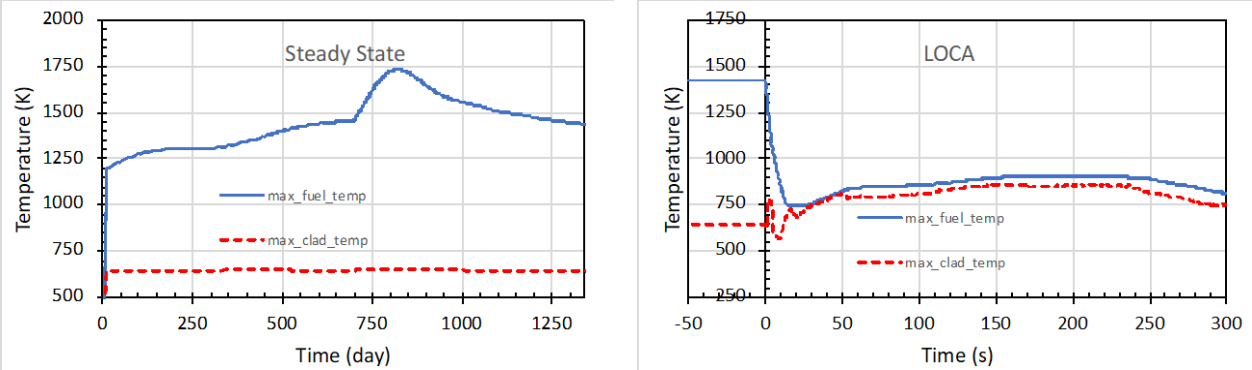

Figure 100. Maximum temperature evolution of fuel and cladding in the steady-state (left) and LOCA (right) for Core Design Option 4. Zero in the LOCA time is the beginning of LOCA and the end of the steady-state operation.

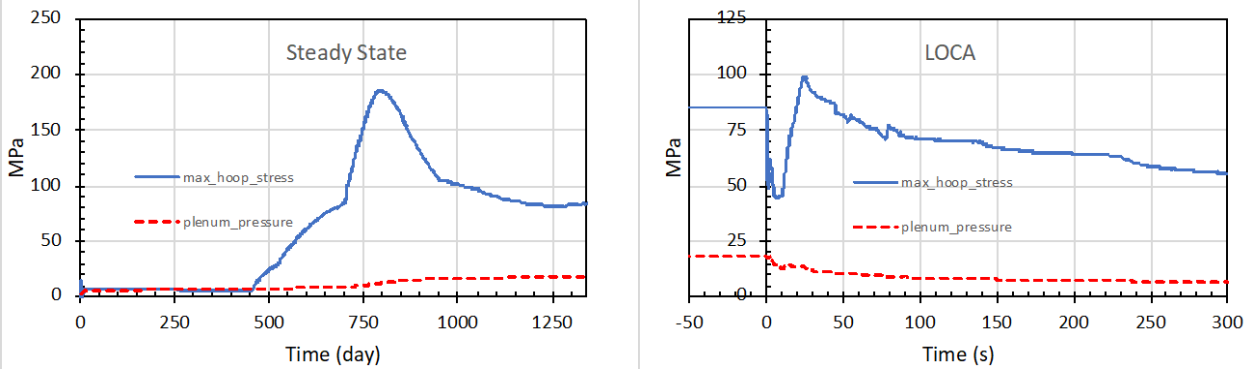

Figure 101. Evolution of max hoop stress and plenum pressure in the steady-state (left) and LOCA (right) for Core Design Option 4. Zero in the LOCA time is the beginning of LOCA and the end of steady-state operation.

7.4 Fuel Rod Bursting Evaluation using BISON for Core Design Option 5

For Core Design Option 5, the fuel rod burst mechanisms under LOCA were evaluated through the BISON simulations. The main parameters to simulate a full-length fuel rod with burnup extension are the same for Core Design Option 3, which is listed in Table 23. The combination of OS/PI is selected as the failure criterion for cladding during transient conditions. The BISON simulations were carried out for the same once-burned fuel rod in the same assembly presented for Core Design Option 3. No burst is found.

Figure 102 shows the maximum temperature evolution of fuel and cladding in the steady-state (left) and LBLOCA (right). It can be seen that in the steady-state, the maximum cladding temperature around

650 K is quite stabilized in the whole steady-state operation, which is very similar with the result for Core Design Option 3. Meanwhile, the maximum fuel temperature increases from ~1250 K to ~1530 K around Day 698 near the end of the first cycle, then drops to ~1475 K at Day 705 (in ~ 1 week). After that, the fuel temperature increases again and reaches a peak value of ~1625 K on Day 840. At the end of MOC in the steady-state operation, the maximum fuel temperature decreases to ~1560 K. With Core Design Option 5, the profile of the maximum fuel temperature is flatter than that for Core Design Option 3 and Core Design Option 4. Meanwhile, the peak value of the fuel temperature is also the lowest.

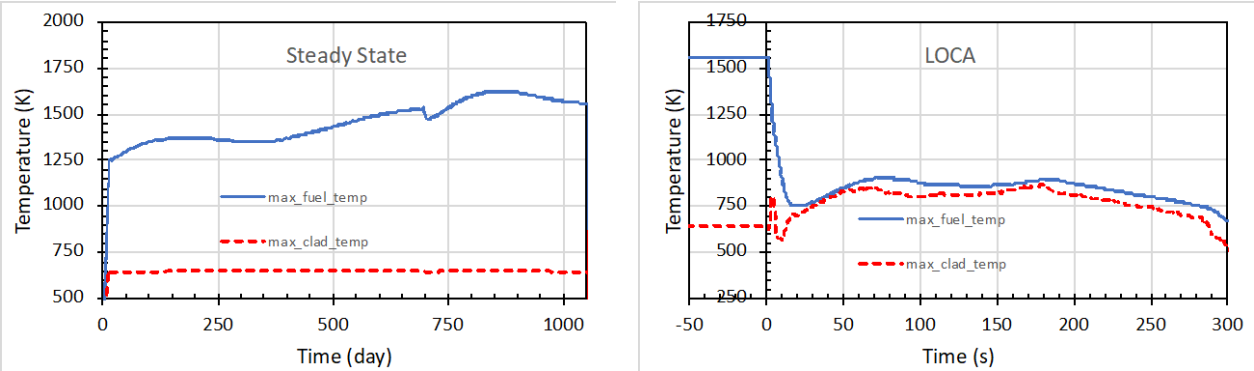

Figure 102. Maximum temperature evolution of fuel and cladding in the steady-state (left) and LOCA (right) for Core Design Option 5. Zero in the LOCA time is the beginning of LOCA and the end of the steady-state operation.

As LBLOCA starts after the reactor scram, the maximum fuel temperature drops rapidly from ~1560 K at the steady-state to below 710 K in a few seconds, then increases slightly and stays below 900 K until the end of LOCA. Meanwhile, the maximum cladding temperature initially increases from about 650 K to ~790 K in 5 seconds, then drops to below 567 K at 11 seconds. This corresponds to the blow-down phase, the cladding temperature first rises rapidly as the initial stored energy in the fuel pellets is transferred to the cladding. After the initial heat-up, the cladding temperature will decrease due to the down flow of high velocity steam through the core. It is clear that with Core Design Option 5, the profile of the maximum fuel temperature is lower than that for Core Design Option 3.

Figure 103 shows the evolution of the maximum cladding hoop stress and plenum pressure evolution in the steady-state (left) and LBLOCA (right). In the steady-state, the maximum cladding hoop stress is near zero (below 8 MPa) for ~435 days, increases to the peak value of ~142 MPa on the 810 day, then decrease to ~109 MPa at the end of MOC. Meanwhile, the plenum pressure increases slowly from ~6 MPa in begin of steady-state to ~17 MPa at the end of MOC. As shown in the left of Figure 103, the evolution of the maximum cladding hoop stress is very similar with those of the Core Design Option 3 and 4, with a lower magnitude.

As LBLOCA starts after the reactor scram, the plenum pressure drops from ~17 MPa at the steady-state to below 6 MPa in end of LOCA. Meanwhile, the maximum cladding hoop stress initially decreases from about 109 MPa to ~40 MPa at 11 seconds, then increases to ~89 MPa at 30 seconds. Again, this may indicate that in LOCA, the maximum cladding hoop stress is determined by the coolant temperature as discovered previously. With the current Core Design Option 5, we didn't observe such behavior under LBLOCA.

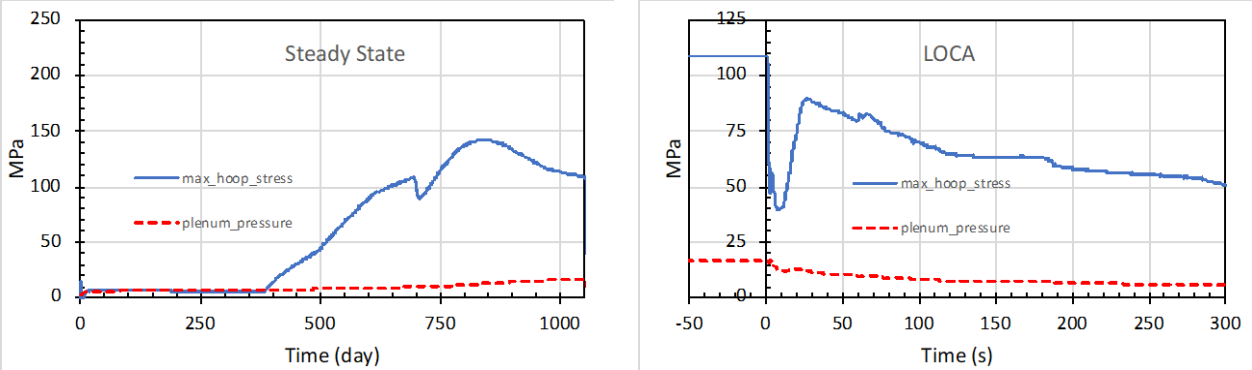

Figure 103. Evolution of max hoop stress and plenum pressure in the steady-state (left) and LOCA (right) for Core Design Option 5. Zero in the LOCA time is the beginning of LOCA and the end of the steady-state operation.

7.5 Summary of Fuel Rod Bursting Evaluation Using BISON

Under LBLOCA, it is expected that significantly higher RIP (aka plenum pressure) and cladding temperature will be observed. However, through this comparative study of the fuel rod burst mechanism using the BISON simulation, no rod burst was observed in Core Design Option 3, Core Design Option 4, or Core Design Option 5. In contrast, significantly higher hoop stress and fuel temperature were observed in the steady-state, induced by the axial average power. Thus, it is crucial to optimize power distribution in order to keep the maximum RIP and temperature below a limit value for the operational safety. Among the three Core Design Options, it was found that Core Design Option 5 provides better fuel performance at the steady-state, and relatively better fuel rod behavior in LBLOCA.

It was also found that the BC of coolant temperature in LBLOCA is paramount since it determines the cladding hoop stress and whether or not the fuel rod will burst. Though no rod burst was observed, it was suggested that the margin for coolant temperature is between 50 K and 150 K with Core Design Option 3.

8. CORE DESIGN OPTIMIZATION AND ECONOMIC CONSIDERATIONS

Utilizing the fuel in an efficient manor helps to reduce the overall cost of fuel and operations for a NPP. This report has shown the viability of producing a two-year cycle length utilizing an increased enrichment—up to 6.0 w/o—and burnup limit—up to 75 GWd/MTU. These results provide an initial insight into the ability to run a two-year cycle length and several different shuffling and optimization schemes remain to provide additional savings and utilization. This section examines a subset of reactor designs that attempt to increase the batch average burnup while decreasing the batch size.

The current designs from Section 4 utilize a batch fraction of ~0.41, where there were 80 fresh assemblies, 81 once-burned assemblies, and 32 twice-burned assemblies. This meant that 49 assemblies were only once-burned and then removed from the core at a lower average burnup than the twice-burned assemblies. For the Core Design Option 5 from Section 4, the batch average discharge is ~61.6 GWd/MTU with a peak pin burnup of 76.17 GWd/MTU. The goal of the core designs in this section is to reduce the amount of fresh fuel required to maintain a critical reactor for a two-year cycle and increase the fuel utilization. Only core design optimization work is performed here, fuel rod bursting evaluations are not performed for these optimized core designs.

8.1 Optimized Core Design Option 1 – Reduction of Batch Size with Constant Core Configuration

For Optimized Core Design Option 1, the batch fraction was reduced from 0.41 to 0.39 where the number of fresh assemblies is reduced to 76. Similarly, the number of once-burned assemblies is reduced to 76. The reduced fresh and once-burned assemblies are replaced by 8 additional twice-burned assemblies, bringing the total number of twice-burned assemblies to 41. A total of 24 assemblies contained 6% enriched fuel rods, while 52 assemblies contained 5% enriched fuel. The shuffling scheme and layout, aside from the central region and the replacement of eight 6 w/o IFBA assemblies with eight 6 w/o IFBA + 8 Gd assemblies, is consistent with Option 5 and can be seen in Figure 104.

Two different methods were used to flatten the power distribution in the core. The first continued the trend from Option 5 and employed gadolinia in 36 assemblies, where the distribution of gadolinia between the two enrichments was 20 assemblies with 5% enrichment and 16 assemblies with 6% enrichment. The second method used to flatten the power distribution in the core was to load the center of the core with five 6% enriched and four 5% enriched twice-burned assemblies. This will not only increase the fuel utilization, but will also push the flux out of the center and into the ‘ring of fire.’ The gadolinia rods were changed from Option 5 and now contain only 3% gadolinia by mass. This reduction is offset by enriching the gadolinium to 70% by weight gadolinium-157, which is the primary neutron absorber. This provides an increase in the w/o of the fuel in the gadolinia pins, and an increase in the allowable enrichment for the gadolinia pins. The enrichment was increased to 85% of the standard fuel, 4.25% for 5% fuel, and 5.1% for 6% fuel, respectively.

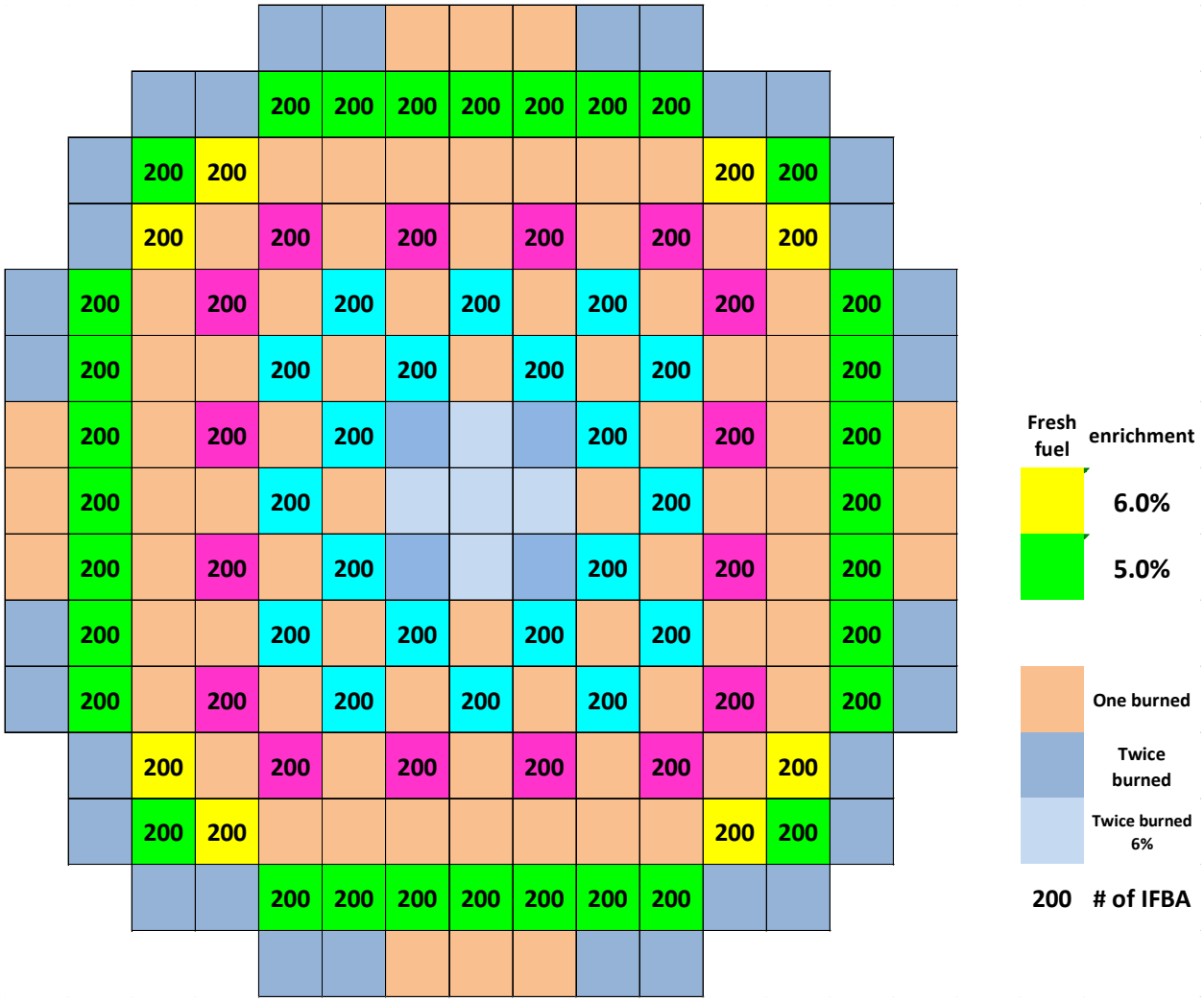

Figure 104. Loading pattern for Optimized Core Design Option 1.

Figure 105 and Figure 106 show the Peak power peaking factors and EOC burnup distribution for Optimized Core Design Option 1. The power peaking has a maximum value of 1.879, which is within the desired value of 1.9. The maximum burnup is also much higher than acceptable, where the maximum burnup is 79.23 GWd/MTU, which is ~5 GWd/MTU over the limit of 75 GWd/MTU. This design used a shuffling scheme based on Option 5, where the center assemblies were the lowest once-burned 6% enriched from that design. The high burnup associated with many of the central assemblies may indicate the need to replace the remaining 6% enriched twice-burned assemblies with 5% enriched assemblies. In addition, there are five assemblies in the periphery that exceed 75 GWd/MTU. Again, the shuffling scheme was based on Option 5, where a further iteration may help to reduce the high burnup in these areas. Along with this, the batch average burnup was increased from 61.6 GWd/MTU to 65.5 GWd/MTU, a 6% increase in the burnup achieved in the previous option. However, this increase causes some of the assemblies to reach peak burnups that were not within acceptable limits, which may reduce the batch average burnup. Once a target reactivity is reached, adjusting the shuffling scheme could provide a decrease in the peak burnup, thereby maintaining a high batch average burnup.

Figure 107 shows the critical boron concentration for Optimized Core Design Option 1, where the core does not have sufficient reactivity to last the full two-year cycle and drops below a critical configuration at burnup step 28 or 30. Replacing some 5% enriched assemblies with 6% enriched

assemblies has the potential to overcome this deficit and provide the reactivity necessary to last the entire two-year cycle. Figure 108 shows the axial offset for Optimized Core Design Option 1, where the initial offset is much higher than that for the original designs. It is currently unclear what caused this large difference in axial offset and may need to be investigated further.

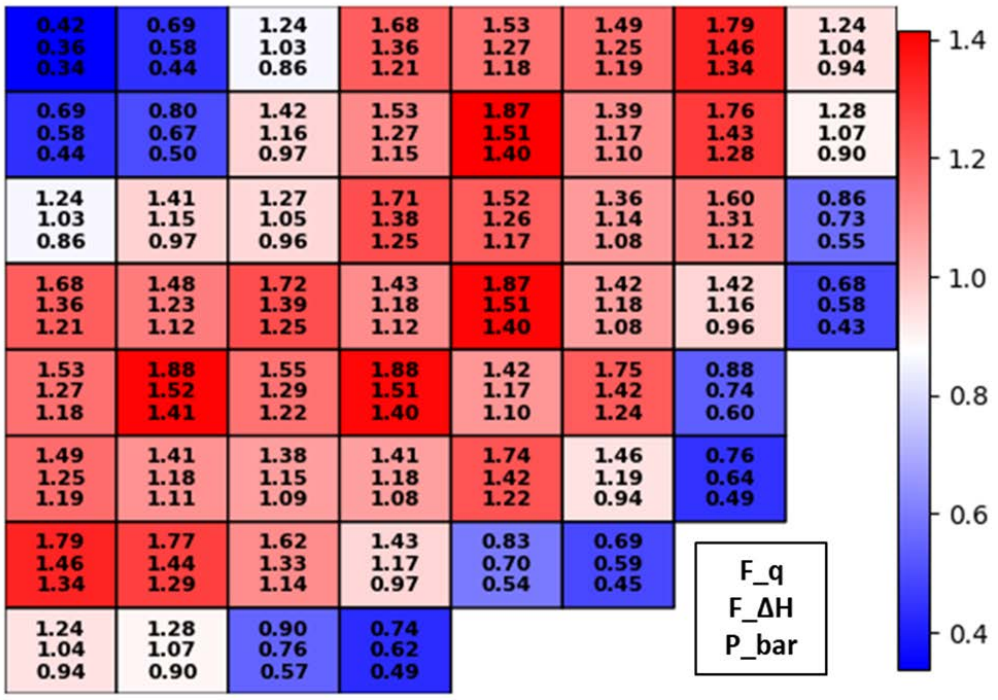

Figure 105. Peaking factors at Peak for Optimized Core Design Option 1.

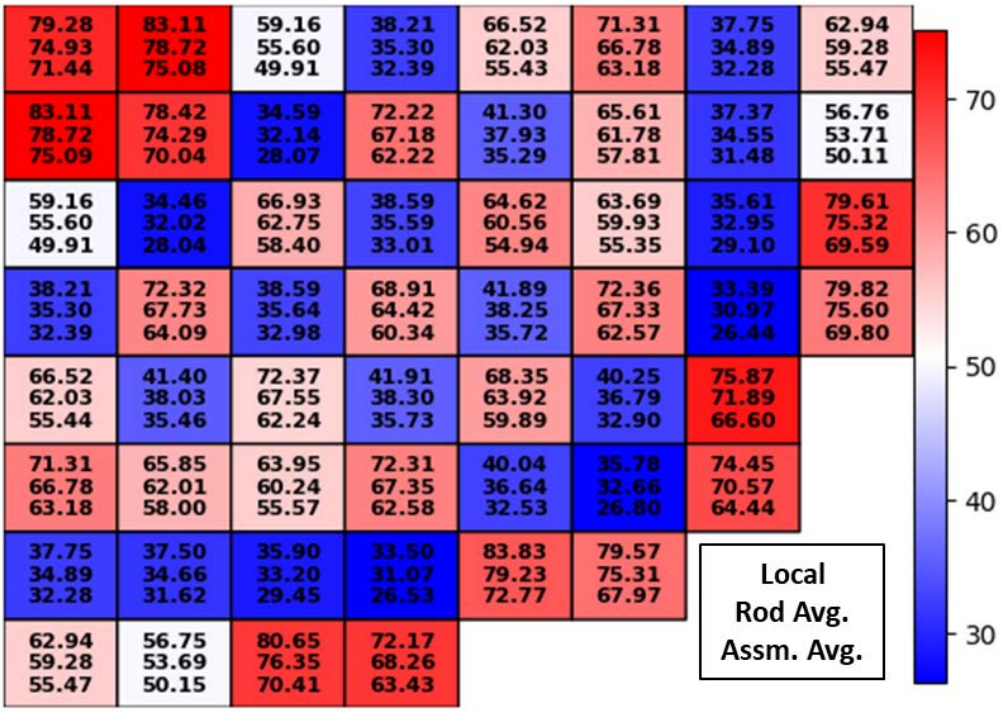

Figure 106. Burnup distribution at EOC for Optimized Core Design Option 1.

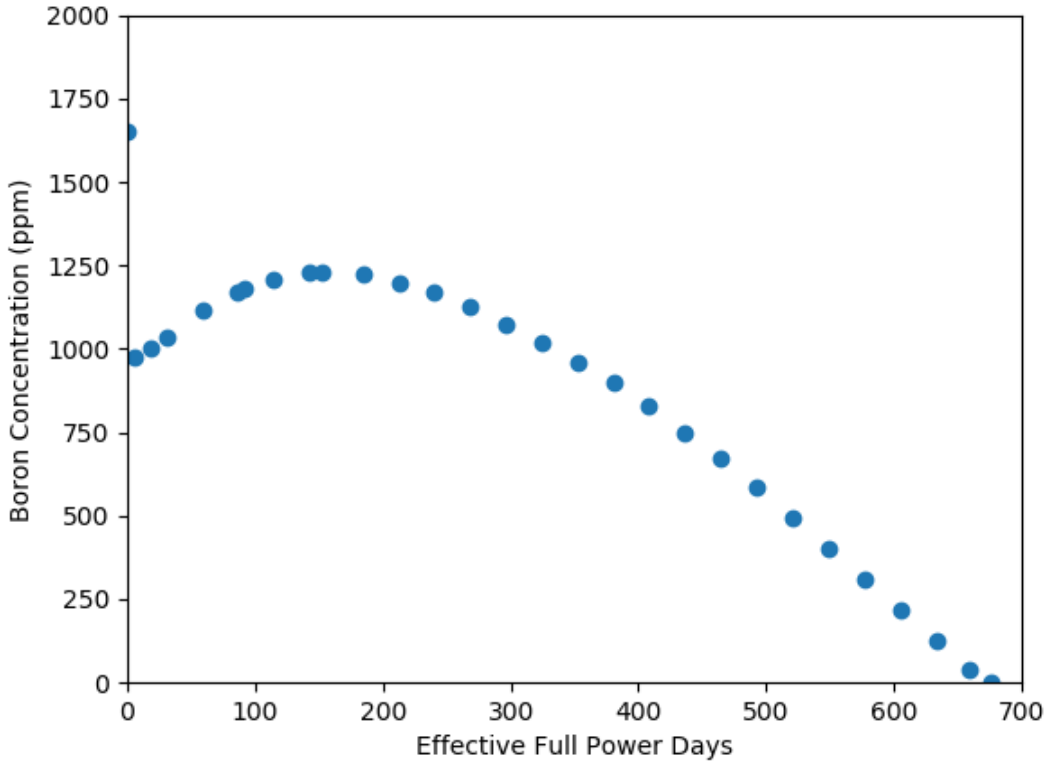

Figure 107. Critical boron concentration in PPM for the equilibrium cycle for Optimized Core Design Option 1.

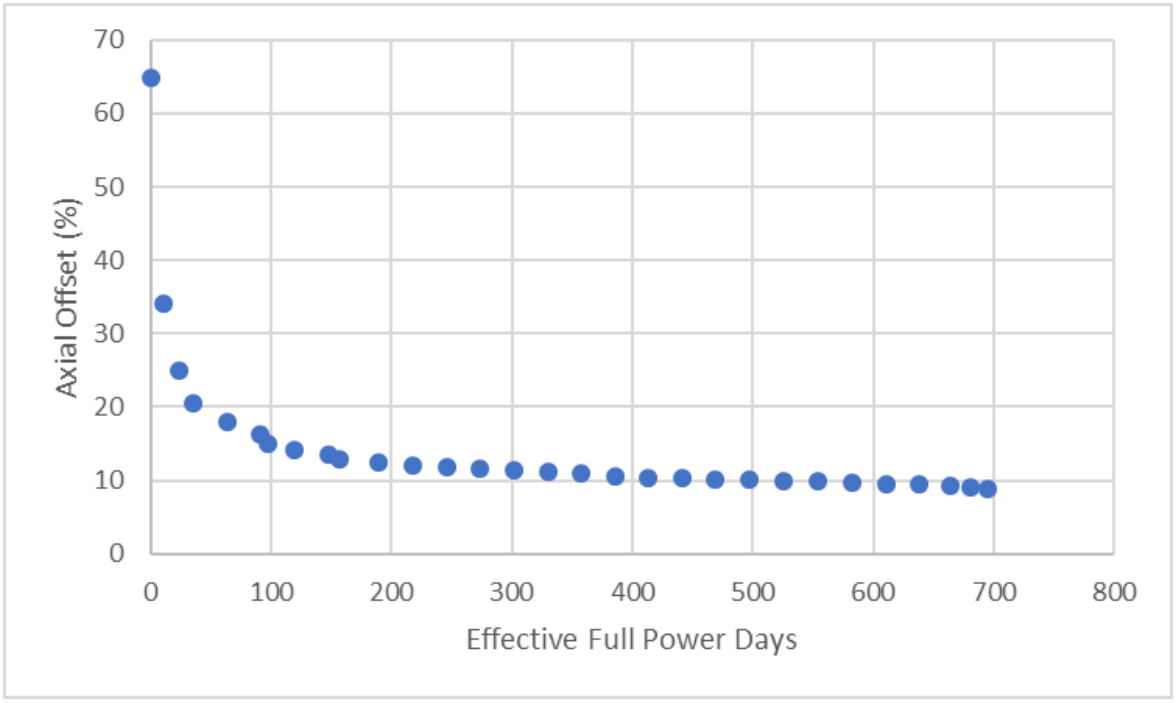

Figure 108. Axial offset for Optimized Core Design Option 1.

Table 24 and Table 25 summarize the peaking factors, burnup values, boron concentration, and axial offset for Optimized Core Design Option 1. This option has the potential to reduce the number of fresh assemblies required for each refueling cycle and reduce peaking in the center of the core by replacing the central core region with twice-burned fuel. This first design iteration fails to deliver on the burnup limits and the total amount of reactivity required to last for a two-year life cycle. Further design iterations will focus on reducing these aspects. Despite the shortcomings, the design has promise to reduce the cost of refueling and increase the fuel utilization for the two-year cycle core.

Table 24. Summary of peaking factors and burnup values for Optimized Core Design Option 1.

	BOC	**Peak**	**MOC**	**EOC**
P_bar	1.403	1.414	1.414	1.324
F_ΔH	1.547	1.517	1.531	1.421
F_q	1.755	1.879	1.756	1.604
Radial assembly burnup (GWd/MTU)	62.07	55.20	67.03	75.09
Radial pin burnup (GWd/MTU)	67.30	60.05	71.55	79.23
Peak burnup (GWd/MTU)	72.21	64.57	76.36	83.83

Table 25. The critical boron concentration and axial offset values for Optimized Core Design Option 1.

Critical boron concentration at hot zero power	1650.91 ppm
Peak critical boron concentration at full power	1230.49 ppm
Maximum axial offset	64.94%

8.2 Optimized Core Design Option 2 – Reduction of Batch Size with Increased 6% Enriched Assemblies

Optimized Core Design Option 1 provided an increase in batch average burnup and a reduction in the batch size which would help reduce the cost of refueling a reactor. For Optimized Core Design Option 2, the batch fraction remained constant but the number of 6% enriched assemblies was increased from 24 to 32 to increase the core reactivity to maintain the full two-year cycle length. Along with this, nearly all of the fresh fuel assemblies were placed into a checkerboard pattern to reduce the peaking factor associated with using the higher enriched fuel. Finally, the placement of the twice burned assemblies was adjusted to reducing the maximum burnup in the central assemblies, Figure 109 shows the core assembly loading pattern for Optimized Core Design Option 2.

Figure 110 and Figure 111 show the peak power peaking factors and EOC burnup distribution for Optimized Core Design Option 2. The power peaking has a maximum value of 2.093, which is has degraded slightly from Optimized Core Design Option 1 due to replacing four 5 w/o assemblies with 6.0 w/o assemblies. The maximum burnup is still much higher than acceptable, because the shuffling scheme was left relatively untouched in an attempt to find a critical core for the two-year cycle length. Once an OCDO core has been found to maintain a critical core for the two-year cycle length, the shuffling will be updated.

Figure 112 shows the critical boron concentration for Optimized Core Design Option 2, where the core does not have sufficient reactivity to last the full two-year cycle and drops below a critical configuration at burnup step 30, indicating that the replacement of a few additional 5 w/o assemblies with 6 w/o assemblies will reach a critical cycle length. Figure 106 shows the axial offset for Optimized Core Design Option 2, where the initial offset is still much higher than the original designs.

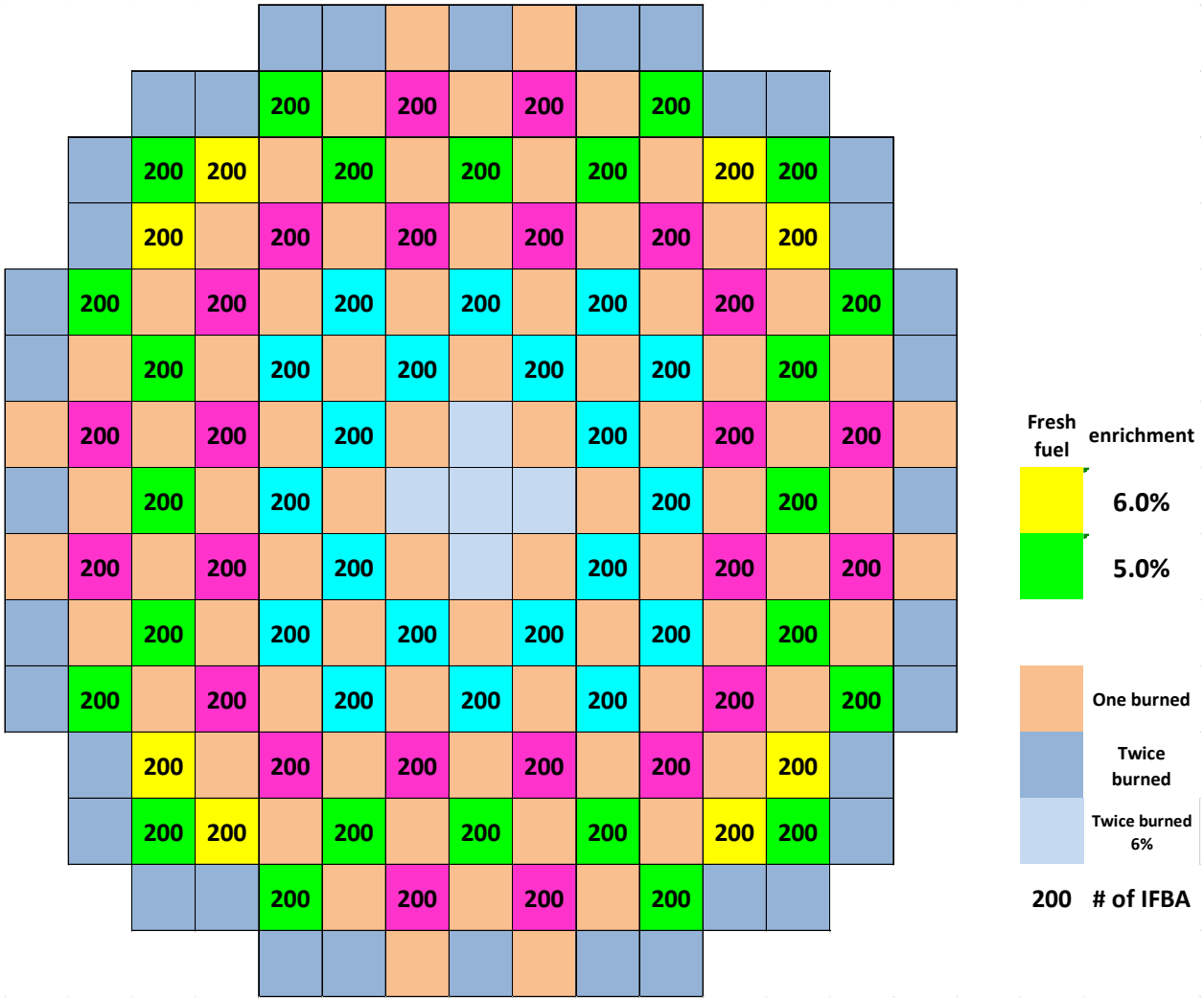

Figure 109. Loading pattern for Optimized Core Design Option 2.

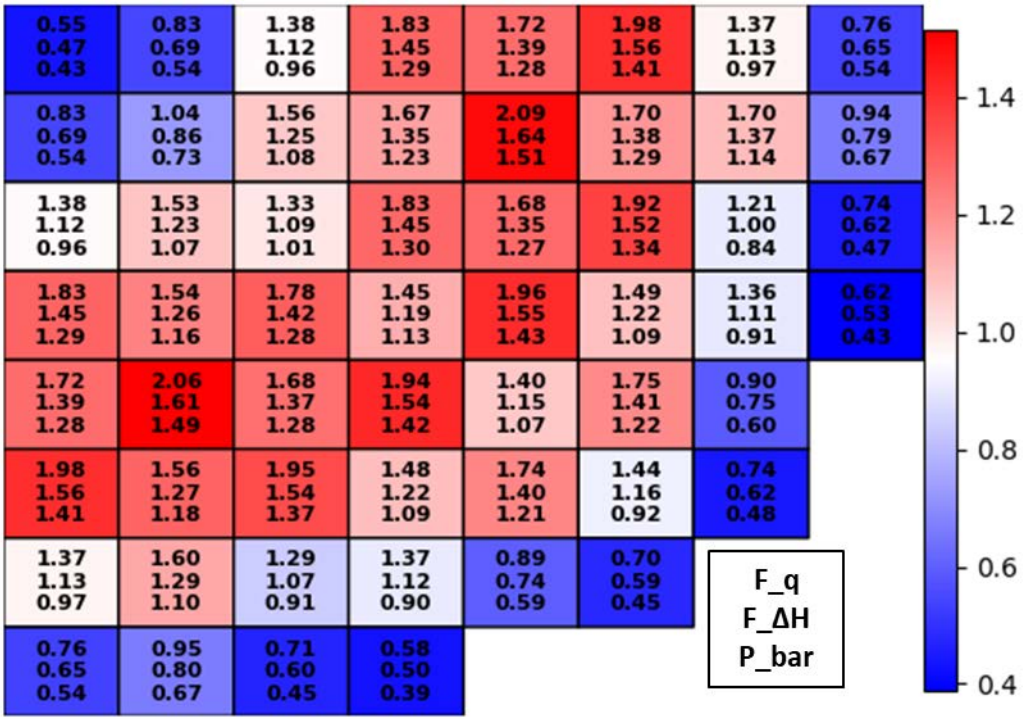

Figure 110. Peaking factors at Peak for Optimized Core Design Option 2.

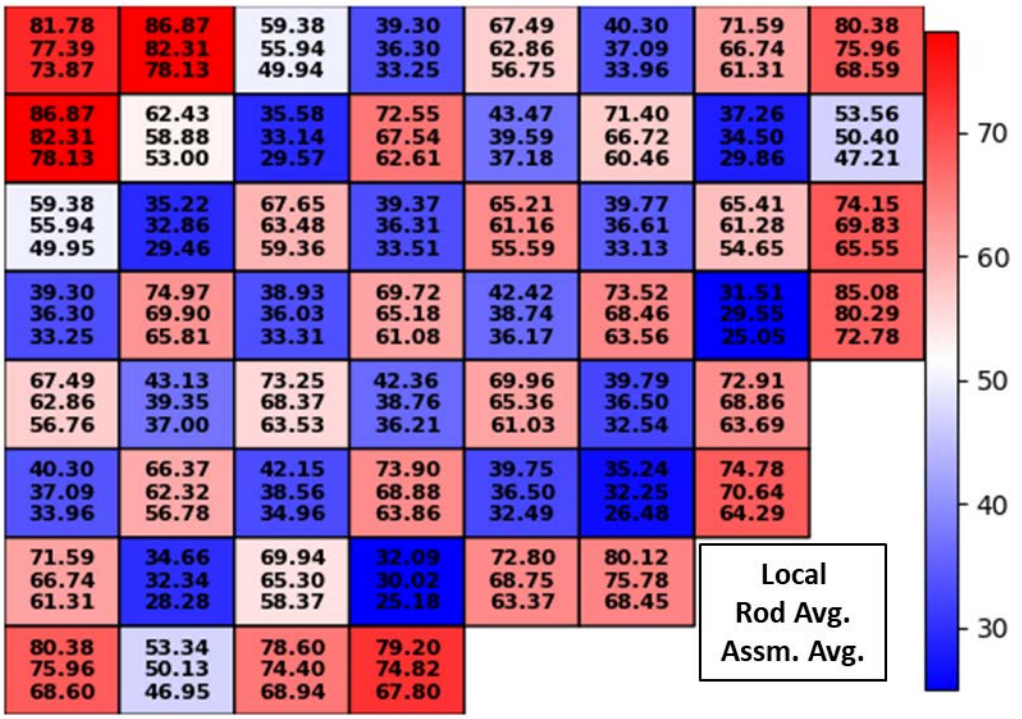

Figure 111. Burnup distribution at EOC for Optimized Core Design Option 2.

Table 26. Summary of peaking factors and burnup values for Optimized Core Design Option 2

	BOC	Peak	MOC	EOC
P_bar	1.417	1.514	1.482	1.334
F_ΔH	1.547	1.638	1.585	1.417
F_q	1.748	2.093	1.809	1.642
Radial Assembly Burnup (GWd/MTU)	63.33	66.26	69.38	78.13
Radial Pin Burnup (GWd/MTU)	68.06	70.67	73.50	82.31
Peak Burnup (GWd/MTU)	72.82	75.43	78.29	86.87

Table 27. Summary of critical boron concentration and axial offset for Optimized Core Design Option 2

Critical Boron Concentration at Hot Zero Power	1697.83 ppm
Peak Critical Boron Concentration at Full Power	1322.27 ppm
Maximum Axial Offset	65.34 %

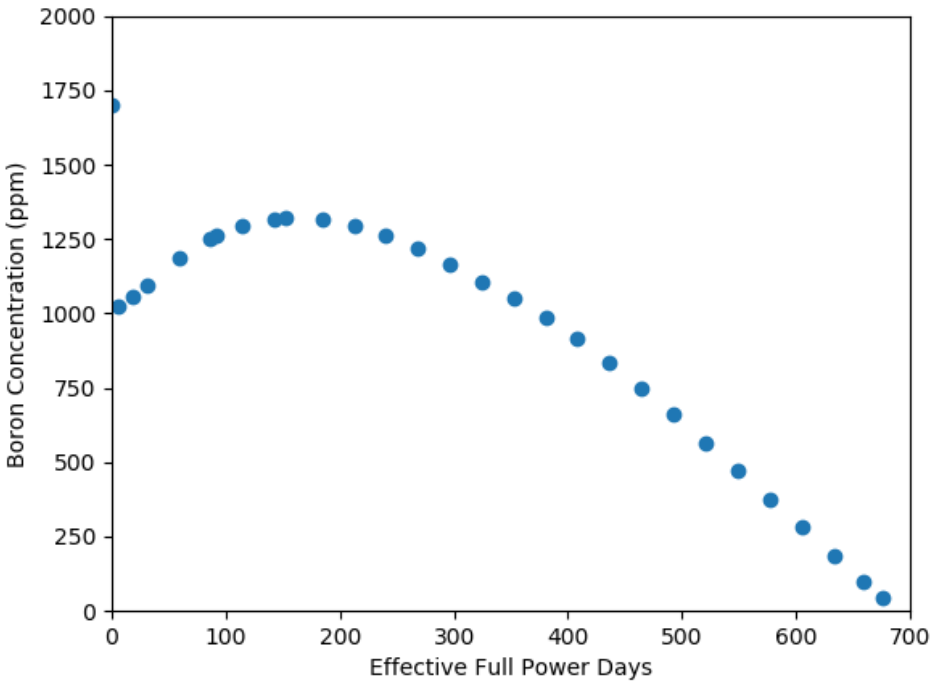

Figure 112. Critical boron concentration in PPM for the equilibrium cycle for Optimized Core Design Option 2.

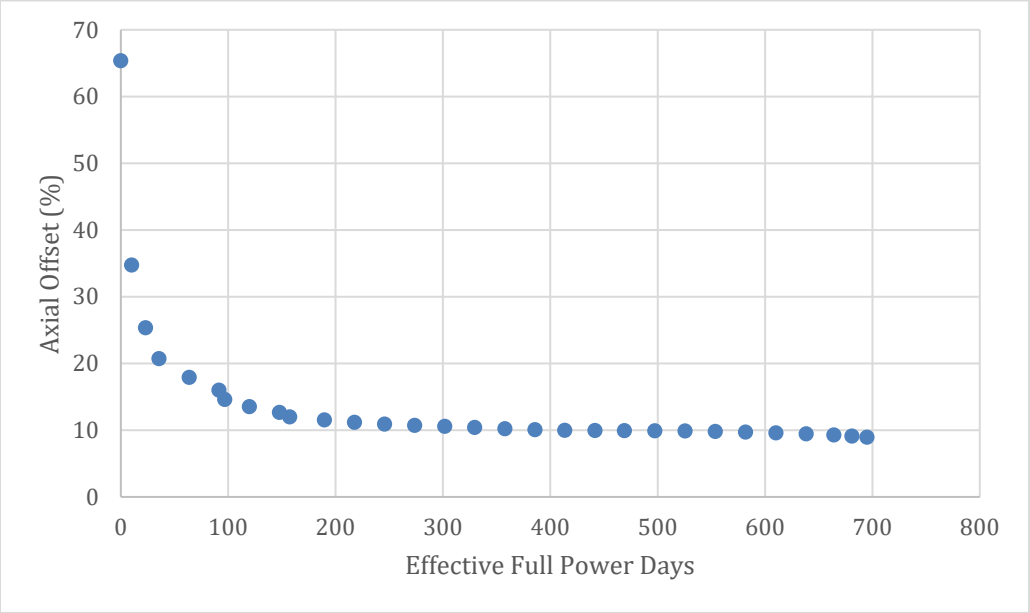

Figure 113. Axial offset for Optimized Core Design Option 2.

Tables 26 & 27 summarize the peaking factors, burnup values, boron concentration and axial offset for Optimized Core Design Option 2. This option has increased the reactivity for the design in Optimized Core Design Option 2 and maintains criticality until burnup step 30. Replacing some 5 w/o assemblies with 6 w/o assemblies can increase the reactivity to maintain a two-year life cycle. Along with this, once the two-year life cycle has been achieved, the position of fresh assemblies and shuffling scheme can be updated to reduce the power peaking and burnup. Performing these changes to the shuffling and assembly placement will be the focus of further design iterations.

9. CONCLUSIONS AND FUTURE WORK

Increasing the fuel assembly discharge burnup is the most efficient means to achieve fuel cycle cost reduction for NPPs. In this work, we have further developed the MP-BEPU analysis framework LOTUS by integrating DOE's advanced simulation tools VERA-CS and BISON to demonstrate the feasibility of 24-months core designs for a PWR with burnup extension and increased enrichment and to perform the fuel rod busting evaluations under LBLOCA conditions. In this report, five core design evolutions (Core Design Options 1 – 5) are presented for 24-months equilibrium cycles for a generic four-loop PWR with burnup extension up to 75 GWd/MTU and increased enrichment up to 6 w/o. As the core design options progress, the assembly and core design become more complex and the core power peaking factors would need to be controlled and decreased, as needed. Core Design Option 5 has the lowest power peaking factors among all the core design options and could be a potential candidate for a practical 24-months core design. Due to the high power peaking factors obtained for Core Design Options 1 and 2, they are unlikely to be adopted in the practical core designs and the burst evaluations are not performed for these two core design options. Instead, fuel rod burst potential evaluations are performed under LBLOCA conditions for Core Design Options 3 - 5 using LOTUS. Both best estimate and MP-BEPU calculations are performed to evaluate fuel rod burst potential. The best estimate calculations using empirical cladding deformation model in RELAP5-3D are performed for Core Design Options 3 – 5 and found that only the hot rod in 4 symmetric location assemblies could experience bursting at MOC for Core Design Option 3 which has relatively higher power peaking factors than those from Core Design Options 4 & 5. However, more mechanistic evaluations of fuel rod bursting using the advanced fuel performance code BISON indicate that the fuel rod integrity is maintained under LBLOCA conditions. Fuel rods would not experience bursting at other exposure points in the equilibrium cycle for Core Design Option 3 - 5. For the MP-BEPU calculations performed for Core Design Option 5, only a small fraction (less than 3.5%) of fuel rods would experience bursting at MOC and EOC under LBLOCA conditions. The twice-burned fuel on the periphery would not experience bursting from either the best estimate or MP-BEPU calculations. The results indicate that high burnup does not necessarily contribute to fuel rod bursting. The power history (e.g., high peaking factors causing high RIP) is a more important contributing factor to fuel rod bursting potential. Advanced fuel and core design techniques will be investigated to control the peaking factors, especially for the once-burned fuel to prevent fuel rods from bursting under LBLOCA conditions. The first area of future work is to further investigate advanced fuel design and optimization techniques to control power peaking in the cycle and to lower the fuel rods' internal pressures during normal operations.

It is noted that the fuel cladding temperature rise from the generic plant model studied in this work exhibits modest rise of cladding temperatures under the LBLOCA conditions. Since the LBLOCA responses are plant specific, the conclusions drawn from this work should be not applied to the PWRs which would have higher temperature rises under LBLOCA conditions. The second area of future work is to perform plant specific analysis to ensure fuel rod integrity.

Since a fundamental requirement for DBA analysis is that there should be no or very limited radiological consequences released to the public, therefore the third area of the future work will be to extend LOTUS to include the radiological consequence analysis resulted from fuel rod bursting. This would involve integrating the accident consequence code, such as the Methods for Estimation of Leakages and Consequences of Releases (MELCOR) and the MELCOR Accident Consequence Code System (MACCS) [53] into the LOTUS framework to determine the acceptable level of fuel rod busting under LBLOCA conditions. MACCS is an NRC code used to perform probabilistic offsite consequence assessments for hypothetical atmospheric releases of radionuclides. The purpose of this code is to simulate the impact of severe accidents at NPPs on the surrounding environment. The code models atmospheric transport and dispersion, emergency response and long-term protective actions, exposure pathways, early and long-term health effects, land contamination, and economic costs. MACCS was designed as a tool for level-three Probabilistic Safety Assessment analysis and is used by NPPs in the

U.S. to obtain license renewal applicants to support the plant specific evaluation of severe accident mitigation alternatives (SAMAs) as part of an applicant's environmental report for license renewal. MACCS is also used in severe accident mitigation design alternatives and severe accident consequence analyses for environmental impact statements for new reactor applications. The NRC uses MACCS in its cost-benefit assessments supporting regulatory analyses that evaluate potential new regulatory requirements for NPPs. Integrating MACCS into the LOTUS framework provides the necessary capability to perform the radiological consequence analysis.

Tightly coupled calculations between RELAP5-3D and BISON, and RELAP5-3D and FRAPTRAN during LOCA and RIA conditions are required to provide a detailed assessment of the fuel rod burst potential, fuel fragmentation, relocation, and dispersal. The tightly coupled calculation capability for RELAP5-3D/BISON and RELAP5-3D/FRAPTRAN is the fourth area for future work.

10. REFERENCES

[1] NEI, "U.S. Nuclear Plant Actual and Expected Uprates by Plant," June 2019. [Online]. Available at: https://www.nei.org/resources/statistics/us-nuclear-plant-actual-and-expected-uprates (last accessed on September 19, 2019).

[2] EPRI, "Optimum Cycle Length and Discharge Burnup for Nuclear Fuel – A Comprehensive Study for BWRs and PWRs: Phase 1: Results Achievable Within the 5% Enrichment Limit," Palo Alto, CA, and U.S. Department of Energy, Washington, DC: 2001. 1003133.

[3] EPRI, "Optimum Cycle Length and Discharge Burnup for Nuclear Fuel: Phase 2: Results Achievable With Enrichments Greater than 5 w/o," Palo Alto, CA, and U.S. Department of Energy, Washington, DC: 2002. 1003217.

[4] NRC, "Evaluation of Fuel Fragmentation, Relocation, and Dispersal under Loss-of-Coolant (LOCA) Conditions Relative to the Final Draft Final Rule on Emergency Core Cooling System Performance during a LOCA," November 30, 2015. [Online]. Available at: https://www.nrc.gov/docs/ML1523/ML15230A200.pdf (last accessed on September 19, 2019).

[5] NRC, "§ 50.46, Acceptance Criteria for Emergency Core Cooling Systems for Light-Water Nuclear Power Reactors," August 29, 2017. [Online]. Available at: https://www.nrc.gov/reading-rm/doc-collections/cfr/part050/part050-0046.html (last accessed on September 19, 2019).

[6] NRC, "Proposed Rulemaking 10 CFR 50.46c: Emergency Core Cooling System Performance During Loss-of-Coolant Accidents (RIN 3150-AH42)," SRM-SECY-12-0034, January 7, 2013 (ML13007A478).

[7] NRC, "Standard Review Plan for the Review of Safety Analysis Reports for Nuclear Power Plants: LWR Edition," NUREG-0800 (formerly issued as NUREG-75/087), November 6, 2017. [Online]. Available at: https://www.nrc.gov/reading-rm/doc-collections/nuregs/staff/sr0800 (last accessed on September 19, 2019).

[8] CASL, Website Homepage, n.d. [Online]. Available at: https://www.casl.gov/ (last accessed on September 19, 2019).

[9] Labworks, "FRAPCON/FRAPTRAN User Group," March 31, 2017. [Online]. Available at: https://frapcon.labworks.org/ (last accessed on September 19, 2019).

[10] INL, "RELAP5-3D," n.d. [Online]. Available at: https://relap53d.inl.gov/SitePages/Home.aspx (last accessed on September 19, 2019).

[11] INL, "BISON: A Finite Element-Based Nuclear Fuel Performance Code," n.d. [Online]. Available at: https://bison.inl.gov/SitePages/Home.aspx (last accessed on September 19, 2019).

[12] The HDF Group, "The HDF5 Library & File Format," n.d. [Online]. Available at: https://www.hdfgroup.org/solutions/hdf5/ (last accessed on September 19, 2019).

[13] Frepoli, C., "An overview of Westinghouse realistic large break LOCA evaluation model," 2008, *Science and Technology of Nuclear Installations*, Vol. 2008, Art. ID 498737.

[14] Martin, R., and L. D. O'Dell, "Development considerations of AREVA NP Inc's realistic LBLOCA analysis methodology," 2008, *Science and Technology of Nuclear Installations*, Vol. 2008, Art. ID 239718.

[15] Nine Engineering, "BEPU 2018: Best-Estimate Plus Uncertainty International Conference," May 13–18, 2018, Lucca, Italy. [Online]. Available at: http://www.nineeng.com/bepu/ (last accessed on September 19, 2019).

[16] Zhang, H., R. H. Szilard, and R. Sugure, "A Strategic Approach to Employ Risk-Informed Methods to Enable Margin Recovery of Nuclear Power Plants Operating Margins," INL, INL/EXT-18-51491, September 2018. [Online]. Available at: https://inldigitallibrary.inl.gov/sites/sti/sti/Sort_12310.pdf (last accessed on September 19, 2019).

[17] Boyack, B., et al., "Quantifying Reactor Safety Margins," NRC, NUREG/CR-5249, 1989. [Online]. Available at: https://www.nrc.gov/docs/ML0303/ML030380473.pdf (last accessed on September 19, 2019).

[18] NRC, "Best-Estimate Calculations of Emergency Core Cooling System Performance," NRC Regulatory Guide 1.157, May 1989. [Online]. Available at: https://www.nrc.gov/docs/ML0037/ML003739584.pdf (last accessed on September 19, 2019).

[19] NRC, "Transient and Accident Analysis Methods," NRC Regulatory Guide 1.203, December 2005. [Online]. Available at: https://www.nrc.gov/docs/ML0535/ML053500170.pdf (last accessed on September 19, 2019).

[20] International Atomic Energy Agency, "Live Chart of the Nuclides," IAEA Nuclear Data Section, 2019. [Online]. Available at: https://www-nds.iaea.org/relnsd/vcharthtml/VChartHTML.html (last accessed on September 19, 2019).

[21] Iwasaki, K., T. Matsui, Y. Arita, T. Nagasaki, N. Yokoyama, I. Tokura, K. Yanai, R. Yuda, K. Une and K. Harada, "Thermal conductivity of Gd_2O_3-dispersed UO_2 pellet," *Atalante*, May 19–22, 2008. [Online]. Available at: https://inis.iaea.org/collection/NCLCollectionStore/_Public/40/034/40034680.pdf (last accessed on September 19, 2019).

[22] Yilmaz, S., "Multilevel Optimization of Burnable Poison Utilization for Advanced PWR Fuel Management," PhD Thesis, The Pennsylvania State University, April 20, 2005. [Online]. Available at: https://etda.libraries.psu.edu/catalog/6671 (last accessed on September 19, 2019).

[23] Sanders, C., and J. Wagner, "Study of the Effect of Integral Burnable Absorbers for PWR Burnup Credit," NRC, NUREG/CR-6760, March 2002. [Online]. Available at: https://www.nrc.gov/docs/ML0207/ML020770436.pdf (last accessed on September 19, 2019).

[24] Wagner, J., and C. Parks, "Parametric Study of the Effect of Burnable Poison Rods for PWR Burnup Credit," NRC, NUREG/CR-6761, March 2002. [Online]. Available at: https://www.nrc.gov/docs/ML0207/ML020770329.pdf (last accessed on September 19, 2019).

[25] Blakely, C., H. Zhang, and J. Yu, "Two-Year PWR Core Design with Burnup and Enrichment Extension using VERA-CS," *Transactions of the American Nuclear Society*, Vol. 121, 2019.

[26] World Nuclear Association, "Nuclear Fuel and its Fabrication," June 2019. [Online]. Available at: https://www.world-nuclear.org/information-library/nuclear-fuel-cycle/conversion-enrichment-and-fabrication/fuel-fabrication.aspx (last accessed on September 19, 2019).

[27] Wikipedia, "Control rod," September 17, 2019. [Online]. Available at: https://en.wikipedia.org/wiki/Control_rod (last accessed on September 19, 2019).

[28] CASL, "MPACT User's Manual Version 2.0.0," CASL-U-2015-0077-000, February 20, 2015. [Online]. Available at: https://www.casl.gov/sites/default/files/docs/CASL-U-2015-0077-000.pdf (last accessed on September 19, 2019).

[29] CASL, "CTF – A Thermal-Hydraulic Subchannel Code for LWRs Transient Analysis User's Manual, Revision 0," CASL-U-2015-0055-000, March 10, 2015. [Online]. Available at: https://www.casl.gov/sites/default/files/docs/CASL-U-2015-0055-000.pdf (last accessed on September 19, 2019).

[30] Oak Ridge National Laboratory, "ORIGEN," n.d., [Online]. Available at: https://www.ornl.gov/division/rnsd/projects/origen (last accessed on September 19, 2019).

[31] Oak Ridge National Laboratory, "SCALE," n.d., [Online]. Available at: https://www.ornl.gov/scale (last accessed on September 19, 2019).

[32] CMake, Website Homepage, n.d. [Online]. Available at: https://cmake.org/ (last accessed on September 19, 2019).

[33] IAPWS, "Revised Release on the IAPWS Industrial Formulation 1997 for the Thermodynamic Properties of Water and Steam," IAPWS R7-97(2012), August 2007, http://www.iapws.org/relguide/IF97-Rev.html (last accessed on September 19, 2019).

[34] ParaView, Website Homepage, n.d. [Online]. Available at: https://www.paraview.org/ (last accessed on September 19, 2019).

[35] NRC, "South Texas Project Electric Generating Station (STPEGS) Updated Final Safety Analysis Report (UFSAR)," Rev. 18, June 29, 2007. [Online]. Available at: https://www.nrc.gov/docs/ML1620/ML16207A534.pdf (last accessed on September 19, 2019).

[36] Szilard, R., H. Zhang, A. Epiney, C. Parisi, and P. Talbot, "Loss of Coolant Accident/Emergency Core Coolant System Evaluation of Risk-Informed Margins Management Strategies for a Representative Pressurized Water Reactor," INL/EXT-16-39805, September 2016. [Online]. Available at: https://inldigitallibrary.inl.gov/sites/sti/sti/7365842.pdf (last accessed on September 19, 2019).

[37] NRC, "Westinghouse Technology Systems Manual, Section 2.2: Power Distributions Limits," n.d. [Online]. Available at: https://www.nrc.gov/docs/ML1122/ML11223A208.pdf (last accessed on September 19, 2019).

[38] Beyer, C. E., C. R. Hann, D. D. Lanning, F. E. Panisko, and L. J. Parchen, "GAPCON-Thermal-2: A Computer Program for Calculating the Thermal Behavior of an Oxide Fuel Rod," BNWL-1898, November 1975. [Online]. Available at: https://www.osti.gov/servlets/purl/4113463 (last accessed on September 19, 2019).

[39] NEA, "Nuclear Fuel Behaviour in Loss-of-Coolant Accident (LOCA) Conditions: State-of-the-Art," ISBN 978-92-64-99091-3, 2009. [Online]. Available at: https://www.oecd-nea.org/nsd/docs/2009/csni-r2009-15.pdf (last accessed on September 19, 2019).

[40] Wilks, S. S., "Determination of sample sizes for setting tolerance limits," *The Annals of Mathematical Statistics*, Vol. 12, no. 1, pp. 91–96, 1941.

[41] Ikonen, T., "Comparison of global sensitivity analysis methods–application to fuel behavior modeling," *Nuclear Engineering and Design*, Vol. 297, pp. 72–80, 2016.

[42] Brown, C., and H. Zhang, "Uncertainty quantification and sensitivity analysis with CASL Core Simulator VERA-CS," *Annals of Nuclear Energy*, Vol. 95, pp. 188–201, 2016.

[43] Zhang, H., R. Szilard, A. Epiney, C. Parisi, R. Vaghetto, A. Vanni, and K. Neptune, "Industry Application ECCS / LOCA Integrated Cladding/Emergency Core Cooling System Performance: Demonstration of LOTUS-Baseline Coupled Analysis of the South Texas Plant Model," INL, INL/EXT-17-42461, June 2017. [Online]. Available at: https://www.osti.gov/servlets/purl/1376207 (last accessed on September 19, 2019).

[44] Guba, A., M. Makai, and L. Pál, "Statistical aspects of best estimate method—I." *Reliability Engineering & System Safety*, Vol. 80, Iss. 3, pp. 217–232, 2003.

[45] Szilard, R., et al., “Industry Application Emergency Core Cooling System Cladding Acceptance Criteria Early Demonstration,” INL, INL/EXT 15 36541, September 2015. [Online]. Available at: https://lwrs.inl.gov/RiskInformed%20Safety%20Margin%20Characterization/INL-EXT-15-36541%20Industry%20Application%20ECCS%20Cladding%20Acceptance%20Criteria.pdf (last accessed on September 19, 2019).

[46] INL, “MARMOT,” n.d. [Online]. Available at: https://moose.inl.gov/marmot/SitePages/Home.aspx (last accessed on September 19, 2019).

[47] INL, “MOOSE,” n.d. [Online]. Available at: https://moose.inl.gov/SitePages/Home.aspx (last accessed on September 19, 2019).

[48] Pastore, G., S. R. Novascone, R. L. Williamson, J. D. Hales, B. W. Spencer, and D. S. Stafford, “Modeling of Fuel Behavior during Loss-of-Coolant Accidents using the BISON Code,” Proc. of the Reactor Fuel Performance Meeting – Top Fuel 2015. Zurich, Switzerland. Part 1, pp. 552–561. 2015.

[49] Erbacher, F. J., H. J. Neitzel, H. Rosinger, H. Schmidt, and K. Wiehr, “Burst criterion of Zircaloy fuel claddings in a loss-of-coolant accident,” Franklin, D. G., (Ed.) ASTM International: West Conshohocken, PA. pp. 271–283, 1982.

[50] Di Marcello, V., A. Schubert, J. van de Laar, and P. van Uffelen, “The TRANSURANUS mechanical model for large strain analysis,” *Nuclear Engineering and Design*, Vol. 276, pp. 19–29, 2014.

[51] Pastore, G., R. L. Williamson, S. R. Novascone, B. W. Spencer, and J. D. Hales, “Modelling of LOCA Tests with the BISON Fuel Performance Code,” Proc. of the Enlarged Halden Programme Group Meeting – EHPG 2016. Fornebu, Norway, 2016.

[52] Pastore, G., R. L. Williamson, S. R. Novascone, B. W. Spencer, W. Liu, K. A. Gamble, R. J. Gardner, A. Casagranda, and J. D. Hales, “LOCA Demonstration with Experimental Assessment (IFA-650.10),” 2017.

[53] Jow, H.-N., J. L. Sprung, J. A. Rollstin, L. T. Ritchie, and D. I. Chanin, “MELCOR Accident Consequence Code System (MACCS),” NRC, NUREG/CR-4691, 1989. [Online]. Available at: https://www.nrc.gov/docs/ML0635/ML063560409.pdf (last accessed on September 19, 2019).